DEVELOPMENT OF THREE-DIMENSIONAL WIND TURBINE WAKE MODELS AND OFFSHORE WIND FARM LAYOUT OPTIMIZATION STRATEGIES

SUN HAIYING

PhD

The Hong Kong Polytechnic University

2019

The Hong Kong Polytechnic University

Department of Building Services Engineering

Development of Three-Dimensional Wind Turbine Wake Models and Offshore Wind Farm Layout Optimization Strategies

SUN Haiying

A thesis submitted in partial fulfillment of the requirements for the Degree of Doctor of Philosophy

June 2019

Certificate of Originality

I hereby declare that this thesis is my own work and that, to the best of my knowledge and belief, it reproduces no material previously published or written, nor material that has been accepted for the award of any other degree or diploma, except where due acknowledgement has been made in the text.

_____ (Signed)

Sun Haiying (Name of student)

Abstract

Wind energy plays an increasing important role in substituting fossil fuels and solving environmental issues all around world. Wake effect is a common problem in all wind farms, which decreases energy output as well as causes structural damages to wind turbines. If the knowledge of wake effect is well acknowledged, it will be helpful to improve the benefit of wind farms by optimizing layouts of wind turbines to avoid severe deficits and turbulences caused by upstream wind turbines. Therefore, this research project focuses on the investigations of three-dimensional (3-D) wind turbine wake models and new optimization strategies of wind farm layout. Novel 3-D wake models have been developed to describe the wake distribution in spatial, wind farm experiments have been conducted to study the characteristics of wakes and validate wake models, and new layout optimization strategies have been come up with to capture more wind energy and save the cost of offshore wind farms. The output of this project contributes to predicting the wake effect and improving the energy generation of wind farms.

Firstly, the novel 3-D wake models have been developed. To solve the wind farm optimization problems spatially, an original analytical 3-D wind turbine wake model for a single wind turbine has been developed and validated. The newly presented 3-D wake model considers the wind variation in the vertical direction, therefore it is more accurate and closer to reality. The wake model is based on the flow flux conservation law and it assumes that the wind deficit downstream of a wind turbine is Gaussian-shaped. The wake model has been validated by the published wind tunnel measurement data. The adopted horizontal wake profiles were obtained from Marchwood Engineering Laboratory's atmospheric boundary-layer wind tunnel and were published by Schlez, Tindal, and Quarton (2003). The adopted vertical wake profile data were obtained from the atmospheric boundary-layer wind tunnel at St. Anthony Falls Laboratory and were published by Y.-T. Wu and Porté-Agel (2011). The relative errors are mostly within 5%

in the horizontal profile validation and within 3% in the vertical profile validation. Based on the wake model, a series of wind prediction results have been demonstrated.

For further consideration of the 3-D problems of wind farm optimization, the average wind speed of a single wind turbine has been investigated considering the influence of vertical wind distribution, and the 3-D wake model for multiple wind turbines have been developed. For one wind turbine, assuming the incoming wind is distributed as power law in the vertical direction, the average wind speed has a close relationship to the power exponent α , hub height h_0 and rotor radius r_0 . When $\alpha = 0.4$, the average wind speed can decrease to 96% of the speed at the hub height, therefore, the wind variation in vertical direction should not be ignored. Then, the 3-D wake model for multiple wind turbines has been developed based on the wake model for single wind turbine. The method of Sum of Squares has been adopted to consider the wake adding principle. The wind tunnel data of two layouts have been used to validate the model. The experimental data come from the wind tunnel in the Saint Anthony Falls Laboratory at the University of Minnesota (L. P. Chamorro & Porte-Agel, 2011). For the first layout, most of the relative errors at the hub and the top heights are smaller than 6%. For the second layout, the largest errors are 8.5% at the top height, 17.8% at the bottom height and 21.2% at the hub height. The results predicted by the wake model for multiple wind turbines have also been presented.

Secondly, the experimental study of wake effect and validations of wake models have been carried out by wind field measurements. An overview of available full-scale wind field measurements for investigating wake effect has been conducted. Typical measurements about wake effect in onshore wind farms, offshore wind farms and isolated wake effect have been studied. Information about the site, equipment and process of each experiment have been described in details. Significant results and experience from experiments are discussed. The

validations for wake models are the main purposes of some experiments, which have also been demonstrated.

Our wind field measurements have been conducted for validating the developed wake models, which were conducted in a complex-terrain wind farm in northern China. The experiment of an upstream-and-downstream arrangement has been made to investigate how wakes of the upstream turbines affect the downstream turbines. It is observed that the range of the wake-influenced area expands, whereas the largest wind speed deficit decreases gradually in the downwind direction. Meanwhile, the wake centerlines of upstream and downstream wind turbines could be different. Another experiment of the side-by-side arrangement was also made to investigate how wake interactions distribute downwind of a row of wind turbines. It has been found that huge deficits of wind speed exist in all analyzing lines behind the wind turbines. The wind speeds reduced to as small as 2.8 m/s at 1D downwind position in Line 2. Fluctuations were observed in the far-wake zone. The range of the wake-influenced area was not easy to be identified in the far-wake zone, and the wakes of two adjacent turbines demonstrated a complicated interaction.

The presented 3-D wake models have been validated by the on-site measured wind data. In the vertical direction, the wake model for a single wind turbine can predict the wind speeds with an acceptable accuracy, especially at positions beyond 10D downstream distance or over 100 m height. Because of the complex terrain, some large errors happened at positions less than 40 m height, and wind speeds in two symmetrical side sections showed different distributions at the same downwind positions. Whereas in the horizontal direction, the wake model for multiple wind turbines also has a reliable accuracy at the far wake positions and near the inflow measuring site, only except that wake model could not predict the wind deficits before an

operating wind turbine, and it was not accurate enough in some particular complex-terrain positions. Suggestions have been given to improve the wake models in the future.

Thirdly, for practical use of the proposed wind wake models, a new repowering strategy and a directional restriction method have been proposed to better optimize offshore wind farm layouts. In the repowering optimization strategy, the service time of the wind turbine foundation is extended to two generations' service time. The costs of removing the first-generation foundations and installing the second-generation foundations can be saved. With the layout optimization method, the wind loss caused by wake effect can decrease. Both aligned and optimized layouts are analyzed, and a case study (an offshore wind farm with the size of 3,740 m × 5,828 m) in Waglan Island seawater area in Hong Kong has been discussed as well. This offshore wind farm (the number of 4.2 MW wind turbine is 54) can generate 2.15×10^4 GWh electricity in 20 years. If the repowering strategy is applied, by reusing the wind turbine foundations and replacing the original wind turbines with the optimized wind turbine combination, the LCoE is expected to reduce by nearly 16.63% and to only 1.0310 HK$/kWh.

An original directional spacing restriction method, Directional Restriction, has been presented to restrict the spacing between wind turbines. The new method considers the influence of wind directions, and the restriction for each wind turbine is related to its rotor diameter. With the Directional Restriction, a wind farm optimization process applying the Multi-Population Genetic Algorithm (MPGA) has been developed. Four representative cases are then studied and discussed. Through these cases, the utilization rate of a non-uniform wind farm with five types of wind turbines can increase to 99.21%, and the minimum utilization rate of a single wind turbine is 94.27%. A potential offshore wind farm in Sha Chau Island in Hong Kong is then analyzed. The results demonstrate that the proposed optimization method is practical in

engineering design of local wind farms.

In summary, this project has developed the novel 3-D analytical wind turbine wake models, carried out wind filed measurements and proposed two novel strategies for offshore wind farm optimization problems. The wake models can help to investigate the distributions and characteristics of wakes. The presented strategies combined with the optimization process can exploit the wind resource effectively and can be used to optimize the layout of non-uniform wind farms. It is expected that the work from this thesis can help develop wind power generation in Hong Kong, mainland China and in the world.

Publications during PhD Study

Journal papers

[1] Sun, H., & Yang, H. (2018). Study on an innovative three-dimensional wind turbine wake model. Applied Energy, 226, 483-493.

[2] Sun, H., Yang, H., & Gao, X. (2019). Investigation into spacing restriction and layout optimization of wind farm with multiple types of wind turbines. Energy, 168, 637-650.

[3] Sun, H., Gao, X., & Yang, H. (2019). Investigation into offshore wind farm repowering optimization in Hong Kong. International Journal of Low-Carbon Technologies, 14(2), 302-311.

[4] Sun, H., & Yang, H. (2020). Numerical investigation of the average wind speed of a single wind turbine and development of a novel three-dimensional multiple wind turbine wake model. Renewable Energy, 147, 192-203.

[5] Sun, H., Gao, X., & Yang, H. A review of full-scale wind field measurements on wind turbine wake effect. (Under Review)

[6] Sun, H., Gao, X., & Yang, H. Experimental study on wind speeds in a complex-terrain wind farm and analysis of wake effects. (Under Review)

[7] Sun, H., Gao, X., & Yang, H. Validations of three-dimensional wake models with the wind field measurements in complex terrain. (Under Review)

[8] Gao, X., Li, B., Zhao, F., Sun, H., Yang, H., Wang, T., Wang, Y., & Han, Z. Investigation of wind turbine performance coupling wake and topography effects based on LiDAR measurements and SCADA data. (Accepted by Applied Energy)

Conference papers

[1] Sun, H., Yang, H., & Gao, X. (2017). Study on offshore wind farm layout optimization based on decommissioning strategy. World Engineers Summit - Applied Energy Symposium & Forum: Low Carbon Cities & Urban Energy Joint Conference (WES-CUE), 18-21 July 2017, Singapore.

[2] Sun, H., & Yang, H. (2017). Study on three wake models' effect on wind energy estimation in Hong Kong. Applied Energy Symposium and Forum, REM2017: Renewable Energy Integration with Mini/Microgrid, 18-20 October 2017, Tianjin, China.

[3] Sun, H., Gao, X., & Yang, H. (2018). Study on Offshore Wind Farm Repowering Strategies in Hong Kong. The 17th International Conference on Sustainable Energy Technologies: Sustainable Energy Technologies for Eco Cities and Environment, 21-23 August 2018, Wuhan, China.

[4] Sun, H., & Yang, H. (2018). Comparative study on a newly-developed three-dimensional wind turbine wake model. The 10th International Conference on Applied Energy: Innovative Solutions for Energy Transitions, 22-25 August 2018, Hong Kong, China.

[5] Sun, H., Gao, X., & Yang, H. (2019). Wake effect measurements on a complex-terrain wind field. Applied Energy Symposium: MIT A+B (AEAB2019), 22-24 May 2019, Boston, USA.

Acknowledgements

Firstly, I would like to express my sincere gratitude to my supervisor Prof. Yang Hongxing, Department of Building Services Engineering of The Hong Kong Polytechnic University, for the continuous support of my PhD study and related research, for his patience, motivation, and immense knowledge. His professional guidance helped me in all the time of research and writing of this thesis. His optimism and friendly personality also set an example for my life-long learning.

I would like to thank Prof. Lu Lin, for her encouragement and insightful comments which incented me to widen my research from various perspectives. In particular, I am grateful to Dr. Gao Xiaoxia at North China Electric Power University (Baoding), for enlightening me the first glance of research and supporting me on the wind farm experiments. My sincere thanks also goes to all members of the Renewable Energy Research Group (RERG), for the assistance they gave me during my study, and for all the fun we have had in the last three years in The Hong Kong Polytechnic University.

My special appreciation is also devoted to Prof. Rebecca J. Barthelmie, who provided me an oversea exchange opportunity to join her team in Wind Energy Research Lab, Cornell University, where I expanded my knowledge and exposed myself to different cultures.

Last but not the least, I would like to thank my parents for supporting me spiritually throughout writing this thesis and my life in general. Without their love, the accomplishment of this thesis should never be possible.

Table of Contents

List of Figures

List of Tables

Nomenclatures

Abbreviations

1-D	One-dimensional
2-D	Two-dimensional
3-D	Three-dimensional
CFD	Computational Fluid Dynamics
D	The rotor diameter of the wind turbine
EWTW	ECN Wind Turbine Test Station Wieringermeer
FLORIS	Flow Redirection and Induction Steady State
LCoE	Levelised Cost of Energy
LES	Large Eddy Simulation
LM	Land Mast
MHK$	Million Hong Kong dollar
MPGA	Multi-Population Genetic Algorithm
PPI	Plan Position Indicator
RHI	Range Height Indicator
SCADA	Supervisory, Control and Data Acquisition
SD	Standard Deviation
SMS	Sea Mast South
SMW	Sea Mast West
WT	Wind Turbine

Variables

Variable	Description	unit
a	axial induction factor	
$A(x)$	parameter in 3-D wake model	m^2
$B(x)$	parameter in 3-D wake model	m/s
C	parameter in 3-D wake model	
Δd	horizontal distance of wind turbines perpendicular to downstream direction	m
d_{normal}	normal distance between two wind turbines	m
$d_{vertical}$	vertical distance between two wind turbines	m
h_0	wind turbine hub height	m
Δh	hub height difference between two wind turbines	m
I_0	incoming free stream turbulence intensity	
I_{wake}	wake turbulence intensity	
k_0	rate of the wake expansion	
k_{wake}	wake decay constant	
$Q(x)$	total flow flux	m^3/s
r	radial distance to the centerline	m
r_0	rotor radius of the wind turbine	m
r_0	radius of the wake area	m
S_0	swept area of the wind turbine	m^2

S_{r_0}	circular area with radius r_0	m^2
$S_{r_w(x)}$	circular area with radius of $r_w(x)$	m^2
S_w	wake area of the downstream wind turbine	m^2
u	incoming wind velocity of the downstream wind turbine	m/s
u_0	incoming wind velocity at z_0 height	m/s
u_a	average wind speed on a wind turbine	m/s
$U(x)$	wind velocity in 1-D wake model	m/s
$U(x,r)$	wind velocity in 2-D wake model	m/s
$U(x,y,z)$	wind velocity in 3-D wake model	m/s
$U_0(z)$	incoming wind speed distribution	m/s
v	wind speed at height of z	m/s
v_0	average wind speed just behind the wind turbine	m/s
V_g	gradient wind velocity	m/s
x	distance between the upstream and the downstream wind turbines	m
z_0	roughness length of aerodynamic surface	m
z_r	reference height	m
α	wind speed power law parameter	
δ	boundary-layer thickness	m
$\sigma(x)$	parameter in 3-D wake model	m

Chapter 1

Introduction

1.1 Status of wind energy development

Wind energy is widely accepted as a representative clean and renewable energy source. It is inexhaustible and environment-friendly, which is an ideal energy source to deal with the pressure from the on-going global warming and pollutions. Wind energy was developing fast in recent years, has palyed an important role in many regions and is regard as a reliable and affordable source of energy (Zhou et al., 2014).

In the year 2018, the new global installation of wind turbines was in excess of 51.3 GW, which brings the new global total up to 591 GW (Global Wind Energy Council, 2019). In the onshore market, 46.8 GW was installed, China and USA remained the largest onshore markets with 21.2 GW and 7.6 GW new capacity, respectively. The European onshore market installed 9 GW, whereas the Middle East, Latin America and South-East Asia installed a combined 4.8 GW during 2018.

Compared with onshore wind resources, their counterpart offshore wind resources tend to be stronger, more abundant, and more consistent in terms of their availability (Perveen, Kishor, & Mohanty, 2014). The offshore wind also has higher efficiency of energy production, saves more land area (Hou, Hu, Soltani, & Chen, 2015b) and has less impact on residents (Hou, Hu, Soltani, Zhang, & Chen, 2016). As expected, offshore wind power is more and more becoming a major source of energy globally and is already a major development in electricity generation for many

marine countries (Twidell & Gaudiosi, 2009, p. v). Offshore wind farms are relatively new but develop fast. The global offshore market remained stable in 2018 with 4.5 GW of new additions, and the total cumulative installations has now reached 23 GW, representing four percent of total cumulative installations (Global Wind Energy Council, 2019). China installed 1.8 GW in 2018, taking the lead for the first time, followed by the United Kingdom (1.3 GW). Globally, the share of offshore installations continues to increase and reached eight percent for new installations and four percent of the total installations in 2018 (Global Wind Energy Council, 2019). Offshore wind energy is regarded as the most potential renewable energy resource to coastal regions in the future (Sun, Yang, & Gao, 2017).

The decommissioning phase, which is also the last phase for a wind farm project, has just been given little attention to date (Heritage, 2013). In the year of 2015, seven offshore wind turbines in the UK and Sweden were decommissioned (Global Wind Energy Council, 2016), which also declared that the first generation of offshore wind turbines arrived their final stage of the 20-year service time and an unprecedented decommissioning market was emerging (Heba Hashem, 2014). The incalculable high decommissioning costs becomes a new challenge. Saving the decommissioning cost could cut down the total cost to a great extent, which is a commonly seen solution to decrease the levelised cost of energy (LCoE) of a wind farm.

Hong Kong is also an ideal coastal region to make use of offshore wind energy, with an annual power generation potential of 1.13×10^{10} kWh (Gao, Yang, & Lu, 2014b), accounting for 25.54% of the total annual electricity consumption in 2014 (Reichardt, Negro, Rogge, & Hekkert, 2016). However, the energy in Hong Kong now is either imported directly (oil products and coal products), or produced using imported fuel inputs (nuclear electricity and gas), only excluding a very small scale of wind power generation as from early 2006 (Korsnes, 2016), and with no

energy supplement from the offshore wind yet. It is reported that around 90% of the total greenhouse gas emissions (44,400 kilotons CO2) originated from the consumption of energy (Reichardt et al., 2016). Therefore, Hong Kong stands a good chance to develop the offshore wind energy industry in the near future.

1.2 Research objectives of the thesis

The wind energy industry has been developed for several decades. With an increasing number of wind turbines have been erected in wind farms, the wake effect and wake-generated loads have a more significant impact on modern wind farms (Bingöl, Mann, & Larsen, 2010). At present, wind turbines tend to have larger capacities with longer blades and higher hub heights. An increasing high-power wind farms that contain more and larger wind turbines have been put into operations as well. The energy losses and structural damages caused by the wake effect become obvious in the current wind farms. However, the wakes caused by operating wind turbines have complicated characteristics, which are still unveiled yet. Scholars and engineers all around the world have been conducting studies to solve the wake-induced problems and to prevent economic losses. This project tries to build analytical wake models, investigate the characteristics of wakes and predict the wake distributions, and avoid the influence of wakes through optimizing the layouts of wind farms from the very beginning phase of the projects. The main research objectives of this thesis are summarized as follows:

(1) To develop 3-D wake models for a single wind turbine and multiple wind turbines. The wake models should be able to predict the wind speeds at any downwind positions of a wind turbine and the wind interactions behind several wind turbines as well. The variation of wind speed in the vertical direction should be taken into the consideration by applying different inflow functions. With the 3-D wake models, it will be possible to obtain the wind

distributions with relatively less computational cost and high accuracy.

(2) To validate the 3-D wake models with data from wind tunnel experiments and demonstrate the predictions from the models. The wake models should be proved to have the acceptable accuracies before taken into application of wind farm optimization process. They will firstly be used to calculate wind speeds under the circumstance of some wind tunnel experiments, and then the results will be compared to the experimental data. The errors should be analyzed from the theoretical aspects.

(3) To conduct wind farm experiments and study the characteristics with the experimental data. Measurements will be conducted in a wind farm of the typical terrain, and then the first-hand data of wind speeds downstream of the operating wind turbines could be obtained. Characteristics of wakes will be studied based on the experimental data in depth, including the centerline, wake width and wind deficit of wakes from both single and multiple wind turbines.

(4) To validate the 3-D wake models with measured wind data and come up with the directions to improve the models. The predictions of wind speeds from the 3-D wake models will be compared to the data from measurements. The applicability of wake models in real wind farms should be verified with the consideration of the complex-terrain conditions. Analyses of errors and shortages of the 3-D wake models will be conducted both theoretically and experimentally based on the comparisons. Methods to improve the wake models will be proposed for the future works.

(5) To develop the wind farm layout optimization process and present strategies for offshore

wind farm optimizations based on the new wake models. The optimization process should be effective to design the layout of a wind farm with a specific number of wind turbines. Novel strategies for offshore wind farm should be proposed based on the optimization process. With the new strategies, the energy efficiency of the whole wind farm should be raised and the LCoE should decrease dramatically.

(6) To conduct case studies based on the developed optimization process and the presented strategies. Hong Kong will be a target region for designing the new offshore wind farms. The real wind data should be applied in the studies and different layouts from optimization process and strategies will be compared and analyzed. This part of study should be able to guide the offshore wind energy development for Hong Kong and other offshore regions as well.

1.3 Organization of the thesis

The overall structure of this thesis takes the form of nine chapters. Following the background introduction and the proposed research objectives, Chapter 2 will provide a comprehensive literature review on a number of significant issues related to wake models and the offshore wind farm development. To begin with, existing wake models are briefly introduced, of which the expressions, advantages and disadvantages and the scopes of applications of the models are comparatively studied. Next, the historical and current status of measurements related to wake effect are summarized. Information will be carried on from the aspects of the tested wind farms or wind turbines, set-ups of experiments and the important conclusions from the experiments. Finally, the advanced strategies for offshore wind farm optimization problems will be presented. To cope with the development of current wind farms, this part of review will focus on the methods about repowering the offshore wind farms and designing layouts of non-uniform wind

farms.

Chapter 3 focuses on the development of the analytical 3-D wake model for a single wind turbine. Three assumptions of the wake model and the derivation process are introduced in details. The wake model takes the vertical wind speed variation into consideration and can obtain wind speeds at any downstream positions with little computational cost. The 3-D wake model will be validated by the available wind tunnel experimental data. The predictions of wind distribution from the wake model will be demonstrated at a series of positions and from different views.

Chapter 4 follows the study of the presented 3-D wake model in Chapter 3, further investigating the average wind speeds with the consideration of wind variation in the vertical direction and developing the 3-D wake model for multiple wind turbines. The commonly used power law is adopted to simulate the inflow. The average wind speeds are compared with the wind speeds at the hub height under the circumstances of various inflow shapes. The deep study on average wind speeds reveals the significance of investigating the wake effect with the vertical wind speed variation. After that, the 3-D wake model for multiple wind turbines is developed. The model applies the method of Sum of Squares to solve the wake overlap problem. The wake model is validated by the wind tunnel experimental data as well.

Chapter 5 introduces a series of measurements of wind speeds in a complex-terrain wind farm. The wind farm information, measuring equipment and results are described comprehensively. Two measuring plans of wind turbines with upstream-and-downstream and side-by-side arrangements are included to study the interactions of wakes. The characteristics of wakes are summarized from the measured data. Besides the analyses of significant experimental results,

some suggestions have also been come up with for the further wind field experiments.

Chapter 6 aims to validate the 3-D wake models with the wind farm experimental data. The wind speeds measured at vertical sections are applied to validate the 3-D wake model for single wind turbine, whereas those measured at horizontal sections are used to validate the 3-D wake model for multiple wind turbines. The relative errors and the applicability of wake models in complex-terrain wind farms are analyzed in depth. The limitations of wake models are pointed out and the improvements are proposed for the future work.

Chapter 7 presents a wind farm layout optimization process with a novel repowering strategy. MPGA is adopted as the optimization tool. With the local wind resources data, the optimization process can give out the optimized high wind efficient wind farm layout for the specific area and the number of wind turbines. Then, a repowering strategy aims to save the decommissioning cost of offshore wind farms has been proposed. The strategy is applied to Sha Chau Island in Hong Kong and is evaluated by comparing the economic performance of original and optimal wind farm layouts. The strategy turns out to be effective for the offshore wind farm layout optimization problem. The newly developed 3-D wake models are applied in the optimized layouts, and it turns out that the 3-D wake models tend to predict less energy output than 2-D wake models.

Chapter 8 presents a novel Directional Restriction method to restrict the minimal distance between wind turbines. The wind directions are involved in the consideration of the new restriction. With the new method, more wind energy can be taken use by installing more wind turbines in the crosswind directions. Several cases with different layouts and different wind directions are studied to demonstrate the effectiveness of the Directional Restriction. It has been

proved to have obvious influence on wind farms with high-centralized incoming wind directions and the non-uniform wind farms.

Chapter 9 summarizes the major conclusions and achievements of this project and proposes the recommendations for the future research.

Chapter 2

Literature Reviews

2.1 Wake effect

In an operating wind farm, the wake effect appears in the wind flow field downstream of operating wind turbines (Rados et al., 2001), because the wind turbines not only generate energy but also induce wakes behind their swept areas (Z. Song, Zhang, & Chen, 2016). The wake effect is characterized by lower wind speeds and higher turbulence levels than the upstream conditions (Samorani, 2013). Wind turbine blades are rotating and the presence of the turbine itself is an obstacle to the inflow (J. Lundquist, Churchfield, Lee, & Clifton, 2015). The wake effect makes the downstream wind contain more turbulence and less energy than the upstream wind (Amaral & Castro, 2017). The wake spreads a long distance downstream of a wind turbine and returns to the surrounding wind gradually. This explains why in an operating wind farm, a wind turbine may be under the wake influence of more than one upstream wind turbines.

If the wake effect is not evaluated properly, the overestimation of energy yields will cause a higher requirement of the electrical equipment's voltage level and the cables' capacity, influencing the operating reserve (Ela et al., 2010) and control strategy of the whole wind farm (P. Wang, Goel, Ding, & Chang, 2009), which will finally induce a waste of investment on components' redundancy (Hou, Hu, Soltani, & Chen, 2015a). The wake effect is also a principle factor that affects the energy output efficiency of a wind farm. The wind loss and turbulence level in the wake of wind turbines are the aspects that have special relationship with the wind farm layout optimization process (L. P. Chamorro & Porte-Agel, 2011). The turbulent flow in a wind farm is particularly characterized by the interaction and superposition of wakes from

multiple wind turbines. In large wind farms, wakes may cause 10~20% power losses of the total energy output (Barthelmie et al., 2009; Sanderse, 2009). For offshore wind farms, understanding the turbulence increase and power loss caused by wakes is of great importance to design the layout of a wind farm (Barthelmie et al., 2007). Several studies on offshore wind suggested that the wake interaction with the surface might be measured even beyond 5~10D (D represents the rotor diameter of the wind turbine) downstream distance from the wind turbines (Barthelmie et al., 2010). Wake characterization can also provide significant insights for optimizing wind farm layout. If the wake effect is taken into account when designing a wind farm, much power loss could be avoided and the cost of wind energy could be reduced (Bodini, Zardi, & Lundquist, 2017).

Wakes with low energy air are created with characteristics influenced by the wind turbines, the incoming wind, and the weather conditions. In wind farms, the downwind wind turbines suffer from wind speed deficit, therefore resulting in the power loss. This degradation in performance has really important effect on the efficiency of wind farm layouts. Since the wake effect is complicated and its characteristics are still unveiled, the most common method to estimate wind losses in wind farm layout optimization is adopting simplified wake models, which can both meet the demands of desired computation time and the necessary accuracy of prediction.

2.2 Wake models

Many researchers have worked on wake models to assess the wake effect. The research has been carried on from the aspects of cutting down the computational cost and improving the accuracy (Sun & Yang, 2018). Various wake models were presented for wake calculation (N. O. Jensen, 1983), which makes it possible for scholars to carry out wind farm-related works. However, via comparisons among different wake models (six models of varying complexity

(Rados et al., 2001), three commonly seen wake models (VanLuvanee, 2006), and a number of wake-induced turbulence models (Sørensen, Thøgersen, Nielsen, & Jernesvej, 2008)), a crucial conclusion has been drawn that all wake models perform with high uncertainties (Pérez, Mínguez, & Guanche, 2013). As problems surface, challenges to the wake model issues are faced by researchers attempting to develop more accurate models.

The requirements of wake assessment methods are considerably distinct when handling different problems. Generally, wake models can be divided into analytical wake models (Tong, Chowdhury, Zhang, & Messac, 2012) and numerical wake models (Schmidt & Stoevesandt, 2015). In view of optimizing locations of wind turbines, numerical models tend to be more precise, but analytical models have more advantages because of their simplicity and fast computational speed (Ishihara, Yamaguchi, & Fujino, 2004).

2.2.1 Analytical wake models

Analytical wake models are the most commonly used measures to estimate wind losses when optimizing the layout of a wind farm (Niayifar & Porté-Agel, 2016). Analytical wake models are relevantly simple and are likely to meet the demands of both the desired computational time and the necessary accuracy of prediction. Several scholars have proposed wake models including, Jensen, Ainslie and G.C. Larsen (Thogersen, Sorensen, Nielsen, Grotzner, & Chun, 2006). All these models can be used in energy yields estimation, however, only the Jensen wake model has been used in most wind farm layout design work (Eroğlu & Seçkiner, 2012; Kusiak & Zheng, 2010; Pérez et al., 2013; Pookpunt & Ongsakul, 2013; Y.-K. Wu, Lee, Chen, Hsu, & Tseng, 2014).

The Jensen wake model, also known as Park model, is a one-dimensional (1-D) wake model

(Charhouni, 2015). It is the most common choice to estimate the energy losses in wind farm due to its simplicity and relatively high accuracy. The calculation based on Jensen wake model requires the least computation time compared with other models (Shakoor, Hassan, Raheem, & Wu, 2016). Jensen wake model is based on momentum conservation theory, and it assumes a linear wake expansion behind the upwind wind turbine (N. O. Jensen, 1983), as shown in Figure 2.1.

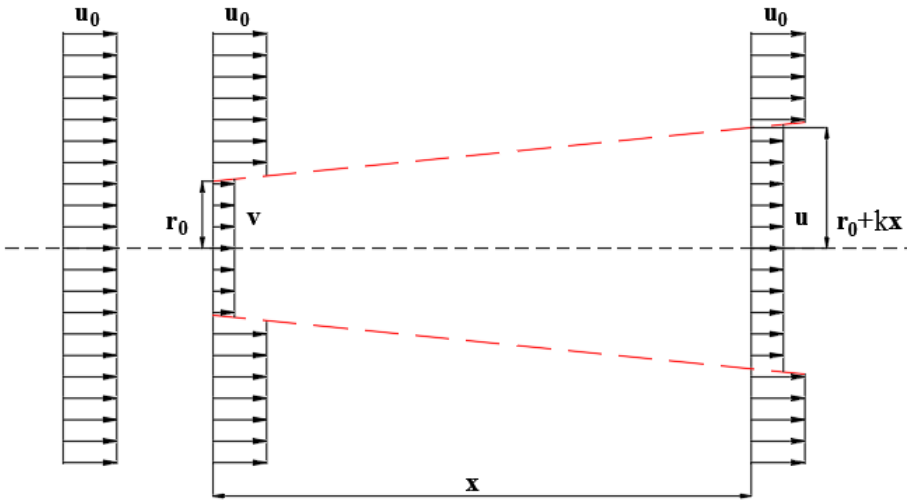

Figure 2.1 The Jensen wake model

The equation of the Jensen wake model is shown as equation (2.1) and equation (2.2). If a wind turbine is under another wind turbine's wake influence, equation (2.1) should be adopted; whereas if a wind turbine is under several other wind turbines' wake influence, a more complicated equation (2.2) should be used additionally.

$$u = u_0 \left[1 - \frac{2ar_0^2}{(r_0 + kx)^2} \right] \tag{2.1}$$

$$u_i = u_0 \left[1 - \sqrt{\sum_{i=1}^{N} \left(1 - \frac{u}{u_0} \right)^2} \right] \tag{2.2}$$

u_0 is the original wind velocity; r_0 is the radius of wind turbine; a is the axial induction factor; x is the distance between the upstream wind turbine and the downstream wind turbine; and u is the incoming wind velocity of the downstream wind turbine.

Although Jensen wake model is widely accepted, one apparent problem is that the wind velocity distribution behind the wind turbine blades is not 1-D in reality. According to the assumption of Jensen wake model, at any particular downstream distance, the inside wind velocity is seen to be constant across the wake plume, which is far from reality. Dufresne and Wosnik (2013) studied the classical shear flow theories in the wakes, whereas Leonardo P Chamorro and Porté-Agel (2009) organized wind tunnel experiments to study one single wind turbine's wind deficit. Both investigations found that after a certain downwind distance, the wind deficit is approximate Gaussian axisymmetric-shaped. The linear wake model was then further investigated.

Ishihara et al. (2004) considered how turbulence affects the rate of wake recovery and developed a universal wake model. The wake can be predicted by the proposed model for any thrust coefficient and ambient turbulence. Larsen (2009) presented a semi-analytical algorithm for computation of stationary wind farm wind fields. The model considers wakes as linear perturbations on the ambient non-uniform mean wind field. Although they considered other factors in the following models later, the simplification models were only constrained for the flat terrain.

Recently, some two-dimensional (2-D) wake models were developed based on the Jensen wake model. Bastankhah and Porté-Agel (2014) built the Bastankhah wake model in 2014, and the model was validated by a large-eddy simulation and experimental case studies. Although the wake model contains three variables, the wind distribution is only related to two factors, the downstream distance to the wind turbine and the distance to the hub axis. In 2015, L. L. Tian, Zhu, Shen, Zhao, and Shen (2015) developed a Cosine wake model in which the wind distribution on the horizontal plane is cosine-shaped. A similar principle Jensen-Gaussian wake model was then developed by Gao, Yang, and Lu (2016), in which the wind distribution is as its name describes, Gaussian-shaped.

Admittedly, the 2-D wake models are more effective in forecasting wind losses than the Jensen wake model, but practical limitations still remain. 2-D wake models do not consider the wind velocity variation in the height direction, the spatial optimization problems are tough or even more serious than before. Because a great number of wind farms are built in rugged and uneven areas, the wind turbines are not actually fixed in the same horizontal plane. The 2-D wake models simplify the wind farm layout optimization to a plane problem, which is apparently unreasonable.

2.2.2 Numerical wake models

Numerical wake models or more complicated analytical wake models are based on various theories, such as linear RANS ((Ainslie, 1988) and (Ott, Berg, & Nielsen, 2011)), dynamic wake meandering (Larsen et al., 2007), and the stochastic wake model (Manuel, Veers, & Winterstein, 2001). Kuo, Rehman, Romero, and Amon (2018) proposed a numerical wake model to simulate wake effects over complex terrains. It implemented simplifications and assumptions to solve a simplified variation of the Navier-Stokes equations. However, this model was not applied to

multiple wake effect. M. X. Song, Wu, Chen, Zhang, and Wang (2016) simulated the turbulence of wind turbine's wake flow and the effect of velocity decay as well. They decoupled the wake flow solution from the wind speed field. The wake model regarded the wake intensity as a diffusive and convective virtual matter. The model can predict the turbulence of wake and the distribution of wind speed decay in the complex terrain with a non-uniform flow field.

On the other hand, to conduct the detailed numerical simulation, some researchers applied Computational Fluid Dynamics (CFD) and took experiments of wind turbine wake flow, especially in the fluid mechanics field. They tried to better understand the nature and the interaction of multiple wake flows. Jimenez, Crespo, Migoya, and García (2007) programmed a CFD code based on LES approach. Concentrated drag forces were applied to simulate wind turbines, which were fixed in anisotropy turbulence. The results were in good agreement with analytical correlations and experimental data. Y.-T. Wu and Porté-Agel (2011) also used LES to study the characteristics of wind turbine wake in a flow of neutral turbulent boundary-layer. The simulation results were validated by the high-resolution measuring data from a hot-wire anemometry behind a wind turbine model. Yang and Sotiropoulos (2013) validated an LES-actuator disk model by wind tunnel measurements. For the case of single wind turbine, good agreement was obtained between model simulation and the tested data at far downstream locations, discrepancies existed in the near wake zone. For the wind farm case, perfect downwind results were obtained at both bottom and top tip heights. Some discrepancies were at the hub height of wind turbines. Sedaghatizadeh, Arjomandi, Kelso, Cazzolato, and Ghayesh (2018) developed a fully numerical wake model by LES. The LES model was more accurate compared to the semi-empirical wake models that were commonly applied in the industry. It was also used as a benchmark to compare the accuracy of those semi-empirical models. Leonardo P Chamorro, Arndt, and Sotiropoulos (2011) studied the basic properties of wake

flow in a staggered wind farm through wind tunnel tests. The staggered configuration was more efficient than the aligned layout in both streamwise and spanwise directions. The maximum turbulence intensity level of the staggered configuration was similar to that of a single wind turbine, but substantially different from that of the aligned layout with a similar spacing. W. Tian, Ozbay, and Hu (2014) conducted an experiment and found that the discrepancies from the upper stream wind could significantly influence the characteristics of wake and the loads on the wind turbine model. The formation, shedding and breakdown of different unstable wake vortices were found to determine the flow characteristics of the wind turbine wake. Wildmann, Kigle, and Gerz (2018) used long-range lidar instruments to detect and analyze the wake of a single wind turbine in the complex terrain. A wake tracking algorithm was proposed to detect the wake center in the lidar scans for three periods with distinct atmospheric stability conditions.

With development, the fidelities of these models continue to increase (Churchfield, 2013), which adds to the computational complexity and to the cost. These models can estimate wind losses and wake distribution, but they are more widely used in aerodynamic analysis, blade structure studies, and mechanical loads (Cao, Wang, Long, Ke, & Xu, 2015). For the wind farm layout optimization process, the trial calculation of the optimal layout may be thousand times, and all wind directions should be involved in each calculation, a balance of accuracy and computation cost of estimating the wind loss is of critical importance The heavy computation cost of numerical wake models makes them impossible to apply to the wind farm layout optimization problem (Hu, 2016).

2.3 Full-scale wind field measurements on wind turbine wake effect

Plenty of wind farms are operating presently, however, there are key problems that need to be solved for the sake of satisfying the increasing need for the larger, more efficient, and more

reliable wind farms. To better use wind energy, the data from full-scale wake experiments are necessary in wind energy community. The experimental wind field testing of wake steering is meaningful to study whether the predicted and observed advantages of the simulation can be realized. State-of-the-art wind farm models are needed in the development and validation processes based on more comprehensive and accurate wake measurements (Trujillo, Bingöl, Larsen, Mann, & Kühn, 2011). Wake characterization based on wind field data can be applied to validate and improve the numerical models. Wind field data can avoid typical limitations from wind tunnels, such as low Reynolds numbers and down-scaled geometric dimensions (Iungo, Wu, & Porté-Agel, 2013). Therefore, the interactions between wakes of multiple wind turbines must be obtained from the experiments in large wind farms, as done by (Aubrun, Garcia, Boquet, Coupiac, & Girard, 2016; Clive, Dinwoodie, & Quail, 2011; Hirth, Schroeder, Gunter, & Guynes, 2015; Hirth, Schroeder, Irons, & Walter, 2016; Kumer, Reuder, Svardal, Sætre, & Eecen, 2015; H. Wang & Barthelmie, 2015) and (van Dooren, Trabucchi, & Kühn, 2016).

2.3.1 Measurements in onshore wind farms

In this section, measurements in six onshore wind farms are analyzed. They are Goodnoe Hills wind farm, Sexbierum wind farm, Nørrekær Enge wind farm, ECN test farm, Iowa wind farm and Myres Hill wind farm.

2.3.1.1 Measurements at Goodnoe Hills wind farm

Three 2.5 MW wind turbines were erected in 1980 in a site close to Goldendale, Washington, providing the possibility for studying the interactive influence of large-scale wind turbines that were integrated into a utility network (Zambrano & Gyatt, 1983). The terrain of the wind farm sloped smoothly upwards from west to east and a steep gully existed in the northwest (Lissaman, Zambrano, & Gyatt, 1983). Figure 2.2 demonstrates the site layout of Goodnoe Hills and

distances between wind turbines (feet).

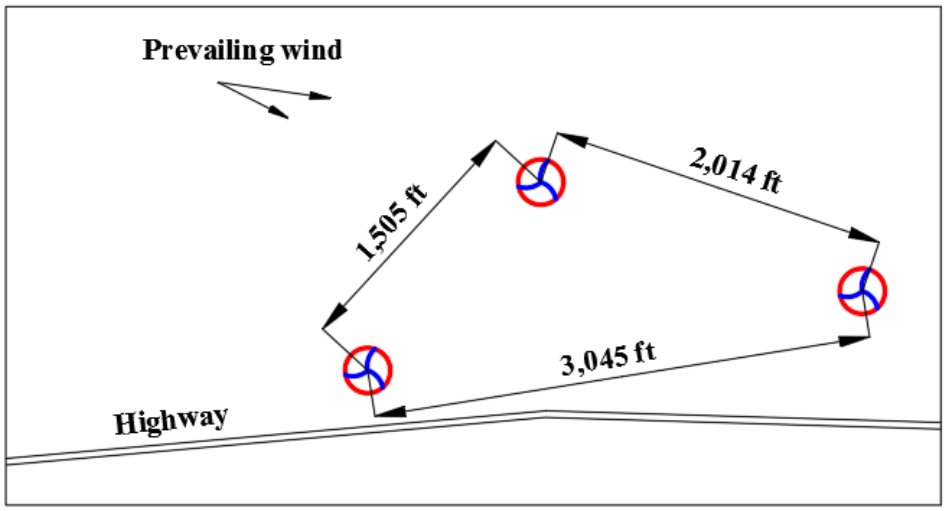

Figure 2.2 Site layout and distances between wind turbines at Goodnoe Hills (Lissaman et al., 1983)

A wind field experimental program was conducted at the hub height (200 feet) from July 12 to August 1, 1982 (Lissaman et al., 1983). Wind velocities were captured by a radiosonde suspended from a tethered balloon, the position of which was determined from a grid of ground stakes. A total of 21-hour data from free stream and simultaneous balloon were collected. During that period, the direction of significant wind energy was west. Measurements were taken to decide the rate of downstream wind speed deficit at centerline in different ambient turbulences and wind turbine drag coefficients. Downwind distances at 3D, 5D, 7D, and 9D from the wind turbine were investigated. At the wind speed from 30 to 45 mph, it revealed that the deficits of wind speed were up to around 50% at 3D and 5% at 5D downwind distances.

Findings indicated that there was obvious terrain-induced influence on the flow at the tower site. However, the measured deficit sometimes is a speed-up, revealing that the deficit could not be specified due to the experimental accuracy. Terrain-induced non-uniformities in the wind farm

may account for some observed scatter. An anomalous behaviour was also observed that the measured deficits of wind velocity were much smaller than what theory predicted at speeds less than 35 mph. This may be because at low wind speeds, there were extensive flow meander.

Some recommendations were also made on the basis of experimental conclusions. Firstly, analysis of the data indicated that at that stage, attention should be paid on the experimental accuracy, and the appropriate methods of statistically processing wind data. It proved the advantages of collecting data for a long period at the fixed downstream positions rather than adjust the wake centerline according to changes in the wind direction. Secondly, tethered sonde systems should be used at least one for upstream and one for downwind flow. This can make sure that the reference anemometer of free stream describes a realistic picture of the winds met by rotors. Besides, it can also avoid differences between upwind and downwind measurement systems from aspects of sampling rate and response, etc. Thirdly, the topography of the wind site was complex enough, so the wake effect could be masked (or exaggerated) by terrain-induced non-uniformities in the wind farm. In addition, an experimental program should be taken in to consideration at a wind field site with a uniform background wind and flatter terrain.

2.3.1.2 Measurements at Sexbierum wind farm

Sexbierum wind farm experiments have resulted in a useful data base for the validation of wake and wind farm models and for input to wind turbine load calculation programs.

The Dutch experimental Sexbierum wind farm was situated at a distance of around 4 km from the sea, West of Leeuwarden (Cleijne, 1993). The wind farm was in a flat homogenous terrain with grassland. In the immediate vicinity of the wind farm, there were only a few scattered farms. The total capacity of Sexbierum wind farm was 5.4 MW, and there were 18 wind turbines with

rated power of 300 kW (Schlez et al., 2003). The wind turbines were from HOLEC and had three WPS 30/3 blades. The diameter of rotor was 30.1 m, and the hub height was 35 m. The layout of Sexbierum wind farm is demonstrated in Figure 2.3. The direction of the rows was at 7° with North. Around the wind farm, there were seven meteorological masts. Masts M4 and M6 were parallel to the prevailing wind direction, of which the sensors were at three different heights. The sensors of the other five masts were at the hub height.

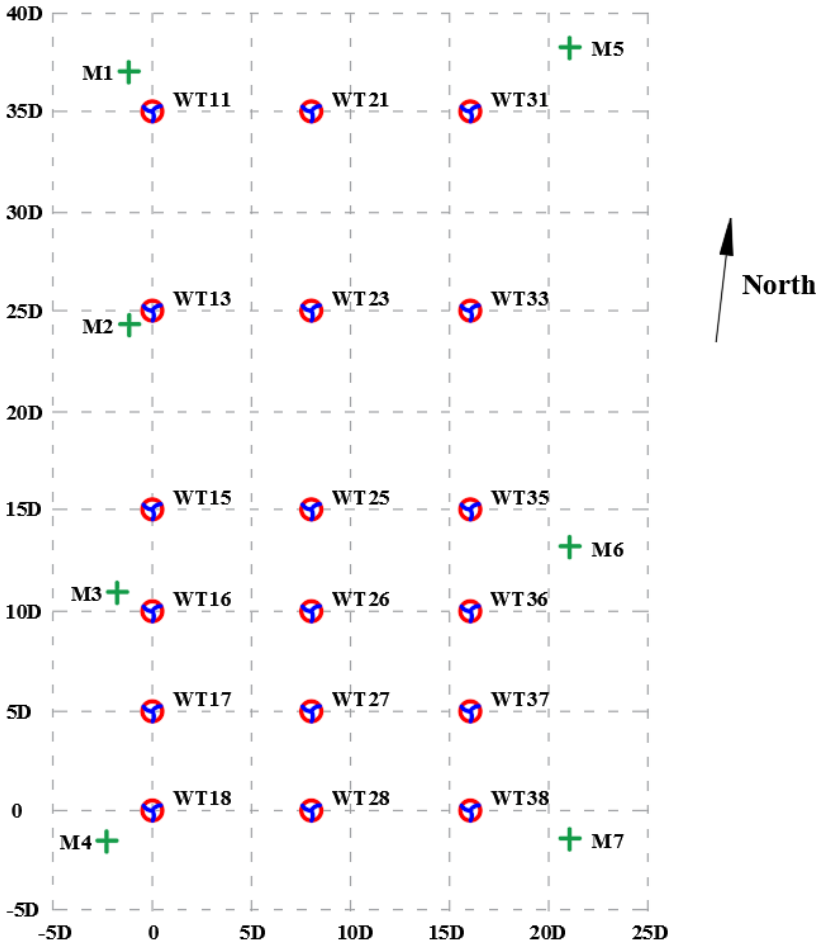

Figure 2.3 Lay out of Sexbierum wind farm (Cleijne, 1993)

During 1992, several experiments were done in the Sexbierum wind farm to collect the data on wind velocity, turbulence intensity and shear stress downwind of a single wind turbine at a series of distances of 2.5D, 5.5D and 8D (Cleijne, 1993). Further, the WT36 was instrumented to study

the wake effect on loads. The prevailing wind direction of the wind farm is along the line from WT18 to WT36. The wind speed at hub height was given by Weibull frequency distribution, of which the scale factor is $a_{hub} = 8.6\ m/s$ and shape factor is $k_{hub} = 2.1$. The average wind velocity was 7.6 m/s.

In these Sexbierum wind farm experiments, the monitored quantities included: fast rate wind speed data in wakes: spectra and wake data, wind turbine power, and fatigue loads. The measurements had no serious problems, but some systematic errors in the measurement of the undisturbed wind was detected, for which the data had to be corrected. From the experimental data, it was found that at x = 2.5D, the wake profile deviated markedly from a Gaussian shape, at larger distances this deviation disappears. At the same position, turbulence intensity showed peaks at the maximum wind speed gradient, which then disappeared for positions further downstream the wind turbine (x = 5.5D and x = 8D). As for shear stresses, they had also been measured successfully, and the course of the individual shear stresses was explained qualitatively based on the assumption that the wind velocity was gradient in wakes.

Besides, the data from the Sexbierum wind farm also enabled to compare the power output with wind direction in the wind farm (Schlez et al., 2003). The comparisons then indicated the ability of the WindFarmer software in predicting the power output on a realistic level including complicated wake interactions. It is worth noting that WT11 and WT31 were non-operational for a significant proportion in the measurement program. Therefore, all data from WT11, WT21 and WT31 were omitted.

2.3.1.3 Measurements at Nørrekær Enge wind farm

Nørrekær Enge II wind farm was situated at the south bank of Limfjord in the northern area of

Jutland, Denmark. The terrain in the wind farm was generally extremely flat, but had some features in the south, west and north of the site. The terrain in south was slightly irregular with the largest irregularity of a 50 m hill. The west of the wind farm contained some farm buildings, whereas to the north of wind farm, the Limfjord was located about 200 m away. The wind farm had a capacity of 12.6 MW, and there were 42 stall regulated Nordtank wind turbines of 300 kW rated power. The wind turbines were fixed in two regular grids of 7 by 3 rows with inter spacing of 6D along the grid line of 166° direction, whereas 7D to 8D along the other line of 258° direction. The separation between the two blocks of wind turbines was around 28D. The layout of Nørrekær Enge II wind farm is showed in Figure 2.4.

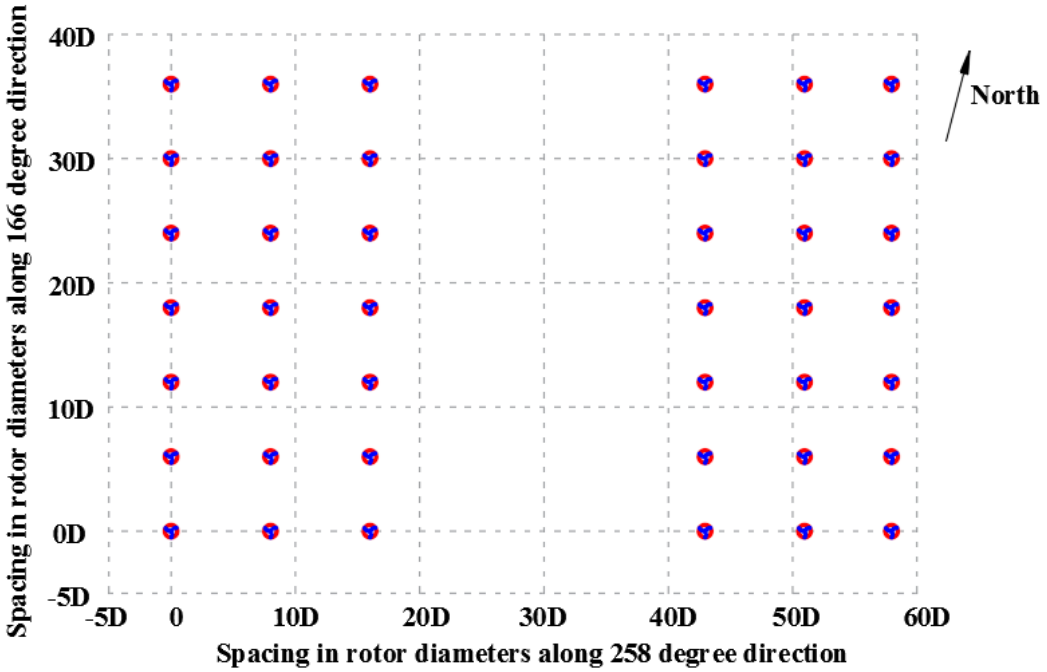

Figure 2.4 Layout of the Nørrekær Enge II wind farm (Schlez et al., 2003)

The Nørrekær Enge wind farm was used to demonstrate the effectiveness of the WindFarmer software in predicting the power output of wake affected wind turbines, in rows with different spacing (Schlez et al., 2003). The data included power output from all wind turbines in the wind farm, averaging over a number of 10-min periods, where the wind was blowing along the lines

of wind turbines. The measured data was grouped into direction bins with a width of 2.5˚.

For the wind direction of 166˚, mean wind speed and power data were grouped by wind speed. A set of thirteen data points were applied to figure out the average power output of each wind turbine. Each data point had the same mean wind velocity of around 8 m/s, and the same standard deviation (SD) of means, indicating similar wind conditions. For the direction of 258˚, no wind speed information was available. The powers from the wind turbines of the front row in the wind farm were applied to calculate the ambient mean wind velocity.

The agreement between the predictions from WindFarmer and measurements from the experiments was generally good. For the 166˚ direction, there appeared to be a tendency to over predict the power at the third and fourth lines. For the 258˚ direction, the power was over-predicted at the third line.

2.3.1.4 Measurements at ECN test farm

ECN Wind Turbine Test Station Wieringermeer (EWTW) was situated in a flat open farmland (Eecen et al., 2006). It is 35 km northeast away from the ECN premises in the Netherlands (MacHielse, Eecen, Korterink, Van Der Pijl, & Schepers, 2007). The tested wind farm belonged to EWTW, and contained 5 rows of the wind turbines of 2.5 MW and a 108 m high meteorological measurement mast. The wind turbines were oriented in one line with a mutual 3.8D spacing (Schepers, Obdam, & Prospathopoulos, 2012). The wind turbines were variable-speed and can be pitch controlled at the 2.5 MW rated power. The hub height of the wind turbine was 80 m, whereas the rated speed was about 15 m/s. The rotation speed can vary from 10.9 rpm to 19.1 rpm. The 3-year averaged wind velocity in the wind farm was 7 m/s at the height of 71.6 m. The direction of the predominant wind was from southwest to northwest. Figure 2.5

demonstrates the directions and distances from the individual wind turbines to the mast.

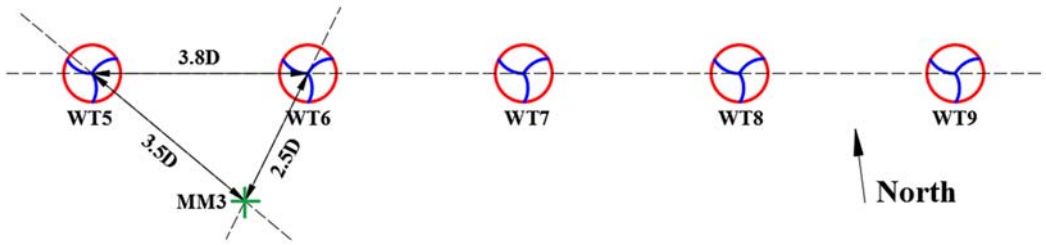

Figure 2.5 Dimensions and the direction of the test farm (MacHielse et al., 2007)

A unique test facility became available since the summer of 2003 (Eecen et al., 2006). The 2-year data were used to validate the models for simulating wakes and designing wind farms. The measured data consisted of wind turbine performances and wind properties, including average wind speeds, turbulence ratios and turbulence intensities.

It was revealed that for the particular configuration of the wind farm, the wake zone had a core whose performance had a close relationship with the ambient conditions, but was flanked by small sectors where the performance did not depend on the ambient conditions. The effect of the ambient turbulence intensity on the power loss tended to be large when there was stronger wake effect with a low turbulence level. The power loss could reach 80% at the low turbulence intensity range of 2 ~ 4%. The maximum deficits of wind velocity in wakes were around 45% at 2.5D distance downstream of the wind turbine and 35% at 3.5D distance downstream the wind turbine. The load along the blade still existed in the wake zone within 2.5D distance, which caused the wind speed distribution a hump shape in the centre of the wake. The wake rotation effect was still visible in the vertical velocities until 3.5D downwind of the wind turbine. The profiles of wind velocity at hub height at 2.5D and 3.5D distances downstream of the wind turbine were compared to preliminary numerical results from ECN's WAKEFARM model. It

was found that the wake width was well predicted and the fair agreement was observed with the magnitude of the wind speed deficit. However, the turbulence in wakes was not well predicted right downstream the rotor.

For either the westerly or easterly wind directions, the maximum power loss existed at the second array of wind turbines in the farm, whereas that for the third to the fifth array of wind turbines were slightly less. The maximum power loss of the second array of wind turbine was in the order of 67% in the westerly wind directions. The higher 73% power loss was in the easterly wind directions, which was due to the lower turbulence intensity in the wind came from the IJsselmeer. An obvious diurnal cycle reflected on the vertical turbulence intensity, wind shear and temperature gradient, especially when less rated wind speeds and in summer. In the evening, a significant positive vertical temperature gradient was observed with a higher wind shear and much lower turbulence level. This leaded to the stronger wake effect during the night time.

2.3.1.5 Measurements at Iowa wind farm

The CWEX experiments were conducted in wind farm in central Iowa (Rajewski et al., 2013). The 200-wind turbine wind farm comprised of two kinds of wind turbines. The southernmost 100 wind turbines were GE 1.5 MW wind turbines, which were super-long extended and feature with rotor diameters of 74 m, the hub height of 80 m and the rated wind velocity of 14 m/s. The northern 100 wind turbines were GE 1.5 MW wind turbines, which were extra-long extended and feature with rotor diameters of 77 m and 82.5 m, whereas the rated wind velocity was 11.5 m/s. The land in wind farm was flat in general, with a slope less than 0.5° at the direction from southwest to northeast. There were crops in the wind farm, most of which were soybeans and corn. There were also some lower terrain and wetland on the southern edge of the wind farm.

(1) The CWEX-10 and CWEX-11 experiments

Two experiments were carried out to investigate surface and elevated meteorological conditions in the wind farm. The CWEX-10 experiment was conducted in the summer of 2010, in which four flux stations were deployed in the cornfields in the wind farm. The upper-air observations were also conducted in a while of the summer. In the next period of summer measurement, the 10-week CWEX-11 experiments were conducted. Experiments were completed on the southwest edge of the farm. The layout of the tested area as shown as Figure 2.6.

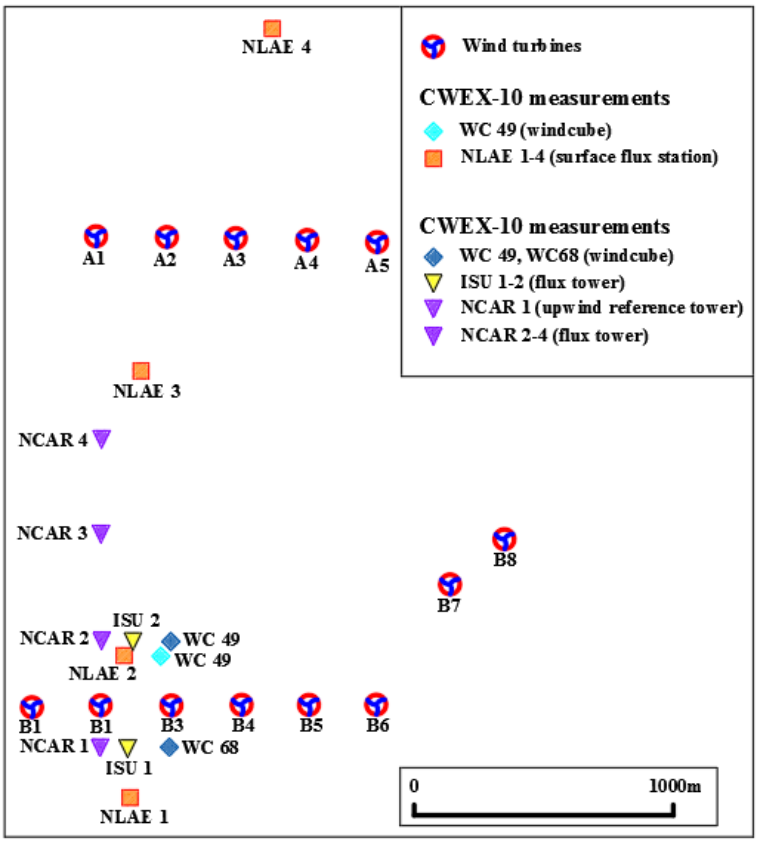

Figure 2.6 The expanded view of CWEX-10 and CWEX-11 measurement locations (Rajewski et al., 2013)

Both those CWEX-10 and CWEX-11 experiments were conducted within and above a corn

canopy. At late June, the beginning of two experiments, the height of crop was around 1.5 m, when it came the second and the third weeks of July, the canopy grew to the maximum height of almost 2.8 m. The roughness length therefore changed from 0.05 m to around 0.4 m for neutral stratification conditions, which followed the parameterization of one-tenth the canopy height.

The CWEX-10 and CWEX-11 experiments (Rajewski et al., 2013; Rhodes & Lundquist, 2013) revealed the one row wind turbines' influence on the local environment. CWEX-10 experiment was conducted to study the differences of mean variables and surface fluxes at various positions in the surround area of one line of wind turbines. The important variability of wind turbine wakes got from CWEX-10 showed the necessity for more comprehensive experiments about surface flux differences at the closer distances from the leading line of wind turbines. Consequently, more flux towers were deployed closer to the wind turbines in CWEX-11.

CWEX-10 and CWEX-11 demonstrated the evidence that flow structures changes near a single wind turbine and a line of wind turbines. They suggested wind turbines modify fluxes to crops importantly, such as CO2 and heat. CWEX-10 and CWEX-11 experiments demonstrated that wind turbines can enhance daytime CO2 flux down into the crop canopy, but also caused higher night time temperature, which enhanced respiration.

Based on the experimental data, Rajewski et al. (2013) proposed three mechanisms that affect the surface micrometeorological conditions where it was near lee of wind turbines: First, overhead wake did not reach the surface but modified the turbulence intensity, vertical mixing, and wind profile between the overlying boundary layer and surface. Second, wakes intersecting the surface allowed the turbulence to modify the surface microclimate. Third, static pressure

fields surrounding each wind turbine and each line of wind turbines generated perturbations in surface flow and fluxes within a short distance of the wind turbine line.

(2) The CWEX-13 experiments

CWEX-13 campaign (J. K. Lundquist et al., 2014) was conducted in the same wind farm studied in the CWEX-10 and CWEX-11 campaigns and from the late of June to the early of September in the year of 2013. The area demonstrated frequent nocturnal low-level jets and strong diurnal cycles of atmospheric stability (Vanderwende, Lundquist, Rhodes, Takle, & Irvin, 2015). In the CWEX-13 measurement, several remote sensing instruments quantified the 3-D distribution of wind speed and turbulence level through the complex flow of several rows wind turbines. Figure 2.7 demonstrates the schematic view of the tested wind field, and the row of wind turbines that were measured by the scanning lidar pointed out with a red ellipse.

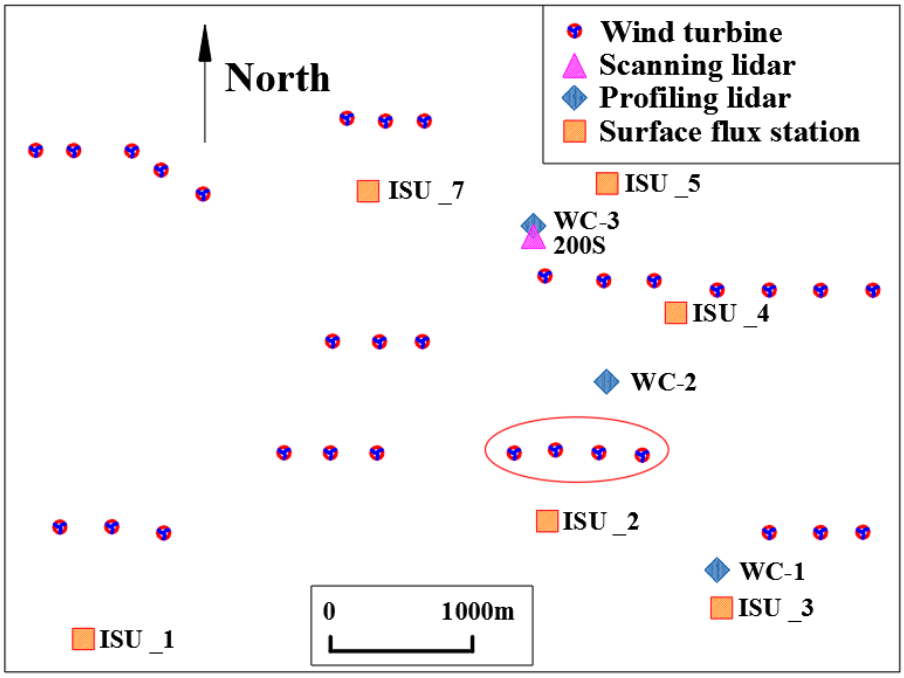

Figure 2.7 Schematic view of tested wind farm and the row of wind turbines (Bodini et al., 2017)

CWEX-13 focused on the interaction of wakes from multiple wind turbines in different atmospheric stability conditions, which was different from what was discussed by Mirocha et al. (2015); Rajewski et al. (2013); Rhodes and Lundquist (2013) and J. C. Lee and Lundquist (2017). With the multiple horizontal scanning, a 3-D wake structure from the row of wind turbines can be created. It was found that wakes erode fast in unstable conditions and may therefore be measured in stable conditions primarily. During the stable conditions, significant differences appeared in the wakes caused by inner and outer wind turbines. Wakes caused by a row of four wind turbines at the leading edge of the tested area were focused to investigate the difference between outer and inner wakes. Furthermore, the strong wind condition connected to the stable condition resulted in a stretching of wake distributions, and that stretching demonstrated variously for wakes from inner and outer wind turbines. These conclusions could be involved in low-order wake models for optimizing layouts of wind farms and forecasting wind powers.

Bodini et al. (2017) extended the algorithm from the single wake detection presented by Aitken, Banta, Pichugina, and Lundquist (2014) to the multiple wake characterization. Based on wind measurements from the scanning lidar, plenty of algorithms were applied to assess the wake parameters, like the wind speed deficits, wake boundaries, and wake centerlines. They firstly quantified the influence of ambient wind condition on the vertical stretching of wakes.

2.3.1.6 Measurements at Myres Hill wind farm

Myres Hill test facility is outside Eaglesham near Glasgow, Scotland. A Long Range Inland Galion was fixed on the southern edge of the wind farm. The Galion swept its probe using a 3˚ azimuthal increment to survey the region under investigation. Each sweep took approximate

one minute to complete. Wake structures were immediately evident approximate 600 m upwind of the Galion. The wakes of several nearby wind turbines were studied with Plan Position Indicator (PPI) scan geometries. The location of the Galion relative to the wind turbines studied is demonstrated in Figure 2.8.

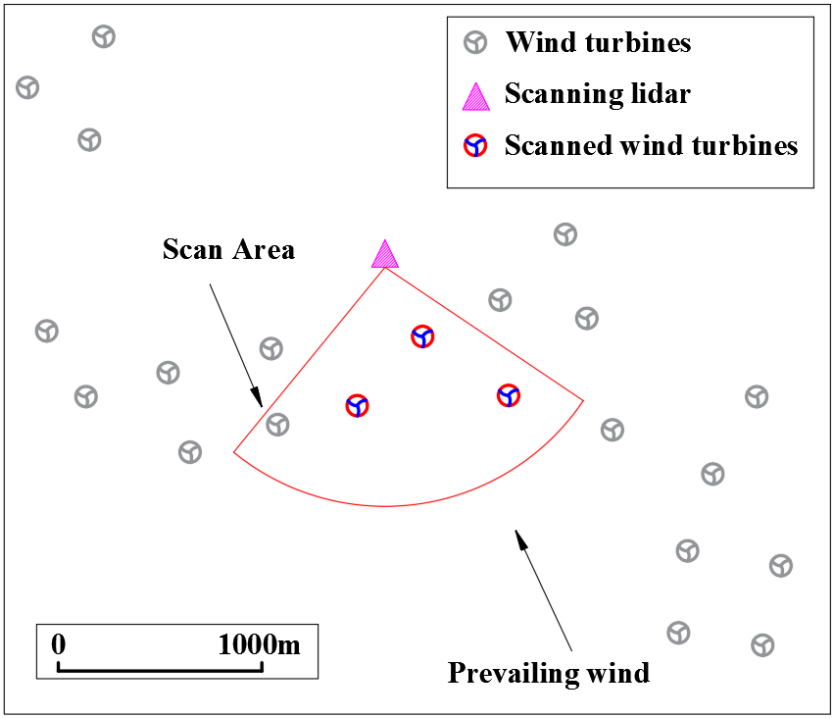

Figure 2.8 The location of Galion and wind turbines (Clive et al., 2011)

The wake of the wind turbine lying centrally in the area surveyed was modelled using ANSYS WindModeller software and the direct measurements were compared to the model results.

The horizontal wind speed was estimated by observing the sinusoidal variation of the line-of-sight component with azimuth. The results obtained from the conventional k-ε model were the least successful at reproducing the measurements acquired by the Galion. The lack of agreement in the near wake was due to the actuator disc approach adopted in the models: full resolution of the blades would improve this. Good agreement in the far wake was achieved for k-ε RNG and

k-ω SST models.

2.3.2 Measurements in offshore wind farms

In this section, measurements in three offshore wind farms are analyzed. They are Vindeby wind farm, Horns Rev wind farm, and Middelgrunden wind farm.

2.3.2.1 Measurements at Vindeby wind farm

Vindeby offshore wind farm has been in operation since 1991, with eleven 450 kW wind turbines (Barthelmie et al., 2003). It was located in Denmark and was around 2 km to the coast. The water depth of the wind farm was only about 2 ~ 5 m, therefore made swell and wave heights relatively low in comparison to other exposed sites.

The wind farm had two offshore monitoring masts and one coastal monitoring mast, taking comprehensive meteorological measurements to the height of 48 m. The offshore masts were sea mast west (SMW) and sea mast south (SMS), whereas the coastal mast was the land mast (LM). The wind turbines were in two rows in the same direction as the prevailing wind (toward the southwest). The rotor diameter was 35.5 m and the hub height was 38 m. The locations of masts and the layout of the wind farm are demonstrated in Figure 2.9.

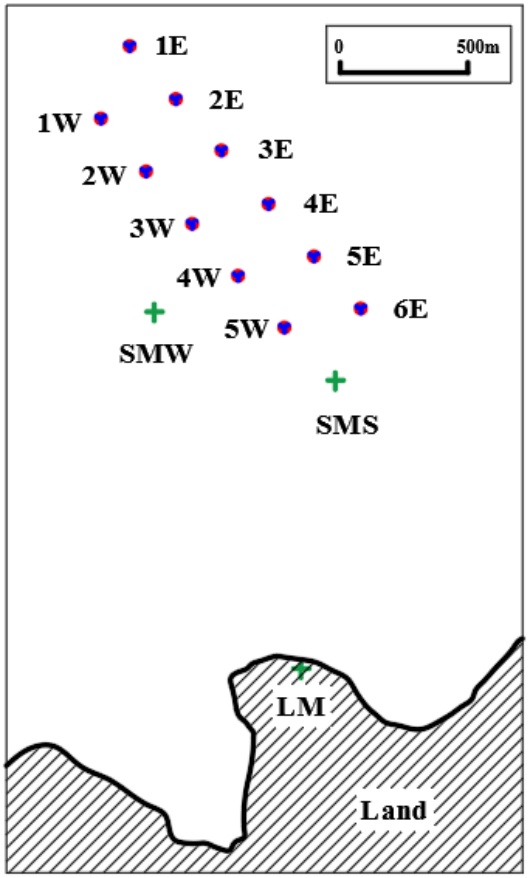

Figure 2.9 Locations of masts and the layout of wind turbines in Vindeby wind farm (Barthelmie et al., 2003)

A total of 36 experiments were done from 21st to 28th April 2001. The average wind speed at 10 m above sea level at SMW was 7.4 m/s in April from 1996 to 1999 inclusive, with average water temperature of 5.88℃ and average air temperature of 5.98℃. During the experiments, a sodar was mounted on the Seaworker ship to measure wakes of wind turbines. The Seaworker was a highly-stable ship regarding to both position and tilt. It was equipped with four anchors, however only three were used during the most experiments. The vertical extent and magnitude of wake were obtained by detecting the profile of wind speed downstream of an operating wind turbine, then turning down the wind turbine and detecting the profile of the free stream. The experiments were compared to meteorological experiments on one coastal and two offshore masts at the same site.

From those experiments, the utility was evaluated that sodar can be used for obtaining profiles of offshore wind speed. It also provided the first offshore wake measuring experiments with different distance from a wind turbine. After excluding the periods that were unsuitable for experiments, a series of turbine-on, turbine-off pairs were studied for the function between deficit of wind speed at the hub height and various distances from the wind turbine. The sodar were also operating well when mounted on an offshore ship. Vertical wind profiles obtained by the sodar also showed great agreement with the data from the mast. It was proved to be possible to detect wind velocity profiles that obviously demonstrated a wind speed deficit near the hub height when wind turbine operating, which disappeared while the wind turbine stopped operating. The noise of wind turbine caused no difficult to measuring the wind velocity profile at the high of 100 m. The experiments also indicated that the offshore wind farms within 3 km distance to coast could be modelled by onshore wake models.

Barthelmie et al. (2006) gave an evaluation of the six most usually applied models for predicting the wake effect behind of a wind turbine. Those models were Risø engineering model (Larsen, Carlen, & Schepers, 1999; Larsen, Højstrup, & Madsen, 1996; Larsen, Madsen, & Sørensen, 2003), Risø WAsP model (Katic, Højstrup, & Jensen, 1986), Risø analytical model (Frandsen et al., 2006), UO FLaP model (Ainslie, 1988), ECN Wakefarm model (Crespo, Hernandez, Fraga, & Andreu, 1988) and RGU computational fluid dynamics model (Magnusson, Rados, & Voutsinas, 1996). The evaluation was based on the experiments to detect the wind speed in both free stream and wake conditions at a series of distances from 1.7D to 7.4D downwind of the wind turbine. Evaluation of those models were carried out by comparing the predicted and measured deficits of wind speed at the hub height.

It was found that there was a great scale of deficits of wind velocity at the hub height between measured data and the predictions from models, and it did not appear to systematically relate to the distance from the wind turbine. The study demonstrated that some models tended to have high or low predictions, however, which was not completely consistent. For predicting wind speeds at the hub height, the mean absolute error of predictions from single wake was 15% and the root-mean-square error was 0.88 m/s.

Some experience was gained from the comparisons. It was hardly possible to compare measurements and models accurately. The detected wind speed deficits were subject to a huge uncertainty. Apart from the measuring uncertainty, some corrections were needed in the free stream and wake measuring periods. The experiment also proved the possibility to let sodar operate on floating platforms to monitor wind in the North Sea. Even though the wave heights were relatively low when conducting the measurements, it was possible to detect the transverse and longitudinal tilt angles with high time resolution, which might be applied to calibrate the sodar signal in the further study (Barthelmie et al., 2003).

To get rid of the evaluation of the model performance at the hub height, a new method was proposed based on determining the cumulative deficit of momentum for the whole wake profile. Good agreement was got with the momentum deficit curve obtained from the experimental data. It was concluded that the predicted wake profile was correct generally. The prediction range tended to be of the order of 50% in absolute terms. However, in general, the discrepancy of the values obtained from the detected wind distribution was larger than the predictions from the wake models. The predictions of wake models spread relatively even for the single offshore wake cases, but propagated with much energy losses. Therefore, the need was urgent for further evaluation on models, as well as the more and better-quality experiments, especially for the

multiple wake cases.

2.3.2.2 Wake measurements in the Horns Rev 1 wind farm

The Horns Rev 1 offshore wind farm was situated in the North Sea, around 30 km west of Esbjerg. The distance from the wind farm to the nearest onshore point, Blåvands Huk, was around 13 km (L. Jensen, Mørch, Sørensen, & Svendsen, 2004). It was a relatively large wind farm exposed to the low turbulence flow. There were 80 wind turbines in the wind farm, and the layout was a 10 × 8 matrix, arranged as a slightly oblique rectangle. The distance between two near wind turbines was 7D (560 m) in both directions. The wind turbines were numbered, as shown in Figure 2.10.

Three met masts were fixed surround the wind farm to investigate the flow recovery downstream of the wind farm. The oldest mast was M2, located about 2 km north-northwest of the WT01. It was fixed earlier than the construction of the wind farm and was applied to obtain the wind resource at the site. Two more masts, M6 and M7, were fixed in the summer of 2003. They were located in a line through the middle of the fifth and sixth rows, and were about 2 km and 6 km east of the wind farm respectively.

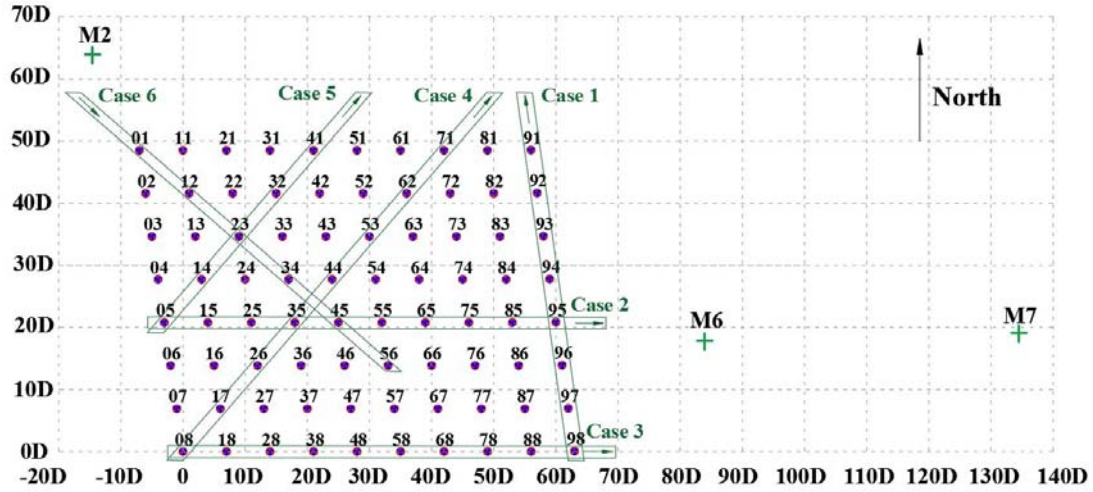

Figure 2.10 Layout of masts and wind turbines in the Horns Rev 1 wind farm (L. Jensen et al., 2004)

(1) Study of the wake flow recovery

L. Jensen et al. (2004) conducted experiments in the Horns Rev 1 wind farm and then demonstrated the main results. The periods of operating the main controller were not involved in the measured data, because of the unpredictability. All operation data of the wind farm were measured and stored by a Supervisory, Control and Data Acquisition (SCADA) system. The SCADA system collected data every 10 minutes from more than 200 sensors. The data were applied to analyse the internal wake effect.

Measurements were conducted on four lines of wind turbines, three aligned and one diagonal lines, as shown in Figure 2.10 (cases 1 ~ 4). Wind speed were analysed based on four cases, whereas turbulence was analysed based on case 2 and case 4. To study the directional dependence of the wake effects, WT35 and WT71 were selected for analysis independently. In addition, external wake effects were studied by measuring the data from the three surround masts, and only the wind velocities within the range of 3 to 10 m/s were selected.

The study showed that a huge reduction of wind velocity existed between the first and the second wind turbines in a row, whereas the wind speed did not reduce much after the second row. The measured wind data revealed that the influence of wakes still exists at 6 km downstream the wind farm both on average wind velocity and turbulence. It indicated that the boundary layer was still not stabilized when the fetch was more than 15 km.

(2) Comparison to wake models

Barthelmie et al. (2009) compared various models including wind farm models and CFD wake models to determine if they were accurate when estimating wake losses compared to measured data. The models included WAsP linearized model, CRES–Farm model, WindFarmer model from GH, WAKEFARM model from ECN, CENER model and NTUA CFD model.

The data were measured in the year of 2005. The wind farm was characterized by low turbulence intensity with less than 8% and plenty of operating hours were in the near-neutral stability. The direction of predominant wind was from south to west. The analysis was focused on westerly flow to maximize the amount of observed data. Directions of the three simulation cases were: Case 2 at 270º with 7D spacing, Case 5 at 221º with 9.4D spacing and Case 6 at 312º with 10.4D spacing. The wind velocity at the first wind turbine was 8.0 ± 0.5 m/s.

For the narrowest wind direction sector of ±1º and the smallest spacing of 7D, the wind speed at the second wind turbine in the row dropped dramatically compared to the free stream. The powers at the second and subsequent wind turbines were around 60% of the free stream. However, if wider sectors were chosen, the decrease of wind velocity at the second wind turbine was less severe, but the wind velocity in the row continued to reduce. The power generation of each wind turbine in row was normalized to that of the wind turbine in free stream. The power

generation from the outside rows tended to have less wake losses than that of the central rows.

2.3.2.3 Measurements at Middelgrunden offshore wind farm

The Middelgrunden offshore wind farm was situated in the Øresund strait between Sweden and Denmark, which was around 2 km east away from the coastline of Copenhagen harbour (Barthelmie et al., 2007). The wind farm belonged to Middelgrunden Wind Turbine Cooperative and Energi E2, providing at least 3% of the electricity in Copenhagen. The wind farm consisted of twenty 2 MW Bonus wind turbines situated in a distinctive bow-shaped layout. WT1 was located in the furthest north and the number of wind turbine increases southwardly until the southernmost WT20. The rotor diameter was 76 m, the hub height is 64 m and the wind turbine spacing was 2.4D. The layout of the wind farm is shown in Figure 2.11.

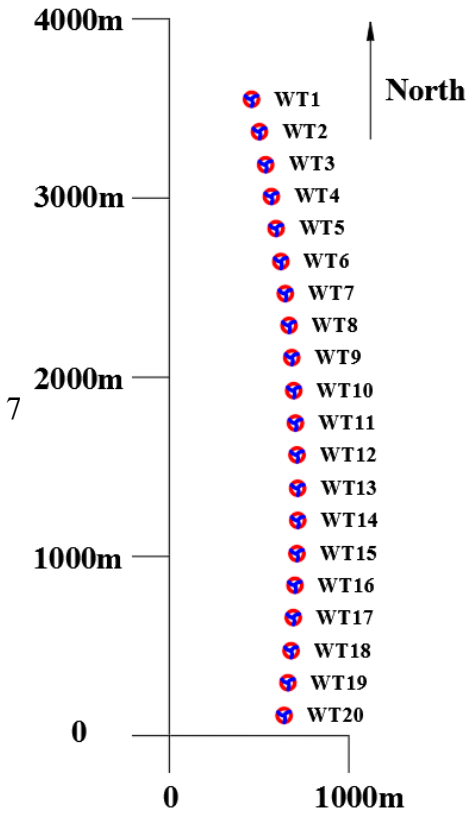

Figure 2.11 Location and layout of Middelgrunden wind farm

The measured data of each wind turbine were 10-min averages from the SCADA system between the years from 2001 to 2004. Only the data with all variables available and all wind turbines working were chose, which was around 35% of all experimental time. The variables included mean wind speed, SD of wind speed measured by the nacelle anemometer, yaw angle, mean power output and SD of the power output. The extracted data were not evenly distributed, which were 47% in autumn, 17% in winter, 18% in spring and 18% in summer. The main observations were between 4 and 12 m/s, which were dominated by the prevailing directions from west to south-westerly. For the daily measurements, more observations were during the night (44% between 07:00 and 18:00), whereas a minimum was between 09:00 and 12:00. In addition, the 30 min average mean wind speed and SD of wind speed were used to compare with the operating data. The measured data was obtained from a 50 m height meteorological mast fixed and operated between October 1997 and December 1999. To be specific, the wind speed was from a cup anemometer at the 50 m height, whereas the wind direction was measured at the 48 m height.

Average ambient turbulent levels were about 13%. Turbulence levels were minimum at 6.5% when wind speed was 11 m/s and then increased with the wind velocity. Barthelmie et al. (2007) described two methods to estimate turbulence intensity. One was based on the mean wind speed and SD of wind speed from the nacelle anemometer, whereas another one was from mean and the SD power output. Compared with the turbulence intensity derived from data at the nacelle anemometers, those derived from power measurements had a better agreement with the data from the meteorological mast.

Power loss and turbulence increase caused by wakes were quantified by data from the wind

farm and state-of-the-art models. On average, wakes caused about 10% of the measured power losses. Measurements indicated that the turbulence intensity was approximate 9% higher than that derived from the power measurements in absolute terms. Conclusion was received that in non-wake conditions, the power SD method represented ambient turbulence better than the nacelle anemometer method. The turbulence from WAsP model increased about 20% in absolute terms when flow was directly along the row. Turbulence intensity was also strongly dependent on wind direction. Although the 2.4D wind turbine spacing was beyond the limitation of most wake models, the WAsP model has a great agreement with the measured results.

Because of the wind farm layout, wake losses at Middelgrunden were limited to two wind direction sectors and could be well predicted by the WAsP model reasonably. Observed wake loss was the highest when wind speeds were low and decreased with the increase of the wind speed. The estimation of the efficiency of the whole wind farm was 90% with the measured data between 2001 and 2004, and was 86% with the WAsP model. Then, the discrepancy existing in the results was pointed out, such as the time period for modelling was independent on the production of wind farm and the wind turbines produced 5.7% more power than that estimated by the power curve.

2.3.3 Measurements of isolated wind turbines

Plenty of wake validation focus on individual isolated wind turbines and are from remote sensing measurements (Aitken et al., 2014; Aitken & Lundquist, 2014; Bastine, Wächter, Peinke, Trabucchi, & Kühn, 2015; Bingöl et al., 2010; Hirth & Schroeder, 2013; Hirth, Schroeder, Gunter, & Guynes, 2012; Käsler, Rahm, Simmet, & Kühn, 2010; Kumer et al., 2015; Trujillo et al., 2011), with some research that aims to reconstruct the 3-D distribution of wind turbine wakes (Banta et al., 2015; Iungo et al., 2013). In this section, eight measurements about

the isolated wind turbine are analyzed.

2.3.3.1 Light detection and ranging measurements of wake dynamics

A serious of tests were performed to validate the instrument in the Risø DTU Høvsøre Test Centre in Denmark (Bingöl et al., 2010). The test period was from the end of 2004 to the beginning of 2005. To face the downwind flow field, the ladar system was installed on the back of a small wind turbine's nacelle. The wind turbine was the stall regulated Tellus 95 kW, the hub height was 29.3 m and the rotor diameter was 19.0 m (Trujillo et al., 2011). The laser beam was moved across the wake in both vertical and horizontal directions. The wind speed was detected at the frequency of around 136 times every second. The instrument was focused on the downstream distances from 1D to 10D, therefore it was possible to investigate the shape, the widening, the meandering and attenuation of wakes.

Bingöl et al. (2010) presented an experimental technique to directly detect the instantaneous wind speed deficit. The technique can quantify the instantaneous wake expansion and the wake meandering expressed in a meandering frame of reference. The measurement was carried out firstly to validate the hypothesis that the wind speed deficit was advected passively by eddies that were larger than rotors in the atmospheric flow, meanwhile the wake widens gradually, because the small-scale atmospheric eddies caused the mixing. The experimental results were used to preliminarily verify a wake meandering model, in which the wake was essentially considered as a passive tracer.

Trujillo et al. (2011) developed and tested a method for tracking wake based on 2-D lidar measurements. The method delivered the instantaneous transversal wake position and compared to the predictive result of the Dynamic Wake Meandering model quantitatively. The

aim was to quantify the wake quasi-steady, the wake meandering and the turbulence intensity. The method was applied to various data of measurements, and two 10-min time series measurement in stable atmospheric stratification were demonstrated in details. The results showed that the measurement and analysis techniques had a high potential for the understanding and recording the full-scale wind turbine wakes. The obtained data of the organized wake flow distribution was useful for validating energy output assessment models in wind farms. Hypothesis was made that the slightly rotating wake slants downwind to one side and then loses symmetry quickly.

2.3.3.2 Wind velocity from multiple wind lidars

Debnath et al. (2018) retrieved vertical distributions of spatial wind from triple Range Height Indicator (RHI) scans, performing with five simultaneous Doppler wind scanning lidars. The test was conducted at the National Oceanic and Atmospheric Administration's Boulder Atmospheric Observatory, which is close to Erie, Colorado. The experimental period was from 2nd March to 31st May 2015. Three components of wind velocity were retrieved. They were compared to the data from different profiling wind lidars and the wind data with high frequency from sonic anemometers, which were fixed on a 300 m high meteorological tower.

Specifically, lidars are widely used in wind industry for the investigating the characterization of atmospheric boundary layer. It is mainly because of their characteristics of the non-intrusiveness, relatively easy deployment, lower maintenance costs and lower deployment cost than traditional met towers (Barthelmie et al., 2010; Schepers et al., 2012).

The results showed that the direction and the magnitude of the horizontal wind obtained from the triple RHI scans have a good accuracy in general. However, for the vertical velocity, the

accuracy was pretty poor. The small magnitude, the error propagation related to the accuracy of experimental setup and the data retrieval procedure maybe responsible for it.

2.3.3.3 Wake Measurements with Coherent Long-Range Pulsed Doppler Wind Lidar

Long-range Doppler lidar measurements at a wind turbine were conducted in the northern part of Germany where was close to the coastline of Bremerhaven. The tested wind turbine was of the Areva Multibrid M5000 type, with rated power of 5 MW. It was the prototype for Alpha Ventus, a German offshore test site. The 2-μm lidar was situated at approximate 1820 m northeast away from the wind turbine M5000.

Azimuth scans and elevation scans were conducted to analyse the ambient wind distribution of the prototype of the tested wind turbine. For the scan of azimuth, the laser beam was elevated constantly and the azimuth angle was adjusted continuously, with the azimuth scan duration of 15 s and the speed of 2°/s. Whereas for elevation scans, the elevation increased continuously, but the azimuth angle was fixed. The single elevation scan period was 10 s and the scan speed was 1°/s. One merit of the measurement was that it can simultaneously get the data of airflow before and after the wind turbine. The layout of the 2-μm lidar and wind turbines in the wind farm in Bremerhaven are demonstrated in Figure 2.12.

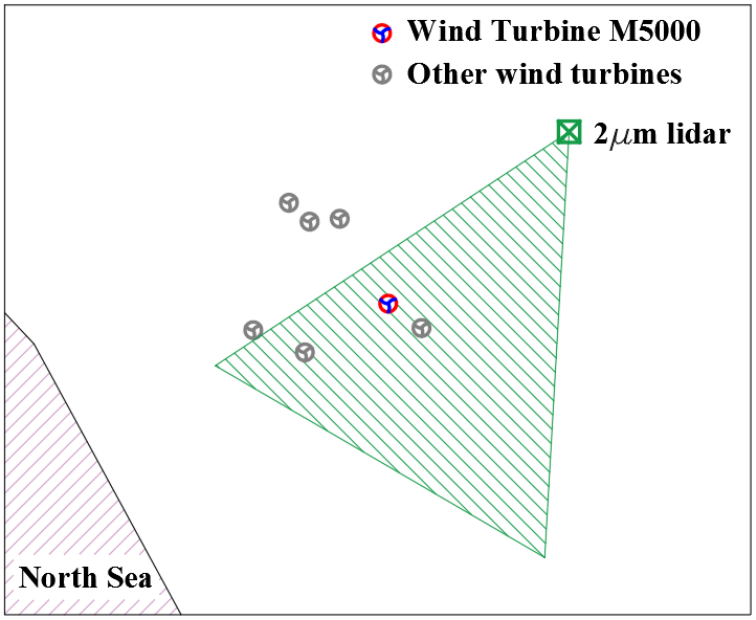

Figure 2.12 The top view of azimuth scan in the wind farm (Käsler et al., 2010)

Käsler et al. (2010) discussed the measurement technique and demonstrated the data of the stable nocturnal boundary layer and the diurnal layer. The reduction of the wind velocity at a series of downstream distances of the wind turbine was mainly studied. A method for capturing wake was proposed. It also revealed that the 2-mm Doppler lidar was a reliable tool to research wind energy and can complete the modelling of wakes for a single wind turbine and for wind parks.

2.3.3.4 Study of wake characteristics of a horizontal axis wind turbine

Qing'an Li, Takao Maeda, Yasunari Kamada, and Naoya Mori (2017) demonstrated the wind speed distribution of a horizontal axis wind turbine and investigated the influence of turbulence intensity and wind shear on wake characteristics in the horizontal direction by wind field measurements. The tested wind turbine was three-bladed with a variable pitch mechanism. The rotor diameter of the wind turbine was 10.0 m, the rated power was 30 kW and the hub height was 13.4 m. The arrowhead wind vane and the 3-cup anemometers were fixed on the upwind

of the wind turbine to detect the incoming wind. The flow field of the wake zone had a close relationship with the operation condition. The rotation speed of rotors was set as 70 rad/min, the pitch angle was set as 2˚ and the direction of nacelle was 303˚, which was the same as the predominant wind direction. SAT-550, an ultrasonic current meter, was installed on the downstream measuring equipment, which was applied to detect the wake distribution at multiple points.

The observed wake results of the wind turbine were analyzed under the optimal operating condition, in accordance of the maximum power coefficient (Qing'an Li, Takao Maeda, Yasunari Kamada, & Naoya Mori, 2017). The analyses demonstrated that the non-dimensional wind speed ratio made the minimum value where near the y/R = 0.50 zone, in which y was the lateral coordinate and R was blade radius. Then the ratio increased from y/R = 0.50 in the horizontal direction. The maximum deficit of wind speed was found around y/R = 0.50. The inflow had a gradient of the horizontal wind velocity, and it became smaller where it was close to the positive direction of y/R. For both low and high turbulence intensities, the maximum deficit of wind speed was found at the position of y/R = -0.50, z/R = -0.25. For all wind shear indexes, the maximum wind speed deficit was found at the position of y/R = -0.50, z/R = -0.2.

2.3.3.5 Measurement of a utility-scale wind turbine wake

Hirth et al. (2012) did a wake measurement of a single utility-scale wind turbine on 27th October 2011. The data was collected by Ka-band mobile radars from the Texas Tech University. Two mobile Ka-band Doppler radar systems which were 35 GHz, were designed and constructed in the year of 2006. Those systems were built to obtain the data from different aspects of the atmospheric boundary layer with a high level of spatial and sensitivity resolution.

Scanning techniques of RHI and PPI were applied to analyze various wakes. Preliminary results confirmed that the deficit of wind speed right behind the hub was on the order of 50%. It laid the groundwork for further analyses of evolution and wake distribution with the Ka-band radar systems, which included wake interaction and wake meandering in large wind farm deployments.

2.3.3.6 Full-Scale wind field experiment of wake steering

Fleming et al. (2017) conducted a campaign of wind field experiment, in which the utility-scale wind turbine was operated with a yaw misalignment, and a lidar were installed on the mount of nacelle continually scanning the wake. The campaign started from the September of 2016.

The test wind turbine and meteorological tower were situated in the National Wind Technology Center in Boulder, Colorado. The site was close to the east of the Rocky Mountains, where the dominant direction of the incoming wind was from the mountains to the west. The wind turbine used in this test campaign was a GE 1.5 SLE, which belonged to the U.S. Department of Energy and was operated by the National Renewable Energy Laboratory.

In the experiment, the yaw controller of the wind turbine was set to track various yaw misalignment set points, whereas the lidar scanned the wake at several downwind distances. The experiments of lidar were combined with wind turbine data and the data of the incoming wind collected by a highly instrumented meteorological mast. The measurements were then compared to the predicted results of Flow Redirection and Induction Steady State (FLORIS), which was a control-oriented wake model applied in designing wake steering controllers. Comparisons contained the key predictions of FLORIS, power loss, wind speed deficit, wake recovery, wake deflection and wake skew. Perfect agreement was obtained between the model

results and observed data. Simulations from FLORIS indicated that the wake steering may positively affect the annual energy generation of a wind farm, and may help to further validate the conclusions.

2.3.3.7 Wake characterization in complex terrain

The Perdigão experiment was conducted at the period from May to June in the year 2017. The site of Perdigão experiment was a double ridge, which extended for several kilometers and with the maximum height of 300 m above the local terrain (Vasiljević et al., 2017). Three Doppler lidar systems were used to obtain the wake distribution of a wind turbine on the southwest ridge. All lidar systems were operated in data processing, therefore horizontal and vertical wake profiles can be derived at a series of downstream distances of the wind turbine. Cornell University controlled one lidar system in the bottom of valley, which was around 1 km northeast away from the wind turbine. Two RHI scans and multiple arc scans were conducted every 10 minutes centered on the wind turbine. Technical University of Denmark applied a dual Doppler lidar system to conduct the horizontal scanning from the northeast ridge. Deutsches Zentrum für Luft- und Raumfahrt used three lidars, two of which were in the same plane with the wind turbine from the predominated wind direction, and the third one was on the southwest ridge.

Barthelmie, Pryor, Wildmann, and Menke (2018) described the wake measurements with lidars from the three groups, evaluated the advantages of adopting various scanning strategies and compared wake characteristics obtained from the various systems. The integration process of those datasets were illustrated to distinguish common spatial and temporal frameworks, which can be used for other scans. From the experiments, the study of wake characterization was more difficult in complex terrain, which was firstly because the flow was complexity (Forsting, Bechmann, & Troldborg, 2016), and secondly because the wake behavior itself responded to

the flow and the terrain slope (Politis et al., 2012; Vasiljević et al., 2017). The Perdigão experiments was one of the first experiments to detect wakes by lidar in high complex-terrain wind farms and to study the advantages of integrating results from several scanning and lidar systems.

2.3.3.8 Analytical wake model validation with nacelle-mounted wind lidars

In this test, the selected site was situated at the Kirkwood Community College campus, in Iowa State of the US. The tested wind turbine was a 2.5 MW Liberty C96 model, which was manufactured by Clipper Windpower. The wind turbine had a SCADA system, continuously collecting the data about the operation of the wind turbine at 10-min intervals. Two pulsed scanning Doppler lidars were installed on the wind turbine nacelle. One lidar was upstream installed and detected the incoming wind, including turbulence intensity, average wind speed, vertical and yaw wind shear; the other one was downwind oriented and performed horizontal planar scans of the wind speed deficit in wakes.

Carbajo Fuertes, Markfort, and Porté-Agel (2018), based on the measurement, presented the setup, methodology and results on the characteristic of single wind turbine's wakes under various inflow conditions. It was concluded that the higher turbulence intensity of inflow will enhance the flow mixing and entrainment in the wake zone, then leading a faster wake width growth rate, a shorter near-wake length and a faster wind speed recovery.

2.4 Wind farm optimizations

2.4.1 Offshore wind repowering strategy

Generally, offshore wind farms, including foundations, must be decommissioned after their life

cycle's operation in order to protect marine ecological environment (Ekins, Vanner, & Firebrace, 2006). All the obligations emphasize the responsibility of the wind farm owner to conduct a complete dismantling to minimize the project's impact on the marine ecosystem. Thus, the foundations must be removed, while cables sometimes can be left in situ (Ekins et al., 2006). Some countries, such as Sweden, have already introduced decommissioning regulations to ensure that wind turbines are dismantled once wind farms reach the end of their life service (McCarthy, 2015).

Topham and McMillan (2017) analyzed the main operation parameters that affect the decommissioning process, identified the benefits and drawbacks of the variables and designed a model to compare different transportation strategies. Research has also been conducted on the increased environmental cost of decommissioning of offshore wind turbines when compared to the onshore counterparts (Bonou, Laurent, & Olsen, 2016; Kaldellis, Apostolou, Kapsali, & Kondili, 2016).

The high cost of decommissioning an offshore wind farm is an unavoidable problem and is therefore rising more and more attention. DNV GL, a renewable energy and technical advisory, estimated that the cost to decommission offshore wind turbines will be EUR200,000-500,000/MW, which equals to 60~70% of quoted installation costs (Dodd, 2015). Interviews within the Contact Programme suggested that the average decommissioning cost for offshore wind would make up around 2.5% of the total project cost or 2% of operating cost when spread over the lifetime of a project (Climate Change Capital, 2010). Removal of foundations may need near 50% of the total decommissioning expenses, because the heavy offshore structures require more complex techniques and specialized equipment (Topham & McMillan, 2017).

Commonly, the offshore wind turbine has a longer life expectancy of around 25~30 years

(Carrasco, Bialasiewicz, Guisado, & León, 2006). The foundations are often overdesigned (Hou et al., 2016), which means foundations still have the capability to serve when wind turbines are to be decommissioned. Type and load will influence the specific lifespan of the foundations. For example, some gravity bases can be projected last over 100 years (Yanguas Miñambres, 2012). Under this circumstance, the repowering idea has been proposed recently.

Hou, Enevoldsen, Hu, Chen, and Chen (2017) presented an offshore wind farm repowering strategy, in which other types of wind turbines chose to replace the original wind turbines. The repowering strategy is demonstrated to be better than replacing the old wind turbines with identical ones. Actually, repowering is important if a country faces a scarcity of sites with suitable wind conditions, such as in Germany and Denmark (Ziegler, Gonzalez, Rubert, Smolka, & Melero, 2018). The repowering strategy extents the lifespan of wind farm, as when the first generation offshore wind turbines are decommissioned, foundations remain to be utilized for the second generation of wind turbines after some strengthening work. It is obviously that the huge decommissioning cost can be saved, because the foundations will only be decommissioned once in the original two generation wind farm's lifespan. Since all wind turbines and foundations are decommissioned at the end of the whole lifecycle, no additional marine ecological problems will be caused. On the other hand, the repowering strategy also reduces one undersea construction phase, which is likely to reduce the greatest impact on marine mammals (Dolman & Simmonds, 2010). Consequently, some activities of greatest concern like pile driving and increasing vessel traffic could be dismissed as well.

2.4.2 Spacing restrictions in wind farm optimization

When designing a wind farm, a wind turbine must be considered to be at a distance from other wind turbines. One practical consideration is to avoid the huge influence of wind deficits and

turbulences from the upwind wind turbines, and the other one is to prevent the interaction effect among wind turbines. Consequently, a restriction must be set when designing and optimizing a wind farm.

In the earlier research on the wind farm layout optimization problems, a grid farm was always applied in to restrain the position of wind turbines, as shown in Figure 2.13. Mosetti, Poloni, and Diviacco (1994) used a 10×10 square grid farm to solve wind farm optimization problem. The size of each cell was 5D and wind turbines must be placed at the midpoints of the square cells. Grady, Hussaini, and Abdullah (2005) further studied wake decay effect in wind farm design with Genetic Algorithm, using the same wind farm grid. Zhang, Hou, and Wang (2011) applied a lazy greedy algorithm to optimize the placement of wind turbines, in which a 10×10 square grid farm with 5D side length was also used.

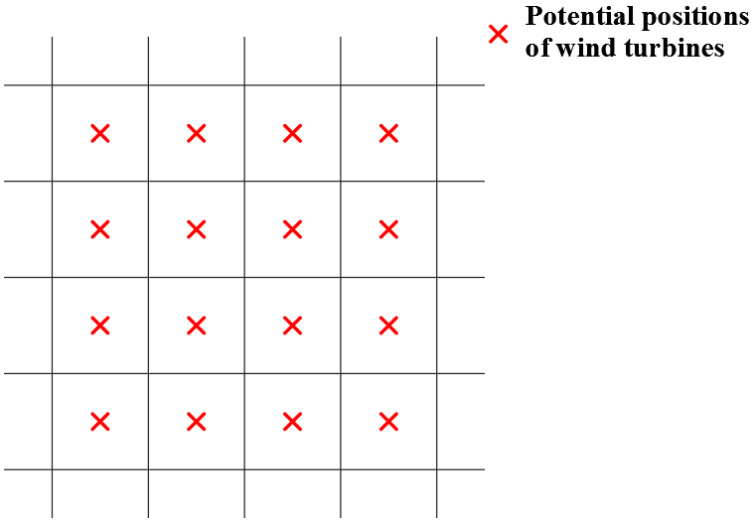

Figure 2.13 Wind farm grid with potential positions of wind turbines

Recently, the more general way is to set a minimum distance between any two wind turbines, which is the empirical Omnidirectional Restriction. It can be interpreted by a circular restrained

area, and 5D restrained radius is mostly used, as shown in Figure 2.14. In the Omnidirectional Restriction, each wind turbine has its restrained area, and any other wind turbines should not be installed in it. If one wind turbine (WT2) is put into the restrained area of another wind turbine (WT1), both two wind turbines (WT1 and WT2) are regarded as out of operation, which means their power outputs are considered as zeros. This restriction is widely used in optimizing the layout of wind farms, because of its simplicity.

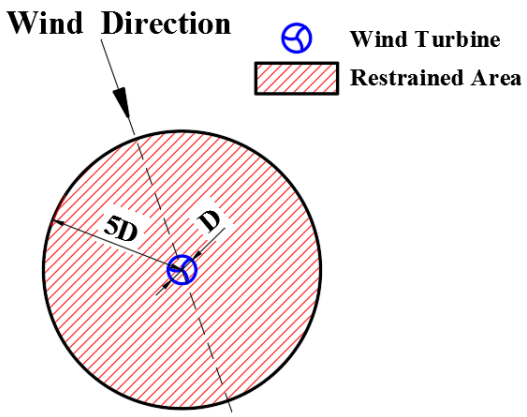

Figure 2.14 Restrained area in the Omnidirectional Restriction

Park and Law (2015) described a method for optimizing the placement of wind turbines with the 5D inter distance constraint. Mittal, Kulkarni, and Mitra (2016) proposed a hybrid optimization method to simultaneously optimize the total number and the locations of wind turbines, in which the minimum distance between wind turbines is 5D. Parada, Herrera, Flores, and Parada (2017) also determined the wind farm layout to maximize the annual energy generated, using the Omnidirectional Restriction with the 5D constraint.

The Omnidirectional Restriction is more advanced than the wind farm grid restriction. However, the irrationality of it is obvious. The wake generates behind the wind turbine blades and then

develops in the wind direction. For a specific wind direction, the wake influenced area is within a long downwind distance but a relatively short crosswind distance. The Omnidirectional Restriction does not consider the directional influence from the wake effect. For the place where the prevailing wind directions are very distinct, it is especially not economical when adopting the Omnidirectional Restriction to design a wind farm.

2.4.3 Nonuniform wind farm optimization

Furthermore, some research has focused on nonuniform wind farm optimization problems. Y. Chen, Li, Jin, and Song (2013) pointed out that the power output will increase by using wind turbines with different hub heights when the total number of wind turbines is the same. Feng and Shen (2017) investigated the design of offshore wind farms with multiple types of wind turbines and hub heights and found that a nonuniform wind farm can achieve a lower levelised cost of energy. Nonuniform wind farm optimizations should not neglect the factor of height difference.

The Directional Restriction also contributes to the layout optimization of nonuniform wind farms, which contain different types of wind turbines. Since the nonuniform wind farms increase the difficulties in optimization, for a long time, studies were only carried out based on one-type-wind turbine wind farm. However, some recent research have found that the nonuniform wind farm may be a better choice.

Herbert-Acero, Franco-Acevedo, Valenzuela-Rendón, and Probst-Oleszewski (2009) addressed the problem of wind turbines lined up in the wind direction through three cases, in which the simulated annealing (Annealing & Machines, 1991) and genetic algorithms (Hand,

1994) were used. From the result, their algorithms can minimize wake effects by placing the wind turbine hubs at two different heights. Y. Chen et al. (2013) used nested genetic algorithm to analyze different hub heights' effect on energy output in a small onshore wind farm. The results showed that the energy output can increase by using wind turbines with various hub heights when the total number of wind turbines is same. Chowdhury, Zhang, Messac, and Castillo (2013) developed an optimization for the commercial-scale wind fields to decide the type and the position of wind turbine to install. The Particle Swarm Optimization algorithm was used. From their results, the capacity factor of wind farm increased to a noteworthy 6.4% when optimizing the position and the type of wind turbine simultaneously. K. Chen, Song, and Zhang (2014) firstly conducted the research on wind turbine height matching problem in wind farm layout optimization. The greedy algorithm was used and the optimal objective was to find the maximum Turbine-Site Matching Index, including cost and production of the wind field. The presented iteration method was then validated through both numerical cases of both flat terrain and complex terrain. Then they continued the study of the multiple wind turbine height optimization with the greedy algorithm (K. Chen, Song, Zhang, & Wang, 2016). A 3-D greedy algorithm was built to optimize the wind farm with various wind turbine hub heights and reduce the cost of energy. The layout of wind farm with different hub heights increased the total energy output and reduced the cost of energy compared to that with identical hub heights, especially for the wind field in the complex terrain. J. Lee, Kim, and Lee (2015) proposed a hub height optimization method with the objective of Annual Net Profit, which provided the economic feasibility of wind turbines. The optimal hub height reduced with the increase of the wind shear exponent and the mean wind speed. Of all wind turbine power characteristics, the optimal wind turbine hub height were mostly affected by the rated speed and the cut-out speed. Feng and Shen (2017) investigated the nonuniform offshore wind farms layout design with both different types of wind turbines and wind turbine hub heights. They built a random search algorithm and it was

validated though the Horns Rev 1 offshore wind farm. The difference between the optimal nonuniform designs and their uniform counterparts was that the nonuniform one achieved a better economical performance, as per MW of the smaller size turbine needs less investment. Vasel-Be-Hagh and Archer (2017) assessed the effect of only one optimal variable, the wind turbine hub height, on the Annual Energy Production of a wind field. Three cases were discussed and then the findings were validated by the large eddy simulations. M. Song, Chen, and Wang (2018) investigated the wind turbine layout optimization of different hub heights on flat terrain with the Gaussian Particle Swarm Optimization. All wind turbine positions and the wind turbine hub heights were optimized simultaneously. Then they drew the conclusion that their method can produce optimum solutions with relatively high energy output and low cost per unit product in most circumstances, which is more obvious in some complicated situations.

From these studies, the investigation on nonuniform wind farm optimization is developing but still not comprehensive at present stage.

2.5 Summary of previous research and research gap

2.5.1 Summary of previous research

Wind energy has developed for several decades, and the wake-related problems have been widely studied as well. In operating wind farms, wakes cause severe wind speed deficits and turbulences to the downwind wind turbines. Economical losses not only come from the wind energy loss but also the damage to the structures of turbines. So far, the wake effect is still too complicated to unveil its characteristics. More investigations should be carried out on the wake effect and the related issues.

Various analytical and numerical wake models have been presented for optimizing the layout of wind farm and studying the characteristics of wakes in depth. Analytical models are regarded as tools that can meet the demands of acceptable computation cost and the relatively high accuracy. Most analytical wake models are 1-D and 2-D models, which can be applied to design wind farms, but excludes the problems in the vertical direction. On the other hand, numerical wake models have been developed to have high prediction precisions.

Besides wake models, some experimental studies have also been conducted to unveil the characteristics of the wake effect. Study on wind field measurement has lasted for more than 35 years. Typical measurements about wake effect based on onshore wind farm, offshore wind farm and isolated wake turbine have studied. For onshore wind farm measurements, experiments were conducted on both flat and complex terrains. From offshore wind farm measurements, sodar was proved to be useful when it was operated from floating platforms for monitoring wind. Several wake models were studied, however, it was not easy to compare the measurements and models accurately. Some models tended to predict low or high wake, but the trends were not absolutely consistent. For the isolated wind turbine experiments, the methods of measurements are various. In several experiments, measuring equipment were installed on the mount of a wind turbine's nacelle. The validations of wake models are the main purposes of some experiments, which are also demonstrated. Those experimental studies are significant for comprehending the development process and research status of the full-scale wind field measurement.

Research on nonuniform wind farm optimization problems was still limited. Among the existing research, most of them (K. Chen et al., 2014; K. Chen et al., 2016; Y. Chen et al., 2013; Herbert-Acero et al., 2009; J. Lee et al., 2015; M. Song et al., 2018; Vasel-Be-Hagh & Archer,

2017) just considered the hub height as the variable, and only two (Chowdhury et al., 2013; Feng & Shen, 2017) adopt different types of wind turbines. To be specific, K. Chen et al. (2016); Y. Chen et al. (2013); Herbert-Acero et al. (2009); Vasel-Be-Hagh and Archer (2017) involved two alternative hub heights. K. Chen et al. (2014); J. Lee et al. (2015); M. Song et al. (2018) considered a series of hub heights within the designated height arrangement. As for the multiple wind turbines studies, Feng and Shen (2017) involved three different types of wind turbines, of which each type of wind turbine has a hub height; whereas Chowdhury et al. (2013) studied three types of wind turbines but with five hub heights.

When designing a wind farm, a spacing restriction must be set to minimize the wake effect and the turbines' interaction effect. The most common methods are the wind farm grid method and the Omnidirectional Restriction. These two methods actually both excessively restrain the crosswind intervals between wind turbines, because the wake develops in downwind direction and the wind turbines in crosswind direction are hardly influenced by the wake effect. Thus, if these methods are adopted, huge space will be wasted, especially where the directions of prevailing wind are strongly centralized.

2.5.2 Research gap

Although wind energy is being widely used and research work has been carried out on the wake effect and layout optimization problems, almost no previous efforts can be identified about analytical wake models involving the variation of wind speed in the vertical direction. As for onshore wind farm experimental studies, little previous studies have focused on complex-terrain wind field measurements. Furthermore, little studies on nonuniform wind farm optimization issues can be found in open literatures. The literature review presented in this chapter has

demonstrated that although there have been significant research interests and efforts to study the wake-related issues, there are still a number of areas where further in-depth research works are required to focus on, which summarized as follows.

(1) Considering the analytical wake models, the 2-D wake models are not sufficiently complete and cannot well support further investigation of the nonuniform wind farm problems. In addition, the trend of power upsizing of single wind turbines dramatically increases the hub height and the rotor diameter, the height distance and the wind speed difference in the swept area also increase correspondingly. The 2-D wake models' uniform wind assumption in the vertical direction ignores these differences, which causes huge errors when estimating the energy output and is no longer applicable. As a result, 2-D wake models cannot provide comprehensive and complicated spatial wind farm optimization anymore. The further development of an analytical wake model from 2-D to 3-D is significant and necessary.

(2) The experiments on complex-terrian wind farms are still insufficient. Significant progress has proved that it is complicated to extract robust and quantitative metrics of wake characteristics like length scale and velocity deficit. In complex terrains, the issues of wake characterization are further enlarged. It is a challenge to describe the freestream with complex waves, turnings, and recirculation zones. The wake behavior also has a close relation to the flow as well as the terrain slope. Therefore, more typical wind farm experiments should be conducted to study the wake characteristics and validate the advanced 3-D wake models.

(3) For offshore wind farm development, although the repowering strategy has been presented,

only the aligned layout of wind farm is considered. If the repowering optimization is considered, variables like positions and heights of wind turbines are involved, the LCoE could continue decreasing. Therefore, a more comprehensive offshore wind farm layout optimization process with the repowering strategy is needed.

(4) With the experience in wind industry is accumulated, it is a trend to develop the nonuniform wind farm, which involves multiple types of wind turbines. So far, few studies have been conducted on how to set restrictions among various types of wind turbines. One rough way is to make sure that the distance between two wind turbines is at least five times of the larger wind turbine's rotor diameter, which is just an extension of the Omnidirectional Restriction. Therefore, some more studies should be conducted to make good use of the space in wind farms, and a new feasible spacing restriction that considers the influence of wind direction is needed. With the new restriction, the wind farm optimization process can be further improved.

Chapter 3

Development of a New Three-Dimensional Wake Model for Single Wind Turbine

To help handle wind farm optimization problems, a new original analytical 3-D wind turbine wake model has been developed and validated. Compared with existing analytical wake models, the presented wake model also considers the wind variation in the height direction, which is more accurate and closer to reality. The wake model is based on the flow flux conservation law, and it assumes that the wind deficit downstream of a wind turbine is Gaussian-shaped. The wake model is validated by published wind tunnel measurement data at both horizontal and vertical sections. Based on the wake model, a series of prediction results from multiple views and at different positions are demonstrated. From the predictions, the 3-D wake model is effective in describing the spatial distribution of wind velocity. It makes a theoretical contribution to the single wake study, and it is also meaningful to the further study of multiple wakes.

3.1 Derivation of the three-dimensional wake model

3.1.1 Introduction of the three-dimensional wake model

Figure 3.1 shows the schematic diagrams of 1-D and 2-D wake models. In the 1-D wake model, the incoming wind is assumed to be evenly distributed and the downwind wind velocity $U(x)$ is only relative to the downstream distance x. In the 2-D wake model, the incoming wind is also assumed to be evenly distributed, whereas the wind deficit is assumed to be Gaussian-shaped. The actual wind velocity $U(x,r)$ in the 2-D wake model is relative to the downstream distance x and the radial distance to the centerline r. However, as matter of fact, the

downstream wind distribution is complicated and absolutely beyond the 2-D distribution.

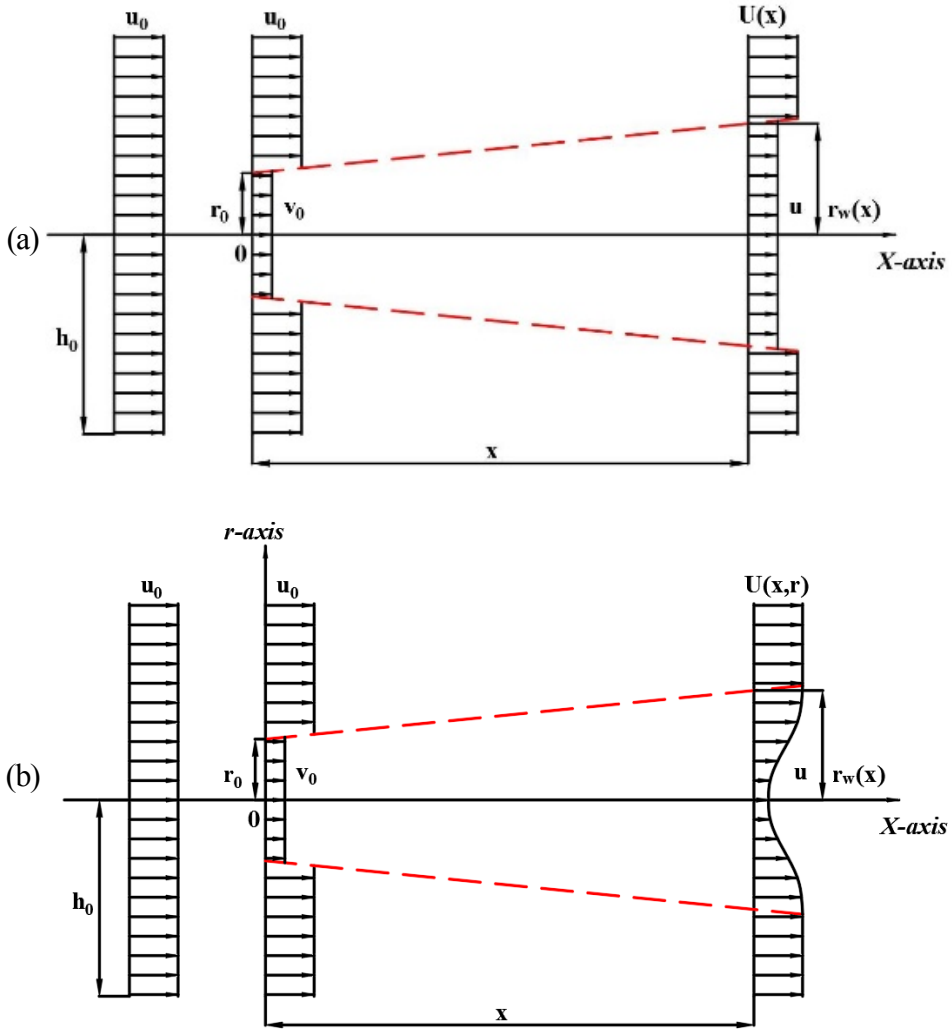

Figure 3.1 Schematic diagrams of analytical wake models: (a) 1-D wake model; and (b) 2-D wake model

Figure 3.2 demonstrates a schematic diagram of the proposed 3-D wake model. In this 3-D wake model, the wake-influenced radius $r_w(x)$ varies along the downstream distance x; the wind deficit is Gaussian-distributed in the 3-D space rather than linearly distributed. Most importantly, this 3-D wake model assumes that the incoming wind distribution $U_0(z)$ varies along the height direction, and the variation is accounted for from the beginning of the derivation process.

Therefore, the wind velocity $U(x, y, z)$ is relative to the X, Y, and Z directions. The X axis and Z axis are shown in Figure 3.2, where the Y axis is perpendicular to the paper and points into it.

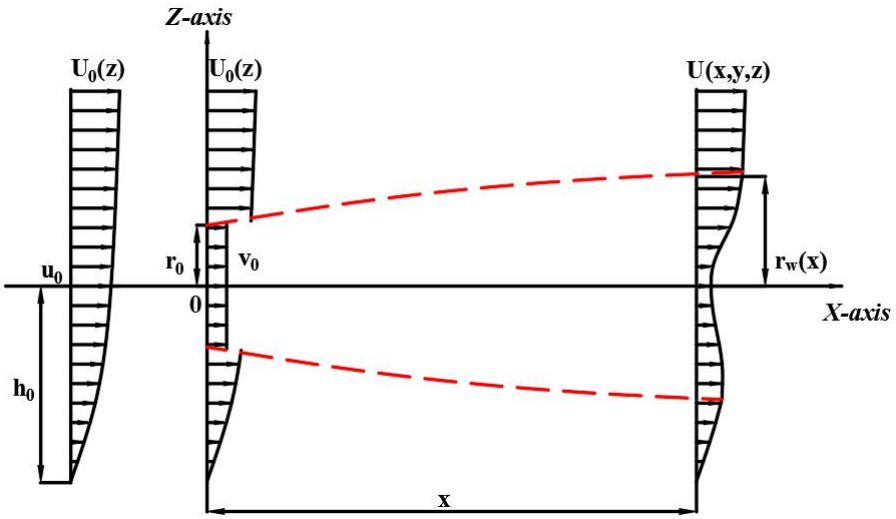

Figure 3.2 Schematic diagram of the 3-D wake model

The assumption of the 3-D wake model is closer to reality and has not been adopted in any other analytical wake model. With the proposed 3-D wake model, it is easy to obtain the wind velocity $U(x, y, z)$ of any spatial position downstream of a wind turbine.

3.1.2 Assumptions of the three-dimensional wake model

There are three basic assumptions of the newly presented 3-D wake model.

The first assumption is that the wind velocity deficit at downstream distance x is Gaussian-distributed, which is expressed as $A(x)(\frac{1}{2\pi\sigma(x)^2}e^{-\frac{y^2+(z-h_0)^2}{2\sigma(x)^2}})+B(x)$. The incoming wind speed distribution is expressed by $U_0(z)$. Consequently, the actual wind velocity

$U(x, y, z)$ at the downstream position can be described by equation (3.1).

$$U(x, y, z) = A(x)\left(\frac{1}{2\pi\sigma(x)^2} e^{-\frac{y^2+(z-h_0)^2}{2\sigma(x)^2}}\right) + B(x) + U_0(z) \tag{3.1}$$

In the equation, h_0 is the wind turbine hub height. $A(x)$, $B(x)$ and $\sigma(x)$ are three important parameters that decide the Gaussian shape of the wind deficit. To simplify the calculation, $\sigma(x)$ is defined as $\sigma(x) = \frac{r_w(x)}{C}$, in which C is a constant and is to be determined according to the real operating conditions. In the 3-D wake model, $A(x)$ and $B(x)$ vary along the downstream distance and their derivation processes will be introduced in the following study.

The second assumption is based on the momentum conservation theory, which refers to the Jensen wake model (N. O. Jensen, 1983), and it means that the flow flux is conservative in a specific area at any wake section.

A circular area with radius $r_w(x)$ is chosen to calculate the total flow flux $Q(x)$. At the plane just behind the wind turbine, the total flow flux $Q(x)$ is calculated from equation (3.2). $Q(x)$ consists of two parts: one is the flow flux within the circular area of rotor radius $\pi r_0^2 v_0$ and the other one $\iint_{S_{r_w(x)}-S_{r_0}} U_0(z)ds$ is the flow flux beyond the circular area but within another circular area with radius $r_w(x)$.

$$Q(x) = \pi r_0^2 v_0 + \iint_{S_{r_w(x)} - S_{r_0}} U_0(z) ds \tag{3.2}$$

In equation (3.2), r_0 is the rotor radius of the wind turbine and v_0 is the average wind speed just behind the wind turbine. In reference (N. O. Jensen, 1983), v_0 is one third of the ambient wind velocity in accordance with classical theory. Therefore, in this study, v_0 is similarly assumed to be one third of the incoming wind speed at the hub height of the wind turbine. $S_{r_w(x)}$ is the circular area with radius $r_w(x)$, whereas S_{r_0} is the circular area with the rotor radius r_0.

At the plane downstream of the wind turbine at x distance, the total flow flux $Q(x)$ is calculated from equation (3.3), which is the integration of the wind velocity $U(x, y, z)$ at the circular area within the radius $r_w(x)$.

$$Q(x) = \iint_{S_{r_w(x)}} U(x, y, z) ds \tag{3.3}$$

Then, combining equation (3.2) and equation (3.3), the final expression of the second assumption is shown as equation (3.4).

$$\pi r_0^2 v_0 + \iint_{S_{r_w(x)} - S_{r_0}} U_0(z) ds = \iint_{S_{r_w(x)}} U(x, y, z) ds \tag{3.4}$$

The third assumption is that the wind velocity is continuous at the wake boundary. Therefore, this assumption can be expressed by equation (3.5).

$$\frac{A(x)}{2\pi\sigma(x)^2} e^{-\frac{y^2+(z-h_0)^2}{2\sigma(x)^2}} + B(x) + U_0(z) = U_0(z), \quad where \;\; y^2 + (z-h_0)^2 = r_w(x)^2 \qquad (3.5)$$

3.1.3 Wind speed variation

Wind speed changes with height and the height of an anemometer is variable at different sites. It is necessary to know the wind speed at wind turbine hub height (Ilinca, McCarthy, Chaumel, & Rétiveau, 2003; Johnson, 1985). In this study, the height of anemometer and different wind turbines' hub heights are also taken into account.

The wind power law is recognized as a useful tool to describe the wind speed variation with height (Peterson & Hennessey Jr, 1978):

$$v = v_0 \cdot \left(\frac{z}{z_r} \right)^{\alpha} \qquad (3.6)$$

where v is the wind speed at hub height z in m/s; v_0 is the wind speed measured at the reference height z_r and the parameter α is the wind speed power law coefficient shown in Table 3.1.

Table 3.1 Power exponent and gradient height for wind (Lu, Yang, & Burnett, 2002)

Terrain type	α	δ (m)
Lake, ocean and smooth hard ground	0.10	200
Open terrain with few obstacles (e.g. open grassland, shores, desert)	0.16	250
Terrain uniformly covered with obstacles 10 ~ 20 m (e.g. residential suburbs, woodland)	0.28	400
Terrain with large irregular objects (e.g. city centre, very broken country)	0.40	500

For the wind blows over a consideration distance of terrain from smooth to rough, the following equations can describe the variation. The gradient wind velocity, V_g , remains unchanged :

$$V_1 = V_g \cdot \left(\frac{z_1}{\delta_1} \right)^{\alpha_1}, \qquad V_2 = V_g \cdot \left(\frac{z_2}{\delta_2} \right)^{\alpha_2} \tag{3.7}$$

Consequently, the following equation can be obtained:

$$\frac{V_2}{V_1} = \left(\frac{z_2}{\delta_2} \right)^{\alpha_2} \cdot \left(\frac{\delta_1}{z_1} \right)^{\alpha_1} \tag{3.8}$$

In this study, the incoming wind speed distribution $U_0(z)$ is expressed by equation (3.9). u_0 is the wind speed measured at the height of z_r .

$$U_0(z) = u_0 \cdot \left(\frac{z}{z_r} \right)^{\alpha} \tag{3.9}$$

3.1.4 Derivation process

The first step is to calculate the flow flux $Q(x)$ behind the wind turbine according to a series of equations (3.10).

$$\begin{cases} Q(x) = \pi r_0^{\,2} v_0 + \iint\limits_{S_{r_w(x)} - S_{r_0}} U_0(z) ds \\ v_0 = (1 - 2a) u_0 \\ U_0(z) = u_0 \left(\frac{z}{z_r} \right)^{\alpha} \\ r_w(x) = r_0 + k_{wake} \cdot x \end{cases} \tag{3.10}$$

In the above equations, a is the axial induction factor and k_{wake} is the wake decay constant, which can be estimated according to equation (3.11).

$$k_{wake} = k_0 \frac{I_{wake}}{I_0} \tag{3.11}$$

The term k_0 is the rate of the wake expansion, which is recommended to be 0.075 for onshore wind turbines (Barthelmie et al., 2006) and 0.04 or 0.05 for offshore wind turbines (Barthelmie et al., 2007); I_0 is the incoming free-stream turbulence intensity and I_{wake} is calculated according to equations (3.12) and (3.13) (Crespo & Herna, 1996).

$$I_{wake} = \sqrt{I_0{}^2 + I_+{}^2} \tag{3.12}$$

$$I_+ = 0.73a^{0.8325} I_0{}^{0.0325} \left(x/D\right)^{-0.32} \tag{3.13}$$

The next step is to solve $A(x)$ and $B(x)$ based on another series of equations (3.14).

$$\begin{cases} \dfrac{A(x)}{2\pi\sigma(x)^2} e^{-\frac{y^2+(z-h_0)^2}{2\sigma(x)^2}} + B(x) + U_0(z) = U_0(z) \quad , where \quad y^2 + (z-h_0)^2 = r_w(x)^2 \\ Q(x) = \iint\limits_{S_{r_w(x)}} U(x,y,z)ds \\ U(x,y,z) = A(x)\left(\dfrac{1}{2\pi\sigma(x)^2} e^{-\frac{y^2+(z-h_0)^2}{2\sigma(x)^2}}\right) + B(x) + U_0(z) \\ \sigma(x) = \dfrac{r_w(x)}{C} \end{cases} \tag{3.14}$$

Put $Q(x)$, solved from equation (3.7), into (3.11); then only $A(x)$, $B(x)$, and C are unknown. Finally, $A(x)$ and $B(x)$ can be expressed by constant C as equation (3.15).

$$\begin{cases} A(x) = \dfrac{Q(x) - \int_{h_0 - r_w(x)}^{h_0 + r_w(x)} 2\sqrt{r_w(x)^2 - (z-h_0)^2} \cdot U_0(z)dz}{\left(1 - e^{-\frac{C^2}{2}} - \dfrac{C^2}{2} \cdot e^{-\frac{C^2}{2}}\right)} \\ B(x) = -\dfrac{A(x) \cdot C^2}{2\pi r_w(x)^2} \cdot e^{-\frac{C^2}{2}} \end{cases} \tag{3.15}$$

C is an empirical parameter that will influence the wind deficit in the wake. In the 2-D Jensen–Gaussian wake model (Gao et al., 2016), C is suggested to be 6.6564 in one case. However, wind deficit is actually affected by many factors, such as the blade shape, the incoming wind

speed, and the turbulence intensity. Therefore, in this study, it is recommended that C be set to different values according to the operating conditions.

In addition, in equation (3.9), $U_0(z) = u_0 \cdot \left(\frac{z}{z_r} \right)^{\alpha}$ is just one of the expressions of the incoming wind distribution. In the 3-D wake model, some other expressions of $U_0(z)$ can also be applied.

3.2 Validation of the three-dimensional wake model

To validate the proposed 3-D wake model, published wind tunnel measurement data are cited in this study to test the accuracy of the model. Both the horizontal and the vertical wake profile validations show the good effectiveness of the proposed 3-D wake model.

3.2.1 Validation with the horizontal wake profile

3.2.1.1 Wind tunnel measurement data

The adopted horizontal wake profiles were published by the reference (Schlez et al., 2003). In 1989, Hassan made an intensive analysis of wind turbine wake at the Marchwood Engineering Laboratory's atmospheric boundary-layer wind tunnel. The analysis used 1/160th-scale horizontal axis wind turbines, which had realistic performance properties and sophisticated data logging components. This analysis process generated comprehensive data on the turbulent and mean flow downstream of single and multiple wind turbines. The model site was flat with artificial surface roughness. The artificial surface roughness in the wind tunnel was uniform and the roughness length was 0.075 m.

As for the wind turbines, the rotor diameter of the models was 0.27 m; the corresponding full-

scale rotor diameter was 43.2 m. The assumed wind turbine hub height was 50 m, where the free wind speed was 5.3 m/s. The model turbines were operated at three ratios of tip speed. In this validation, the model tip speed ratio was chosen as 2.9, with a 6.78 rpm rotor speed. Corresponding to this operating condition, the constant C in the 3-D wake model was set as $C = 1.98$.

3.2.1.2 Result comparisons

Figure 3.3 shows the horizontal wake profile comparisons of the 3-D wake model and the wind tunnel measured data. Figure 3.3(a) is at a 5D downstream distance and Figure 3.3(b) is at a 10D downstream distance. In the figures, the blue lines represent the prediction results from the 3-D wake model; the red dots represent the wind tunnel measured data. The horizontal axis is the dimensionless ratio of y distance and rotor diameter D. The vertical axis is the ratio of wind velocity $U(x, y, z)$ and the incoming wind speed at wind turbine hub height u_0.

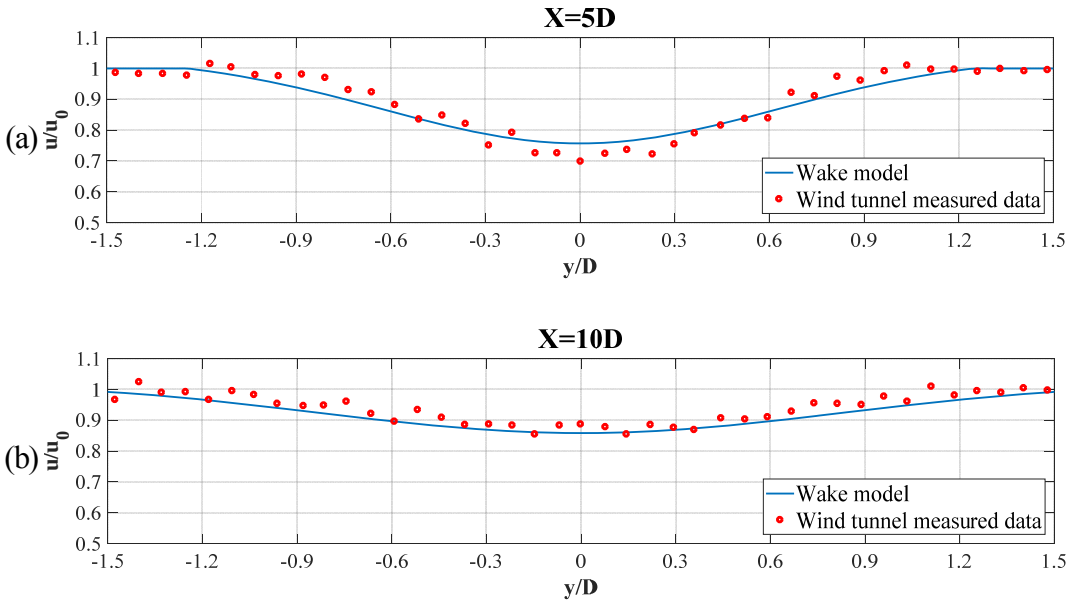

Figure 3.3 Horizontal results comparisons of the measurement data and 3-D wake model-predicted wind velocity at specific downstream distances: (a) x = 5D and (b) x = 10D

From the wake profiles, the presented 3-D wake model apparently predicts the wind velocity well in the horizontal direction at the given wind turbine hub height. At the 5D downstream distance, the wind velocity predicted by the 3-D wake model is greater than that measured at the centerline around but lower than that measured at the y / D ratio range of ± (0.5 ~ 1). At the 10D downstream distance, the 3-D wake model predicts greater wind velocities at most measured positions, but the errors are much smaller. Generally, the 3-D wake model is more accurate at the 10D downstream distance.

The specific relative errors of the comparison results are also analyzed. A total of 41 points are compared according to the wind tunnel experiments. Figure 3.4 shows the error analysis of the comparison results at the 5D and 10D downstream distances.

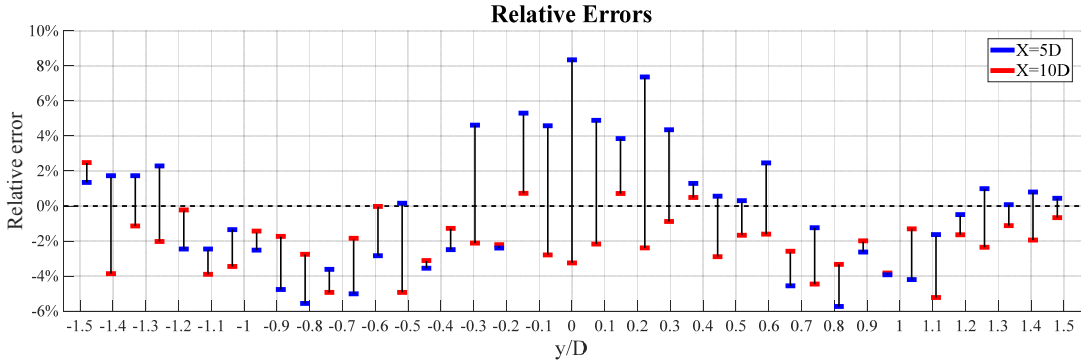

Figure 3.4 Relative errors of horizontal profiles

From the error analysis, the results predicted by the 3-D wake model agree well with the measurement data. The largest error is 8.35% in the 5D downstream distance. Only two errors are beyond ±6%, and other errors are mostly within ±5%. Some large errors are centralized within the ±0.3D area, which shows that the 3-D wake model seems to be somewhat inaccurate in the center wake-influenced area. The reason may be that huge turbulence intensity appears in

the center area, and the 3-D wake model as a simple analytical wake model cannot predict the turbulence well. By contrast, the errors at the 5D distance are larger than those at the 10D distance. The wake model predictions are more accurate at far downstream distance areas. It should also be noted that apart from the center area, most errors are negative, which indicates that the 3-D wake model is likely to predict wind velocities lower than the reality at distances far from the center area. In addition, theoretically, the wind velocity at the lateral areas that are not under the wake effect should be the same as the incoming wind velocity, namely, the same as the wake model predictions. However, some unstable errors appear in the lateral area, which implies that errors may exist in the measurement data and that the experimental errors may also influence the verification of the wake model.

3.2.2 Validation with the vertical wake profile

3.2.2.1 Wind tunnel measurement data

The adopted vertical wake profile data were published by reference (Y.-T. Wu & Porté-Agel, 2011). The test was conducted in the atmospheric boundary-layer wind tunnel at St. Anthony Falls Laboratory. The high-resolution measurement data of the wind distribution downstream a miniature wind turbine were collected by hot-wire anemometry.

In the experiment, a three-blade GWS/EP-6030×3 rotor was fixed on the wind turbine model and linked with a small DC generator motor. The rotor diameter was 0.150 m and the hub height was 0.125 m. The motor was cylindrically shaped, with a length l_m = 0.03 m and a diameter d_m = 0.015 m. The turbine tower was also cylindrically shaped, with a length l_m = 0.118 m and a diameter d_m = 0.005 m. The boundary-layer flow was characterized by a freestream speed of 2.8 m/s and the boundary-layer depth was 0.46 m. The size of the wind tunnel was 16×1.7×1.7 m, and the boundary layer was built at the end of the wind tunnel section in the downwind direction.

The incoming velocity at the hub height of the miniature wind turbine was 2.2 m/s and the wind speed power law parameter α was 0.15. Corresponding to this operating condition, in this validation, the constant C in the 3-D wake model was set as $C = 5.15$.

3.2.2.2 Result comparisons

Figure 3.5 shows the vertical wake profile comparisons of the wake model predictions and the wind tunnel measured data at various downwind distances. The wake profiles are in the wind turbine section, which is also the y = 0 section. Figure 3.5(a) shows the incoming wind distribution; (b) is at the x = 5D downstream distance; (c) is at the x = 7D downstream distance; (d) is at the x = 10D downstream distance; (e) is at the x = 14D downstream distance, and (f) is at the x = 20D downstream distance. In the figure, the horizontal axis is the wind velocity $U(x, y, z)$ and the vertical axis is the dimensionless ratio of z distance and wind turbine rotor diameter D.

(a)

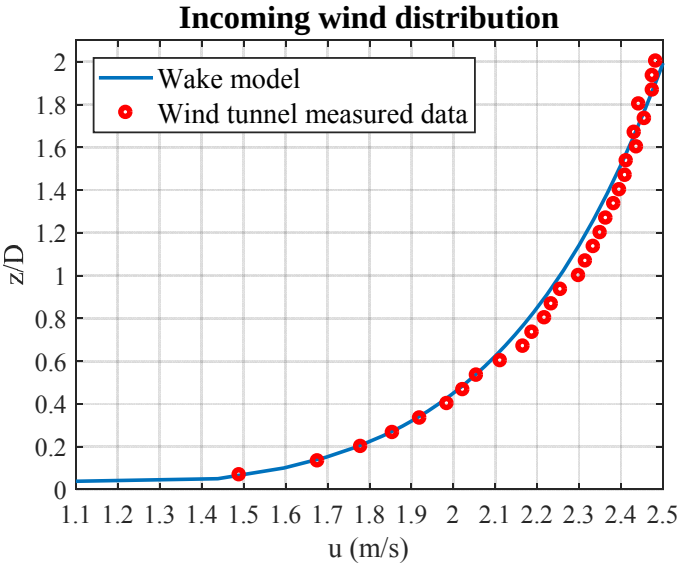

(b)

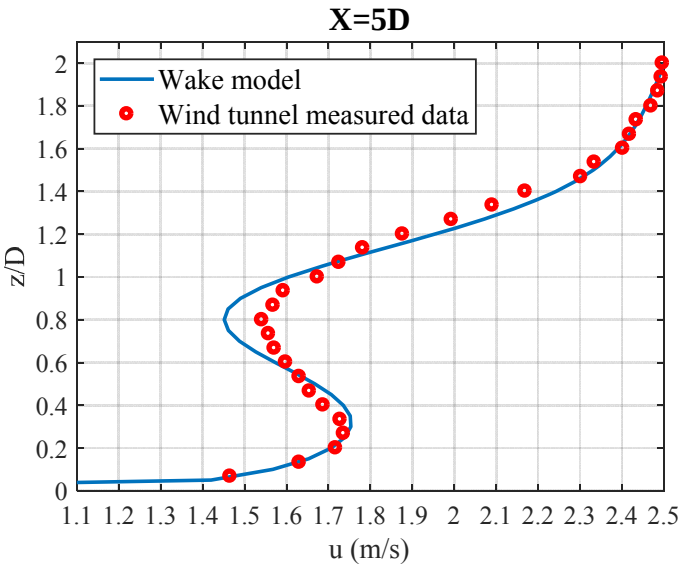
X=5D
Wake model
Wind tunnel measured data
z/D
u (m/s)

(c)

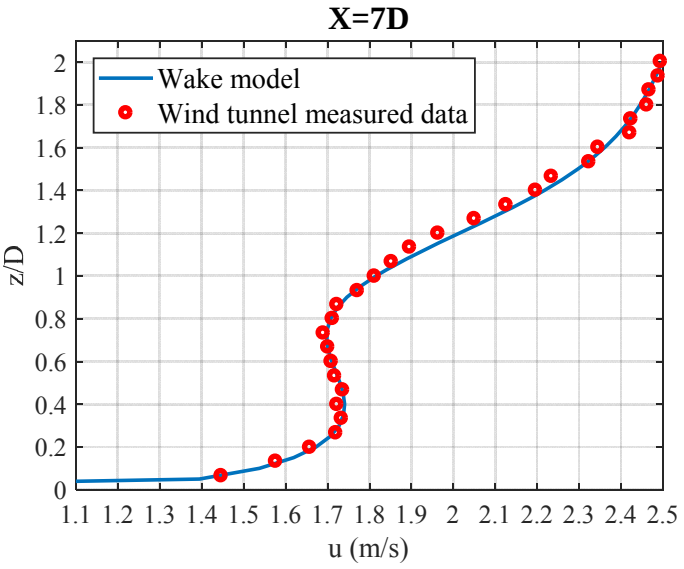
X=7D
Wake model
Wind tunnel measured data
z/D
u (m/s)

(d)

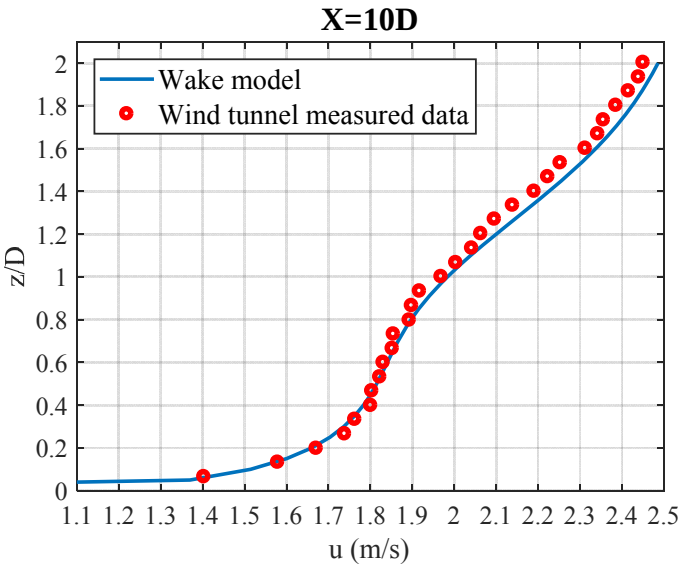
X=10D
Wake model
Wind tunnel measured data
z/D
u (m/s)

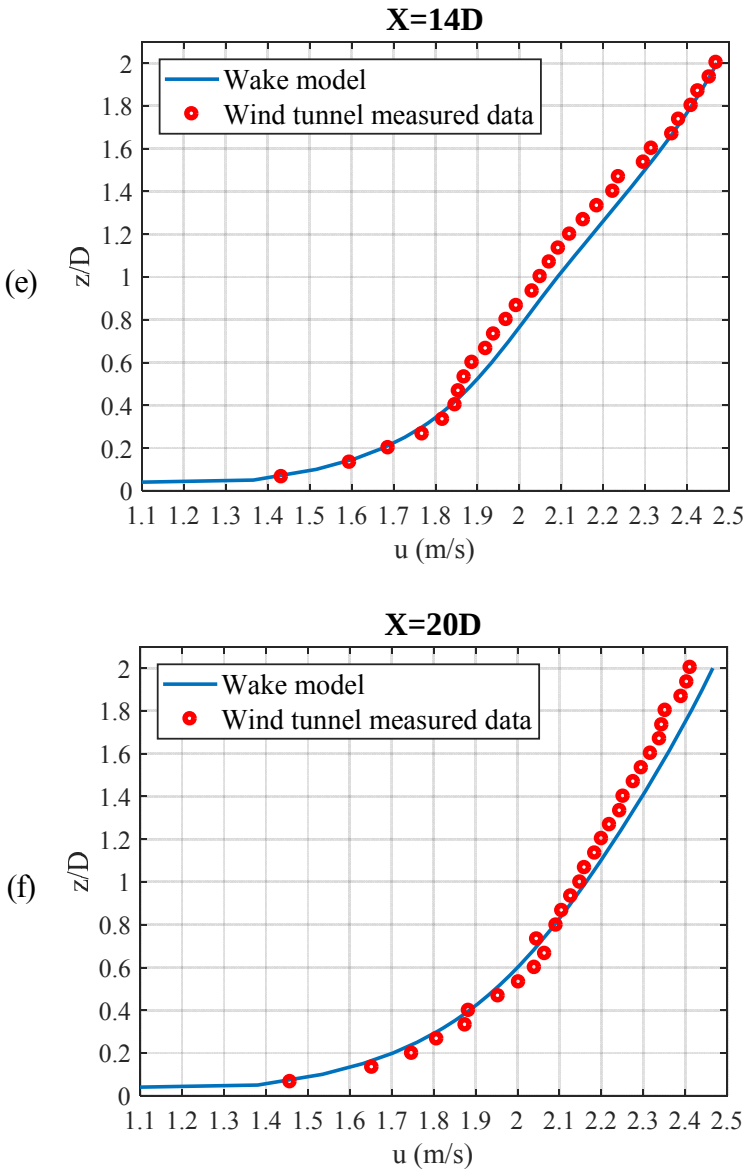

Figure 3.5 Vertical result comparisons of the measurement data and the predicted wind velocity by the 3-D wake model at specific downstream distances: (a) incoming wind distribution; (b) $x = 5D$; (c) $x = 7D$; (d) $x = 10D$; (e) $x = 14D$ and (f) $x = 20D$

From the vertical wake profiles, it is obvious that the proposed 3-D wake model can also predict the wake distribution well in the vertical direction at the wind turbine section. For the incoming wind, the wake model slightly underestimates the wind velocity in the mid-height positions. The predicted wind speeds agree well in all downstream distance positions, especially at the low

height position under a 0.4 z/D ratio. At the 5D downstream distance, the wake model underestimates the wind velocity at around the wind hub height position, where the largest error seems to lie. In most other situations, the wake model slightly overestimates the wind velocity. The specific error analysis of the vertical wind profile comparison results is shown in Figure 3.6, in which 30 measurement points are compared.

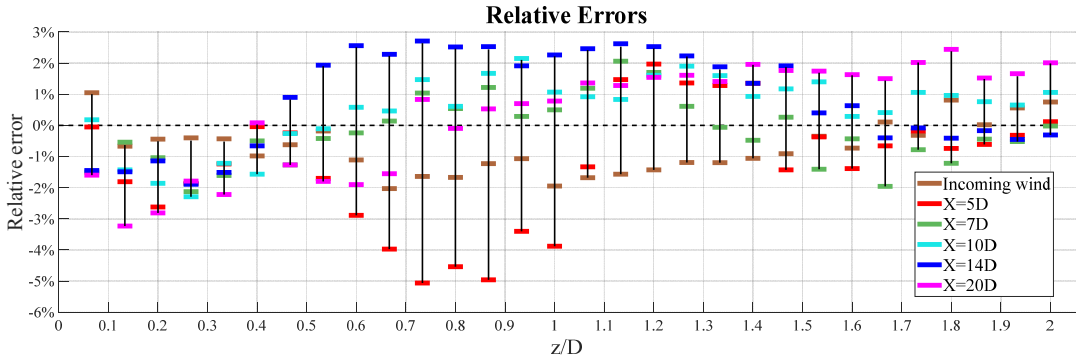

Figure 3.6 Relative errors of vertical profiles

The error analysis further verifies the effectiveness of the proposed 3-D wake model. From the results, the largest error is 5.06% at the x = 5D downstream distance and only five errors are larger than 4%, also at the x = 5D downstream distance, whereas most errors are within ±3%. The predictions at positions near the hub height area tend to have large errors, which is similar to the results of the horizontal analysis, and the rough estimation of the turbulence may be responsible for this finding. It is noteworthy that the wake model tends to underestimate the wind velocity for the incoming wind and the small downstream distance of 5D in this study, but it tended to overestimate it at most other downstream positions. Attention should be paid to this problem when applying the 3-D wake model, and further study should be concentrated on it. Where the incoming wind is totally free from the wake effect, the wake model tends to underestimate the wind velocity, although the largest error is just 2.03%. A more accurate incoming wind speed formula would perform better and should be adopted if necessary.

Because the selected measurement data are from wind tunnel tests, some experimental errors may have affected the results. In Figure 3.3, the measurement data are not symmetrical around the centerline; in Figure 3.5, the wind distributions in the high positions of different downstream distances, where the wind is not under wake's effect, are not quite coincident theoretically. These errors may be caused by some experimental factors, and they have an effect on the validation of the wake model. However, the overall results show that good consistency remains between the 3-D wake model and the wind tunnel measurement data from both the horizontal and vertical wind profiles. Therefore, it is reliable to apply the proposed 3-D wake model to predict any downwind spatial position's wind velocity. In contrast, more comprehensive and accurate wind field tests are necessary to further check the effectiveness of this wake model.

3.3 Predictions of the three-dimensional wake model

Application of the 3-D wake model to predict the wind velocity of a specific point (x, y, z) includes three main steps. The first is to determine the relevant parameters according to the operating conditions and the incoming wind distribution. The second is to calculate the distance from the point to the centerline r according to equation (3.13) and then to judge whether the point is under the wake effect according to the equation $r_w(x) = r_0 + k_{wake}x$. The third step is to calculate the wind velocity according to the judgment of step 2. If $r_w(x) < r$, the point is not within the wake-influenced zone and the wind velocity can be calculated simply by equation (3.6); if $r_w(x) > r$, the point is in the wake-influenced zone and the wind velocity should be calculated from the 3-D wake model as introduced in section 3.1.4.

$$r = \sqrt{y^2 + (z - h_0)^2} \tag{3.13}$$

With the validated 3-D wake model, it is more convenient to study the wake distribution and wake performance in the whole spatial view. In this chapter, a case of multiple views of a wind turbine's wake profile is demonstrated. The rotor radius r_0 is 15 m, the hub height h_0 is 50 m, the incoming wind speed at the hub height is 4 m/s, and the wind speed power law parameter is 0.1. The incoming wind is described by equation (3.6).

3.3.1 Wake profiles from the Y–Z view

Figure 3.7 shows the Y–Z view of the wind profile: (a) is the incoming wind distribution; (b) is at the x = 2.5D downstream distance; (c) is at the x = 5D downstream distance; (d) is at the x = 10D downstream distance; (e) is at the x = 15D downstream distance, and (f) is at the x = 20D downstream distance. The horizontal axis represents the y distance, which ranges from 0 m to 150 m. The vertical axis represents the height, which ranges from 0 m to 120 m. The wind velocity is represented by different colors, which refer to the color bar to the right of each figure.

(a)

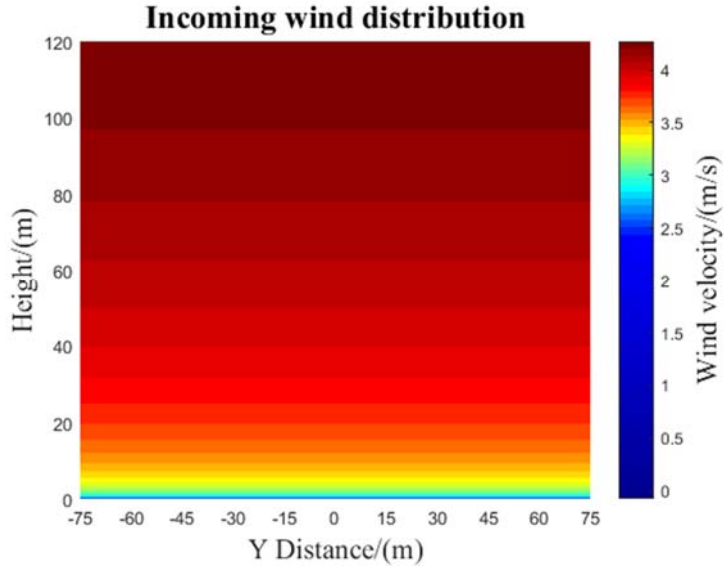

(b)

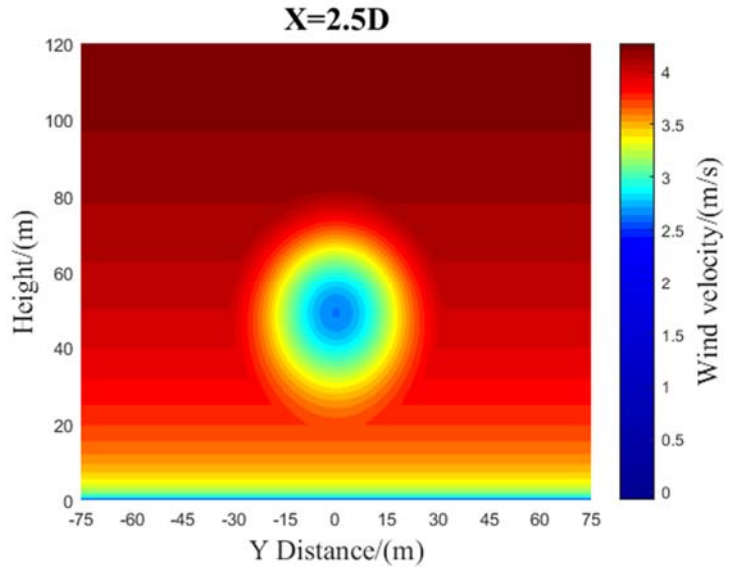
X=2.5D
Height/(m)
Y Distance/(m)
Wind velocity/(m/s)

(c)

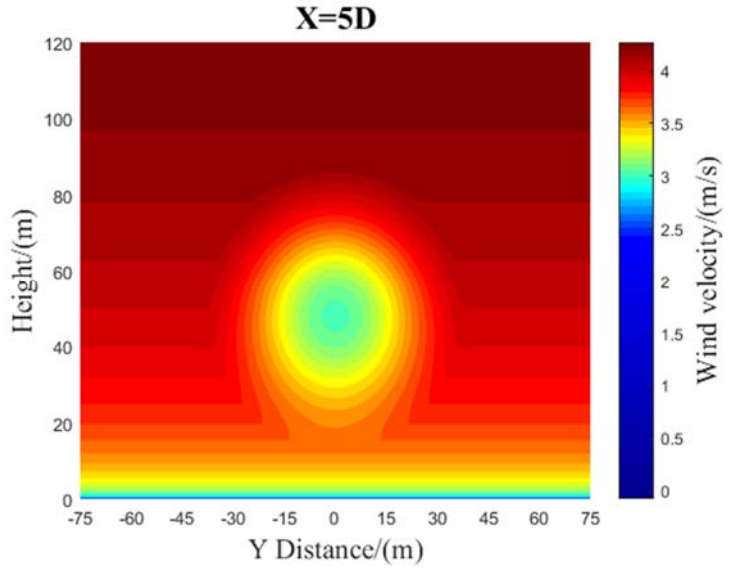
X=5D
Height/(m)
Y Distance/(m)
Wind velocity/(m/s)

(d)

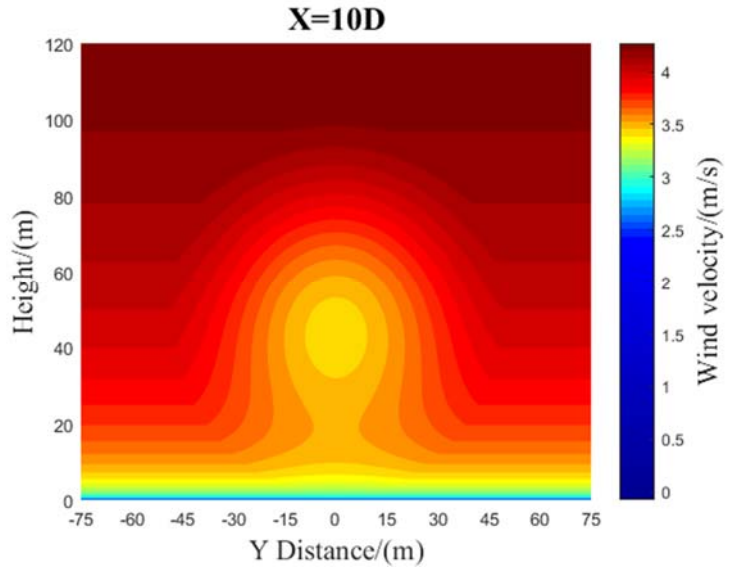
X=10D
Height/(m)
Y Distance/(m)
Wind velocity/(m/s)

(e)

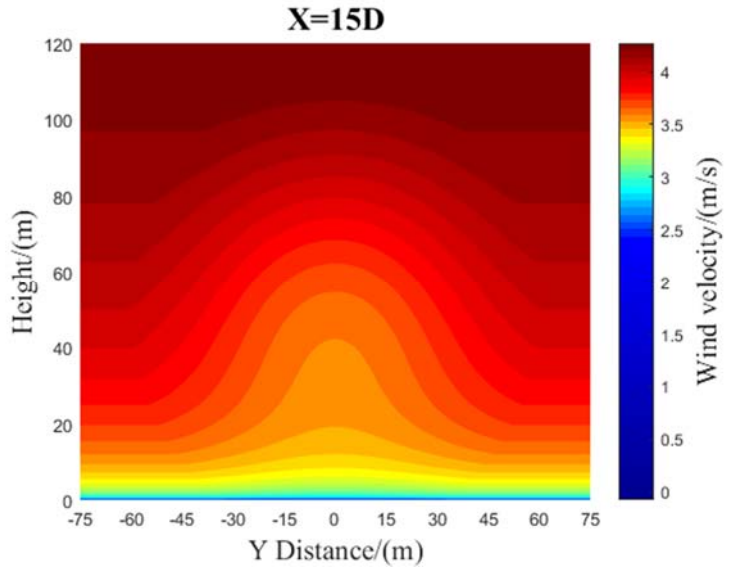

(f)

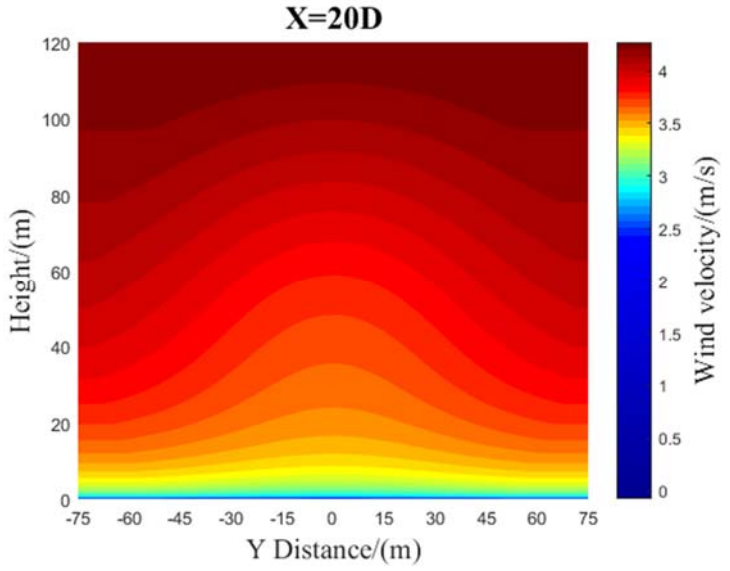

Figure 3.7 Y–Z views of the wind profile at different positions: (a) incoming wind distribution; (b) $x = 2.5D$; (c) $x = 5D$; (d) $x = 10D$; (e) $x = 15D$ and (f) $x = 20D$

From the results, the wake-influenced area expands with the increase of the downstream distance at the same time the wind deficit phenomenon is weakened. This can be explained by the flow flux conservation law. However, it is clear that the wind deficit is not uniformly distributed in any part of the wake-influenced area. In contrast, with expansion of the wake circle, the wake distribution along the height cannot be ignored unconditionally. Within the 5D downstream distance, the wind speed can still be estimated by a particular simple shape, like a

Gaussian shape. However, after the 5D distance, from the figure, the wind speed distribution becomes more complicated, and it is not suitable to apply the original method. It can be seen that the downstream wind distribution is neither the simple uniform distribution predicted by the 1-D wake model nor a simple shape distribution, like a Gaussian or cosine shape, as some 2-D wake models predict. Therefore, application of the proposed 3-D wake model is necessary.

3.3.2 Wake profiles from the X–Z view

Figure 3.8 shows X–Z views of the wind profile at different positions along the Y distance: (a) is the wind turbine section; (b) is the y = 0.2D section; (c) is the y = 0.4D section; (d) is the y = 0.6D section; (e) is the y = 0.8D section, and (f) is the y = 1D section. Because the wake distribution is symmetric about the wind turbine section, half-views from one side of the symmetric section are enough to describe the wake distribution. From these X–Z view results, the wake profile is clearer and more stereoscopic.

At the wind turbine position, the wake effect is serious within 120 m, equivalent to 4D, in the X downstream distance. As the Y distance from the wind turbine position increases, the serious wake-influenced range is narrowed. Therefore, when designing a wind farm, the minimum distance between any two wind turbines should be no less than 4D. It can also be seen that the downstream wind distribution along the height direction is also influenced by the wake effect. In most wind farm layout studies, as 1-D or 2-D wake models are adopted, each wind turbine is considered to have the same incoming wind condition, which is not appropriate. Especially for large wind turbines, the wake effect is more serious and the wake-influenced range is even wider. Considering the wake effect on each wind turbine's incoming wind is of great importance. Consequently, height optimization also deserves to be included in wind farm layout considerations.

(a)

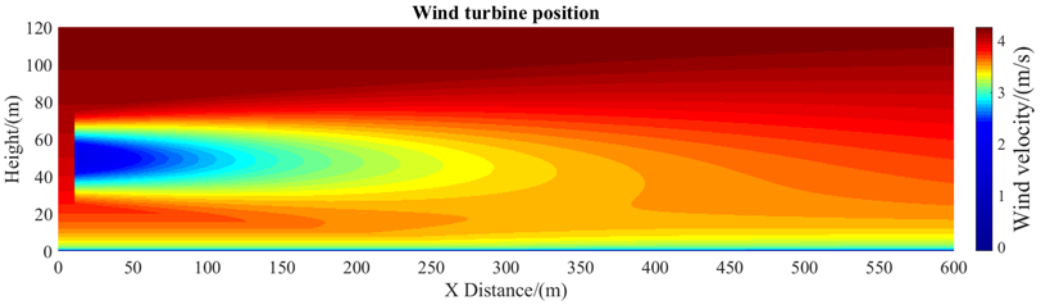
Wind turbine position
Height/(m)
X Distance/(m)
Wind velocity/(m/s)

(b)

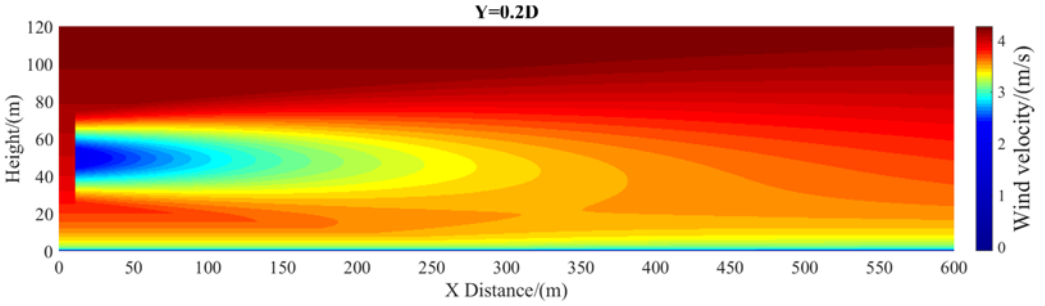
Y=0.2D
Height/(m)
X Distance/(m)
Wind velocity/(m/s)

(c)

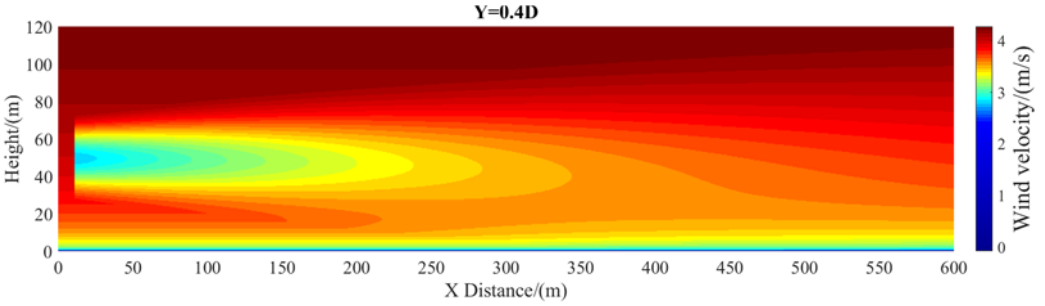
Y=0.4D
Height/(m)
X Distance/(m)
Wind velocity/(m/s)

(d)

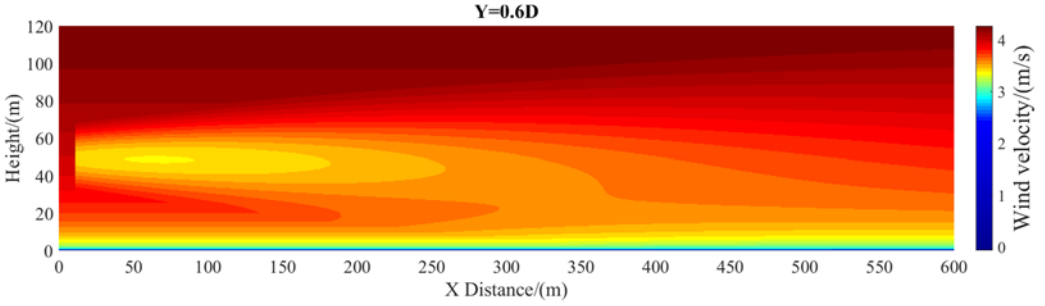
Y=0.6D
Height/(m)
X Distance/(m)
Wind velocity/(m/s)

(e)

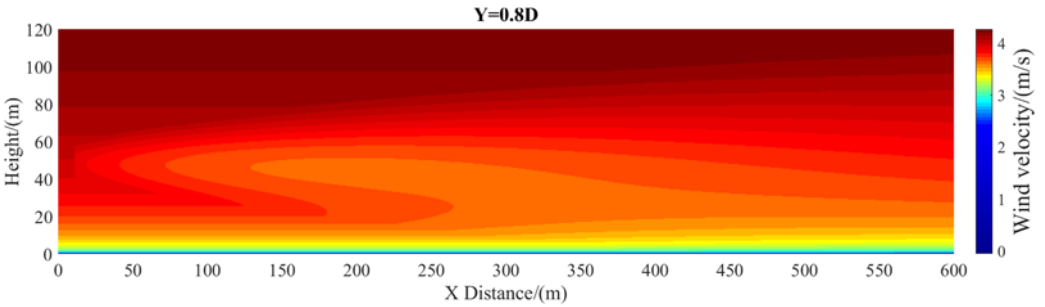
Y=0.8D
Height/(m)
X Distance/(m)
Wind velocity/(m/s)

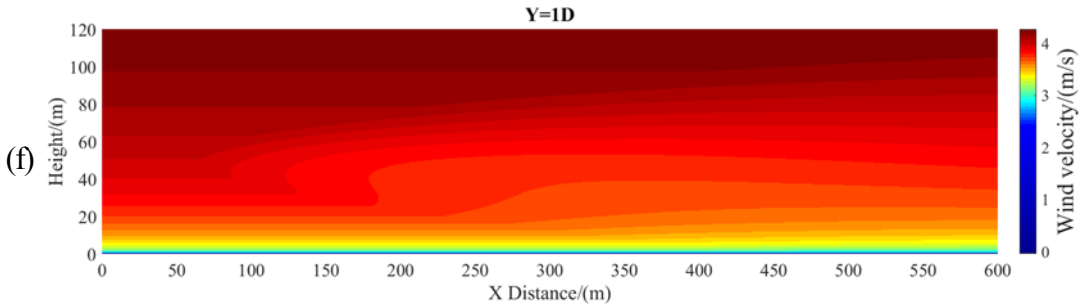

Figure 3.8 X–Z views of the wind profile at different positions: (a) wind turbine position; (b) y = 0.2D; (c) y = 0.4D; (d) y = 0.6D; (e) y = 0.8D and (f) y = 1D

It is noteworthy that the wake estimation at the space near the wind turbine and ground may be far from reality. This is because in the mentioned space, the viscosity causes huge turbulence, which is not considered in the 3-D wake model. Actually, this simplification will hardly affect the wind farm layout because the wind turbines will not be fixed that close to each other or near the ground. Not much turbulence will have a far-reaching effect on the downstream wind turbine, so it is tolerable to not include that turbulence in the consideration of wind farm energy loss problems.

3.3.3 Wake profiles from the X–Y view

Figure 3.9 shows X–Y views of the wind profile at different positions in the height direction: (a) in the Height = h_0 + 1D section; (b) in the Height = h_0 + 0.5D section; (c) in the Height = h_0 section; (d) in the Height = h_0 - 0.5D section, and (e) in the Height = h_0 – 1D section.

Because the effect that wind varies in the height direction is considered, it is clear that the wind distributions at various heights are not symmetrical to the wind turbine hub height plane. It can be inferred that each horizontal plane has a unique distribution of the wake and that both the wake boundary and the wake intensity are different.

(a)

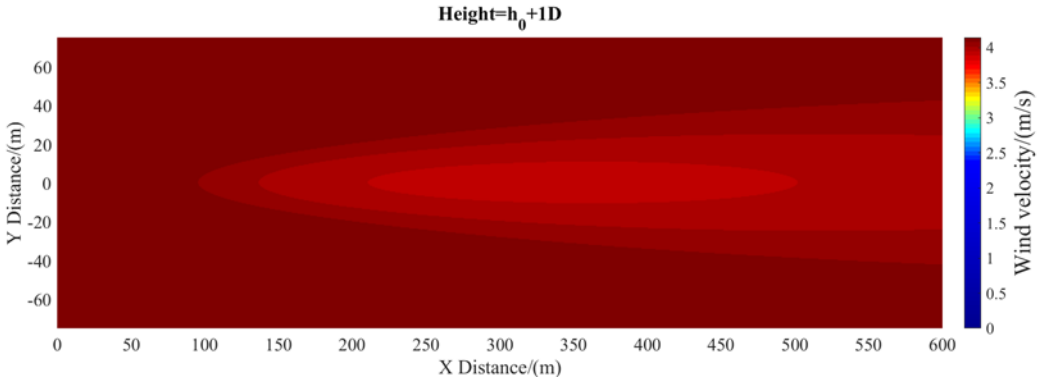
Height=h0+1D
Y Distance/(m)
X Distance/(m)
Wind velocity/(m/s)

(b)

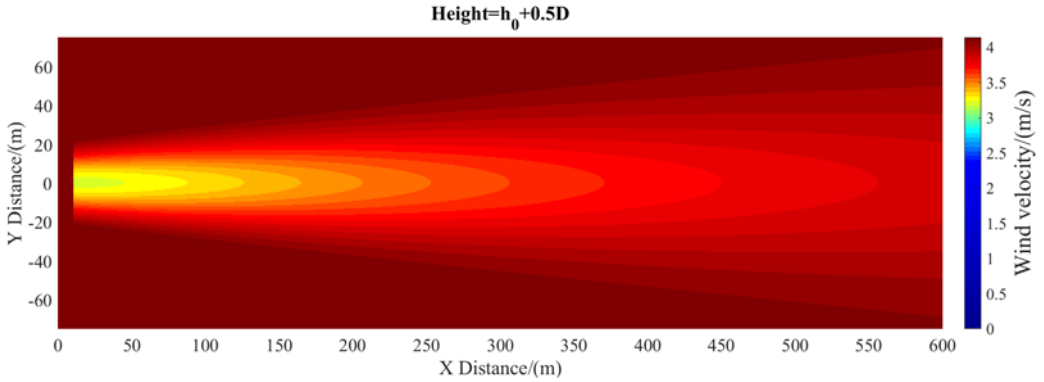
Height=h0+0.5D
Y Distance/(m)
X Distance/(m)
Wind velocity/(m/s)

(c)

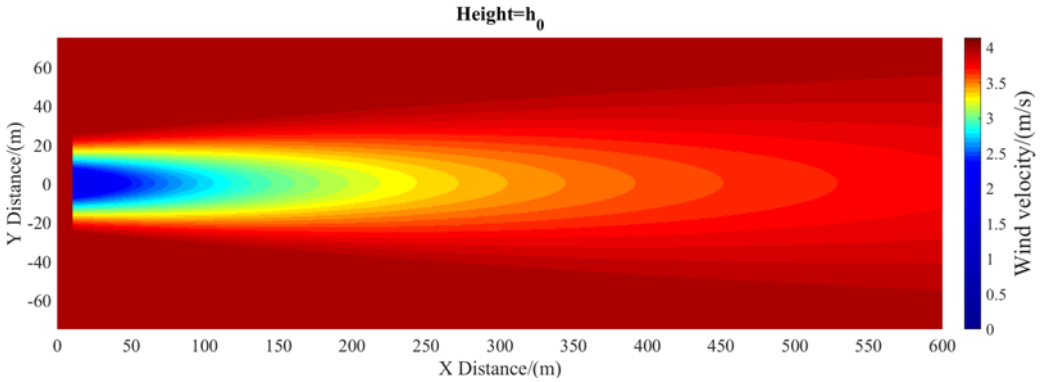
Height=h0
Y Distance/(m)
X Distance/(m)
Wind velocity/(m/s)

(d)

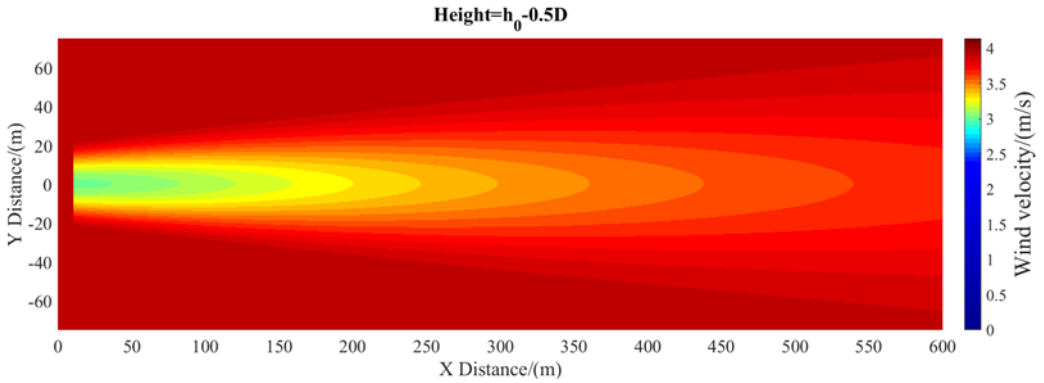
Height=h0-0.5D
Y Distance/(m)
X Distance/(m)
Wind velocity/(m/s)

(e)

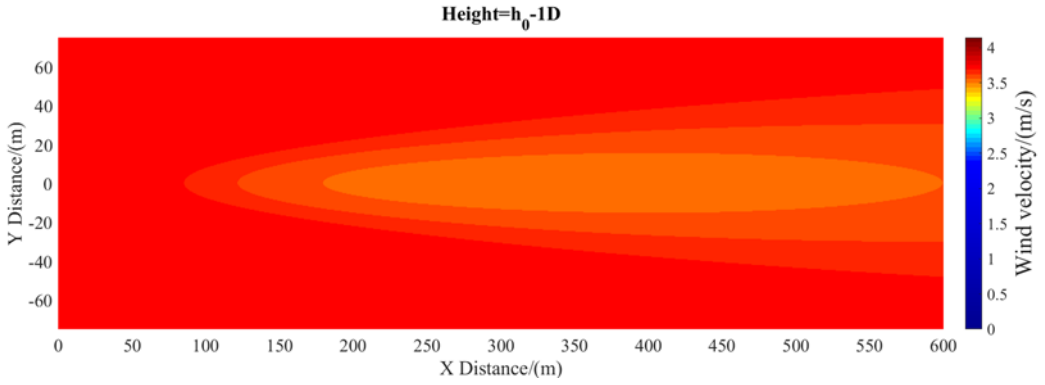

Figure 3.9 X–Y views of the wind profile at different positions: (a) Height = h_0 + 1D section; (b) Height = h_0 + 0.5D; (c) Height = h_0; (d) Height = h_0 - 0.5D and (e) Height = h_0 – 1D

The demonstration of wake profiles from the three views show the effectiveness of the 3-D wake model. It can forecast the wind distribution at any position either before or after the wind turbine and within or without the wake boundary. Especially in the height direction, the superiority of the 3-D wake model is obvious.

3.4 Summary

In this chapter, a novel analytical 3-D wake model is presented to help describe the wind distribution in space at a wind farm. The main conclusions are summarized as follows:

(1) The wake model is based on the momentum conservation theory and assumes that the wind deficit is Gaussian-shaped and the wind velocity is continuous at the wake boundary. It can calculate the wind velocity at any spatial position with high accuracy and little computational cost. The wake model considers the height direction's influence, which makes it more advanced than other analytical wake models.

(2) Wind tunnel measurement data were used to validate the 3-D wake model. In the

validation of the horizontal wake profile, the largest error was 8.35%, most errors were within ±5%, and some large errors were centralized within the ±3D area. Apart from the center area, most errors were negative, which indicates that the 3-D wake model is likely to predict wind velocities smaller than the reality at distances far from the center area. In the validation of the vertical wake profile, the largest error was 5.06%, most errors were within ±3%, and the predictions at positions near the hub height area tended to have large errors. The wake model tended to underestimate the wind velocity for the incoming wind and the small downstream distance, but it tended to overestimate it at most other downstream positions. The 3-D wake model, as a simple analytical wake model, cannot predict the turbulence well, but its predictions are quite accurate far downstream beyond the 5D downstream distance. In addition, according to the analysis, some experimental errors affected the validation of the wake model to some extent.

(3) A series of Y–Z view, X–Z view, and X–Y view wake profiles predicted by the 3-D wake model were demonstrated. From the Y–Z view, the wake-influenced area expanded with the increase of the downstream distance, and the wind deficit phenomenon was also weakened. The wind deficit is not uniformly distributed in the wake-influenced area, and the wake distribution along the height cannot be ignored unconditionally. From the X–Z view, the serious wake-influenced range narrowed with the increase of the Y distance from the wind turbine position, and the minimum distance between any two wind turbines should be no less than 4D. Considering the wake effect on each wind turbine's incoming wind is also of great importance. From the X–Y view, the wind distributions at different heights were not symmetrical to the wind turbine hub height plane, and each horizontal plane had a unique distribution of the wake boundary and the wake intensity.

The study concludes that the 3-D wake model is a reliable tool to describe the wind distribution. As for its simplicity, the wake model also makes a potential contribution to wind farm height optimization and nonuniform wind farm layout optimization problems.

Chapter 4

Average Wind Speed of Single Wind Turbine and Development of a Three-Dimensional Wake Model for Multiple Wind Turbines

This chapter reports the average wind speed of single wind turbine and newly developed analytical 3-D wake model for multiple wind turbines. Firstly, the average wind speed of a single wind turbine is studied. Assuming the incoming wind is distributed as power law along height, the average wind speed has a close relationship to the power exponent α, hub height h_0 and rotor radius r_0. When $\alpha = 0.4$, the average wind speed can decrease to 96% of the speed at the hub height. Secondly, the 3-D wake model for multiple wind turbines is developed based on the wake model for single wind turbine. The available wind tunnel experimental data of two different layouts are used to validate the wake model. Then, the results predicted by the 3-D wake model for multiple wind turbines are demonstrated as well. The presented wake model can be used to describe the wind distribution and optimize the layout of a wind farm.

4.1 Average wind speed derived from the three-dimensional wake model

In the 3-D wake model, the distribution of wind velocity varies in the height direction. Therefore, u_0, the wind speed at the wind turbine hub height, is different from the average wind speed of the wind turbine. To evaluate the energy output of wind turbines more precisely, the analytical average wind speed is firstly derived (Sun & Yang, 2020).

Supposing u_a is the average wind speed on a wind turbine. The flow flux is conservative within a certain area at downstream wake section. In the swept area of the wind turbine, S_{r_0} is the circular area, of which the center is at the hub position and the radius is r_0. The flow flux conservation theory is expressed as equation (4.1):

$$\pi r_0^2 u_a = \iint_{S_{r_0}} U_0(z) ds \tag{4.1}$$

Then, applying hub height into the above equation, $\frac{u_a}{u_{h0}}$ can be solved by equation (4.2).

$$\frac{u_a}{u_{h0}} = \frac{1}{\pi r_0^2} \iint_{S_{r_0}} \left(\frac{z}{h_0} \right)^{\alpha} ds \tag{4.2}$$

MATLAB software is applied as the calculation tool in this study. Figure 4.1 demonstrates the average wind speeds of wind turbines with a series of rotor radii at different hub heights. Four typical values of α are chosen. The results of five rotor radii from 40 m to 120 m are compared. The hub height range is from 60 m to 130 m.

(a)

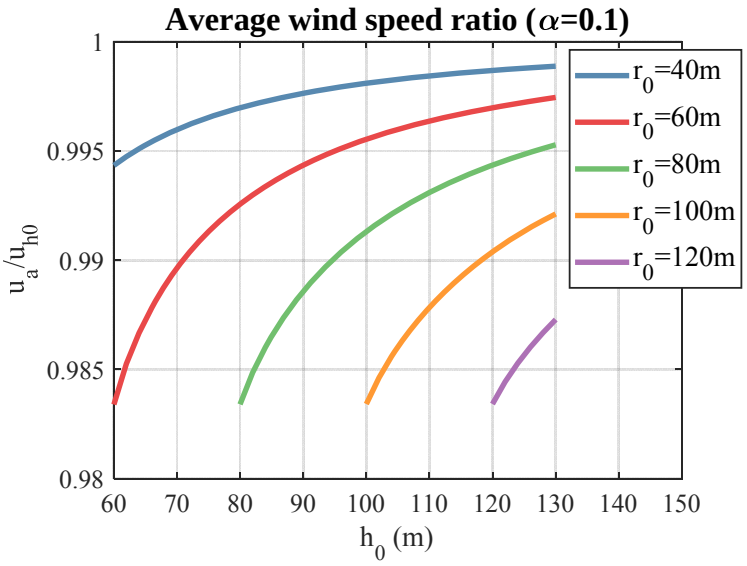
Average wind speed ratio (α=0.1)
u_a /u_h0
h_0 (m)
r_0=40m
r_0=60m
r_0=80m
r_0=100m
r_0=120m

(b)

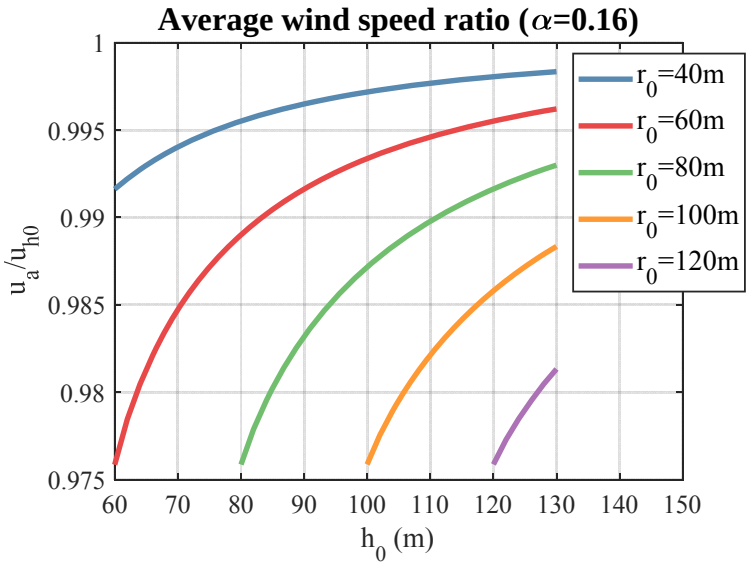
Average wind speed ratio (α=0.16)
u_a /u_h0
h_0 (m)
r_0=40m
r_0=60m
r_0=80m
r_0=100m
r_0=120m

(c)

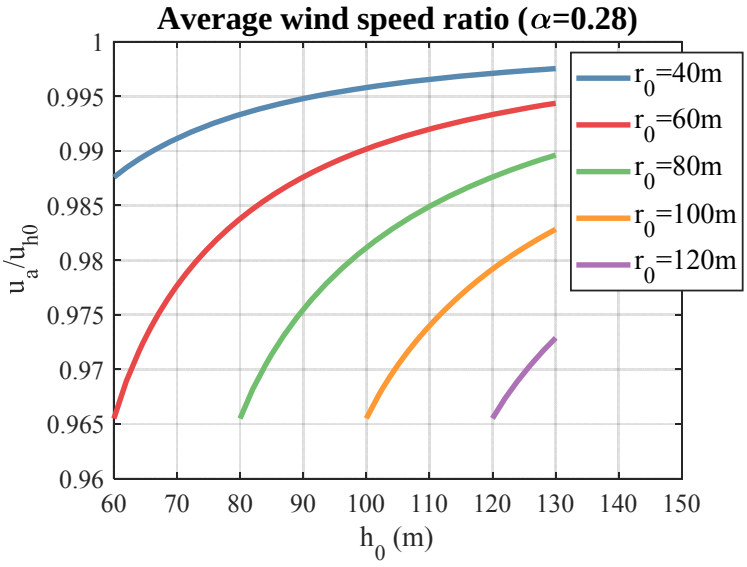
Average wind speed ratio (α=0.28)
u_a /u_h0
h_0 (m)
r_0=40m
r_0=60m
r_0=80m
r_0=100m
r_0=120m

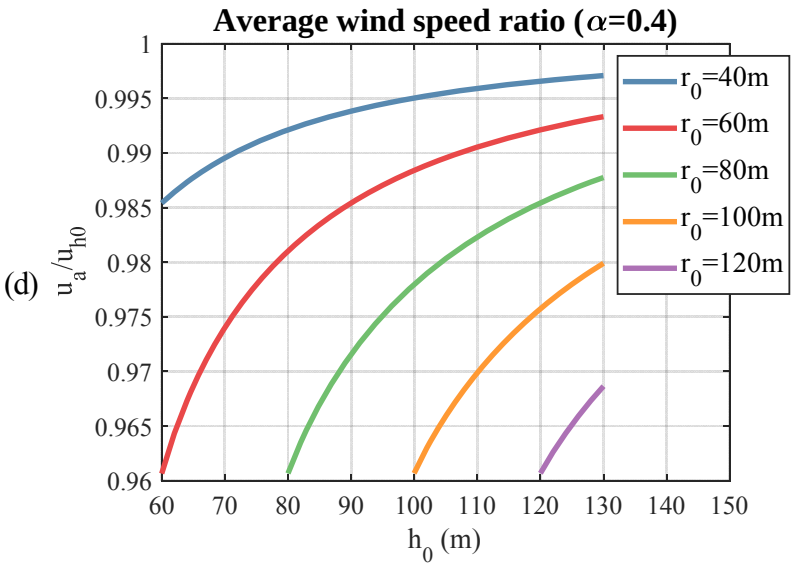

Figure 4.1 Average wind speed with different values of α : (a) $\alpha = 0.1$; (b) $\alpha = 0.16$; (c) $\alpha = 0.28$ and (d) $\alpha = 0.4$

From the results, the conclusion can be drawn that the average wind speed of a wind turbine tends to be lower than that at the hub height, under the condition of power law distributed incoming wind. For the same power exponent α , the average wind speed increases with the hub height, but decreases with the rotor radius. At the same hub height, the average wind speed of $r_0 = 40m$ is successively higher than those of $r_0 = 60m$, $r_0 = 80m$, $r_0 = 100m$, $r_0 = 120m$. For a particular rotor radius, the average wind speed increases gradually from $h_0 = 60m$ to $h_0 = 130m$. The power exponent α also influences the average wind speed. When $\alpha = 0.1$, the average wind speed reduces by 2% to the most, and the reduction raises with the increase of α. When $\alpha = 0.4$, the average wind speed can decrease to 96%. To sum up, the reduction of average wind speed should be considered especially when the rotor has large radius, wind turbines are fixed at high positions and large irregular objects exist on the wind farm terrains.

4.2 Derivation of the three-dimensional wake model for multiple wind turbines

In a real wind farm, a wind turbine may be affected by several other wind turbines' wake effect, thus the study on 3-D wake model should not only be limited to single wake distribution, but also extend to multiple wakes. Therefore, a new 3-D wake model for multiple wind turbines is derivated.

4.2.1 The three-dimensional wake model in a global coordinate

Based on equation (3.1), the 3-D wake model for single wind turbine can be rewritten based on a global coordinate. For the WT_j at the position of (x_j, y_j), the wake induced wind distribution $U_j(x, y, z)$ is shown as equation (4.3):

$$U_j(x,y,z) = \begin{cases} A_j(x)\left(\dfrac{1}{2\pi\sigma_j(x)^2} e^{-\frac{(y-y_j)^2+(z-h_0)^2}{2\sigma_j(x)^2}}\right) + B_j(x) + U_0(z), & \text{within wake region} \\ U_0(z), & \text{, out of wake region} \end{cases} \quad (4.3)$$

The wake region is determined by $r_{w_j}(x)$, which is the radius of the wake influenced circular area at different downwind distance x. If $(y-y_j)^2 + (z-h_0)^2 \le r_{w_j}(x)^2$, the point of (x, y, z) is within the wake region. The equation means that the distance from the point of (x, y, z) to the hub axis is smaller than the radius of the wake influenced circular area. By contrast, if $(y-y_j)^2 + (z-h_0)^2 > r_{w_j}(x)^2$, the point of (x, y, z) is out of the wake region. The equation means that the distance from the point of (x, y, z) to the hub axis is larger

than the radius of the wake affected circular area. In the formula, $r_{w_j}(x)$ can be calculated according to $r_{w_j}(x) = r_0 + k_{wake}(x - x_j)$. Other details about the 3-D wake model for single wind turbine have been described in Chapter 3.

For the WT_i, at the position of (x_i, y_i) with the hub height of h_i, if it is under WT_j's wake effect, the wake effect at WT_i induced by WT_j is $U_{ij}(y,z)$ as shown by equation (4.4):

$$U_{ij}(y,z) = \begin{cases} A_j(x_i)\left(\frac{1}{2\pi\sigma_j(x_i)^2} e^{-\frac{(y-y_j)^2+(z-h_i)^2}{2\sigma_j(x_i)^2}}\right) + B_j(x_i) + U_0(z) & \text{,within wake region} \\ U_0(z) & \text{,out of wake region} \end{cases} \tag{4.4}$$

The two important parameters $A_j(x_i)$ and $B_j(x_i)$ are solved by equation (4.5):

$$\begin{cases} A_j(x_i) = \dfrac{Q_j(x_i) - \int_{h_i - r_{w_j}(x_i)}^{h_i + r_{w_j}(x_i)} 2\sqrt{r_{w_j}(x_i)^2 - (z - h_i)^2}\, U_0(z)\, dz}{\left(1 - e^{-\frac{C^2}{2}} - \frac{C^2}{2} e^{-\frac{C^2}{2}}\right)} \\ B_j(x_i) = -\dfrac{A_j(x_i) C^2}{2\pi r_{w_j}(x_i)^2} e^{-\frac{C^2}{2}} \end{cases} \tag{4.5}$$

4.2.2 Wake addition

For the addition of multiple wakes, several methods can be used (Dobesch & Kury, 2006): Geometric Sum, Linear Superposition, Energy Balance and Sum of Squares. The equations belonging to these models are demonstrated in Table 4.1.

Table 4.1 Methods of multiple wake addition (Renkema, 2007)

Method	Equation
Geometric Sum	$\frac{u_i}{U_\infty} = \prod_j \frac{u_{ij}}{u_j}$
Linear Superposition	$(1-\frac{u_i}{U_\infty}) = \sum_j (1-\frac{u_{ij}}{u_j})$
Energy Balance	$U_\infty{}^2 - u_i{}^2 = \sum_j (u_j{}^2 - u_{ij}{}^2)$
Sum of Squares	$(1-\frac{u_i}{U_\infty})^2 = \sum_j (1-\frac{u_{ij}}{u_j})^2$

where u_i is the wind speed at WT_i, u_{ij} is the wind speed at WT_i under the influence of the WT_j's wake. The summations and the product are taken over the WT_j upwind of WT_i.

A comparative study of four wake models has been conducted with wind tunnel data from GH, i.e. from the documentation of WindFarm software (Djerf & Mattsson, 2000). In comparison, the Sum of Squares method was found excellent for almost all the situations. The next one was the Energy Balance method. Furthermore, it is also recommended that the methods of Linear Superposition and Geometric Sum should not be applied because they tend to make overestimation on the deficit of wind velocity (Renkema, 2007).

In this study, the method of the Sum of Squares is adopted to solve wake adding problem accordingly. A modification of the Sum of Squares and the method to estimate the average wind speed are combined. To calculate the mean wind speed over the swept area, the deficit of momentum is averaged on the area (Lange, Waldl, Guerrero, Heinemann, & Barthelmie, 2003).

If WT_i is only under the wake effect of WT_j, equation (4.6) is adopted. Similarly, u_{a_i} is the average wind speed of WT_i.

$$(u_0 - u_{a_i})^2 = \frac{1}{A}\iint_{S_{r0}} \left(u_0 - u_{ij}\right)^2 ds \tag{4.6}$$

The wind speed affected by several wakes on the swept area is calculated by cumulating all momentum deficits of incoming winds and then integrating them, as shown in equation (4.7).

$$(u_0 - u_{a_i})^2 = \frac{1}{A}\iint_{S_{r0}} \sum_{j=1}^{\text{all wakes}} \left(u_{a_j} - u_{ij}\right)^2 ds \tag{4.7}$$

In the above equation, the momentum deficit of the incoming wind is determined as the square of the difference value between the average incoming wind speed and the in-wake wind speed.

u_{a_i} is the average wind speed of WT_i and it considers all wakes the swept area. With u_{a_i}, the power output of WT_i can be calculated according to the power curve.

4.2.3 The three-dimensional wake model for multiple wind turbines

Applying the 3-D wake model for single wind turbine to estimate the flow speed in the wake, the method of Sum of Squares is rewritten by equation (4.8).

$$[1 - \frac{U_i(x,y,z)}{U_0(z)}]^2 = \sum_{j=1}^{N} [1 - \frac{U_{ij}(y,z)}{U_j(x,y,z)}]^2 \tag{4.8}$$

Next, the same modification of the Sum of Squares as equation (4.8) is made to the equation. The variant equation (4.9) is shown as follows.

$$[U_0(z)-U_i(x,y,z)]^2=\sum_{j=1}^{N}[U_0(z)-U_{ij}(y,z)]^2 \tag{4.9}$$

Therefore, the wind distribution of the WT_i can be expressed by equation (4.10).

$$U_i(x,y,z)=U_0(z)-\sqrt{\sum_{j=1}^{N}[U_0(z)-U_{ij}(y,z)]^2} \tag{4.10}$$

If WT_i is affected by the wake effect of other *n* wind turbines, the formula can be further specified by equation (4.11).

$$U_i(x,y,z)=U_0(z)-\sqrt{\sum_{j=1}^{n}[A_j(x)(\frac{1}{2\pi\sigma_j(x)^2}e^{-\frac{(y-y_j)^2+(z-h_0)^2}{2\sigma_j(x)^2}})+B_j(x)]^2} \tag{4.11}$$

The average wind speed u_a can be calculated by equation (4.12).

$$\iint_{S_{r_w(x)}}[U_0(z)-u_a]^2ds=\iint_{S_{r_w(x)}}[U_0(z)-U(x,y,z)]^2ds \tag{4.12}$$

To simplify the calculation, the incoming wind speed $U_0(z)$ on the left side of the equation can be replaced by u_0, so that the simplified equation (4.13) is shown as follows.

$$(u_0 - u_a)^2 = \frac{1}{A}\iint_{S_{r_0}} \sum_{i=1}^{N} [U_0(z) - U(x,y,z)]^2 \, ds \tag{4.13}$$

4.3 Validation of the three-dimensional wake model for multiple wind turbines

To see the accuracy of the 3-D wake model for multiple wind turbines, the simulations of the wake model are compared with the measured data of the wind tunnel experiment. The experimental data comes from the wind tunnel in the Saint Anthony Falls Laboratory at the University of Minnesota, and the experimental conditions are thermally unstratified (L. P. Chamorro & Porte-Agel, 2011). Two different layouts of the staggered array of miniature wind turbines are demonstrated.

4.3.1 Description of the wind tunnel experiments

The boundary-layer applied to the wind farm model was under neutrally-stratified conditions and grew over a smooth surface. The plan length of the wind tunnel is 37.5 m, the primary fetch of the test section is around 16 m, whereas the cross section size is 1.7 m×1.7 m. The scale ratio of the area was 6.6:1. More descriptions about the wind tunnel can be found in references ((Carper & Porté-Agel, 2008a) and (Carper & Porté-Agel, 2008b)).

The intensity of turbulence in the center, i.e. freestream, of the wind tunnel was around 1% for a freestream speed of 2.5 m/s. A turbulent boundary layer depth was obtained to be $\delta \approx 0.5m$ at the location of wind turbine. The gradient boundary layer was zero pressure, it had a Reynolds number, $\mathrm{Re}_\delta = U_\infty \delta / \nu \approx 1.12 \times 10^5$. δ is the boundary layer height.

The friction velocity u_* was 0.13 m/s. The roughness length of aerodynamic surface z_0 was 0.05 mm. u_* and z_0 were acquired by adjusting the profile of wind velocity to the experimental mean speed in the surface layer.

The wind turbine model consisted of a three-blade GWS/EP-6030×3 rotor, which was linked to a tiny DC generator. The wind turbine angular speed was controlled by altering the generator resistance. The dimensions of the wind turbine model are shown in Figure 4.2.

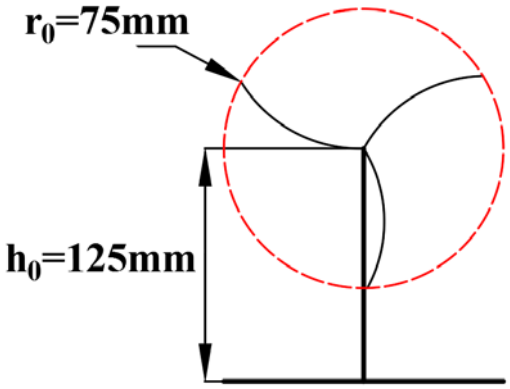

Figure 4.2 Turbine dimensions

In the experiments, the tip speed ratio was set as roughly 4 for the first row of wind turbines ($\lambda = 2\pi r\Omega / [60U_{hub}]$, where U_{hub} was 2.1 m/s and Ω is the angular speed of the wind turbine in rpm.).

4.3.2 Description of the incoming wind

To simulate the incoming wind of the experiments, equation (4) is adopted. To begin with, a vertical velocity profile was selected to see the accuracy of the 3-D wake model for single wind

turbine, of which the position was at downstream distance of $x/D=2$ behind the third row of wind turbines (L. P. Chamorro & Porte-Agel, 2011). The simulation of this study is compared to the measured data, as shown in Figure 4.3. In this process, the power law parameter of wind speed was set as $\alpha=0.1$.

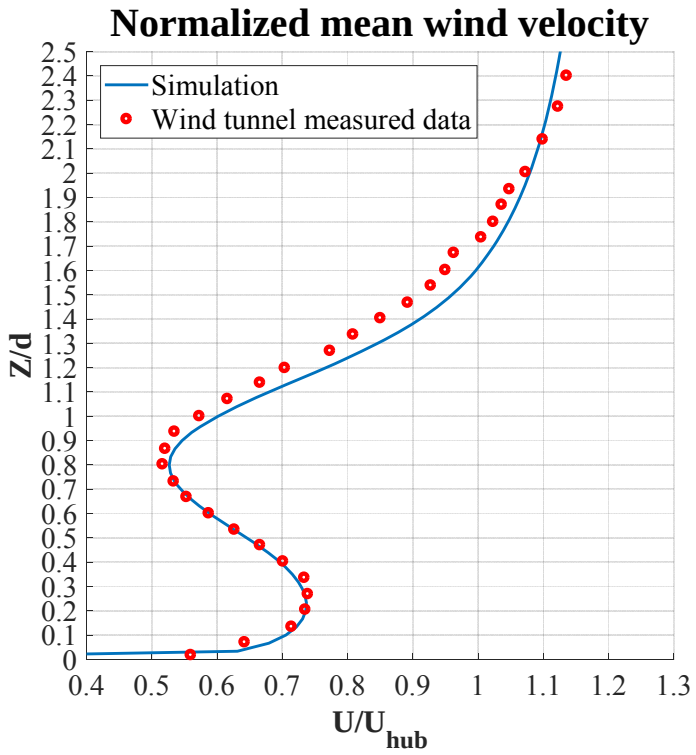

Figure 4.3 Distribution of the normalized streamwise velocity component

The simulation results show a perfect agreement with the measured data, especially at the position of the hub height. The deficit in the wind farm is also given in reference (L. P. Chamorro & Porte-Agel, 2011). To combine the streamwise wind velocity and the wind deficit, the measured incoming wind recovery data in the wind tunnel can also be obtained. The recovery data are then compared with the simulation results, as shown in Figure 4.4.

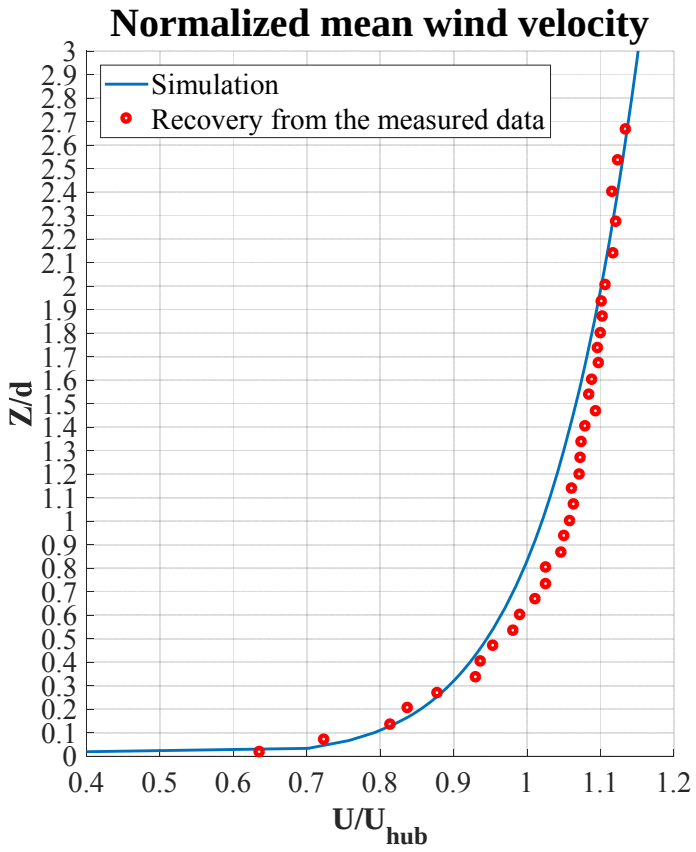

Figure 4.4 Incoming wind distribution

Error comparisons could be done between the simulation results and the measured data through Figure 4.4. Generally, the simulated incoming wind speeds fit well with the experimental data. Some big errors exist in the height range of 0.5D ~1.5D. It is worthy noticing that these errors may have an influence on the validation of the effectiveness of the 3-D wake model for multiple wind turbines.

4.3.3 Result comparisons

The comparisons have been carried out with the experiments of two layouts, which are both the 10 by 3 wind turbine arrays.

4.3.3.1 Results comparison of Layout 1

In Layout 1, the distance between consecutive wind turbines was set to 5D in the direction of the flow and 4D in the spanwise direction. The schematic wind turbine array is demonstrated in Figure 4.5.

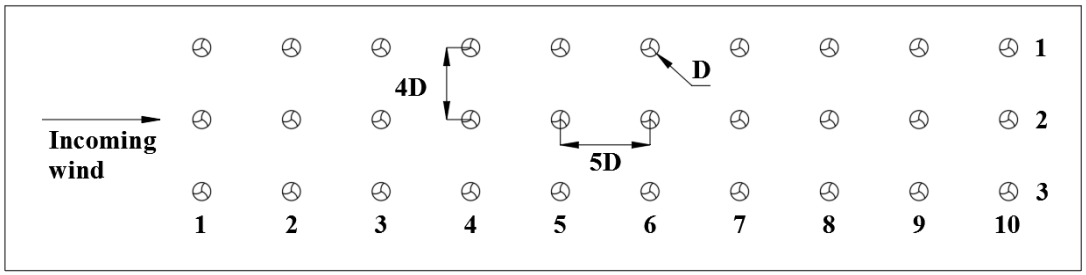

Figure 4.5 Schematic wind turbine array

Figure 4.6 shows the simulation results of the 3-D wake model in Layout 1 and they are compared to the representative measured wind speeds of the wind tunnel experiment at three heights: (a) the bottom tip height; (b) the hub height; and (c) the top tip height.

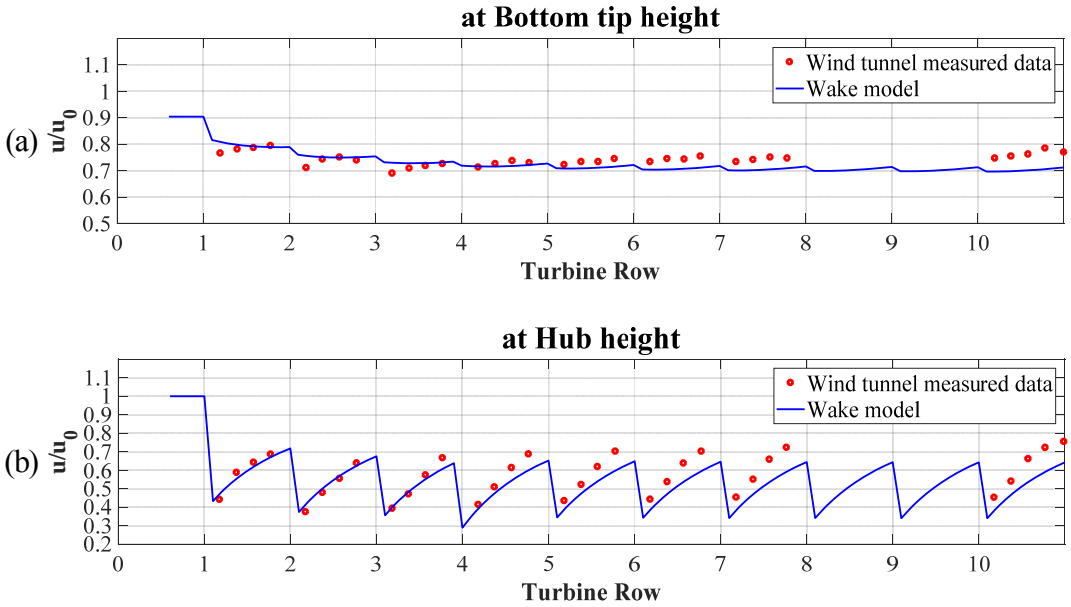

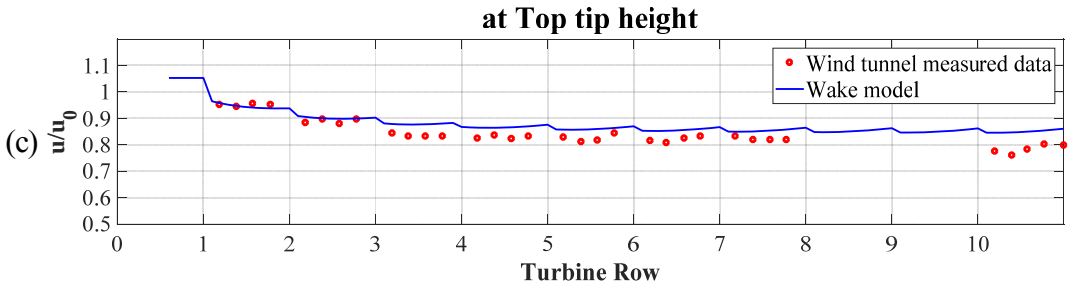

Figure 4.6 A characterization of the average wind speed at (a) the bottom tip height; (b) the hub height and (c) the top tip height

At all three representative heights, the 3-D wake model for multiple wind turbines tends to predict wind speed distribution accurately. For the first two rows, the prediction results are very close to the measured data. For the rest rows, although some deviations exist, the shapes of the prediction and the characterization of the mean flow are in accordance at each height. The 3-D wake model tends to predict smaller wind speed at the bottom tip and the hub heights from the 4th row, while predicting larger wind speed at the top tip height from the 3rd row.

Apart from the simulation errors from the wake model, the errors may also come from the experiment. Taking the hub height data as an example, the measured wind speed at the downwind behind rows tend to be larger than those of the front rows, which is not quite rational. The experimental errors should be involved in the consideration when judge the effectiveness of the 3-D wake model for multiple wind turbines.

The relative errors at three heights of Layout 1 are then analyzed and demonstrated in Figure 4.7.

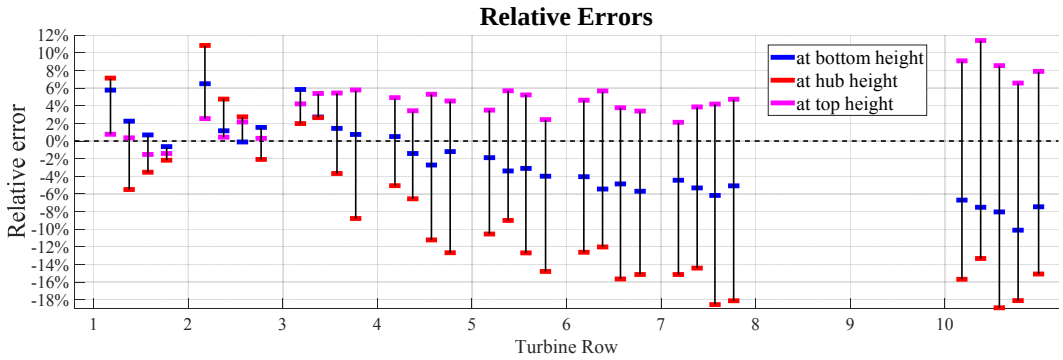

Figure 4.7 Analysis of relative errors of Layout 1

It is apparent that the simulation of the wake model is more precise at the hub and the top heights, where most of the relative errors are smaller than 6%. The wake model does not seem to be that accurate at the top height, but all relative errors are within 20%. The similar conclusion can be obtained that the wake model predicts better in the first three rows than in the rest behind rows.

4.3.3.2 Results comparison of Layout 2

In Layout 2, the distance in the spanwise direction was also 4D, but the distance between consecutive wind turbines was 7D. The schematic wind turbine array is demonstrated in Figure 4.8.

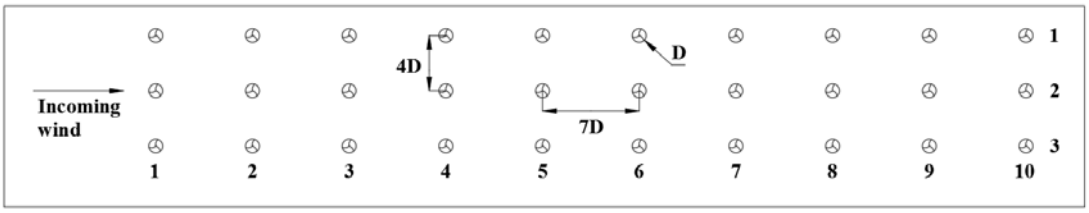

Figure 4.8 Schematic of wind turbine array with 10 lines and 3 rows

Figure 4.9 demonstrates the simulation results of the 3-D wake model in Layout 2. They are also compared with the measured wind speeds of the wind tunnel experiment. The three

representative positions are: (a) the bottom tip height; (b) the hub height; and (c) the top tip height.

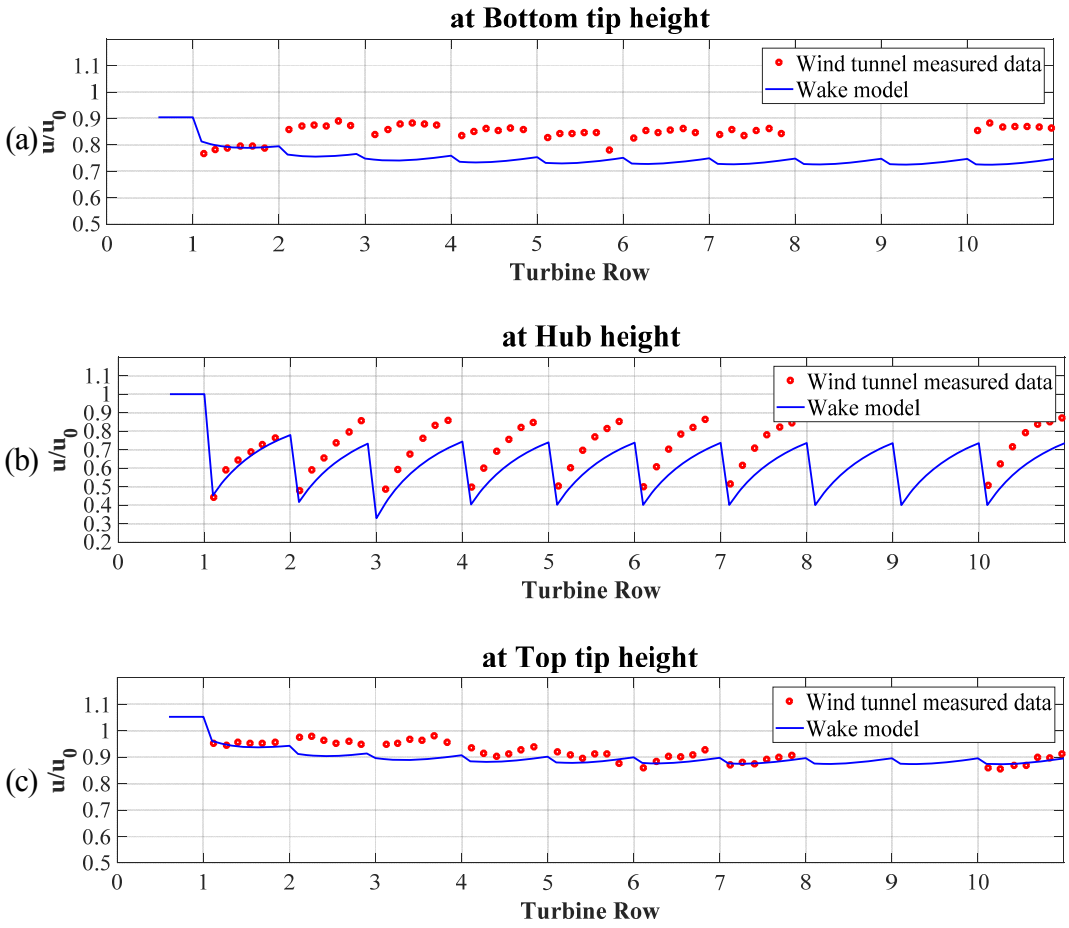

Figure 4.9 A characterization of the average wind speed at (a) the bottom tip height; (b) the hub height and (c) the top tip height

For Layout 2, the 3-D wake model also shows the good accuracy, only tends to underestimate the wind speed at all selected heights. Good agreement between the simulated results and the experimental data is shown at the space between the 1st and the 2nd rows. The wake model is especially precise at the top tip height. For the bottom tip and the hub height, the obvious difference lies between the measured wind speeds of the 1st row and the 2nd row, which may affect the validation of the 3-D wake model. Therefore, some more comprehensive wind tunnel tests should be conducted in future research to explore this 3-D wake model.

The quantitative analysis of relative errors is revealed in Figure 4.10.

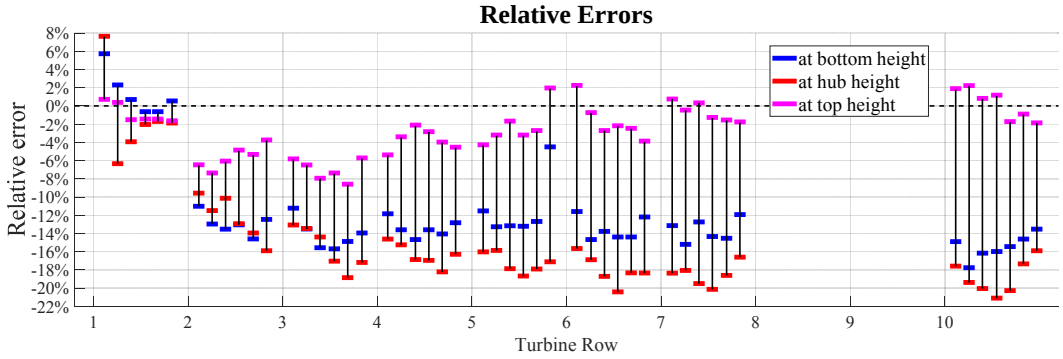

Figure 4.10 Analysis of relative errors in Layout 2

From the figure, for Layout 2, the 3-D wake model simulates the wake effect with acceptable precision, and the largest error is smaller than 22%. The model is more precise within the one-row distance. It is most accurate at the top height, followed by the bottom height and the hub height. At the top height, the largest error of the wake model is just 8.5%, those at the bottom height and at the hub height are 17.8% and 21.2%, respectively.

The 3-D wind turbine wake model tends to underestimate wind speed in some positions. On the one hand, when derivating the wake model, a modification was made from equation (4.8) to equation (4.9). Although it is reasonable according to reference (Lange et al., 2003), it may cause the error to the 3-D wake model. On the other hand, as analyzed before, some of the measured data seems to contain errors themselves, which means the experimental error may affect the validation of the 3-D wake model. Therefore, the 3-D wake model can be further improved and the more accurate wind tunnel experiments should be conducted.

4.4 Prediction from the three-dimensional wake model for multiple wind turbines

After validating the accuracy of the 3-D wake model for multiple wind turbines, some predictions of wake distribution can be obtained. In this chapter, the model is used to simulate the wind speed profiles in the mentioned two layouts from some more views.

4.4.1 Prediction of Layout 1

In this section, the simulated layout of wind farm is the same as Layout 1. Three different views are demonstrated. Figure 4.11 is the X-Z view of wind speed at y = 0D.

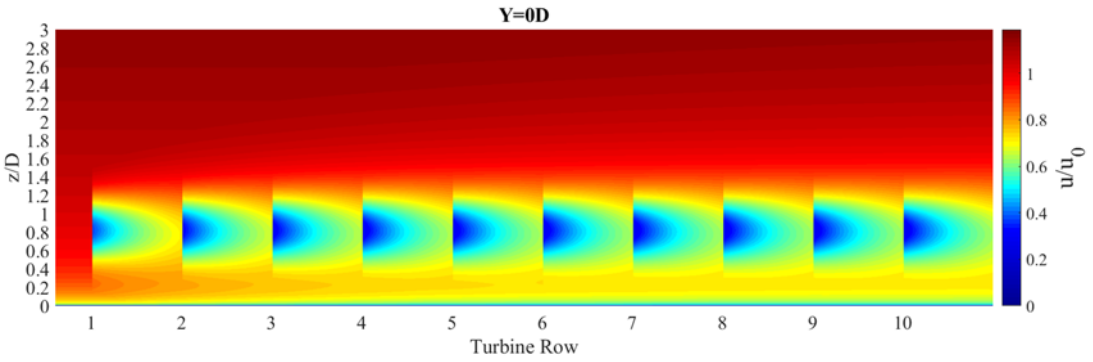

Figure 4.11 X-Z view of wind speed at y = 0D

The wake distributions vary at different downstream positions, which can be seen from Figure 4.11. The wind deficit behind the 1st row of wind turbine is the least. With the wind blows further through wind turbines, the wind deficit phenomenon becomes more obvious. Beyond the 5th row, the wind profiles behind each wind turbines seem to be almost identical. According to Figure 4.11, the downstream intervals between wind turbines are recommended to be no less than 5D. For each vertical section, the largest wind deficit happens at the hub height. That is to say if the hub heights of wind turbines are different, the serious wake-influenced zone can be avoided, and more wind energy can be captured.

Figure 4.12 shows the X-Y view of wind velocity at the position where z = hub height.

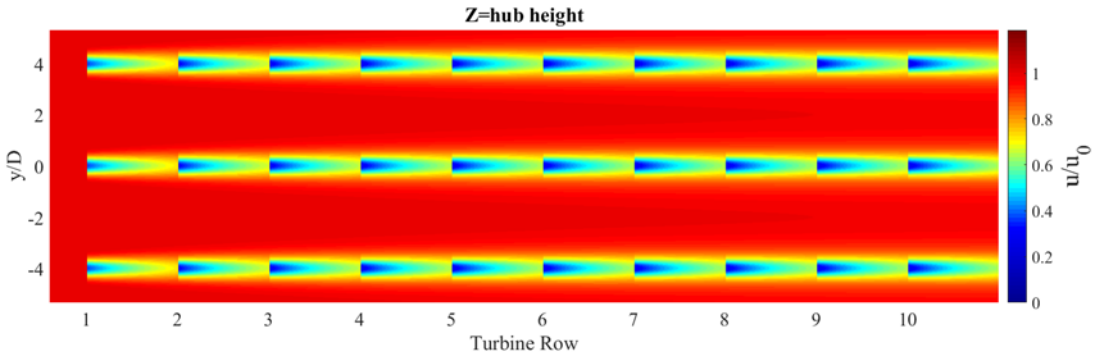

Figure 4.12 X-Y view of wind speed where z = hub height

The 3-D wake model helps to study the X-Y view of wind velocity at all heights. The hub height is where the largest deficit of wind lies. From the figure, the 4D cross interval between wind turbines is long enough to avoid the wakes, because the parallel wind turbines almost have no influence to each other.

Figure 4.13 demonstrates the Y-Z view of wind speed at four typical x positions: (a) x = 1.2 Turbine Row; (b) x = 1.5 Turbine Row; (c) x = 6.2 Turbine Row and (d) x = 10.5 Turbine Row.

(a)

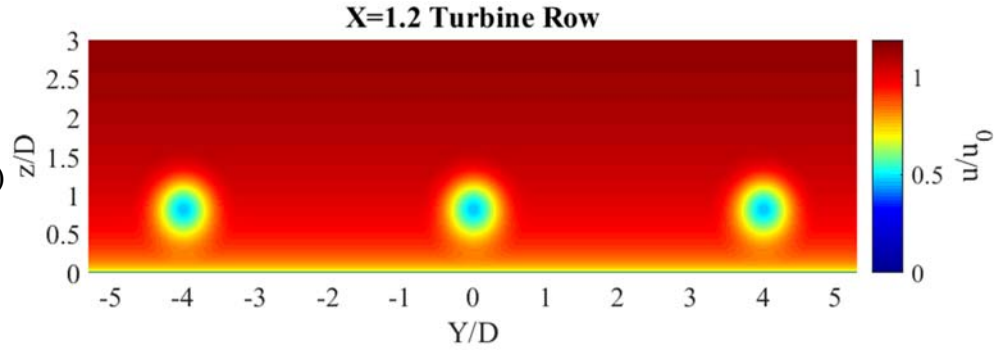

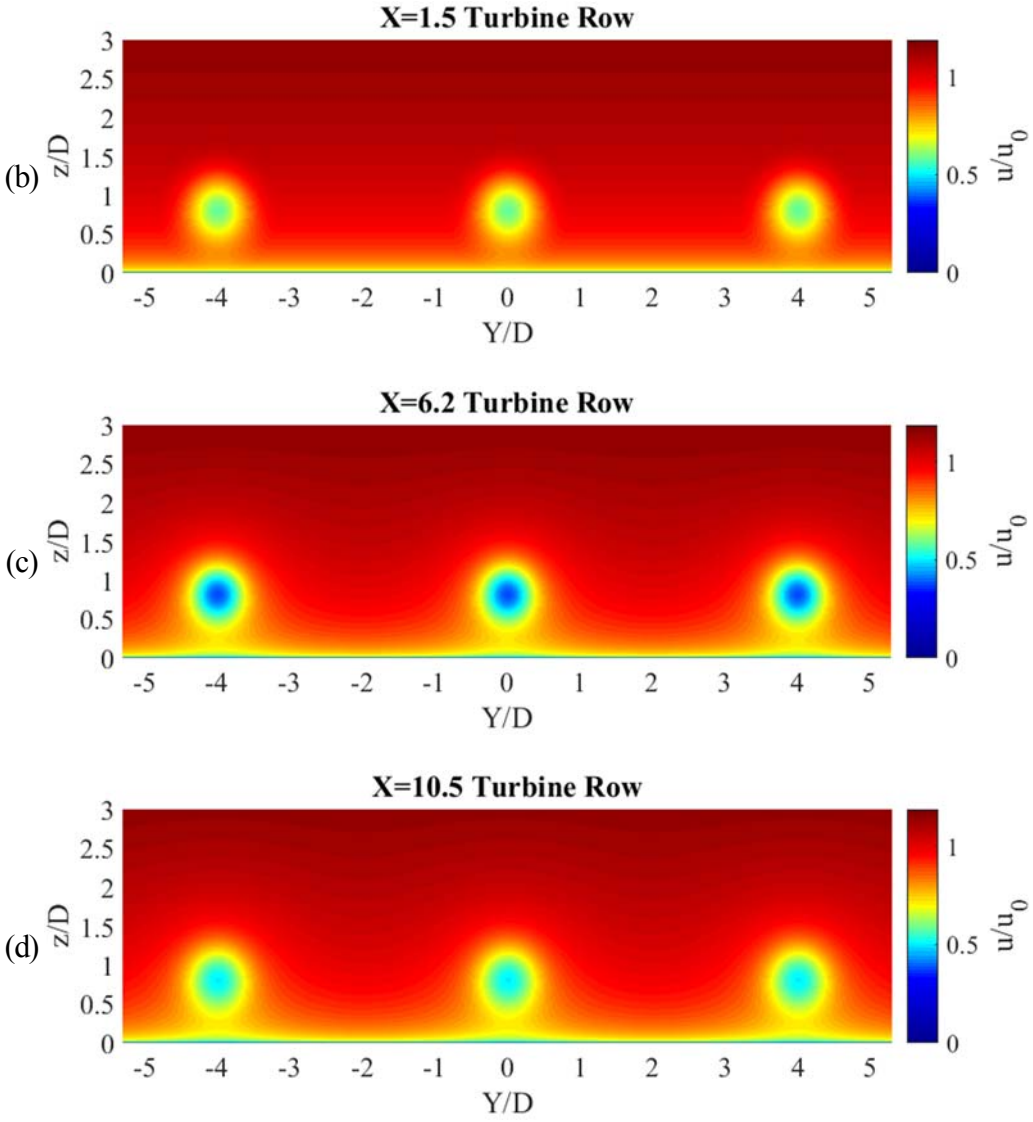

Figure 4.13 Y-Z view of wind speed at (a) x = 1.2 Turbine Row; (b) x = 1.5 Turbine Row; (c) x = 6.2 Turbine Row and (d) x = 10.5 Turbine Row

Comparing Figure 4.13 (a) and (c), the selected sections are at the same distance from the upwind wind turbine, however, the distributions of the wind speeds are much different. This is because that the incoming wind for the 1st row of wind turbines is the environmental wind, which is not influenced by the wake of other wind turbines; whereas the incoming wind for the 6th row of wind turbines is smaller the environmental wind speed, as it is under the wake effect of other upstream wind turbines. This reason can also explain the difference between Figure 4.13 (b) and (d).

4.4.2 Prediction of Layout 2

This section is continuous to section 5.1, and the simulated layout of wind farm is the same as Layout 2. Firstly, Figure 4.14 shows the X-Z view of wind speed at *y*=0D.

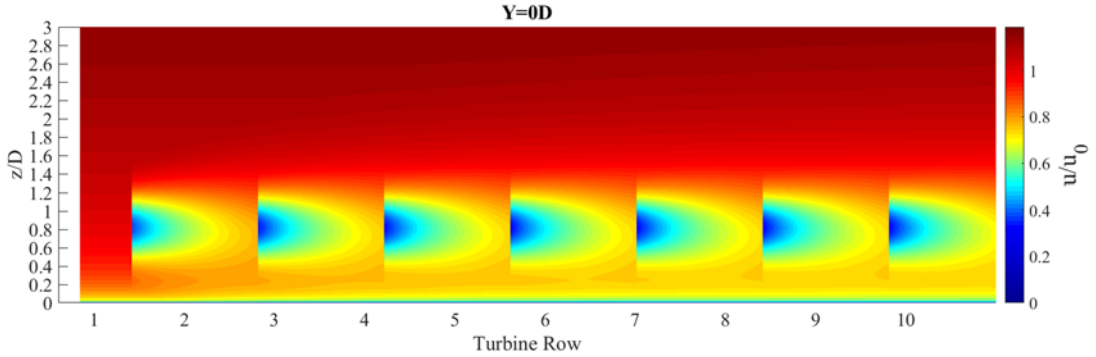

Figure 4.14 X-Z view of wind speed at *y* = 0D

The wind deficit behind the 1st row of wind turbine is also the least, which is similar to that of Layout 1. The little difference is that after the 3rd row, wind profile behind each wind turbine becomes almost identical. This is directly caused by the increase of intervals between downwind wind turbines. Intervals of 7D distance tend to be better than 5D, as the downstream wind turbines are less influenced by the upstream wind turbines.

Figure 4.15 shows the X-Y view of wind speed at *z* = hub height of Layout 2.

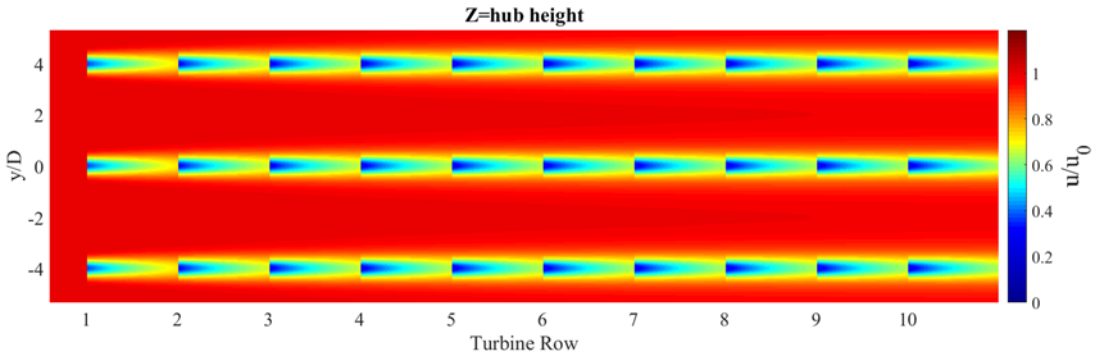

Figure 4.15 X-Y view of wind speed at z = hub height

This figure further confirms that Layout 2 is more efficient. The wake-influenced winds firstly blow through the upstream wind turbines and then recover close to the environmental winds before reach the downstream wind turbines. If the intervals continue to increase, the downstream wind turbines can operate under less wake effect.

Figure 4.16 demonstrates the Y-Z view of wind speed at four typical X position: (a) X=1.2 Turbine Row; (b) X=1.5 Turbine Row; (c) X=6.2 Turbine Row and (d) X=10.5 Turbine Row. These profiles assist to further investigate the characteristics of wind turbine wake models.

(a)

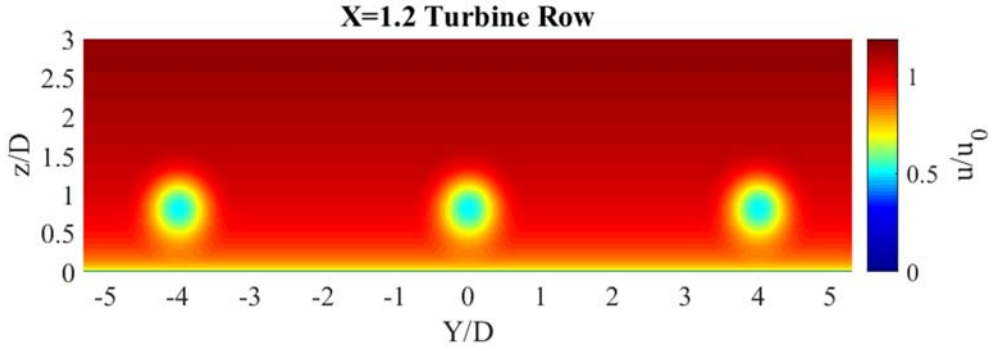

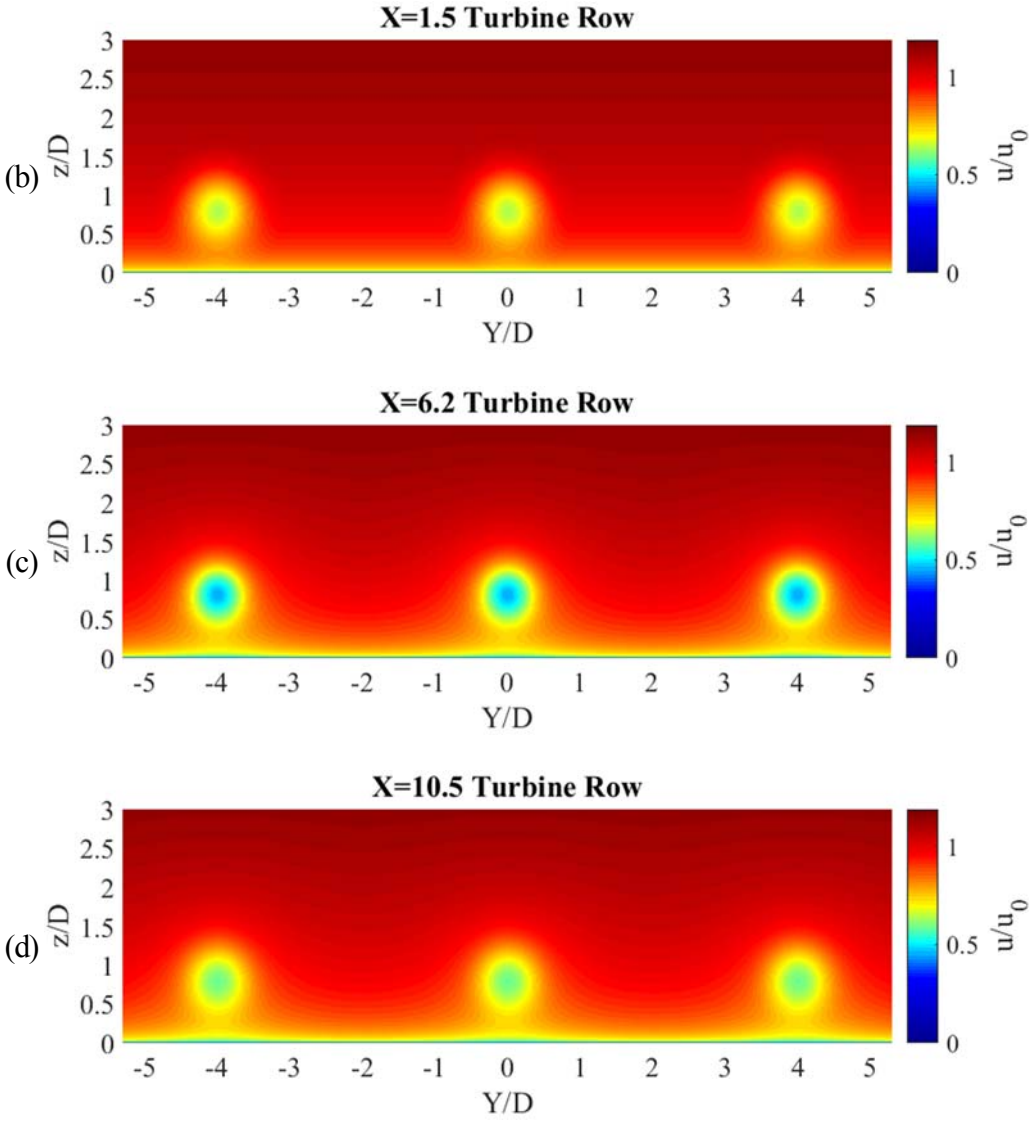

Figure 4.16 Y-Z view of wind speed at (a) X=1.2 Turbine Row; (b) X=1.5 Turbine Row; (c) X=6.2 Turbine Row and (d) X=10.5 Turbine Row

4.5 Summary

In this chapter, an analytical 3-D wake model has been further studied. The method to calculate the average wind speed of single wind turbine is proposed, in which the wind variation in vertical direction is considered. Then, the 3-D wake model for multiple wind turbines is developed. The significant summaries are drawn as follows:

(1) The average wind speed of a single wind turbine is studied in depth. The power law wind profile in 3-D wake model is adopted. The basic theory is the flow flux conservation law. From the results, under the condition of the mentioned incoming wind profile, the average wind velocity of a wind turbine is lower than the measured wind velocity at the hub height. For the same power exponent α, the average wind speed increases with the hub height but decreases with the rotor radius. The power exponent α also influences the average wind speed. To be specific, the wind speed deficit reduces with the increase of α. When $\alpha = 0.1$, the average wind speed is reduced by 2% to the most, whereas when $\alpha = 0.4$, the average wind speed can decrease by 4%. Therefore, the reduction of average wind speed should be considered especially for wind turbines that have large rotor radius, stands at high positions and are built in the terrain with large irregular objects.

(2) The 3-D wake model for multiple wind turbines was derived. The wake model for single wind turbine was rewritten in the global coordinate. The Sum of Squares method was adopted to solve the wake adding problem accordingly. If the WT_i has been judged to be affected by the wake effect of other *n* wind turbines, the formula can be further specified as:

$$U_i(x,y,z) = U_0(z) - \sqrt{\sum_{j=1}^{n} [A_j(x)(\frac{1}{2\pi\sigma_j(x)^2} e^{-\frac{(y-y_j)^2+(z-h_0)^2}{2\sigma_j(x)^2}}) + B_j(x)]^2}$$

(3) The 3-D wake model for multiple wind turbines has been validated by the wind tunnel experimental data of two layouts of miniature wind turbines. In Layout 1, the wake model was pretty accurate at the hub and the top heights, and most of the relative errors were smaller than 6%. At the top height, all relative errors were within 20%. The wake model

predicted better in the first three rows than in the rest behind rows. In Layout 2, the wake model also predicted the wake effect with acceptable precision, and the largest error was smaller than 22%. The model was more accurate within the first-row distance. At the top height, the largest error of the wake model was just 8.5%, which was 17.8% at the bottom height and was 21.2% at the hub height.

(4) Some more prediction of wind distribution of the mentioned two layouts of the miniature wind turbines were obtained from the 3-D wake model. The profiles of wind speeds from some more views were demonstrated. From the predicted results, the largest wind deficit was at the hub height and the 4D cross interval between wind turbines was long enough to avoid the serious wake effect. Comparing two layouts, intervals of 7D distance were better than 5D, as the downstream wind turbines were influenced less from the upwind wind turbines.

Chapter 5

Measurements of Wind Speed at a Complex-Terrain Wind Farm for Analysis of Wake Effects

In this chapter, wind speed deficits were quantified based on field observations from the hilly Shiren wind farm in China. The main purposes of the experiments were to obtain the wind speed profiles with varying distance from a wind turbine and to investigate the wake interactions among multiple wind turbines in complex terrains. Two lidars were applied to measure wind turbine wakes. The experiments involved two layout arrangements of wind turbines. The upstream-and-downstream arrangement was to investigate how the wakes of upstream turbine affect the downstream turbine. From the results, the wake centerlines of upstream and downstream wind turbines could be different. Another side-by-side arrangement was to investigate what the wakes and the wake interaction look like downwind a row of wind turbines. Fluctuations were observed in the far-wake zone. The range of the wake-influenced area was not easy to be identified in the far-wake zone, and wakes of two adjacent turbines may have a complicated interaction.

5.1 Site and layout of the Shiren wind farm

The experiments were conducted in the Shiren Wind Farm, which belongs to Hebei Longyuan Wind Power Co., LTD. The wind farm is located in Shangyi Country, Zhangjiakou City, Hebei Province, China. The booster station is located at 40.985833° N, 114.361667° E with the height of 1814 m. The terrain of the wind farm is characterized with low mountains and hilly areas. The location of the Shiren Wind Farm is shown in Figure 5.1.

Figure 5.1 Location of the Shiren Wind Farm

Shiren Wind Farm has a capacity of 75 MW. The wind farm consists of 50 numbers of 1.5 MW wind turbines, among which 33 are the AW77-1500 type and 17 are the UP77-1500 type. For the AW77-1500 wind turbine, the rotor diameter is 77 m and the hub height is 60 m. For the UP77-1500 wind turbine, the rotor diameter is 77 m and the hub height is 65 m. The layout of wind turbines in Shiren Wind Farm is shown in Figure 5.2. Actually, there are also some wind turbines that belong to other companies in the nearby area, but they are not pointed out in the figure.

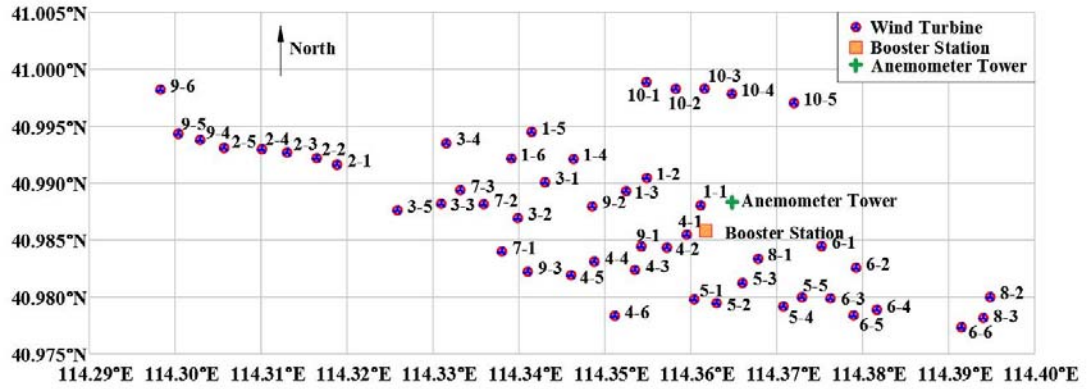

Figure 5.2 Layout of wind turbines in the Shiren Wind Farm

Shiren Wind Farm is built in the hilly terrain, in which the largest difference of altitude is 171.3 m. Among all wind turbines, the highest wind turbine is WT10-5, installed at 1894.1 m high; whereas the lowest one is WT8-2, installed at 1722.8 m high. The layout of Shiren wind farm on satellite map is shown in Figure 5.3.

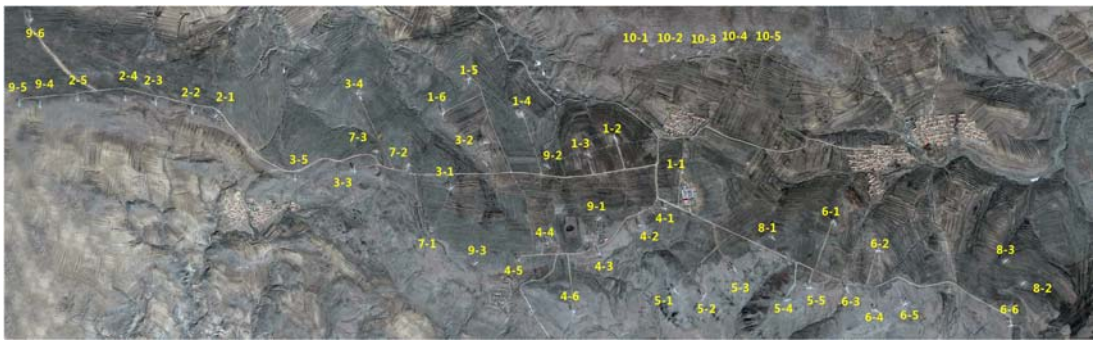

Figure 5.3 Layout of Shiren Wind Farm on satellite map

Shiren wind farm is a good representative of complex-terrain wind farms. The first-hand wind speed data will contribute to both the research study and the engineering application in complex-terrain wind farms.

5.2 Introduction of measuring equipment

5.2.1 Anemometer tower in the wind farm

The wind farm has an anemometer tower with the altitude of 1807.5 m, and the location of which is 40.988352º N, 114.364810º E. The anemometer tower measures wind velocity at two heights, 10 m and 65 m. At each measuring height, an anemometer and a wind vane are applied to measure the wind speed and the wind direction, respectively. Figure 5.4 shows the anemometer tower and the measuring equipment at 10 m height.

(a)  (b) 

Figure 5.4 (a) the anemometer tower and (b) the measuring equipment at the height of 10 m

In the engineering, the data obtained from the anemometer tower provide the evidence for estimating and arranging the power output of the wind farm. However, the anemometer tower cannot monitor the inflow of each wind turbine at different heights. For the wake study, the accurate awareness of the upstream and downstream wind distributions is of extreme importance. Therefore, WindMast WP350, a movable wind mast based on lidar principle was applied to detect the inflow wind of the target wind turbine. Another scanning lidar, Wind3D 6000, was used to obtained the downstream wind speed distribution of wind turbines.

5.2.2 Location of the measuring device

To measure the locations of wind turbines and lidars accurately, Ji Si Bao G128BD, a handheld was used in the experiments. The handheld supports Beidou, GPS and GLONASS three satellite systems perfectly. It has three power supply mode, which are dry battery, lithium battery and USB. The handheld contains electronic compass and barometer. It also supports a variety of

coordinates. The Ji Si Bao G128BD is shown in Figure 5.5.

Figure 5.5 Ji Si Bao G128BD Beidou handheld

5.2.3 Wind speed measuring devices

Two lidars, the WindMast WP350 and Wind3D6000, were used to measure the inflow and downstream wind speeds, respectively. Both two lidars were rented from QINGDAO Leice Transient Technology Co. LTD., and they were calibrated by the data from anemometer tower before the actual experiments.

5.2.3.1 Principle and characteristics of the lidar detection

The atmospheric wind field is the main driving force for atmospheric circulation, material transportation and weather phenomena of various scales. In the field of aviation, wind power and environmental protection, obtaining accurate atmospheric wind fields is always important.

The mentioned two wind lidars adopt the non-contact measurement, which has non-interfering target motion, high spatial and temporal resolution and high measurement accuracy. These lidars are active remote sensors and are capable of measuring 3-D atmospheric wind field in real time.

The mentioned two wind lidar systems both have three parts, a launch system, an optical receiving system, and a signal acquisition processor. The launch system emits laser light into the atmosphere, interacting with the aerosol and generating an echo signal. The signal then is received by the optical antenna, sent to the signal acquisition system for data acquisition and procession. The Doppler shift of the echo signal is then detected through the spectral peak. Finally, the information is inversed into the horizontal wind field.

5.2.3.2 WindMast WP350

WindMast WP350 is a vertical-wind-mast-type lidar, which is designed to replace wind towers. It has a high precision, needs low power, and is designed and manufactured based on the IEC 61400-12-1:2017 standard. The wind speed and wind profile of any 30 height gates from 20 m to 350 m above the lidar can be continuously detected throughout the day. The WP350 used in the experiments is shown in Figure 5.6. Technical specifications of WindMast WP350 are listed in Table 5.1.

(a)  (b) 

Figure 5.6 Wind speed measuring equipment: WindMast WP350

Table 5.1 Technical specifications of WindMast WP350

Specifications	Parameters
Wavelength	1.5 μm, eye-safe
Detection height	20 m ~ 350 m
Spatial resolution	Up to 30 heights in the range of 20 m ~ 350 m, the highest resolution is 1m
Data updating time	1 s ~ 10 min (configurable)
Wind speed range	0 ~ 75 m/s
Wind speed error	≤ 0.1 m/s
Wind direction error	< 3º
Data product	Horizontal and vertical wind speeds, wind direction, mean square error of wind speed, wind shear index, SNR signal to noise ratio data, GNSS position time, radar status data, surface atmospheric temperature, humidity, pressure, etc.
Weight	< 30 kg

The WindMast WP350 is suitable for wind resource exploration and evaluation, wind turbine power curve test, wind power prediction, wind shear analysis, dynamics research of atmospheric boundary layer and other fields.

5.2.3.3 Wind3D 6000

Wind3D 6000 is three-dimensional-scanning-wind lidar, which can realize the detection of 3-D wind fields of the middle and lower troposphere (including the atmospheric boundary layer). Wind3D 6000 has a high precision of optical scanning mirror for 3-D scanning. It also has several scanning modes and the detection radius can be up to 6 km. The device applied in the experiments is shown in Figure 5.7.

(a)

(b)

Figure 5.7 Wind speed measuring equipment: Wind3D 6000

Technical specifications of Wind3D 6000 are listed in Table 5.2.

Table 5.2 Technical specifications of Wind3D 6000

Specifications	Parameters
Wavelength	1.5 μm, eye-safe
Radial detection range	45 m ~ 6000 m
Radial range resolution	15 m/30 m (configurable)
Data updating rate	1 Hz~10 Hz (configurable)
Radial wind speed	-37.5 m/s ~ 37.5 m/s
Wind speed error	≤ 0.1 m/s
Wind direction error	± 0.1°
Data product	DBS/VAD wind profile, vertical flow, RHI/PPI/CAPPI radial velocity, virtual tower stare, turbulence wake, wake vortex, wind shear, backscatter intensity, multi-lidar measurement, GNSS position, lidar status, temperature humidity, pressure
Weight	< 90kg

Wind3D 6000 can meet different requirements of wind measurement such as complex-terrain wind field, wind turbine wake, remote virtual wind tower at sea, and stereoscopic distribution of atmospheric pollutants. Both two lidars are suitable for the experiments in this study.

5.3 Experimental details

The lidars were firstly calibrated by comparing the experimental data with the measurements

from the anemometer tower at the same place. The overall agreement between measurements from lidars and the anemometer was good, which showed the reliable accuracies of two lidars. Then the lidars were applied in measurements of two layout arrangements, one is the upstream-and-downstream arrangement and the other one is the side-by-side arrangement.

5.3.1 Two wind turbines in upstream-and-downstream arrangement

In this experiment, two wind turbines, WT1-4 and WT9-2, were selected to investigate the wake influence of upstream wind turbine on downstream wind turbine. The positions of wind turbines and lidars are shown in Table 5.3.

Table 5.3 Data of wind turbines and lidars

	Longitude	Latitude	Altitude
WT1-4	114.346372˚ E	40.992113˚ N	1794.6 m
WT9-2	114.348533˚ E	40.987956˚ N	1800.6 m
3D6000	114.351035˚ E	40.978225˚ N	1819.6 m
WP350	114.346302˚ E	40.993514˚ N	1766.2 m

To investigate the interaction of wind turbine wakes at a horizontal plane, PPI was applied in the experiments of upstream-and-downstream arrangement. When scanning in PPI mode, the lidar holds its elevation angle constant but varies its azimuth angle. Then the returns can be mapped on a horizontal plane. If the lidar rotates through 360 degrees, the scan is called a *surveillance scan*. However, in this study, the surveillance scan is no need, so Wind3D6000 only conducted a sector scan, which means it rotates through less than 360 degrees.

The prevailing wind directions of the wind farm are between north and northwest. WT1-4 and

WT9-2 were chosen with the consideration of both prevailing wind directions and the obstacles in wind field. Data were collected when the northwest wind blew, i.e. when WT9-2 was right under the wake effect of WT1-4. The positions of lidars and two measured wind turbines are demonstrated in Figure 5.8. The sector enclosed by red lines represents the scanning area of Wind3D 6000.

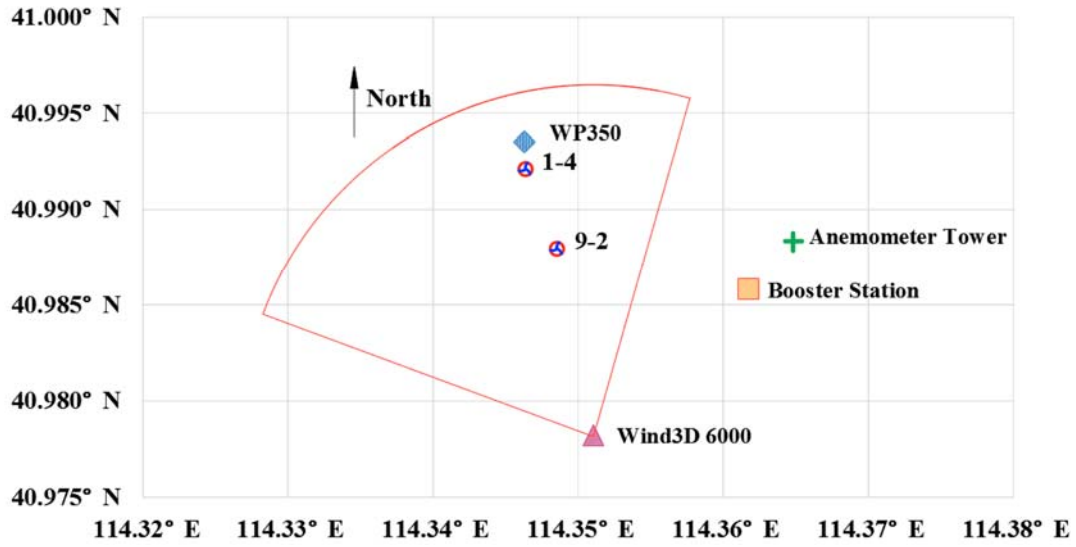

Figure 5.8 The positions of lidars and measured wind turbines

During the experimental period of this plan, wind directions were changing all the time. Therefore, the effective results must be carefully selected from all measured data. WT9-2 must be in the wake-influenced area of WT1-4, the stable wind should last long enough for lidars to measure the wind data, and the aerosol concentration must be within the operating ranges of lidars, in other words, the air could neither be too dirty nor too clean. A qualitied period is 8:33 am to 8:34 am, March 5th, 2019. In that moment, WT9-2 was partly under the wake effect of WT1-4. The inflow wind speed of WT1-4 at this selected period is shown Figure 5.9.

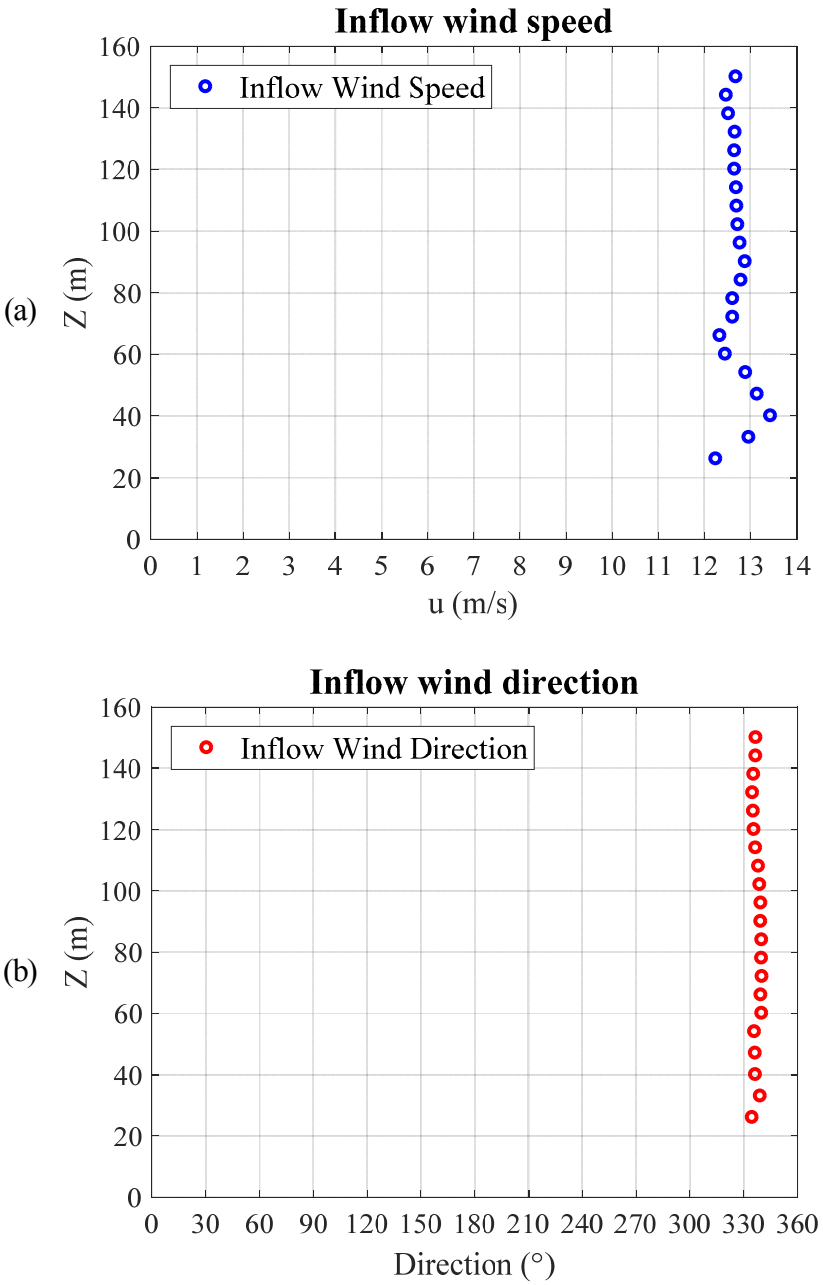

Figure 5.9 Inflow wind: (a) wind speed; (b) wind direction (time: 8:33 am to 8:34 am, March 5th, 2019)

The horizontal wind speed distribution at the height of 50 m is shown in Figure 5.10. Several wind turbines were in the scanning zone of 3D6000, of which the wind speeds are blank in the figure. Actually, it is because that objectives have a negative impact on lidars, so the wind speeds surround wind turbines could not be detected.

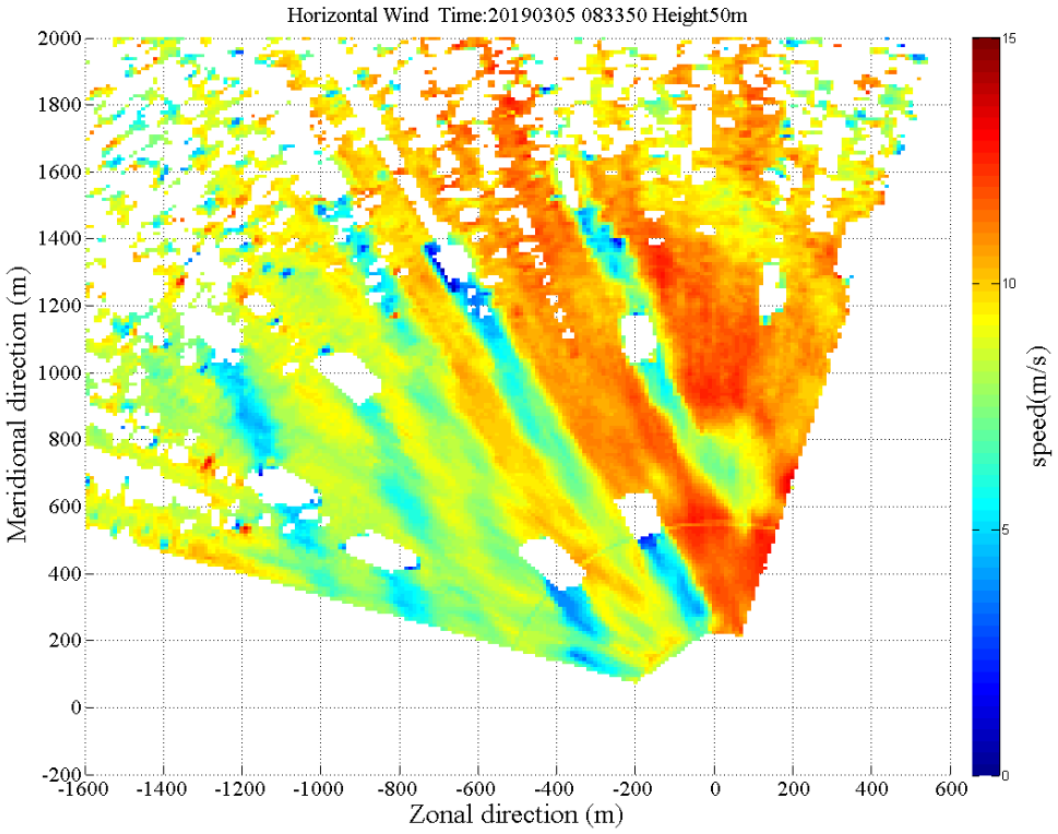

Figure 5.10 Horizontal wind speed distribution at the height of 50 m (time: 8:33 am, March 5th, 2019)

In order to quantitatively analyze the wake effect, wind speed data were filtered according to some analyzing lines, which are shown in Figure 5.11. WT1-4 and WT9-2 are marked as black points. Line 1, Line 2, Line3 and Line 4 are in the direction of wind turbine wakes. To be specific, Line 2 goes through WT1-4 and WT9-2. The other three lines are parallel to Line 2, whereas the spacing between every two adjacent lines is 1/2D. Perpendicular to Line 2, Baseline goes through WT1-4 and is applied to draw parallel lines that are used to study the wake effect in the cross sections. Line_U2D to Line_U6D are five lines to analyze the wind speed downstream of WT1-4 and in front of WT9-2. The distance from WT1-4 to Line _U2D is 2D, and the spacing between any of other two adjacent lines is 1/2D. Similarly, Line_D2D to Line_11D are ten lines

to analyze the wind speed downstream of WT9-2. The distance from WT9-2 to Line _D2D is 2D, and the spacing between any of other two adjacent lines is 1/2D as well.

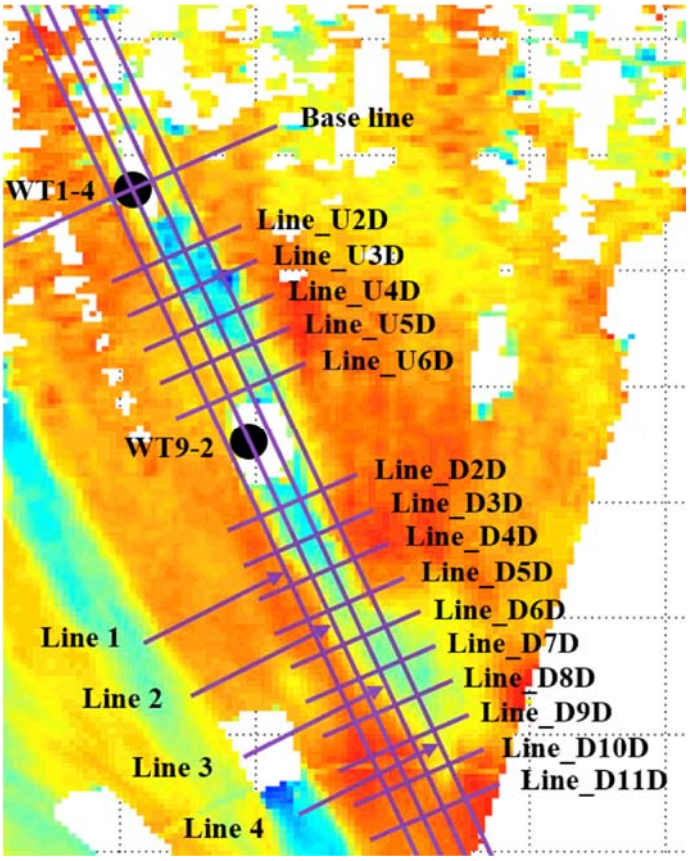

Figure 5.11 Diagram of analyzing lines

The wind speed data and the corresponding altitudes in the four lines in downstream direction are demonstrated in Figure 5.12. The relative positions of WT1-4 and WT9-2 are shown in the figure as well. The distance from WT1-4 to WT9-2 is 6.4D.

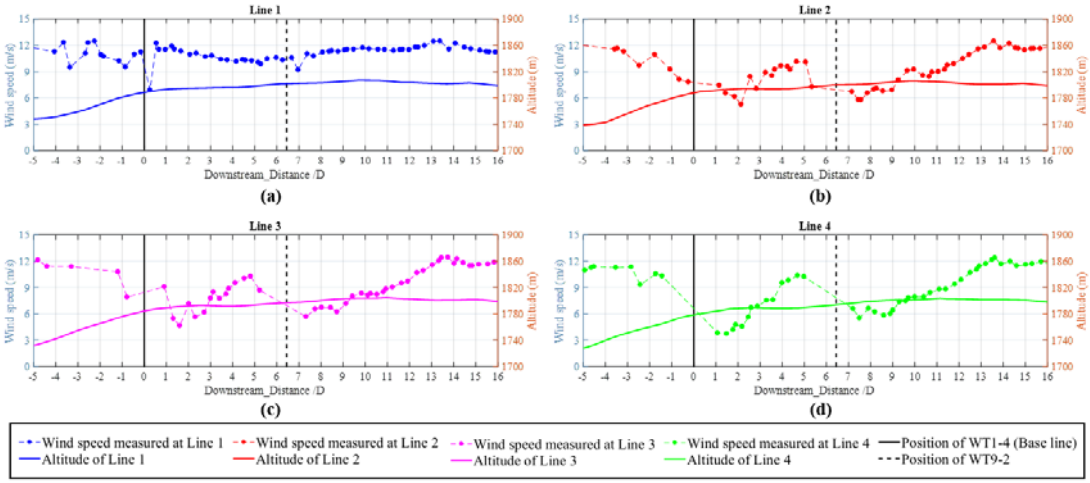

Figure 5.12 Measured wind speed data and altitudes in the downstream direction

The altitudes in four lines have a similar trend. The position of WT1-4 is at the top of the escarpment, therefore, the inflow could have an obvious speed-up phenomenon, which could also be seen from Figure 5.9 (a). After WT1-4, the terrain becomes much more flat, which may not have huge effect on the wake distribution. For the wind speeds, in Line 1, they turn out to be hardly influenced by wake effect. It could be seen that Line 1 is out of the wake zone. For the rest three lines, the severe wind deficits exist between 1D to 2D downstream distance for both WT1-4 and WT9-2. The largest deficit happens in Line 4 at about 1.5D distance downstream of WT1-4, with wind speed dropping from around 11 m/s to 3.8 m/s. The largest wind deficit for Line 2 and Line 3 are at 2.1D and 1.6D downstream distances from WT1-4, respectively. While for WT9-2, all three lines have a very similar trend that wind speeds decrease most at 1D distance downstream of WT9-2 (7.4D distance downstream of WT1-4). From the result, a difference in wake directions exists between the upstream and downstream wind turbines, which explains why the most wind deficit appears downstream of the front turbine rather than the behind turbine.

The measured wind speed data and the altitudes in the corresponding lines in the crosswind

direction behind WT1-4 are shown in Figure 5.13. The position of WT1-4 is set as the center, and the crosswind distance to the center is nondimensionalized by the ratio of turbine diameter.

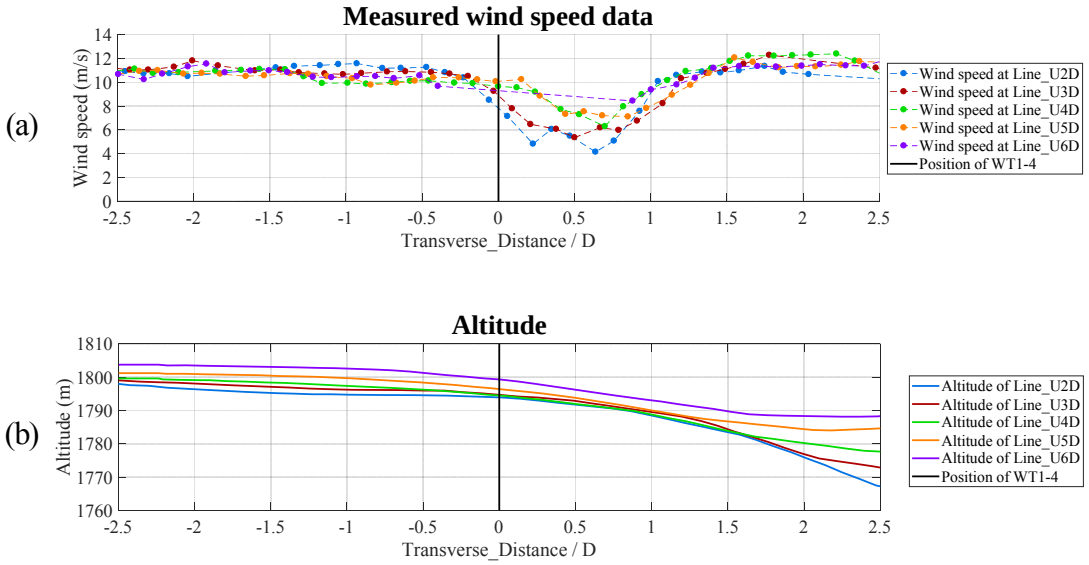

Figure 5.13 (a) Measured wind speed data and (b) Altitude in the crosswind direction (behind WT1-4)

From the crosswind figure, the deficit of wind speed is largest in the near-turbine zone and decreases with the downstream distance. The range of the wake-influenced area varies among different crosswind lines. The range is only 0.8D wide at 4D distance from WT1-4, but rises to 1.8D wide at 6D distance. The largest wind deficit appears at 2D distance downstream of WT1-4, with wind speed reducing from around 11.6 m/s to 4.1 m/s. The wake centerline is not the same as the position of WT1-4, and it tends to move right from 0.49D to 0.83D with the increase of the downstream distance. The altitudes on the left side are similar in four lines, whereas are much different on the right side. They increase in the downwind direction, with the largest difference of more than 30 m. The altitude is one of the main reasons that make the wake distribution asymmetry about the centerline.

The measured wind speed data and altitudes in the crosswind direction behind WT9-2 are shown in Figure 5.14. Similarly, the position of WT9-2 is set as the center in this case, and the crosswind distance to the center is also nondimensionalized by the ratio of diameter of the turbine.

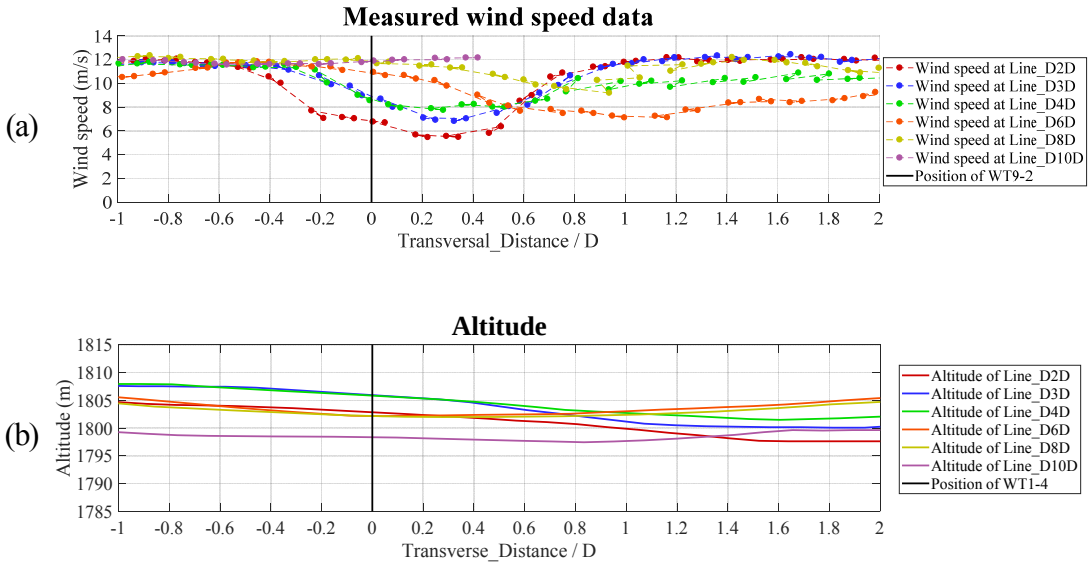

Figure 5.14 (a) Measured wind speed data and (b) Altitude in the crosswind direction (behind WT9-2)

The largest wind speed deficit appears at 2D distance downstream of WT9-2 as expected, with wind speed from around 12.0 m/s to 5.5 m/s. The range of the wake-influenced area is from -0.48D to 1.2D. With the increase of the downstream distance to the turbine, the wake centerline continues moving right from 0.2D to 0.9D at the 8D downstream distance in the crosswind direction. Some of the wind speed data are not available at 10D downstream distance, which is caused by the limitation of scanning area of 3D6000. The wind deficit at the far-wake zone is also not as large as that at near-wake zone. The smallest wind speed is 9.2 m/s at 8D downstream distance. The terrain after WT9-2 is much more flat, with the 10 m biggest altitude difference. Overall, the terrain on the right side is lower than that on the left side. The altitudes fluctuate all

the time in the downwind direction. Meandering ridges exist in this area. The variation of terrain is a main factor that makes the centerlines of wakes change.

From the experiment of the upstream-and-downstream arrangement, some important conclusions could be drawn. Firstly, the results meet well with the expectations in some aspects, with the increase of downstream distance to the wind turbine, the range of the wake-influenced area expands and the largest wind speed deficit at each crosswind line decreases gradually. Secondly, the topographical condition has a considerable effect on the wake distribution. The fluctuation of terrain altitudes makes the downstream wake more complicated. Thirdly, new findings have been pointed out that the wake centerlines of upstream and downstream wind turbines may be different. Under that circumstance, even though the downstream turbine is under the wake effect of the upstream turbine, the wind deficit of downstream turbine is not as much as expected, and the largest wind deficit might even appear before it.

5.3.2 Four wind turbines in side-by-side arrangement

The next experiment is to investigate the wind distribution of turbines in side-by-side arrangement. In this experiment, four wind turbines, WT10-1, WT10-2, WT10-3 and WT10-4 were selected, as they were located almost in one line. The positions of wind turbines and lidars in this experiment are shown in Table 5.4.

Table 5.4 Data of wind turbines and lidars

	Longitude	Latitude	Altitude
WT10-1	114.354838° E	40.998869° N	1857.4 m
WT10-2	114.358255° E	40.998280° N	1884.5 m
WT10-3	114.361603° E	40.998293° N	1880.7 m
WT10-4	114.364788° E	40.997852° N	1877.3 m
3D6000	114.364677° E	40.987484° N	1814.5 m
WP350	114.357298° E	40.999399° N	1872.3 m

PPI scanning mode was also applied in this experiment. The positions of two lidars and four measured wind turbines are demonstrated in Figure 5.15. The sector enclosed by red lines represents the scanning area of Wind3D 6000.

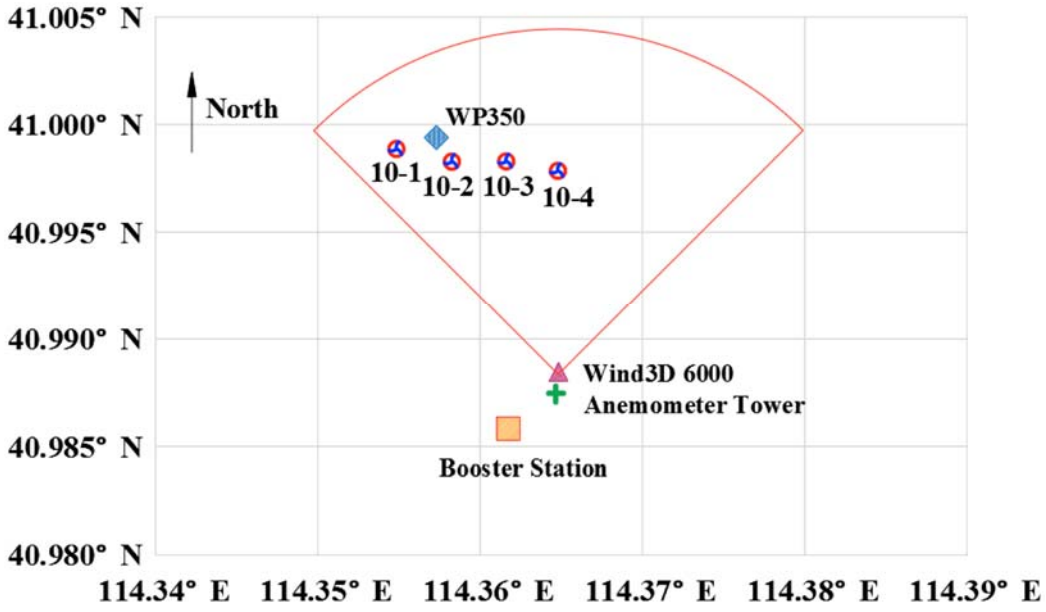

Figure 5.15 The positions of lidars and measured wind turbines

In this experiment, the effective results are supposed to be selected when four wind turbines

were operating simultaneously, and no turbine was under the wake effect of other turbines. The stable wind should also last long enough, and the aerosol concentration must be within the operating ranges of lidars. A qualitied period is 4:14 am to 4:15 am, March 27th, 2019. The most ideal location of WP350 to record the inflow may be in the north of turbines and in the middle of WT10-2 and WT10-3, but the best position cannot be achieved because of the fens and obstacles in the wind farm. Therefore, a position in front of WT10-2 was chosen. The inflow wind speed of WT10-2 of this selected period is shown in Figure 5.16.

(a)

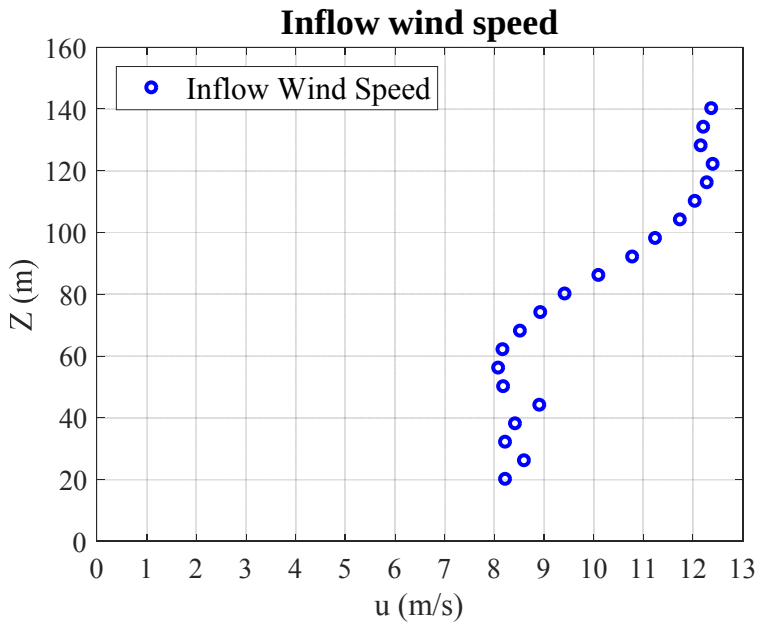

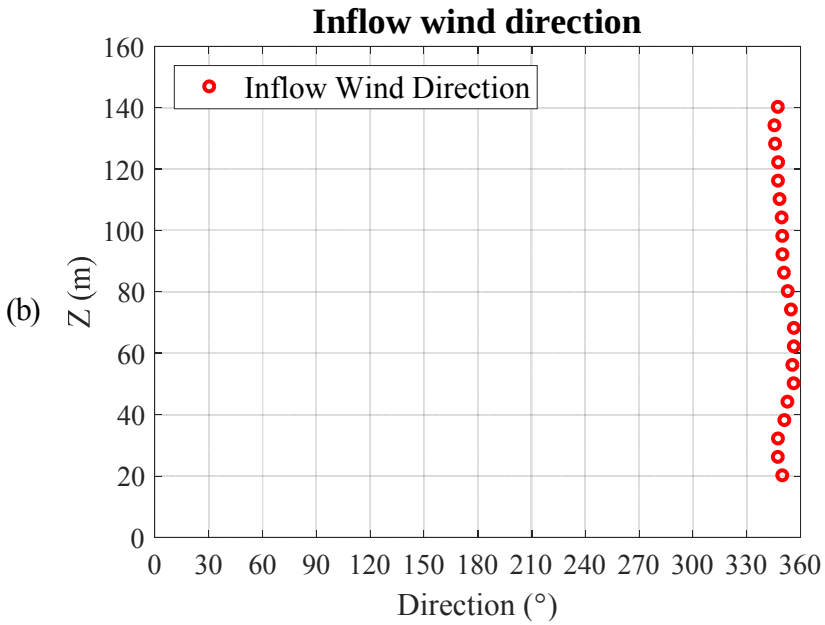

Figure 5.16 Inflow wind: (a) wind speed; (b) wind direction (time: 4:14 am to 4:15 am, March 27th, 2019)

The horizontal wind speed distribution at the height of 135 m is shown in Figure 5.17. Four selected wind turbines were in the scanning zone of 3D6000, and were marked as black spot. In that period, the wind direction was northwest, all four turbines had wakes behind them. The wakes were independent at the beginning, but had some interactions at the positions of far downstream distance.

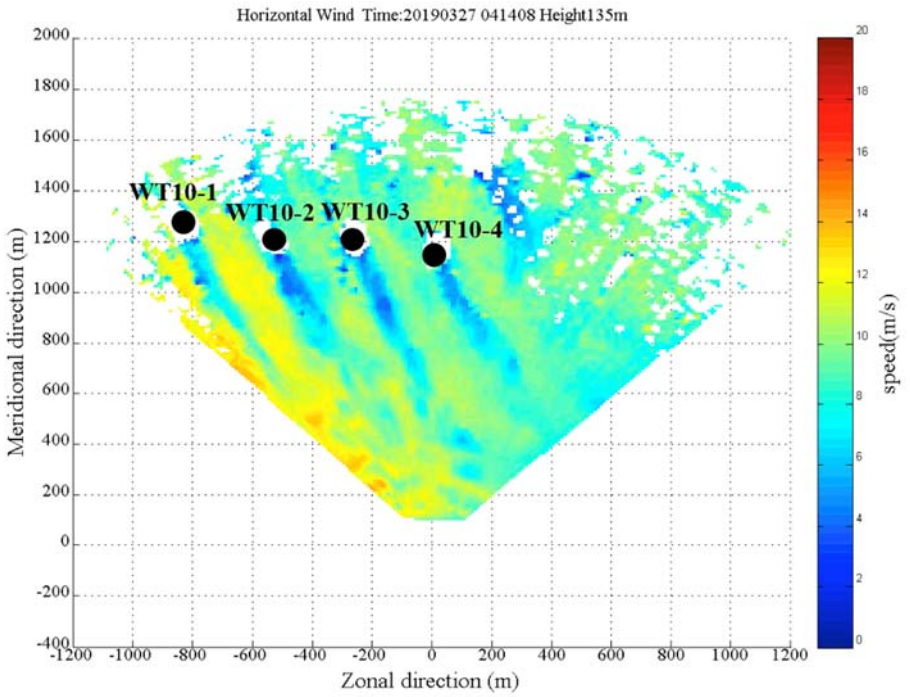

Figure 5.17 Horizontal wind speed distribution at the height of 135 m (time: 4:14 am, March 27th, 2019)

Similar analyzing process has also been done as that in the experiment of upstream-and-downstream arrangement. Wind speed data are filtered according to four downwind and ten crosswind analyzing lines, as shown in Figure 5.18. Line 1, Line 2, Line 3 and Line 4 are in the wake directions and go through WT10-1, WT10-2, WT10-3 and WT10-4, respectively. Baseline is a line fitted by four wind turbines, and it goes through the location of WT10-2. Line_1D to Line_10D are ten lines parallel to Baseline and are applied to analyze the wind speed in the cross sections at different downstream distances of four turbines. The distance from Baseline to Line _1D is 1D, and the spacing between any other two adjacent lines is 1D as well.

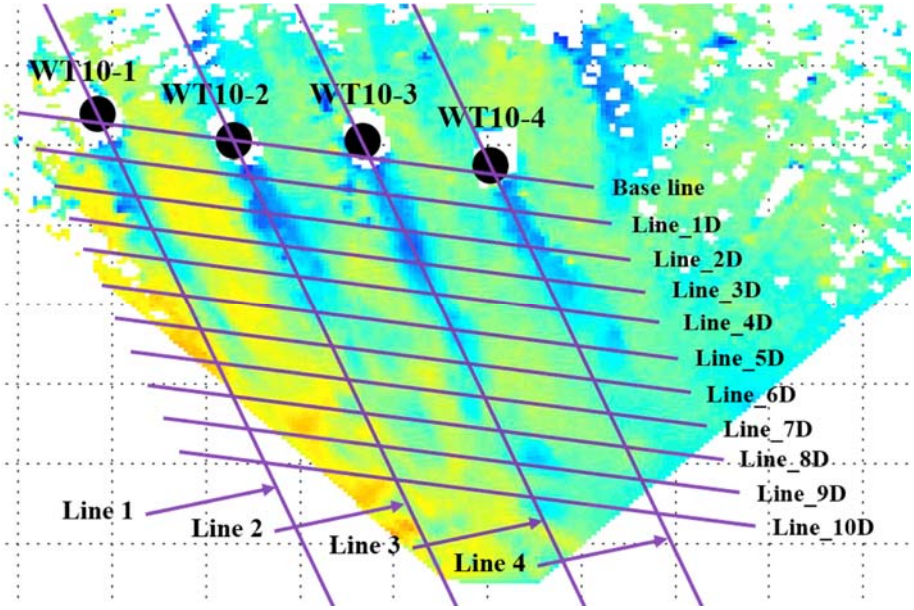

Figure 5.18 Diagram of analyzing lines

The wind speed data and the corresponding altitudes in the four lines in downstream direction are demonstrated in Figure 5.19. The position of wind turbine, i.e. Baseline, is shown in the figure as well.

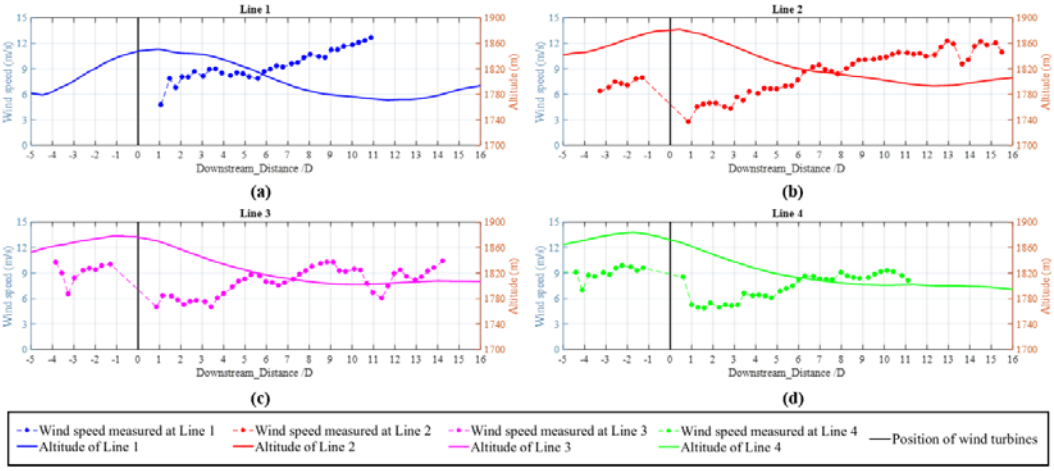

Figure 5.19 Measured wind speed data in the downstream direction

Huge deficits of wind speed in all four lines happen right behind the wind turbines. The wind

speeds reduce mostly to 4.7 m/s, 2.8 m/s 5.0 m/s and 4.9 m/s in four lines, respectively. Fluctuations are observed when winds restoring to the environmental speeds, the amplitude of which are extremely large in the far-wake zone. Referred to Figure 5.17, the wakes are weaker and become unstable in the far-wake zone, this may be caused by the rotations of wind turbines, so the interactions between wakes and environmental winds are far unstable. The topographical condition of this area is also complex. The three left wind turbines are installed on the top of ridges, whereas WT10-4 is installed behind the top of the ridge. The incoming wind of WT10-4 is blocked by the terrain, which explains why the wind speeds are pretty large before it but are much small among four analyzing lines before the turbine.

The measured wind speed data in the crosswind direction behind four wind turbines is shown in Figure 5.20. The positions of turbines are marked as dash line in the figure. A middle point between WT10-2 and WT10-3 is set as original point in the crosswind direction, and the crosswind distances to the original point are nondimensionalized by the ratio of turbine diameter.

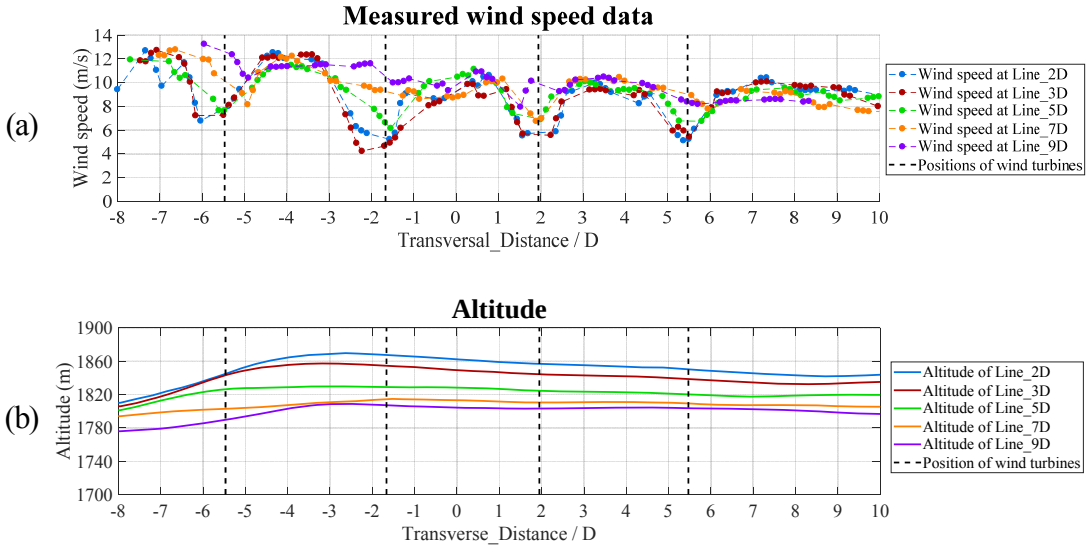

Figure 5.20 (a) Measured wind speed data and (b) Altitude in the crosswind direction

From the above figures, the inflows of four wind turbines are actually pretty different. A decrease trend of wind speed from WT10-1 to WT10-4 is observed. It has a close relationship with the typical topography that the altitudes increase from the left side to the middle of WT10-1 and WT10-2 and then decrease to the right side. The deficit of wind speed is also the largest in the near-turbine zone and decreases with downstream distance increasing. The largest wind deficit appears at 3D distance from WT10-2, with wind speed reducing to 4.2 m/s. The wind deficit could not be ignored even as far as 9D downstream distance, although the wind speeds are all larger than 8.0 m/s. The analyzing lines generally fit well with the wake centerlines of WT10-3 and WT10-4, except for the little difference in lines of WT10-1 and WT10-2.

The range of the wake-influenced area is not easy to be identified, especially in the far-wake zone, where wakes of adjacent turbines may have a complicated interaction. In the analyzing line right behind the turbines, the difference of wind speed at different downstream distances is much larger than that in environmental wind. For example, the range of wind speeds in line 1 is from around 7.3 m/s to 13.0 m/s, whereas at the -4D transversal position, that range is from 11.2 m/s to 12.2 m/s. Similar phenomenon could also be found in other analyzing lines and transversal positions. Therefore, it should be noticed that the wind turbine does have a huge impact on the distribution of wake spatially, especially where it is right behind the wind turbine in the downwind direction.

The distribution of wind speed at the height of 135 m represents a typical situation. To study the spatial wind distribution, more wind data from different heights should be involved. Figure 5.21 demonstrates the measured wind speeds in four heights, 65 m, 100 m, 135 m and 170 m, at a series of downwind distance from 2D to 9D.

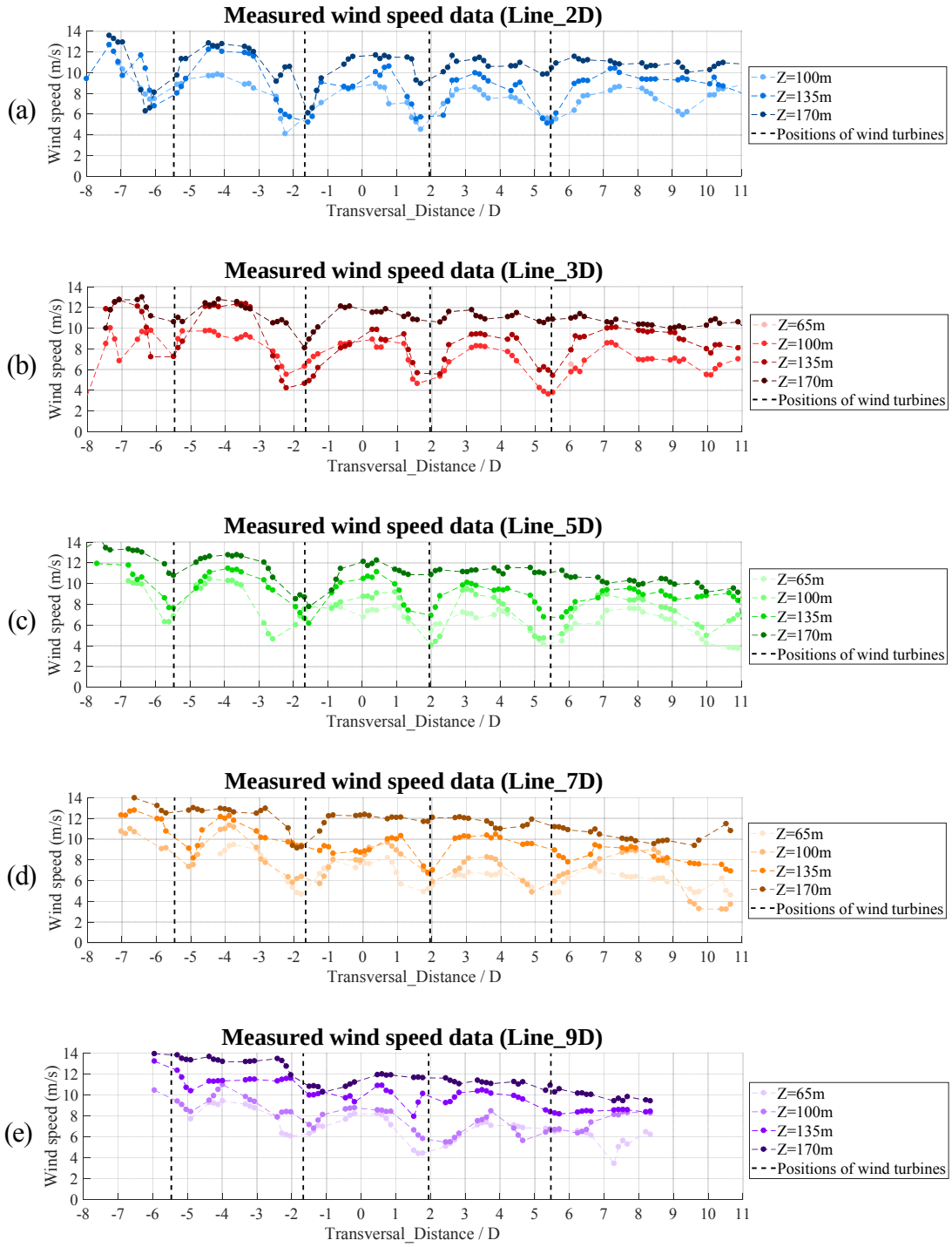

Figure 5.21 Measured wind speed data in different heights in: (a) Line_2D; (b) Line_3D; (c) Line_5D; (d) Line_7D and (e) Line_9D.

The data at 2D downstream distance only involves three heights, which is caused by the limited scanning space of 3D6000. It is also the reason why there are few data at 3D downstream

distance at height of 65 m and the range of wake in the crosswind direction in 9D downwind distance is much smaller than those at other downwind distances.

In the most of the experimental time, wind speeds at higher positions tend to be larger than those at lower positions. However, there are some exceptions when wind speeds did not increase with the height, such as at WT10-4 position in Line_9D, the wind speed at 65 m is higher than that at 100 m. Similar phenomenon is also found at all turbines positions in Line_2D, WT10-1 and WT10-3 positions in Line_3D, WT10-2 and WT10-4 positions in Line_5D, and WT10-2 position in Line_7D. All these positions are around positions of turbines, which also indicates the complex impact of turbines on wake distributions.

From the experiment of the side-by-side layout arrangement, there are also some important conclusions. Firstly, as is drawn from the upstream-and-downstream arrangement, the largest wind speed deficit decreases along the downwind direction and the centerlines of wakes may also be different among the closely-installed wind turbines. Secondly, in the downwind analyzing line right behind turbines, the difference of wind speed at different heights is much larger than that in the environmental wind. Sometimes, nearby the turbines, wind speeds do not increase with the height. All these demonstrate that the wind turbine has a huge impact on the wake distribution in the downwind direction behind the turbine. The reduced wind speeds then restore to the environmental wind beyond the turbine zone.

5.4 Summary

In this chapter, wind field experiments were carried out in order to analyse and better understand wake effect in the complex terrain. The work reported herein is summarized as follows:

(1) The site and layout of the tested wind farm were introduced. The Shiren wind farm has a capacity of 75 MW and consists of 50 numbers of 1.5 MW wind turbines of two types, which are installed at a complex hilly terrain in north China, where the wind resources are relatively rich. The largest difference of altitude is 171.3 m in the farm, with the highest wind turbine installed at 1894.1 m high and the lowest one installed at 1722.8 m. It is a good representative of a complex-terrain wind farm, of which the measured wind data deserves investigating in depth.

(2) Two lidars were applied in the experiments. WindMast WP350 is a vertical-wind-mast-type lidar, which was used to measure the inflow before the wind turbine. The wind speed and wind profile can be continuously detected with 30 height gates from 20 m to 350 m above the lidar. Wind3D 6000 is three-dimensional-scanning-wind lidar. It was used to capture the wake development behind the tested wind turbines. Both two lidars were calibrated by the anemometer tower in the wind farm first, and then were applied in the experiments.

(3) One experiment was based on two wind turbines in the upstream-and-downstream layout arrangement. The aim of this experiment was to investigate the influence of the upstream wind turbine on downstream wind turbine. Data were collected when WT9-2 was right under the wake effect of WT1-4. According to the results, the observed results agreed with the previous studies that the range of the wake-influenced area expands and the largest wind speed deficit at each crosswind line decreases gradually along the downstream direction. Meanwhile, the wake centerlines of the upstream and downstream wind turbines may be different, which shows that the wind deficit of downstream turbine is not as much as expected, and the largest wind deficit might even appear before it. The terrain in this

experiment is pretty flat, which may not have huge effect on the wake distribution.

(4) The other experiment was based on four wind turbines in the side-by-side layout arrangement. The aim of this experiment was to investigate the wake development behind a row of wind turbines. The effective results were selected when four wind turbines were operating simultaneously, and no turbine was under the wake effect of other turbines. The stable wind lasted long enough, and the aerosol concentration were within the operating ranges of lidars as well. From this experiment, huge deficits of wind speed in all four analyzing lines happened right behind the wind turbines. The wind speeds reduced most to 2.8 m/s. Fluctuations were observed in the far-wake zone. The range of the wake-influenced area was not easy to be identified, especially in the far-wake zone, where wakes of adjacent turbines had a complicated interaction. The terrain in this experiment is much more complex, which has huge effect on the wake distribution in terms of deficits of wind speeds, centerlines and restoring wind speeds.

Chapter 6

Validations of Three-Dimensional Wake Models with the Wind Field Measurements in a Complex Terrain

In this chapter, the analytical 3-D wake models for single and multiple wind turbines developed in previous chapters are validated by wind data measured at the complex-terrain hilly wind farm in China. The site and layout information about the measured wind farm has been introduced in Chapter 5. The wake models take into account the variation of wind speed in vertical direction. The 3-D wake models for a single wind turbine and multiple wind turbines are validated by the measurements of one wind turbine and one line of four wind turbines, respectively. RHI was applied to obtain the profiles of wind speed in the vertical direction and PPI scanning modes were adopted to obtain the profiles of wind speed in the horizontal directions. When validating the wake model for a single wind turbine in vertical direction, the model can predict the wind speeds with acceptable accuracy, especially at positions beyond 10D downstream distance or higher than 100 m. When validating the wake model for multiple wind turbines in the horizontal direction, the model also has a reliable accuracy at the far wake positions and near the inflow measuring site, but it cannot predict the deficits of wind speed before an operating wind turbine and was not accurate in some particular complicated situations.

6.1 Comparisons between measurements and model results on wind speeds of a single wind turbine

When validating the wake model for a single wind turbine, the vertical profiles of wind speeds are representative. Therefore, RHI was firstly adopted in the experiments. When scanning in

RHI mode, the 3D6000 holds its azimuth angle constant but varies its elevation angle. The returns can then be mapped on a vertical plane. The elevation angle rotates at a range covers all wake zone. In this experiment, WT10-2 was selected as the target wind turbine. The positions of wind turbines and lidars in this experiment are shown in Table 6.1.

Table 6.1 Data of wind turbines and lidars

	Longitude	Latitude	Altitude
WT10-2	114.358255˚ E	40.998280˚ N	1884.5 m
3D6000	114.364677˚ E	40.987484˚ N	1814.5 m
WP350	114.357298˚ E	40.999399˚ N	1872.3 m

Vertical profiles of three sections are applied to compare with wake models. One section is at the central section and the other two are the side sections that are 39 m from the central section.

6.1.1 At the central section

A clear profile of wind speed was obtained on March 16th, 2019. The overview RHI wind speed distribution is shown in Figure 6.1.

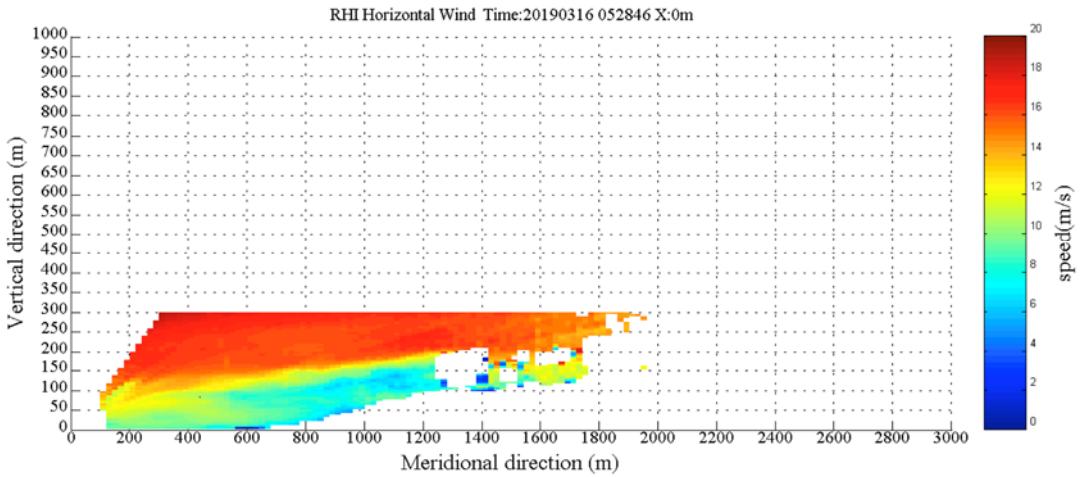

Figure 6.1 RHI wind speed distribution at Y=0 m (time: 5:28, March 16th, 2019)

From the figure, it can be seen that WT10-2 was installed on the top of a hill. The wake developed not along the horizontal axis but along the slope of the hill. The inflow wind speed at the measuring time is shown in Figure 6.2. To calculate the wake distribution with the 3-D wake model, the incoming wind speed distribution $U_0(z)$ should be determined as accurately as possible. The simulation of inflow with the wake model is also compared in the figure.

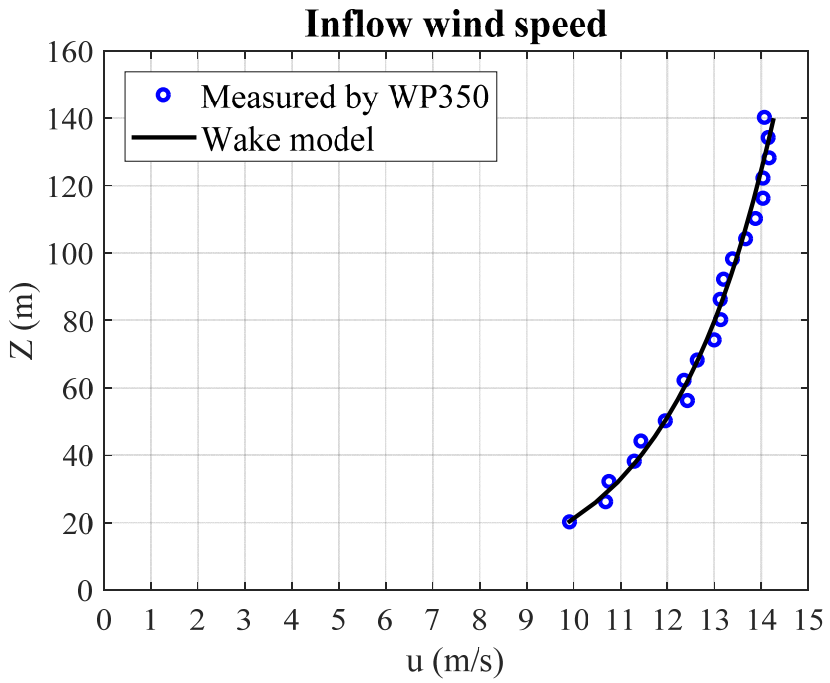

Figure 6.2 Inflow wind speed distribution and the simulation of 3-D wake model (time: 5:28 am to 5:29 am, March 16th, 2019)

The inflow wind speed distribution simulated by the wake model fitted well with the measured wind speeds. Then comparisons of wind speeds were carried out between measurements and simulations from the 3-D wake model at a series of downstream distances. The results of comparisons are demonstrated in Figure 6.3.

(a)

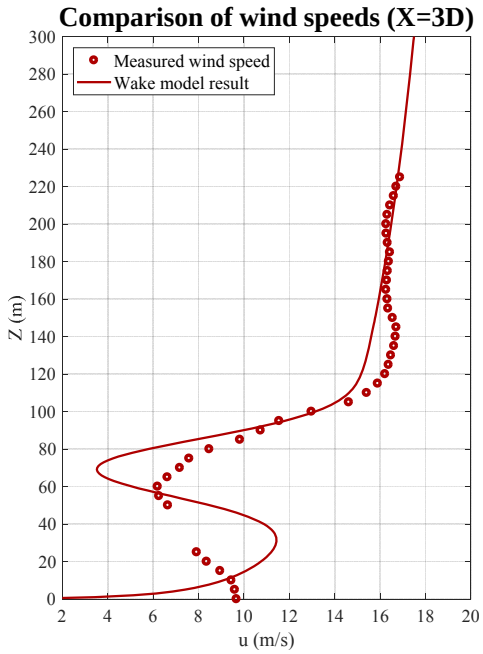
Comparison of wind speeds (X=3D)
Measured wind speed
Wake model result
Z (m)
u (m/s)

(b)

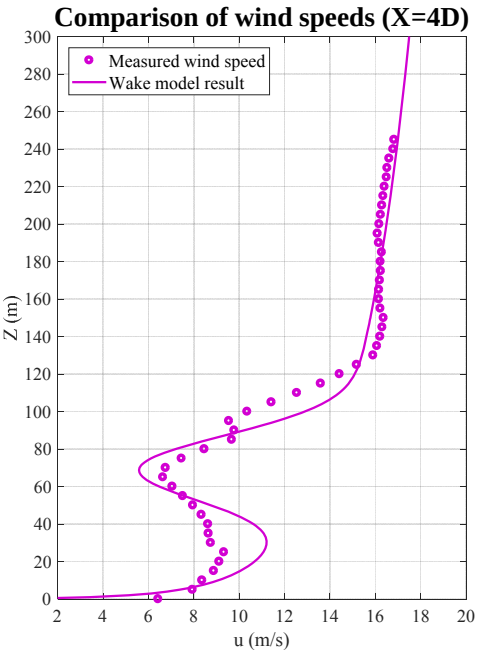
Comparison of wind speeds (X=4D)
Measured wind speed
Wake model result
Z (m)
u (m/s)

(c)

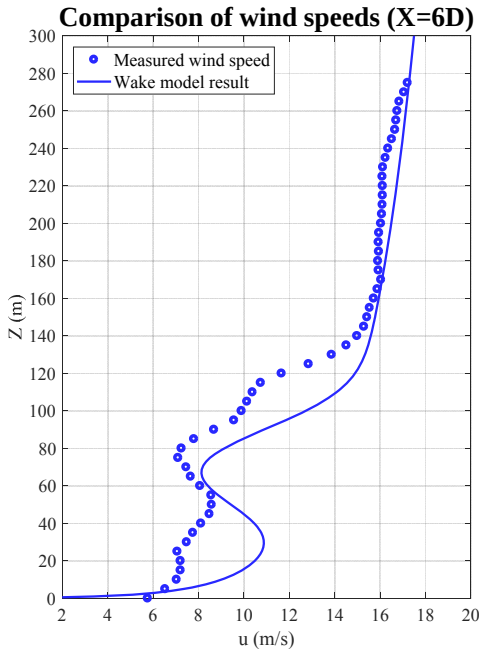
Comparison of wind speeds (X=6D)
Measured wind speed
Wake model result
Z (m)
u (m/s)

(d)

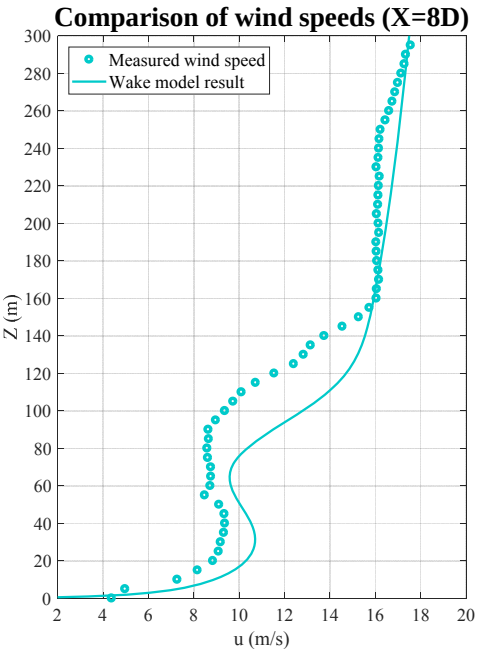
Comparison of wind speeds (X=8D)
Measured wind speed
Wake model result
Z (m)
u (m/s)

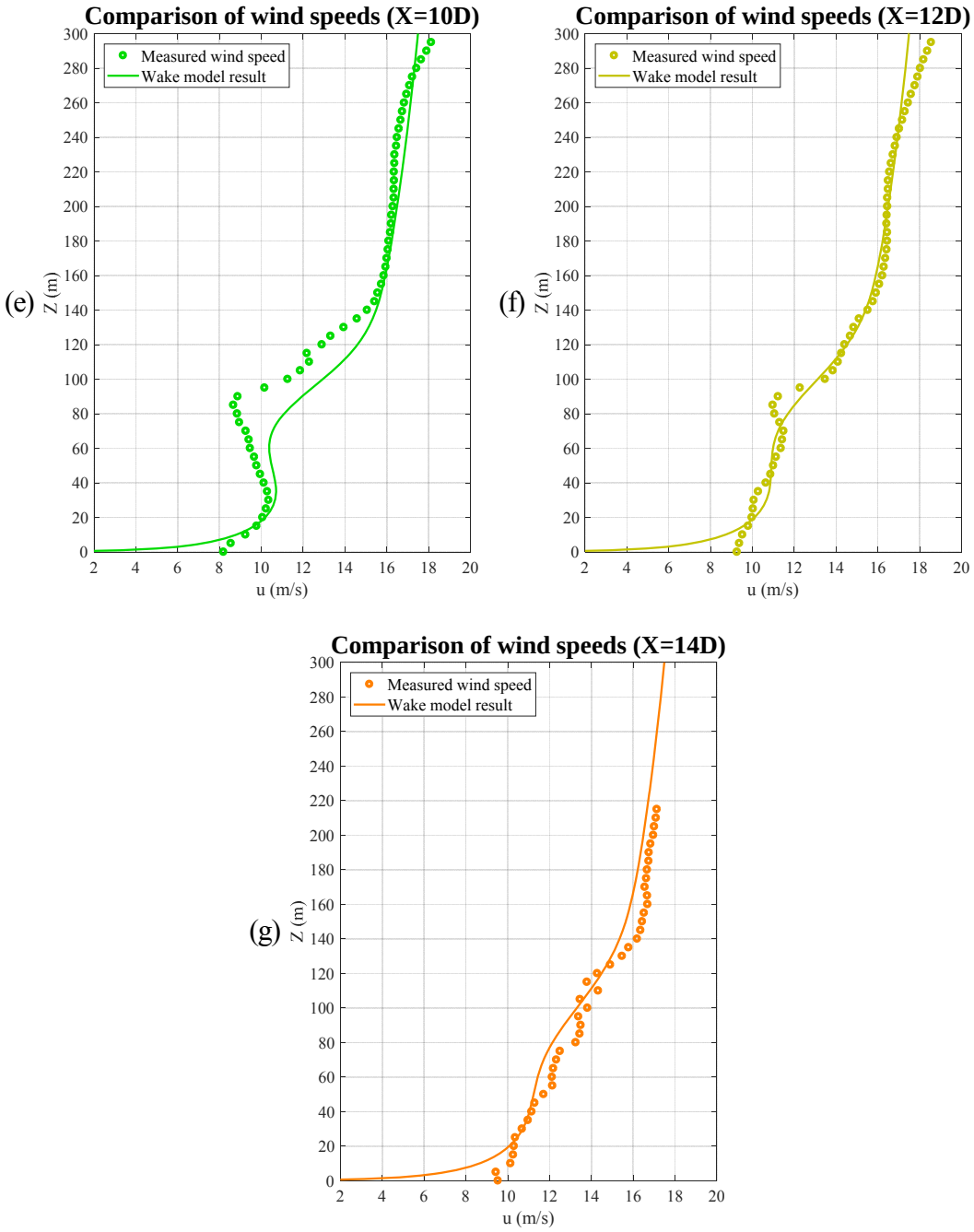

Figure 6.3 Comparisons of wind speeds between measurements and simulations from 3-D wake model at downstream distances of: (a) X=3D; (b) X=4D; (c) X=6D; (d) X=8D; (e) X=10D; (f) X=12D and (g) X=14D

From comparisons, the 3-D wake model can predict the trend of wind speed in the height direction with acceptable accuracy. At the positions beyond 10D downstream distance, the 3-D wake model predicts wind speed well at all heights. Within the range from 6D to 10D, the wake

model tends to overestimate wind speeds under the height of 140 m, but predicts well above that height. In the near-wake zone, the wake model has good accuracy where the positions are higher than 100 m. At the heights near the turbine hub, the 3-D wake model tends to underestimate wind speeds, especially right at the hub height, but still overestimates wind speeds near the ground. The relative errors between wake model and measurement are shown in Figure 6.4.

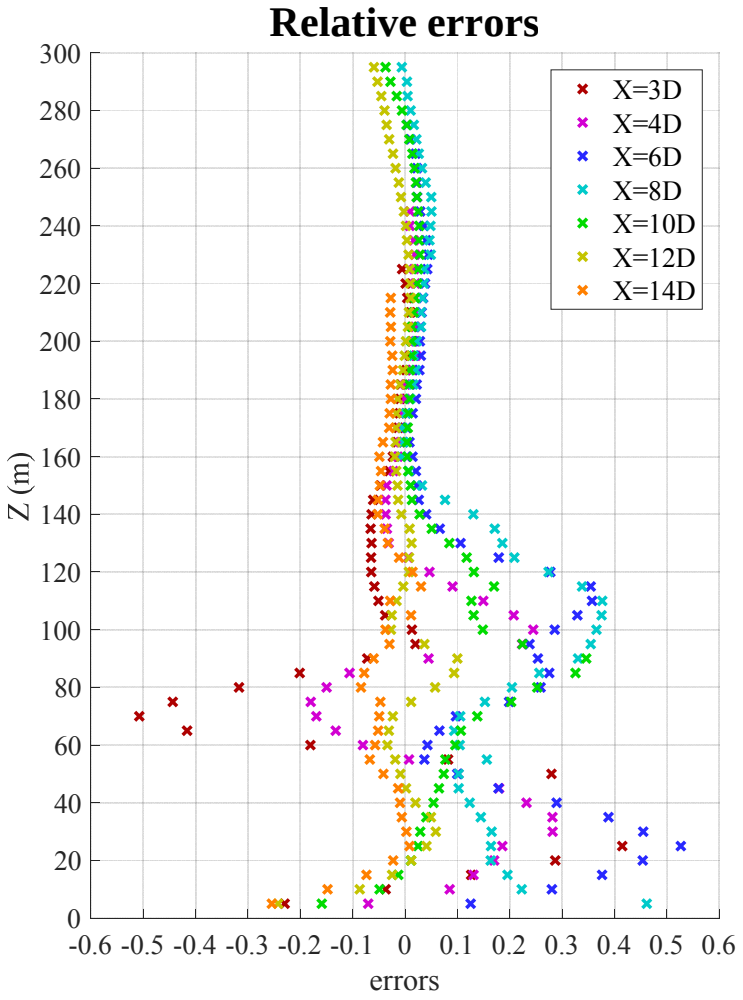

Figure 6.4 Relative errors between 3-D wake model and measured wind speeds at different downstream distances

As analysed before, the 3-D wake model have good accuracy in the higher zone. All relative errors are within 10% where positions are higher than 140 m. Some large errors happen at the

positions lower than 40 m, which may be because that the complex turbulence effect is not considered in the wake model. For the heights between 40 m and 100 m, the largest error happens at the 3D downstream distance and at the hub height, which is approximate -52%. The errors tend to be small with the increase of the downwind distance.

6.1.2 At the side sections

The wake model is then validated at two side sections at the same moment of the central section comparison. The two sections are 39 m away from the central section. To study the wake model in depth, the wind speeds at each sections are compared with the wake model results. The comparisons at different downwind distances are shown in Figure 6.5.

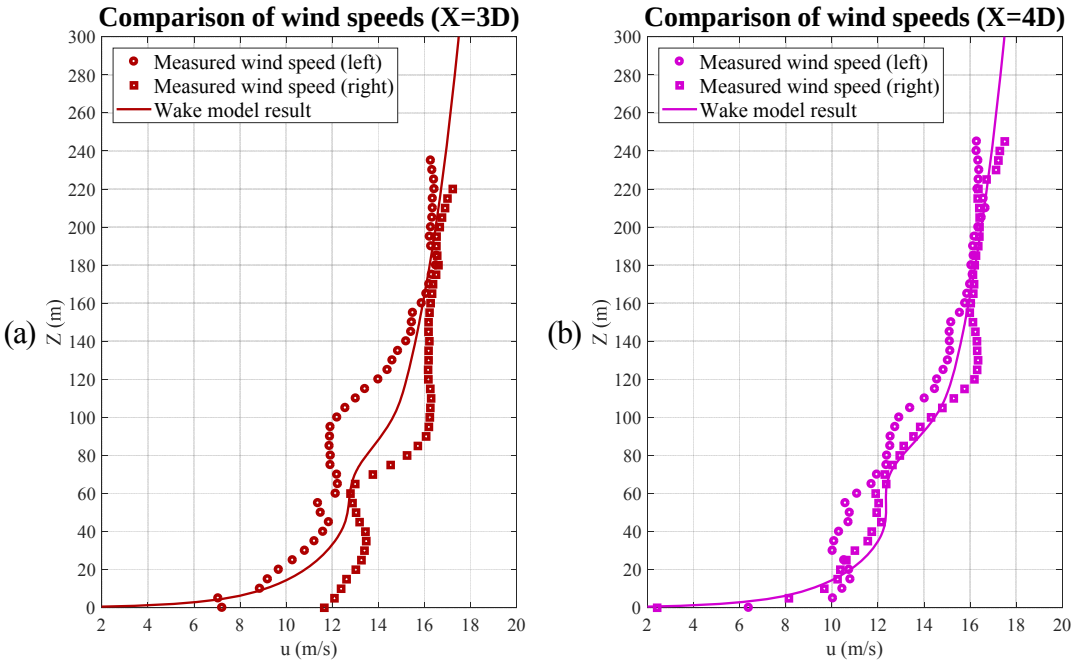

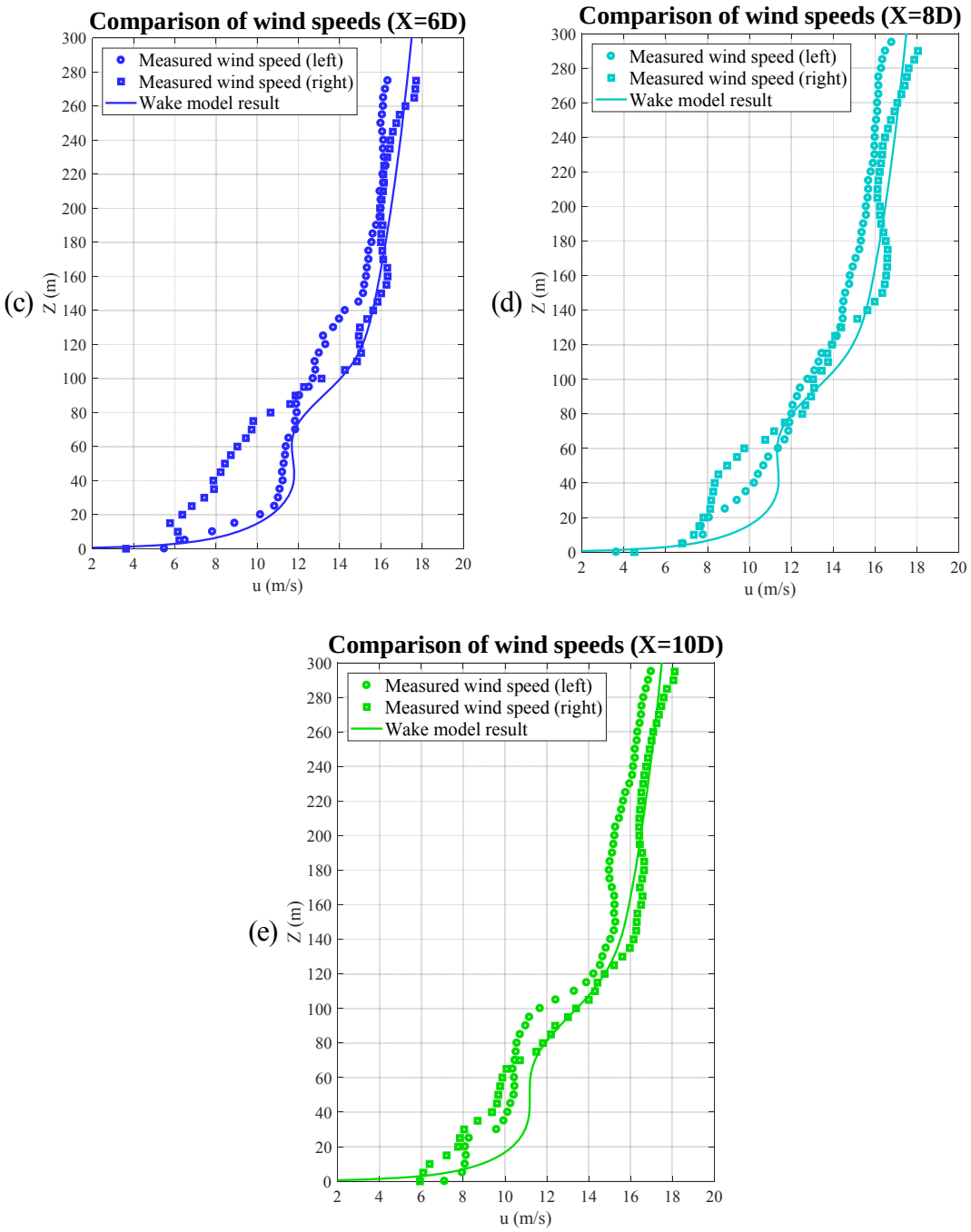

Figure 6.5 Comparisons of wind speeds between measurements and simulations from 3-D wake model at downstream distances of: (a) X=3D; (b) X=4D; (c) X=6D; (d) X=8D and (e) X=10D

From the above figures, the 3-D wake model has a better agreement with the measured wind speed at side sections than those at the central section. Although the wind speeds at the

symmetrical positions are different, the predictions from the 3-D wake model are close to the mean values of the wind speeds from two sides. The 3-D wake model still tends to overestimate wind speeds but at a very small extent. The specific relative errors between the 3-D wake model and the measured wind speeds are shown in Figure 6.6.

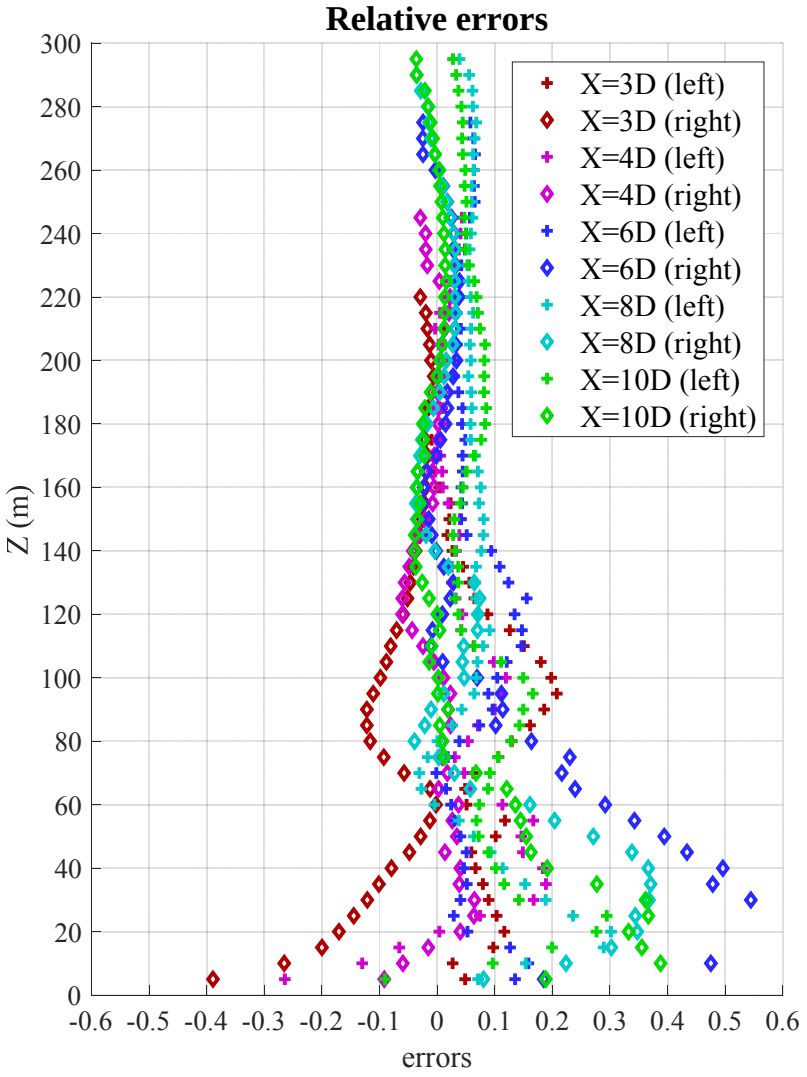

Figure 6.6 Relative errors between the 3-D wake model and the measured wind speeds at different downstream distances

Relative errors at two side sections are much smaller than those at the central section. All errors are smaller than 30% at the positions above 60 m height. The largest error is 54%, and happens

in the right section at 6D downwind distance. The largest error is not at the hub height, but at around the 30 m height, which means the error may be caused by the complex terrain or the turbulence near the ground. If not consider the near-ground errors, the 3-D wake model has a good overall agreement with the measured wind speeds.

6.2 Comparisons between measurements and model results on wind speeds of multiple wind turbines

The next experiment is to validate the 3-D wake model for multiple wind turbines. In this experiment, WT10-1, WT10-2, WT10-3 and WT10-4 were selected. The four wind turbines were installed almost in one line but at various altitudes. The arrangement of this experiment was the same as the side-by-side arrangement in Chapter 5. The positions of wind turbines and lidars can be found in Table 5.4.

To investigate the interaction of wakes from multiple wind turbines in a horizontal plane, PPI was applied in this plan. 3D6000 only conducted a sector scan, which means it rotates through less than 360 degrees. The horizontal wind speed distribution at the height of 135 m is shown in Figure 6.7.

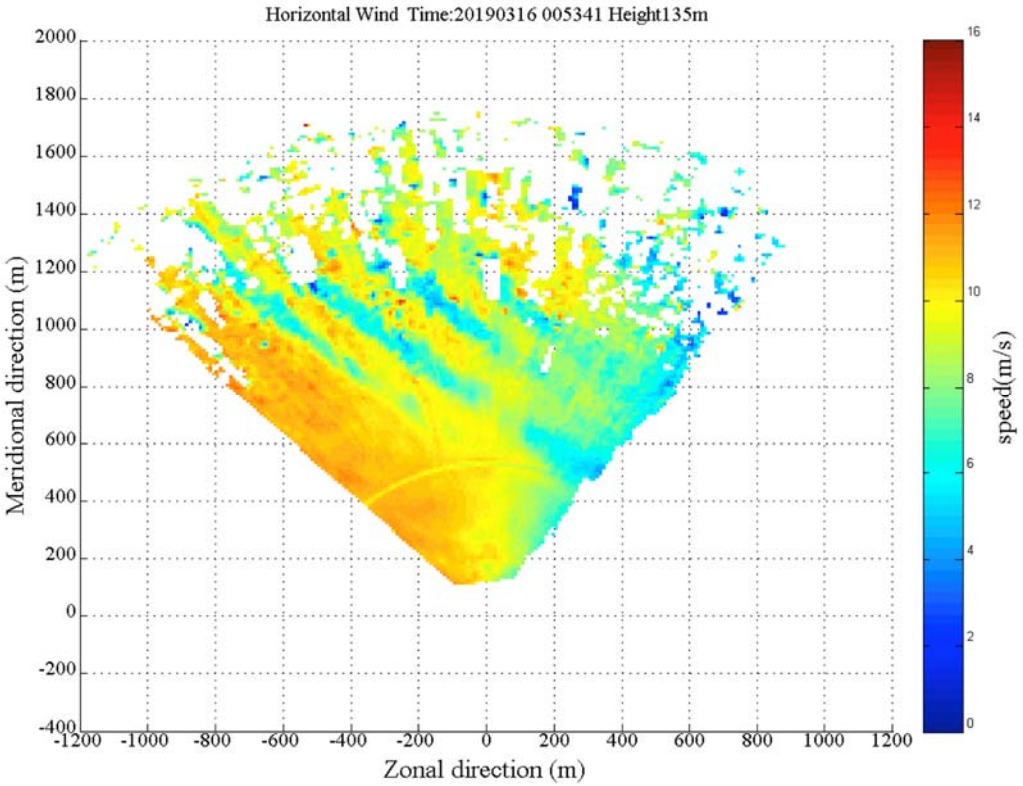

Figure 6.7 Horizontal wind speed distribution at the height of 135 m (time: 0:53 am, March 16th, 2019)

The moment with effective results was selected when four wind turbines were operating simultaneously, and no turbine was under the wake effect of other turbines. It can be seen from the figure that wakes happen behind wind turbines and then develop along the wind direction. The wake-influenced area expands with the increase of the downstream distance. In the far-wake zone, some positions are overlapped with wakes from two upstream wind turbines simultaneously. The inflow wind speed distribution and the simulation of 3-D wake model are shown in Figure 6.8.

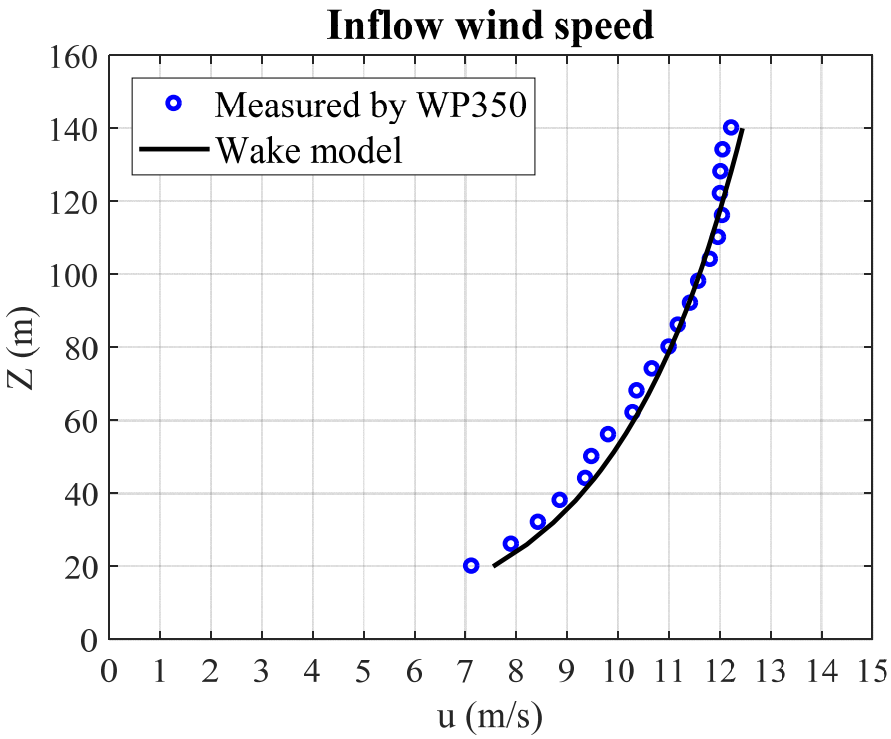

Figure 6.8 Inflow wind speed distribution and the simulation of 3-D wake model (time: 0:53 am to 0:54 am, March 16th, 2019)

The 3-D wake model with log law also shows good accuracy in simulating the inflow wind speed. Then, to quantitatively compare the results of the 3-D wake model to the measured data, some analyzing lines were set according to the wind direction. Wind speed data are filtered according to four downwind and seventeen crosswind analyzing lines, as shown in Figure 6.9.

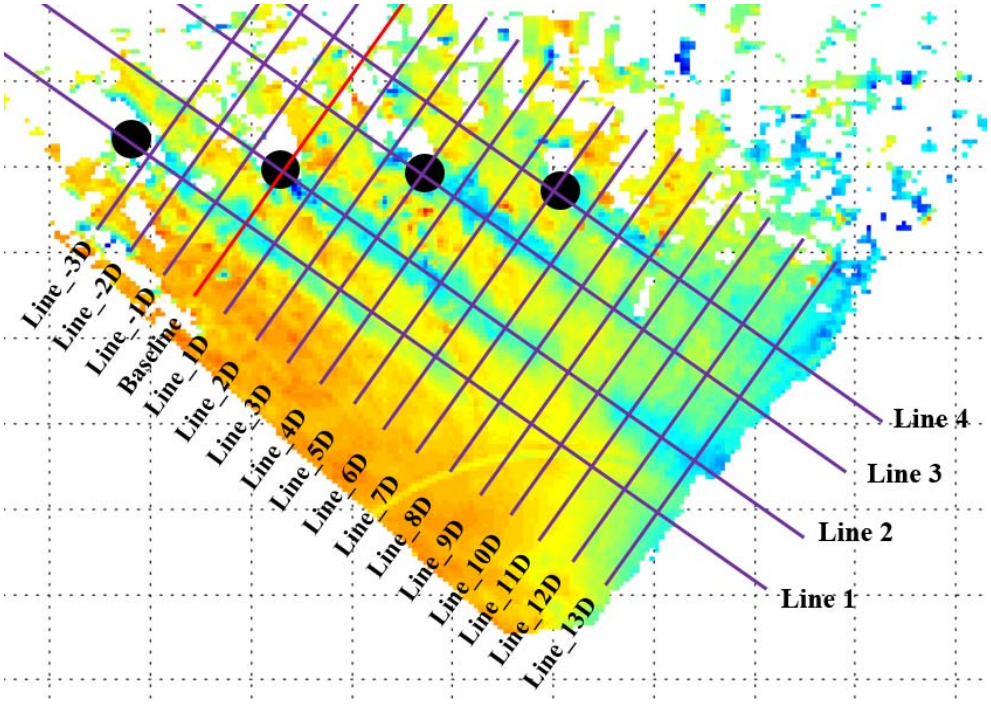

Figure 6.9 Diagram of analyzing lines

Line 1, Line 2, Line 3 and Line 4 are in the wind direction and go through WT10-1, WT10-2, WT10-3 and WT10-4, respectively. The Baseline goes through WT10-2 and is in the crosswind direction. Line_-3D to Line_13D are seventeen lines parallel to the Baseline and are used to analyze the wind speed in cross sections at different downstream distances of four turbines. The distance from Baseline to Line _1D is 1D. The spacing between any other two adjacent lines is 1D as well. Comparisons of wind speeds between measurements and simulations from 3-D wake model at a series of downstream distances are shown in Figure 6.10.

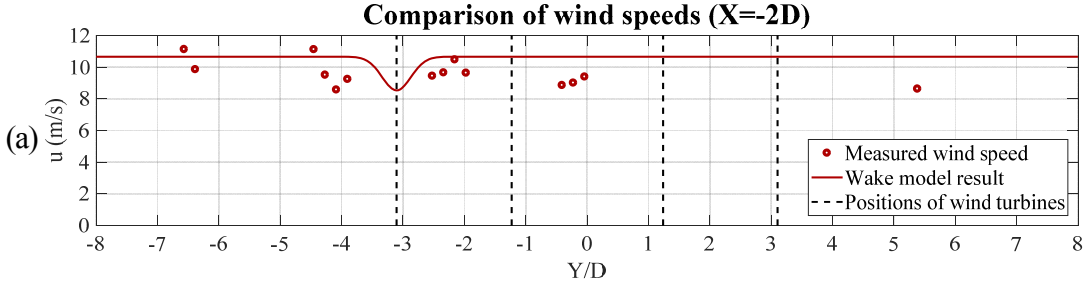

(b)

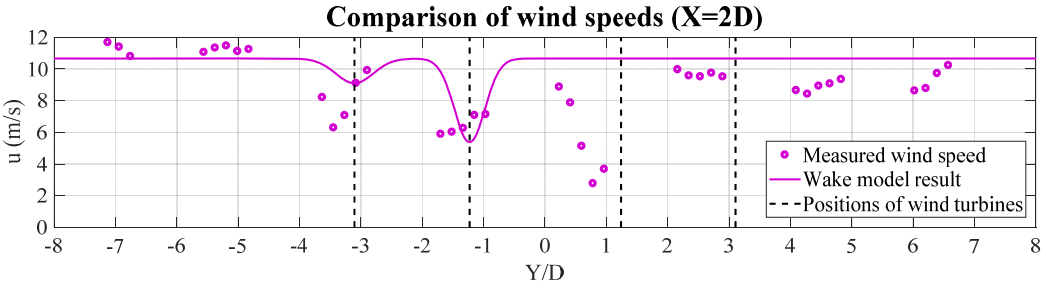
Comparison of wind speeds (X=2D)
u (m/s)
Y/D
Measured wind speed
Wake model result
Positions of wind turbines

(c)

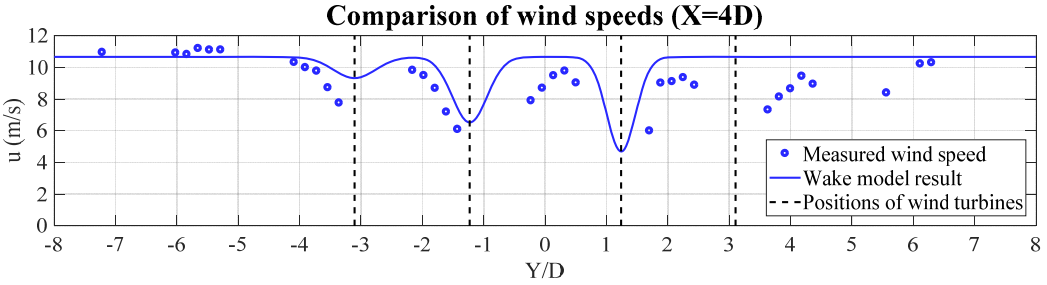
Comparison of wind speeds (X=4D)
u (m/s)
Y/D
Measured wind speed
Wake model result
Positions of wind turbines

(d)

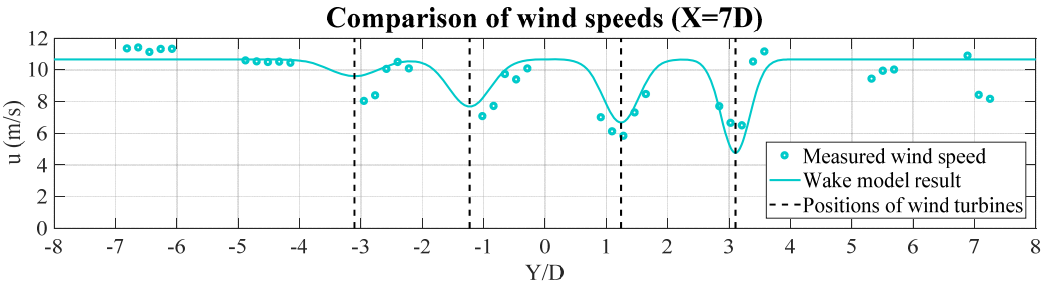
Comparison of wind speeds (X=7D)
u (m/s)
Y/D
Measured wind speed
Wake model result
Positions of wind turbines

(e)

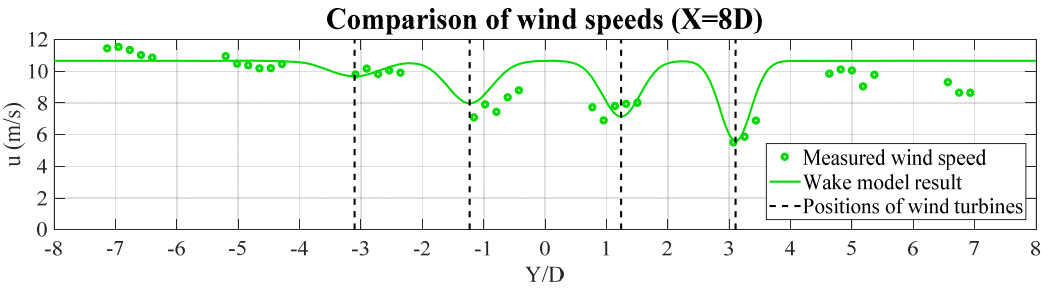
Comparison of wind speeds (X=8D)
u (m/s)
Y/D
Measured wind speed
Wake model result
Positions of wind turbines

(f)

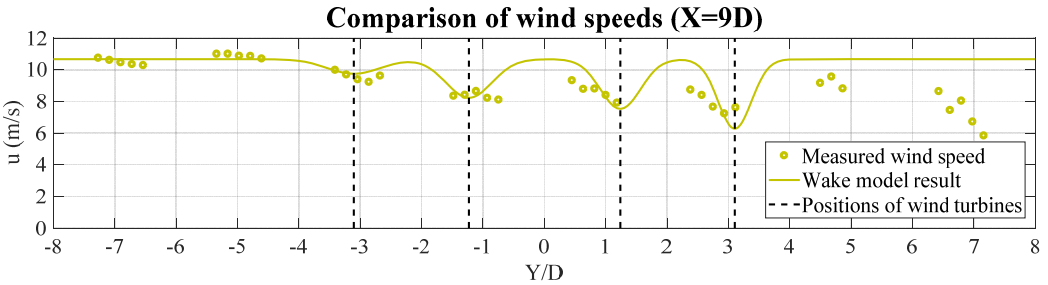
Comparison of wind speeds (X=9D)
u (m/s)
Y/D
Measured wind speed
Wake model result
Positions of wind turbines

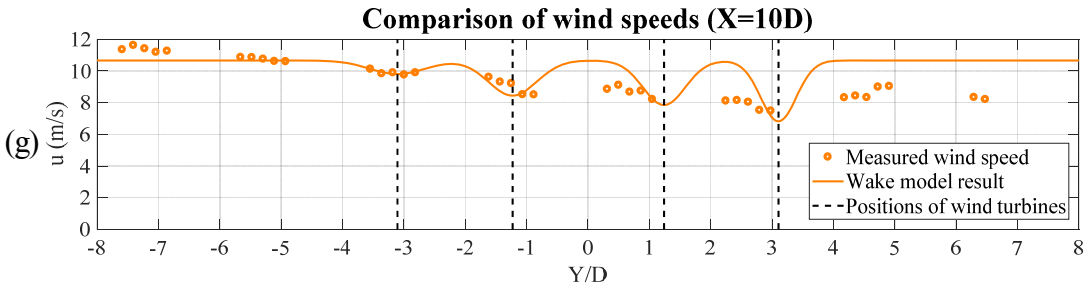

Figure 6.10 Comparisons of wind speeds between measurements and simulations from 3-D wake model at downstream distances of: (a) X = -2D; (b) X = 2D; (c) X = 4D; (d) X = 7D; (e) X = 8D; (f) X = 9D and (g) X = 10D

With the downwind distance increasing form X = -2D to X =10D, the effect of wake interactions also become more obvious. The four wind turbines' wakes only affect positions after Line_7D. Before that line, at X = -2D, X = 2D and X = 4D positions, the wind speeds are only influenced by wakes of one, two or three wind turbines, respectively. For Line_-2D, it should only under the wake effect of WT10-1, but wind speed deficit also exists at the position of WT10-2. Several measured data were obtained, but no data were on the centerlines of wakes. The measurements may be not stable at that position. For Line_2D, the 3-D wake model predicts the deficit of wind speed at the positions right downwind WT10-1 and WT10-2, but could not predict the deficit before WT10-3. The similar situation also happens to Line_4D, where the 3-D wake model estimates the wind speed downwind the three left wind turbines with pretty good accuracy, but did not predict the wind deficit before WT10-4. From the first three lines, according to the measurements data, the deficit of wind speeds not only exists behind the wind turbine but also exists within a short distance before an operating wind turbine. This phenomenon could not be described by the 3-D wake model.

For Line_7D, Line_8D, Line_9D and Line_10D, the wakes of all four wind turbines have an influence on the positions. From the comparisons, the 3-D wake model has a reliable accuracy

in predicting the wind deficits, especially in the far-wake zone. The 3-D wake model tends to estimate the wind speeds very well for positions in Line 2, which are within the wake zone of WT10-2. For Line 4, the 3-D wake model does not show relatively good estimations. The reason could be found from the environmental wind speeds. In the wake model, the inflow is determined by the measured data of WP350, which is installed near WT10-2, so the wake model shows good performance at the positions around WT10-2. Whereas for WT10-4, since it is quite far from WT10-2, the inflow may have a difference from that of WT10-2. This could be seen from the environment wind speeds on the right side of WT10-4, where the environmental wind speeds are actually smaller than the inflow in the wake model.

To sum up, the 3-D wake model has a good overall prediction for wind deficits influenced by multiple wind turbines. Some complicated situations exist in the complex-terrain wind farm, which makes the wake model not accurate in some particular positions. More factors could be considered in the wake model in the future.

6.3 Summary

In this chapter, the 3-D wind turbine wake models for a single and multiple wind turbines were validated by the wind field experiments conducted in complex terrains. The main summaries from this part of study are drawn as follows:

(1) The 3-D wake model for a single wind turbine has been further developed for multiple wind turbines, based on the Sum of Squares method. The analytical wake models could be applied to estimate the distribution of wind speeds in spatial. The inflow wind speed in the wake models could be determined with different functions to fit the distribution of the environmental wind.

(2) Wind field measurements have been carried out in a complex-terrain wind farm in north China. Two scanning modes were adopted to validate the 3-D wake models in both vertical and horizontal planes. The experimental investigation also provided a better understanding of the wind turbine wake characteristics.

(3) The 3-D wake models have been validated by comparing the analytical results with the measured wind speed data. From the comparisons in the vertical direction, the wake models tended to have better predictions in all high positions than those in near-ground positions. The accuracies of the models could also be improved with the increase of the downstream distance and the distance from the centerline. Comparing the wind speeds in the two symmetrical side sections, different distributions were demonstrated in the same downwind positions, which contributed to the errors of the wake models. The asymmetrical characteristics of wakes also deserve further studies.

(4) For horizontal directions, the 3-D wake models showed good accuracies at the far wake positions and also near the inflow measuring site. Deficits of wind speed exist before an operating wind turbine, which could not be estimated from the wake models. In complex-terrain wind farms, the inflows of wind turbines could be different from each other. Therefore, it will cause errors of wake models if inflows of all wind turbines are assumed to be the same.

Chapter 7

Offshore Wind Farm Optimization with the Repowering Strategy

This chapter aims at studying the repowering strategy of offshore wind farm from the very beginning phase of optimizing the positions of wind turbines. The results from both the conventional strategy and repowering strategy are compared. In the repowering optimization process, not only types but also positions of wind turbines are considered. The submarine cable is also considered in this study but not as a variable. Namely, cables also will serve for two generations' period, so the second generation wind turbines remain the same positions as the first generation wind turbines. Hong Kong is an ideal region to adopt the similar strategy. As an application of this study, an economical offshore wind farm layout for Hong Kong is also proposed, which shows the effectiveness of the layout optimization process based on the repowering strategy.

7.1 Calculation models

7.1.1 Wind farm model

The calculation tool adopted in this study is the MATLAB software. To take full advantage of it, the wind farm model is built based on matrixes. Each wind turbine's position is expressed by coordinates and the relative position of two wind turbines is expressed by vector with magnitude and direction (Sun, Gao, & Yang, 2019). The wind loads are also represented by vectors, of which the magnitude and vector are corresponding to wind strength and wind direction. The diagram of distance between turbines along wind direction is shown in Figure 7.1.

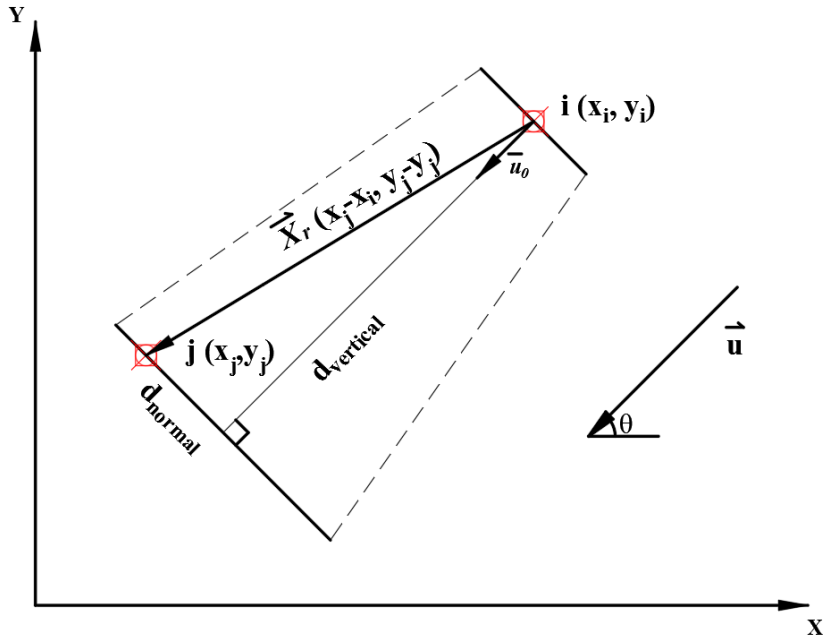

Figure 7.1 Distance between turbines along wind direction

In the figure, X axis and Y axis represent the coordinate axes of the wind farm. The red points represent any two wind turbines i and j in the wind farm. (x_i, y_i) and (x_j, y_j) are the position coordinates of wind turbines. $\overrightarrow{X_r}$ is the vector from i to j, and it can be calculated by $\overrightarrow{X_r} = (x_j - x_i, y_j - y_i)$. $\vec{u}$ is the wind velocity vector. $\overrightarrow{u_0}$ is the unit vector of $\vec{u}$, calculated from $\overrightarrow{u_0} = \frac{\vec{u}}{\left\|\vec{u}\right\|}$. $d_{vertical}$ is a vertical distance to judge the relative position of two wind turbines, whereas d_{normal} is to judge whether a wind turbine is under the effect of wakes. d_{normal} and $d_{vertical}$ are obtained from the following equations:

$$d_{normal} = \overrightarrow{X_r} \cdot \overrightarrow{u_0} \tag{7.1}$$

$$d_{vertical} = \overrightarrow{X_r} \times \overrightarrow{u_0} \tag{7.2}$$

d_{normal} and $d_{vertical}$ are two important parameters to consider the wake effect. $d_{vertical}$ is to judge the relative position of two wind turbines: if $d_{vertical}$ is bigger than 0, it means wind turbine i is the upstream wind turbine and wind turbine j is the downstream wind turbine, vice versa. d_{normal} is to judge whether wind turbine is under the wake's effect. When $|d_{normal}|$ is less than the upstream wind turbine's wake radius, it means the downstream wind turbine is under upstream wind turbine's wake influence. Then $d_{vertical}$ will be utilized to calculate wind losses according to the appropriate wake model.

In the MATLAB program, for the convenience of calculation, wind turbine position coordinate and relative position coordinate are extended from vectors to matrixes. For any two wind turbines, the position matrix $\overrightarrow{X}$ and relative position matrix $\overrightarrow{X_r}$ are as follows:

$$\overrightarrow{X} = \begin{bmatrix} (x_1, y_1) & (x_2, y_2) \\ (x_1, y_1) & (x_2, y_2) \end{bmatrix} \tag{7.3}$$

$$\overrightarrow{X_r} = \overrightarrow{X}' - \overrightarrow{X} = \begin{bmatrix} (x_1 - x_1, y_1 - y_1) & (x_1 - x_2, y_1 - y_2) \\ (x_2 - x_1, y_2 - y_1) & (x_2 - x_2, y_2 - y_2) \end{bmatrix} \tag{7.4}$$

For $\overrightarrow{X_r}$, the diagonal elements will not be involved in the calculation, as no wind turbine is under its own wake effect. On the other hand, when adopting equation (7.1) and equation (7.2), $\overrightarrow{X_r}$ will be replaced by each element of $\overrightarrow{X_r}$ in equation (7.3).

In a real wind farm, a wind turbine may be under multiple wind turbines' wake effect. For

example, in Figure 7.2, the blue wind turbine is under three red wind turbines' wake effect. So the calculation model based on two wind turbines should be further developed.

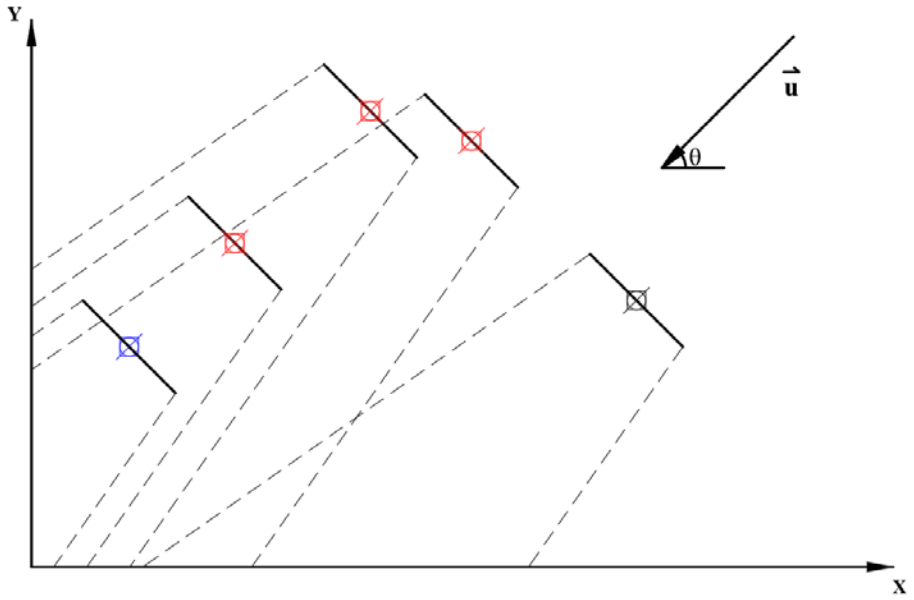

Figure 7.2 The wind turbines under wake effect

To build a whole wind farm's calculation model, a whole wind farm's position matrix is necessary. The position matrix $\overrightarrow{X}$ is extended from a 2-D matrix to a multi-dimensional matrix, and relevantly, $\overrightarrow{X_r}$ is also extended. Supposing the number of the wind turbines is N, $\overrightarrow{X}$ and $\overrightarrow{X_r}$ are as follows:

$$\overrightarrow{X} = \begin{bmatrix} (x_1, y_1) & (x_2, y_2) & \cdots & (x_N, y_N) \\ (x_1, y_1) & (x_2, y_2) & \cdots & (x_N, y_N) \\ \vdots & \vdots & \ddots & \vdots \\ (x_1, y_1) & (x_2, y_2) & \cdots & (x_N, y_N) \end{bmatrix} \tag{7.5}$$

$$\overrightarrow{X_r} = \overrightarrow{X}' - \overrightarrow{X} = \begin{bmatrix} (x_1 - x_1, y_1 - y_1) & (x_1 - x_2, y_1 - y_2) & \dots & (x_1 - x_N, y_1 - y_N) \\ (x_2 - x_1, y_2 - y_1) & (x_2 - x_2, y_2 - y_2) & \dots & (x_2 - x_N, y_2 - y_N) \\ \vdots & \vdots & \ddots & \vdots \\ (x_N - x_1, y_N - y_1) & (x_N - x_2, y_N - y_2) & \dots & (x_N - x_N, y_N - y_N) \end{bmatrix} \tag{7.6}$$

With the multi-dimensional matrix $\overrightarrow{X_r}$, the matrixes of d_{normal} and $d_{vertical}$ can be easily calculated by MATLAB software then. Next, each wind turbine's wake effect status in a wind farm can be obtained according to the mathematical wake model.

7.1.2 Wake model applied in calculation

On the other hand, one apparent problem is that the distribution of wind speed downstream of a wind turbine blade is not a linear problem. The linear assumption of Jensen wake model is far from reality. Therefore, in this study, a 2-D wake model which is a further development of Jensen wake model is applied, as shown in Figure 7.3. In the 2-D wake model, the partial wake effect is taken into consideration. Similar modifications on Jensen wake model have also been made by many other scholars, like Hou et al. (2017), Amaral and Castro (2017), L. Wang, Tan, Cholette, and Gu (2016), and Chowdhury, Zhang, Messac, and Castillo (2012).

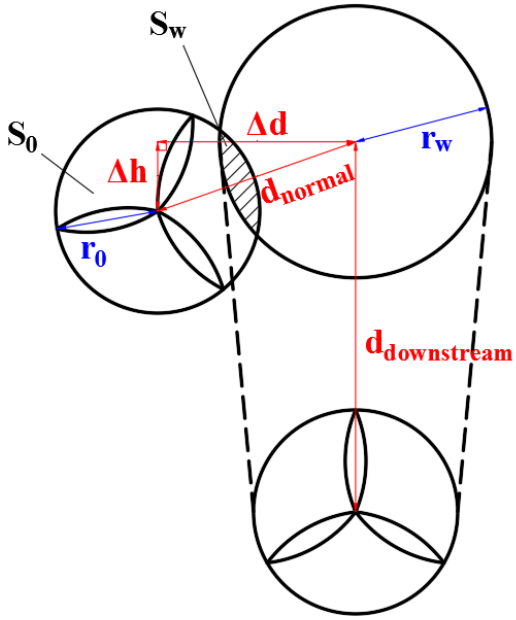

Figure 7.3 2-D wake model

In formulae, r_0 is the radius of the wind turbine blade; r_w is the assuming wake radius; S_0 is the swept area of wind turbine; S_w is the wake-influenced area. d_{normal} is obtained from formula (7.7). Δh is the hub height difference and Δd is wind turbines' horizontal distance that perpendicular to the wind direction.

$$d_{normal} = \sqrt{\Delta h^2 + \Delta d^2} \tag{7.7}$$

Thus, the wake formula for a single wind turbine is modified as (7.8).

$$\begin{cases} u = u_0, & r_w + r_0 < d_{normal} \\ u = u_0 \left[1 - \dfrac{2ar_0^2}{(r_0 + \alpha \cdot d_{downstream})^2} \right] \cdot \dfrac{S_w}{S_0}, & r_w - r_0 \le d_{normal} \le r_0 + r_w \\ u = u_0 \left[1 - \dfrac{2ar_0^2}{(r_0 + \alpha \cdot d_{downstream})^2} \right], & d_{normal} < r_w - r_0 \end{cases} \tag{7.8}$$

7.1.3 Cost estimation

To compare strategies' economical efficiencies, the ways to estimate cost are studied. The total cost of conventional wind farm strategy with one generation of wind turbines is shown in equation (7.9). In this strategy, after one generation's service time, both wind turbines and foundations are dismantled directly. While in repowering strategy, two generations of wind turbines' service time is considered as a complete lifespan. It means when the first generation of wind turbines run out of their service time, wind turbines will be dismantled, while the second generation wind turbines will be installed on the original foundations, and finally all wind turbines and foundations will be dismantled after the second generation's service time. The cost estimation formula is shown as equation (7.10).

$$Total\_Cost_{CS} = Cost_{WT} + Cost_f + Cost_i + Cost_d \quad (7.9)$$

$$Total\_Cost_{RS} = Cost_{WT1} + Cost_{f1} + Cost_{i1} + Cost_m + Cost_{WT2} + Cost_{i2} + Cost_{d2} \quad (7.10)$$

In the formulae, $Cost_{WT}$ is wind turbine cost and consulted from $Cost_{WT} = A_P + B_P \cdot P_{rated}$ (Lundberg, 2003); $Cost_f$ is the foundation cost and assumed to be directly proportional to wind turbine's rated power; $Cost_i$ is the installation cost, which is assumed to be 80% of the corresponding wind turbine cost; $Cost_d$ is the decommissioning cost, which is assumed to be 60% of installation cost; and $Cost_m$ is the maintaining cost, which is assumed to be 10% of installation cost.

In equation (7.9), $Total\_Cost_{CS}$ consists of one generation's wind turbine cost, foundation cost,

installation cost and decommissioning cost. In equation (7.10), $Total\_Cost_{RS}$ consists of two generations' wind turbine costs and installation costs, one generation' foundation cost, maintaining cost and decommissioning cost. The $Cost_{WT1}$, $Cost_{f1}$, $Cost_{i1}$ and $Cost_{d2}$ in (7.10) are the same as $Cost_{WT}$, $Cost_{f}$, $Cost_{i}$ and $Cost_{d}$ in (7.9), respectively. Similarly, $Cost_{WT2}$ and $Cost_{i2}$ are the second generation's costs, also estimated according to the above method.

7.2 Layout optimization of wind farm

7.2.1 Optimization process

When adopting the repowering strategy, apart from the aligned wind farm layout, the optimized layout is also analysed. The optimization in this study is a process directing from the original wind turbine data and wind data to the final optimal wind farm layout. The flow chart of optimization process in this study is shown in Figure 7.4.

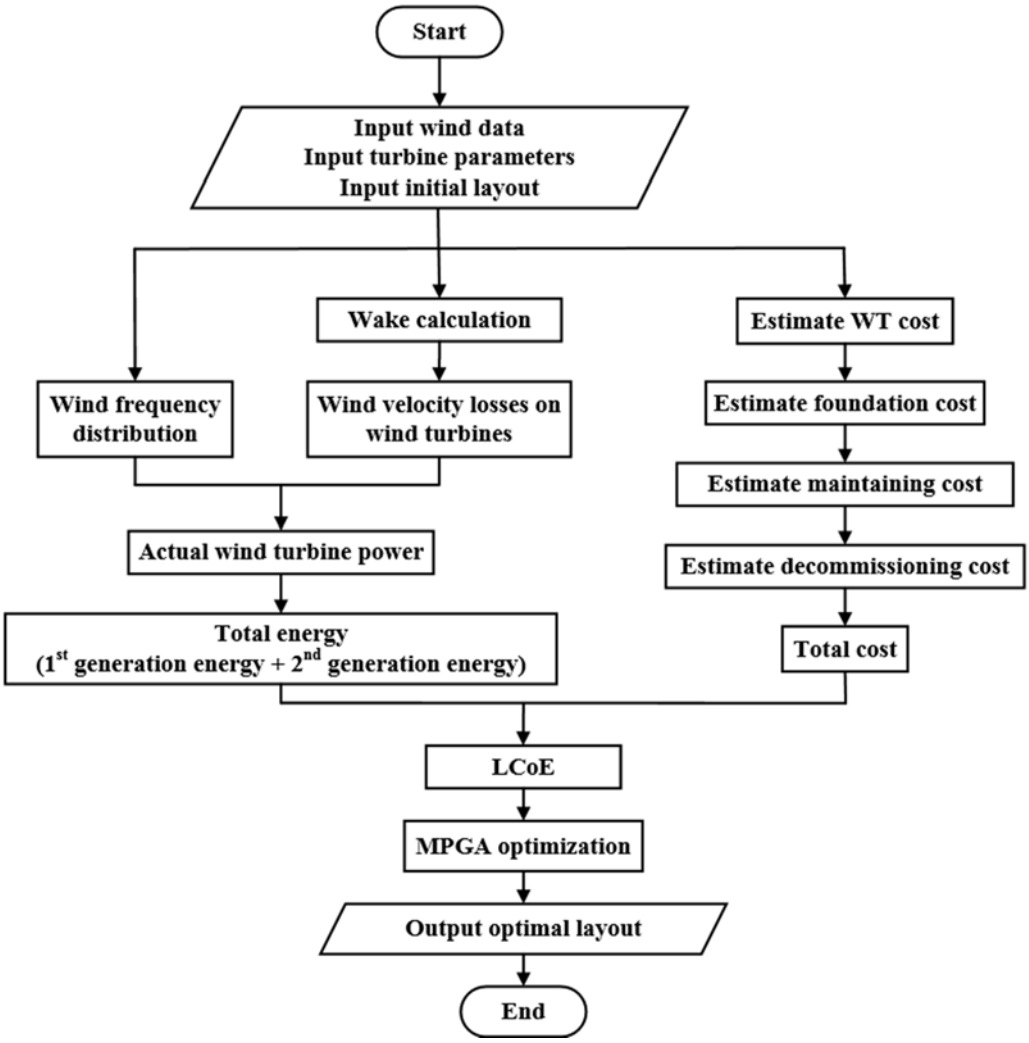

Figure 7.4 Flow chart of the optimization process

LCoE is decided by total energy and total cost, and the lowest LCoE is the objective of this optimization process. Total cost includes wind turbine cost, foundation cost, maintaining cost and decommissioning cost, which are estimated from literatures. In the repowering strategy, the total energy takes account of two generations' energy yields. Each generation's energy yield is decided by the actual wind turbine power, which has close relationship to wind frequency distribution and total wind velocity losses on wind turbines. Wind frequency contains magnitude and direction information of the wind resources and should be obtained from the real wind data. The total wind velocity loss is a more complicated result of multiple effects, and wake effect is mainly considered in this optimization process. To estimate the wake effect, the turbine parameters (rotor

radius, hub height power curve, etc.) and wind farm layout are necessary.

7.2.2 Multi-Population Genetic Algorithm

The optimization tool in this study is the MPGA, which is widely used because of its high-efficiency merit. The effectiveness of applying MPGA in the offshore wind farm optimization problem has been verified by Gao et al. (2014b) and Gao, Yang, and Lu (2014a).

The widely known procedure of the MPGA is shown in Figure 7.5. In MPGA, the first step is to define the objective function by the unresolved problem and set a corresponding optimization criterion. In the second step, the initial population will be generated randomly. In the third step, the population is input to evaluate the objective function. The forth step is to judge whether the optimization criterion is met. If the answer is yes, then the best individuals are received. But if the optimization criterion is not met, the new population will be generated by selection, recombination and mutation, and then go back into the circulation from the third step until the optimization criterion is met.

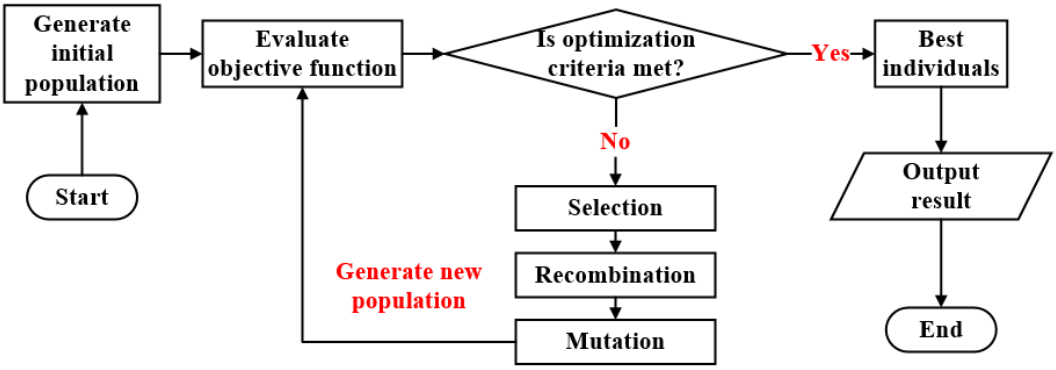

Figure 7.5 Procedure of the MPGA

In this study, the population is the position coordinates of wind turbines, which also represents

the layout of wind farm. LCoE is set as the objective and the optimization criterion here is the judgment that whether the minimum LCoE keeps for 500 generations. If the criterion is met, the optimal layout (i.e. the best individuals) is obtained; if not, the population of the layout will be selected, recombined and mutated until the criterion is met. The number of individuals is 54, which represents the number of wind turbine in the wind farm. Some initial parameters setting for MPGA in this study are listed in Table 7.1.

Table 7.1 The initial parameters setting for MPGA

Parameters	Values
Population number	50
Number of individuals	54
Binary digits of variable	20
Probability of mutation	0.001-0.05
Probability of crossover	0.7-0.9
The least keeping generations	500

7.3 A case study in Hong Kong

The presented offshore wind farm optimization method will be applied in Hong Kong sea area as a case study. In this case, the objective is to find an optimized layout for the particular sea area. The repowering idea is applied in this case, so the optimization criterion LCoE in MPGA is on account of two generations' cost and energy. The final optimization results can provide a useful reference for Hong Kong's offshore wind industry development.

7.3.1 Site selection of the offshore wind farm

In Hong Kong, there are four potential sea areas that are proper to develop offshore wind farms (Gao et al., 2014b). Waglan Island sea area, as shown in Figure 7.6, has huge sea area and good potential of offshore wind energy to build offshore wind farms, which is therefore selected here. The size of the chosen offshore area is 3,740 m×5,828 m. The satellite image of Waglan Island is shown in Figure 7.7.

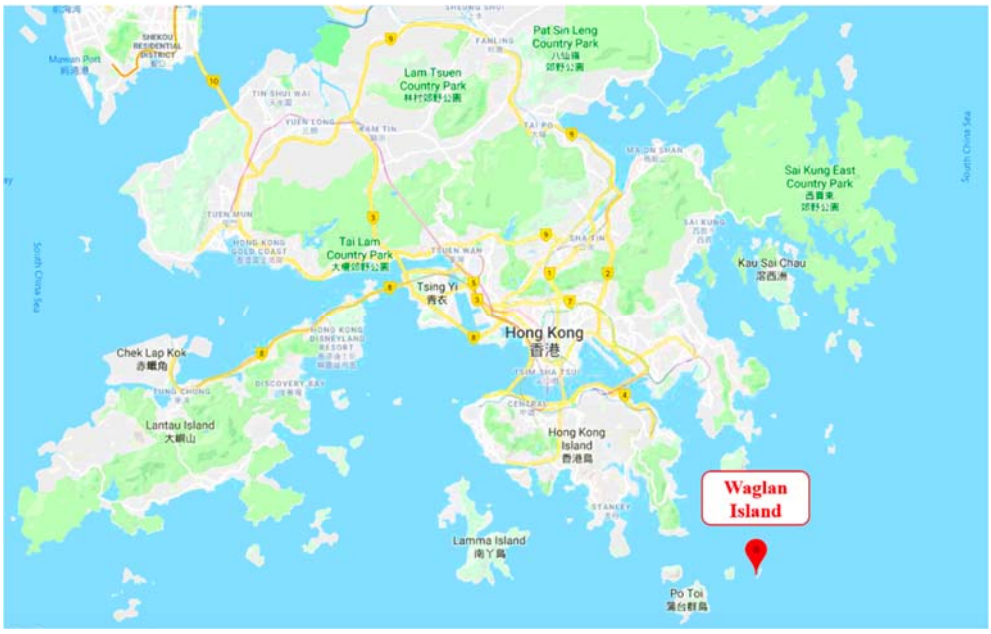

Figure 7.6 The location of Waglan Island (Google Map, 2018b)

Figure 7.7 Satellite image of Waglan Island (Wikipedia)

To simulate the real wind load condition, the actual wind data of Waglan Island sea area is applied in this study. The first-hand wind data is the hourly wind speed data (from the year 2001 to 2011) comes from Royal Observatory, Hong Kong. The site of anemometer tower is 22°10'56" N, 114°18'12" E. The height of anemometer is 83 m and the site height above sea level is 56 m. The hourly wind speed data should be transferred into frequency distribution to be involved in the calculation process. The equation from hourly wind data to frequency distribution is shown as equation (7.11).

$$f(Dir, Spd) = \frac{N(Dir, Spd)}{N_{total}} \tag{7.11}$$

Then the 3-D wind velocity frequency distribution in Waglan Island sea area is shown in Figure 7.8.

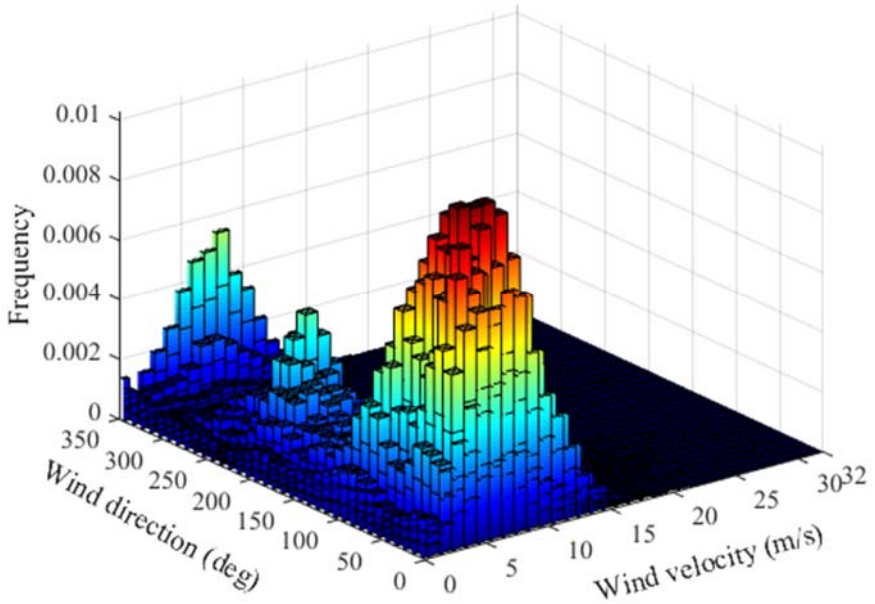

Figure 7.8 Wind velocity frequency distribution in Waglan Island sea area

From the 3-D distribution, it is directly perceived that the wind velocity in this area ranges from 0 m/s to 32 m/s, and mainly centres on around 7 m/s. The wind direction centres on 0 ~ 125 , but also distributes on other directions. The 3-D wind data distribution is convenient for designers to acquire the wind data characteristics at the beginning stage.

7.3.2 Wind turbines

Since the LCoE optimization criterion in MPGA is on account of two generations' cost and energy, two different specifications' wind turbines are considered in this study. The wind turbines are chosen from ENERCON products, the types of which are E-126 EP4 and E-101 (ENERCON GmbH, 2015). As for the service time extending of the foundations, the strength of foundations may decrease in the second generation, the second wind turbines should be smaller than the first ones. The rated powers of two generation wind turbines are 4.2 MW and 3.05 MW respectively. The parameters of wind turbines are listed in Table 7.2.

Table 7.2 The parameters of wind turbines (ENERCON GmbH, 2015)

Parameters	E-126 EP4	E-101
Rated power	4.2 MW	3.05 MW
Rotor diameter	127 m	101 m
Hub height	135 m	99 m
Rated wind speed	14 m/s	13 m/s
Cut-in wind speed	3 m/s	3 m/s
Cut-out wind speed	28 m/s	28 m/s
Service life cycle	20 years	20 years

For the sake of generality, it is common that a generic equation for modelling the power curve will be preferred in analysis of wind energy potential (Jowder, 2009). There are some approximation equations to describe the power curves. In this study, a polynomial power curve is adopted. The equation of the power curve (Carrillo, Montaño, Cidrás, & Díaz-Dorado, 2013) is shown as equation (7.15).

$$P(v) = \begin{cases} 0 & v < v_{ci} \\ C_1 + C_2 \cdot v + C_3 \cdot v^2 & v_{ci} \le v < v_r \\ P_r & v_r \le v \le v_{co} \\ 0 & v > v_{co} \end{cases} \tag{7.15}$$

In the equation P_r is the rated power; v_r is the rated wind speed; v_{ci} is the cut-in wind speed and v_{co} is the cut-out wind speed. C_1, C_2 and C_3 are the coefficients that can be obtained from the equation (7.16) (Carrillo et al., 2013).

$$\begin{cases} C_1 = \dfrac{1}{\left(v_{ci}-v_r\right)^2}\cdot\left[v_{ci}\cdot\left(v_{ci}+v_r\right)-4v_{ci}\cdot v_r\cdot\left(\dfrac{v_{ci}+v_r}{2v_r}\right)^3\right] \\ C_2 = \dfrac{1}{\left(v_{ci}-v_r\right)^2}\cdot\left[4\left(v_{ci}+v_r\right)\cdot\left(\dfrac{v_{ci}+v_r}{2v_r}\right)^3-3v_{ci}-v_r\right] \\ C_3 = \dfrac{1}{\left(v_{ci}-v_r\right)^2}\cdot\left[2-4\left(\dfrac{v_{ci}+v_r}{2v_r}\right)^3\right] \end{cases} \tag{7.16}$$

The corresponding power curves of the selected wind turbines are shown in Figure 7.9.

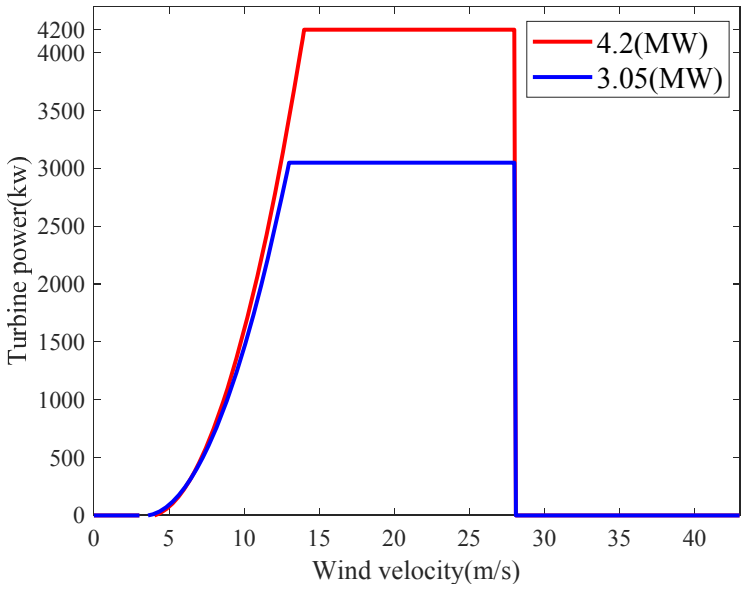

Figure 7.9 Wind Turbine Power Curves

7.3.3 Results

7.3.3.1 Results of aligned layouts

Both aligned layout and optimized layout are compared to evaluate the efficiency of the repowering strategy. In aligned layout, 54 wind turbines are aligned arranged in the wind farm,

with 9 columns and 6 rows. The wind farm layout and each wind turbine's annual average electricity output results are shown in Figure 7.10. From the figure, each wind turbine's energy output is different because of wake's impact. It is also clear that the aligned layout is not the best choice and the layout can be further optimized.

(a)

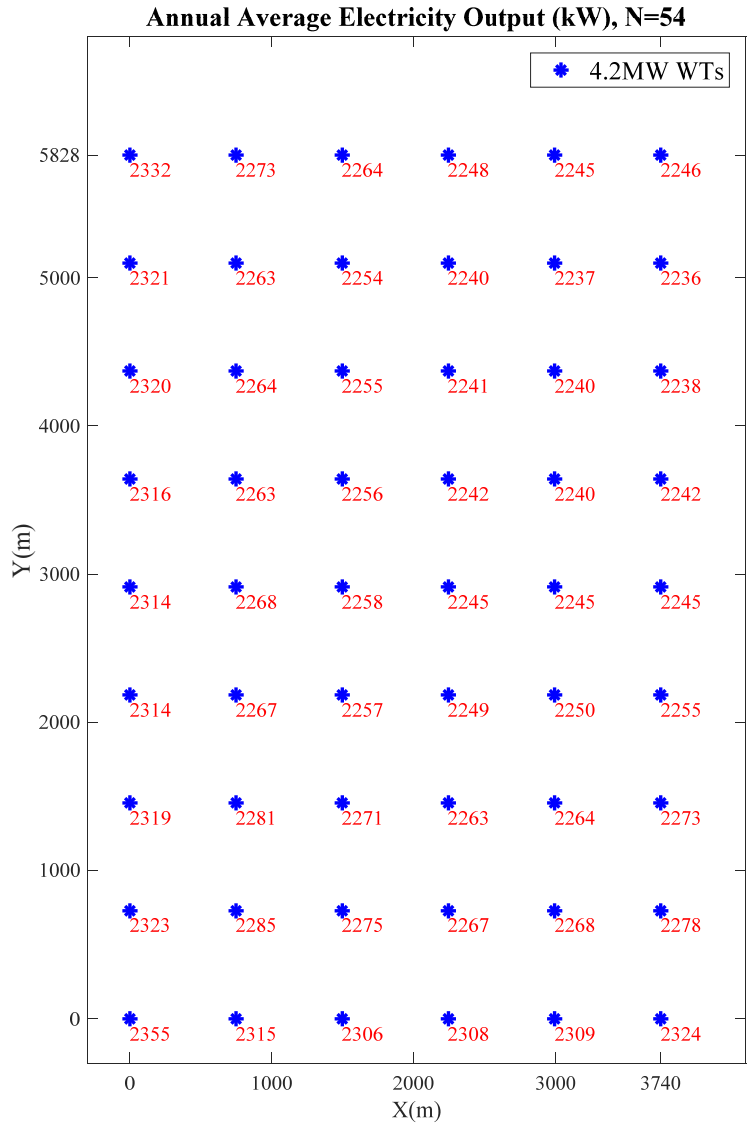

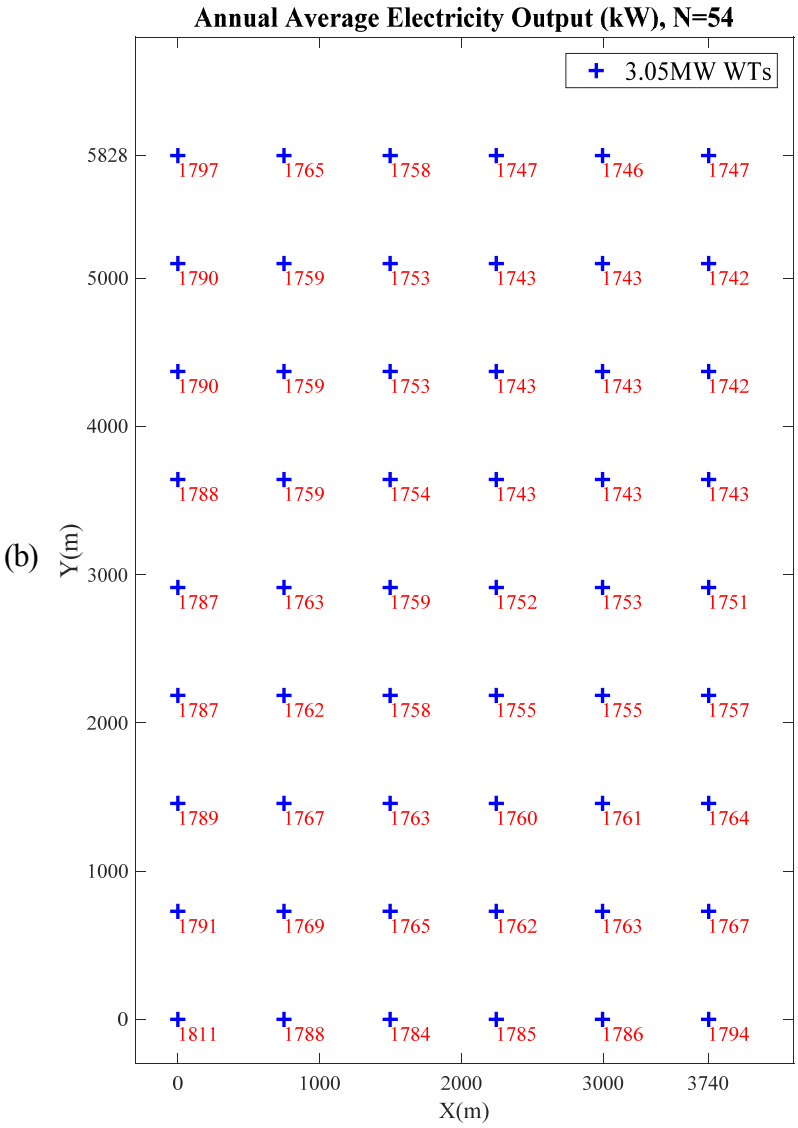

Figure 7.10 Aligned layout and wind turbine power: (a) with 4.2 MW wind turbines and (b) with 3.05 MW wind turbines

More detailed results are calculated and listed in Table 7.3. There are three aligned strategies A1, A2 and A3 in the comparison. A1 is the conventional strategy, in which the foundations and 4.2 MW wind turbines are installed in the beginning phase and dismantled in the end phase and 20-years' service time is taken into consideration. A2 adopts the repowering strategy, to be specific, when the first generation 4.2 MW wind turbines run out of their 20-year service time, the wind turbines are dismantled while the foundations are reserved to support the second generation of

4.2 MW wind turbines for another 20 years. A3 is similar to A2, while the only difference is that the rated power of the second generation wind turbines is 3.05 MW rather than 4.2 MW. Therefore, it is obvious that repowering strategies can reduce huge cost. Benefitting from the lowest total cost, the LCoE of A3 is the lowest, with 1.0573 HK$/kWh.

Table 7.3 Main results of aligned layouts

	A1	A2	A3
Number of wind turbine	54	54	54
Service years	20	40	40
Energy yield (GWh)	2.15×10^4	4.30×10^4	3.82×10^4
Total cost (MHK$)	2.47×10^4	4.56×10^4	4.04×10^4
LCoE (HK$/kWh)	1.2367	1.0604	1.0573

7.3.3.2 Results of optimized layouts

According to the optimization method, both wind turbines' positions and average powers are obtained, which are shown in Figure 7.11.

(a)

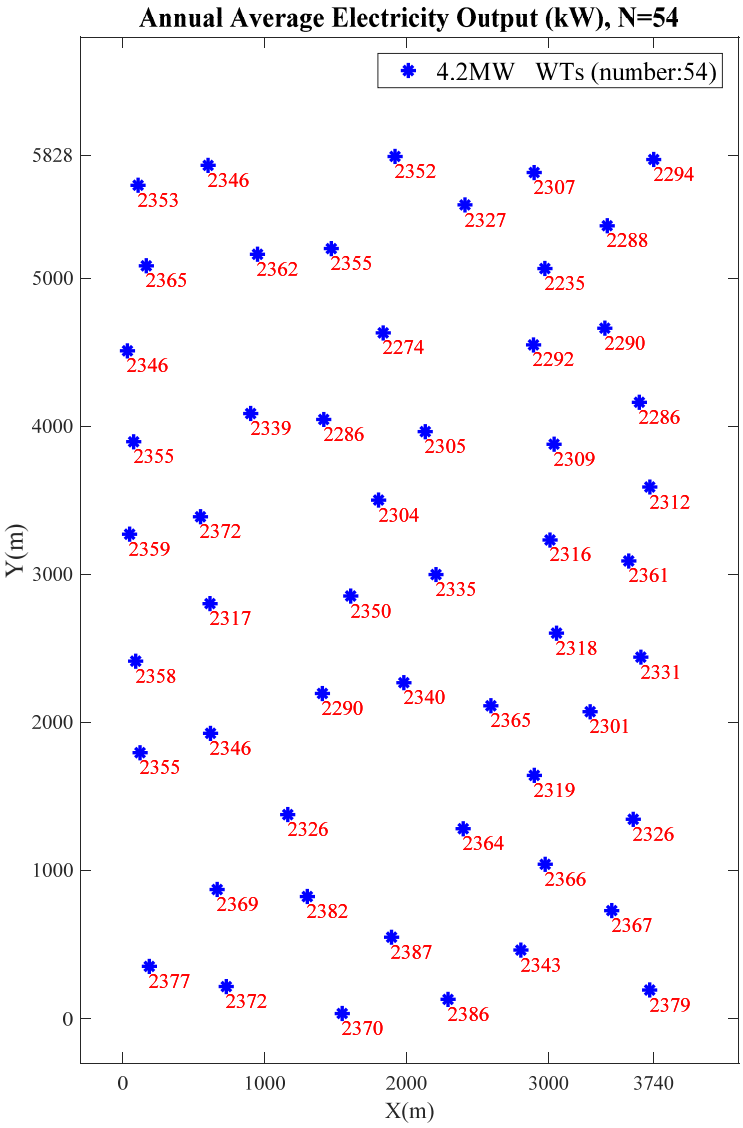
Annual Average Electricity Output (kW), N=54
4.2MW WTs (number:54)
Y(m)
X(m)
0
1000
2000
3000
3740
5828
5000
4000
3000
2000
1000
0
2346
2352
2294
2353
2307
2327
2288
2365
2362
2355
2235
2274
2290
2346
2292
2286
2339
2286
2305
2355
2309
2312
2304
2372
2359
2316
2361
2335
2350
2317
2318
2358
2331
2290
2340
2365
2301
2346
2355
2319
2326
2364
2326
2366
2369
2382
2367
2387
2343
2377
2372
2386
2379
2370

(b)

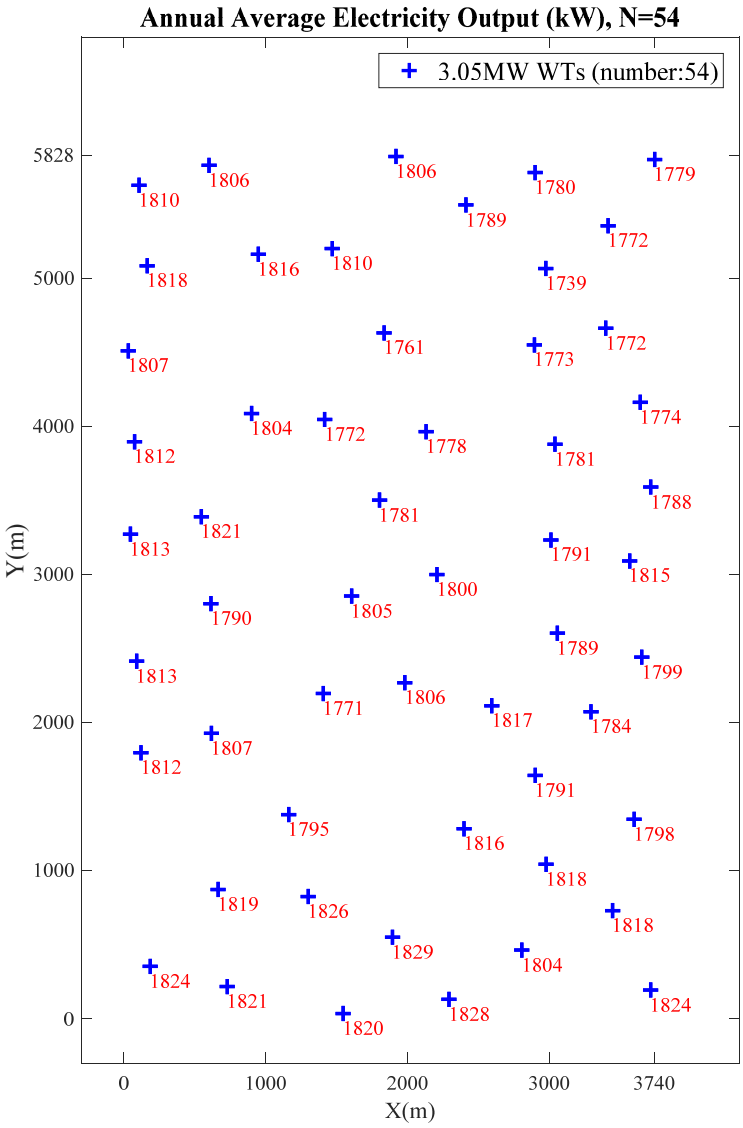
Annual Average Electricity Output (kW), N=54
3.05MW WTs (number:54)
Y(m)
X(m)
0
1000
2000
3000
3740
5828
5000
4000
3000
2000
1000
0
1810
1806
1806
1780
1779
1789
1772
1818
1816
1810
1739
1807
1761
1773
1772
1774
1804
1772
1778
1781
1812
1788
1781
1821
1813
1791
1815
1800
1805
1790
1789
1813
1799
1771
1806
1817
1784
1807
1812
1791
1795
1816
1798
1818
1819
1826
1818
1829
1804
1824
1821
1828
1824
1820

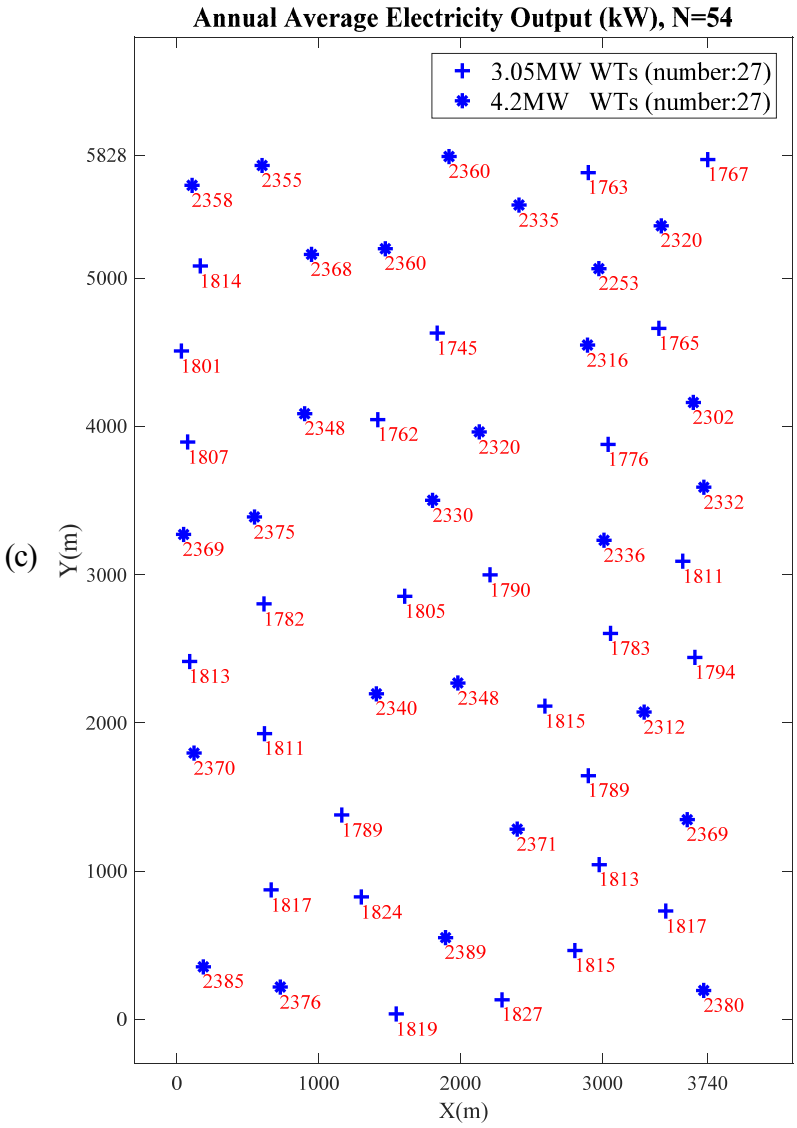

Figure 7.11 Optimized layout and wind turbine power: (a) with 4.2 MW wind turbines; (b) with 3.05 MW wind turbines and (c) with 4.2 MW wind turbines and 3.05 MW wind turbines

The total service time is also in consideration of 40 years. The main results of the optimized layouts are listed in Table 7.4.

Table 7.4 Main results of optimized layouts

	O1	O2	O3
Number of wind turbine	54	54	54
Service years	40	40	40
Energy yield (GWh)	4.4196×10^4	3.4056×10^4	4.1701×10^4
Total cost (MHK$)	4.56×10^4	4.04×10^4	4.30×10^4
LCoE (HK$/kWh)	1.0317	1.1848	1.0312

7.3.3.3 Results with the three-dimensional wake model

To investigate the 3-D wake model's effect on the output of the wind farm, the results from 2-D wake model are compared with those from the 3-D wake model. The 3-D wake model is applied to the obtained optimized layout, and average powers are shown in Figure 7.12.

(a)

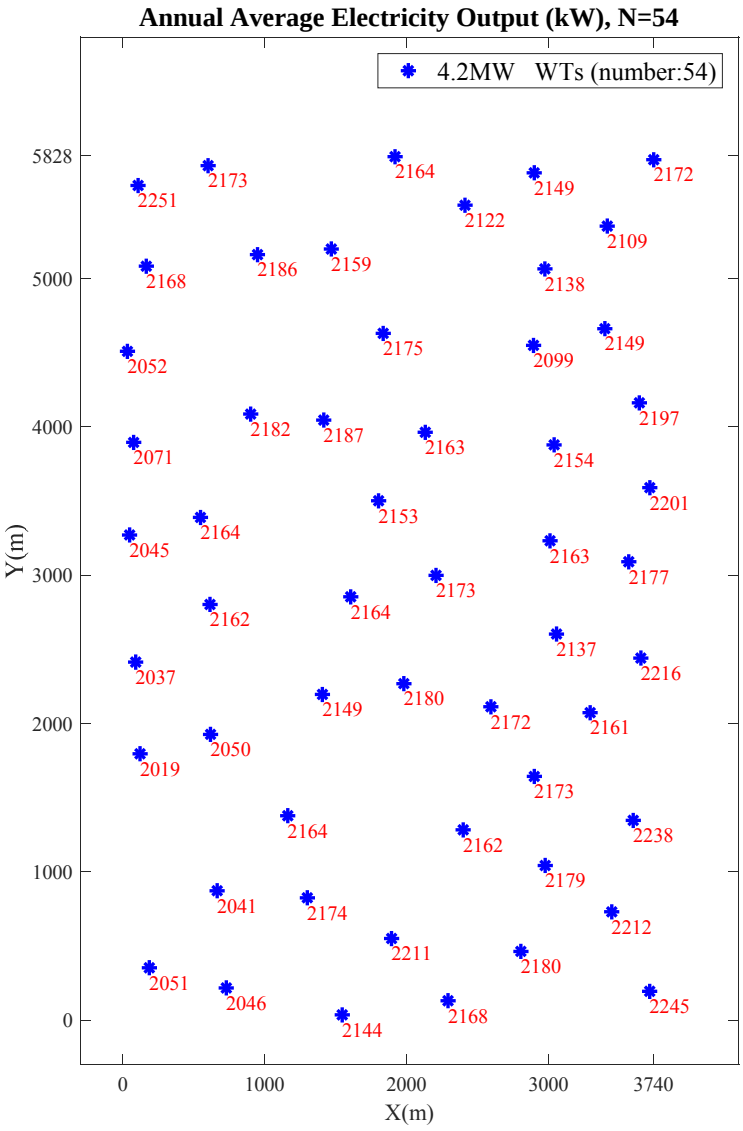
Annual Average Electricity Output (kW), N=54
4.2MW WTs (number:54)
Y(m)
X(m)
0
1000
2000
3000
3740
5828
5000
4000
3000
2000
1000
0
2251
2173
2164
2149
2172
2122
2109
2168
2186
2159
2138
2175
2149
2052
2099
2197
2182
2187
2163
2071
2154
2201
2153
2164
2045
2163
2177
2173
2164
2162
2137
2037
2216
2149
2180
2172
2161
2050
2019
2173
2164
2238
2162
2179
2041
2174
2212
2211
2180
2051
2046
2245
2168
2144

(b)

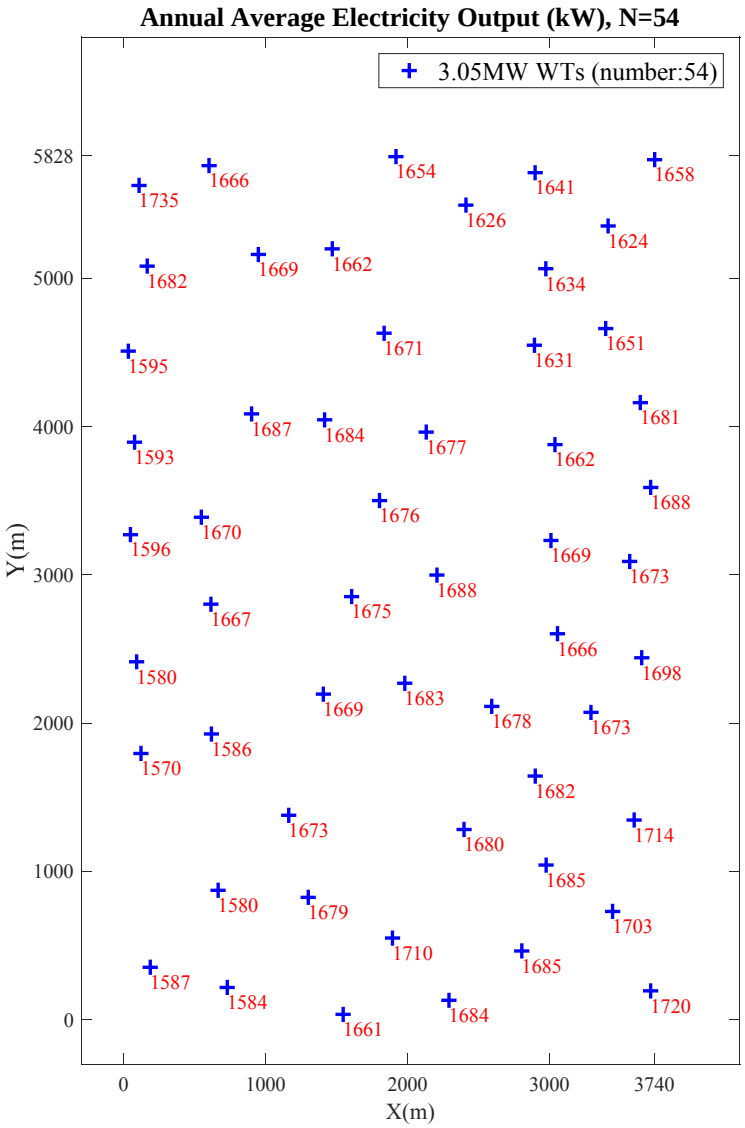
Annual Average Electricity Output (kW), N=54
3.05MW WTs (number:54)
Y(m)
X(m)
0
1000
2000
3000
3740
5828
5000
4000
3000
2000
1000
0
1735
1666
1654
1641
1658
1626
1624
1682
1669
1662
1634
1671
1651
1595
1631
1681
1687
1684
1677
1593
1662
1688
1676
1670
1596
1669
1673
1688
1675
1667
1666
1580
1698
1669
1683
1678
1673
1586
1570
1682
1673
1714
1680
1685
1580
1679
1703
1710
1685
1587
1584
1720
1684
1661

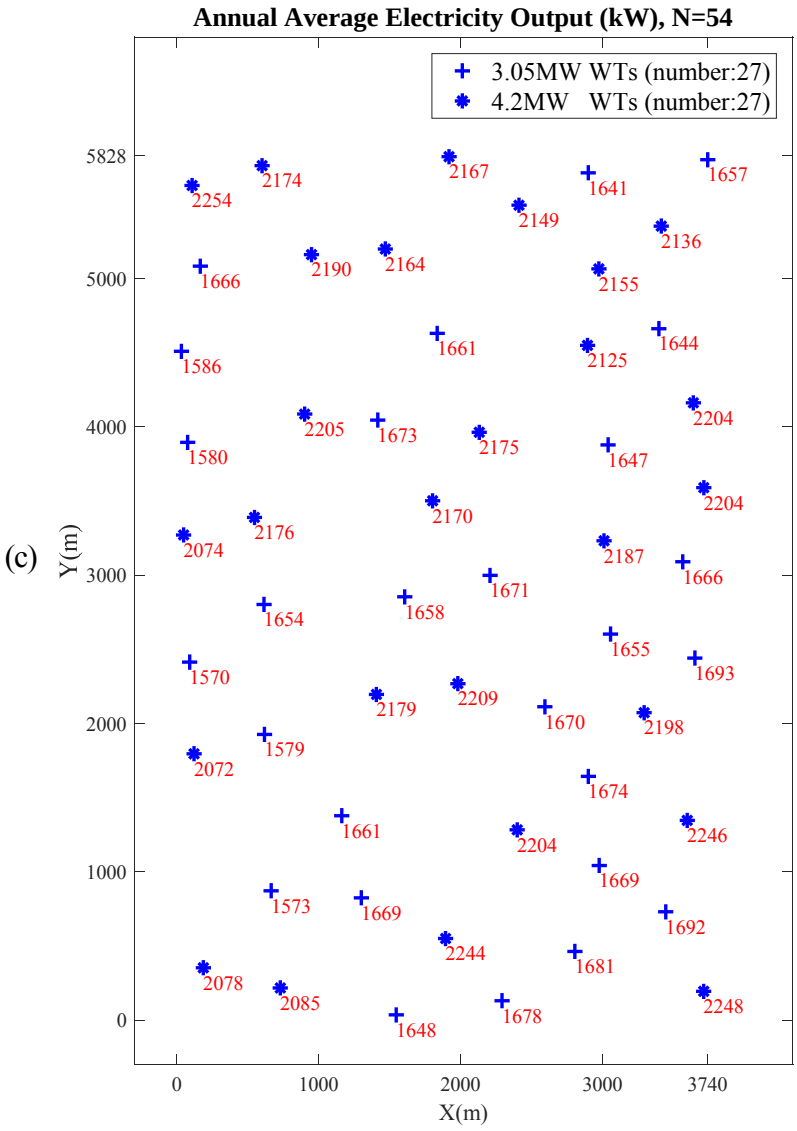

Figure 7.12 Optimized layout and wind turbine power with the 3-D wake model: (a) with 4.2 MW wind turbines; (b) with 3.05 MW wind turbines and (c) with 4.2 MW wind turbines and 3.05 MW wind turbines

Assuming the total service time is also 40 years, the main results of the optimized layouts with the 3-D wake model are listed in Table 7.5.

Table 7.5 Main results of optimized layouts with the 3-D wake model

	O1 (3-D)	O2 (3-D)	O3 (3-D)
Number of wind turbine	54	54	54
Service years	40	40	40
Energy yield (GWh)	4.0692×10^4	3.1400×10^4	3.6158×10^4
Total cost (MHK$)	4.56×10^4	4.04×10^4	4.30×10^4
LCoE (HK$/kWh)	1.1206	1.2866	1.1892

7.3.4 Discussions

The energy yield comparisons of 4.2 MW and 3.05 MW wind turbines with aligned and optimized layout are listed in Table 7.6. From energy yield aspect, optimized layout can improve energy yield distinctly. For 4.2 MW wind turbines, the energy yield of optimized layout within 40 years is 4.42×10^4 GWh, which is 2.79% more than that of aligned layout at 4.30×10^4 GWh. More obvious circumstance happens for 3.05 MW wind turbines, optimized layout produces more energy than aligned layout at 2.10%.

Table 7.6 Energy yield comparisons (40 years)

	Aligned layout	Optimized layout	Change
4.2MW (GWh)	$2.15\times10^4\times2$	4.42×10^4	+2.79%
3.05MW (GWh)	$1.67\times10^4\times2$	3.41×10^4	+2.10%

Table 7.7 and Table 7.8 are the LCoE comparisons of aligned layout and optimized layout. In both layouts, it is obvious that repowering strategy can decrease LCoE. What is more remarkable, if the optimized layout is adopted, the repowering strategy can decrease LCoE to 1.0310

(HK$/kWh), which is equivalent to decrease 16.63% LCoE of A1.

Table 7.7 LCoE comparisons of aligned layout

	A1	A2	A3
LCoE (HK$/kWh)	1.2367	1.0604	1.0573
Change	-	-14.26%	-14.51%

Table 7.8 LCoE comparisons of optimized layout

	A1	O1	O2	O3
LCoE (HK$/kWh)	1.2367	1.0317	1.1848	1.0312
Change	-	-16.58%	-4.20%	-16.62%

With the 2-D wake model, A2 produces most energy and O1 has the smallest LCoE. For the mentioned sea area, if the owner wants to reduce the construction difficulty and choose an aligned layout, A2 is the preferred option. However, if the lowest LCoE is the orientation, O1 is the proper solution. Actually, O2 and O3 can also be considered, as their second generation wind turbines are of the unified types, which makes it easier for construction and management. At the same time the difference of LCoEs among O1, O2 and O3 is not huge and acceptable.

The comparison of optimized layouts with 2-D and 3-D wake models is shown in Table 7.9. The maximum and minimum outputs of wind turbines are demonstrated. The Energy yields and LCoEs are shown and compared as well.

Table 7.9 The comparison of optimized layouts with 2-D and 3-D wake models

		O1	O2	O3
Maximum output of wind turbines (MW)	2-D wake model	2387	1829	2385 (4.2 MW) 1827 (3.05 MW)
	3-D wake model	2251	1735	2254 (4.2 MW) 1693 (3.05 MW)
Minimum output of wind turbines (MW)	2-D wake model	2235	1739	2253 (4.2 MW) 1745 (3.05 MW)
	3-D wake model	2019	1570	2072(4.2 MW) 1570 (3.05 MW)
Energy yield (GWh)	2-D wake model	4.4196×10^4	3.4056×10^4	4.1701×10^4
	3-D wake model	4.0692×10^4	3.1400×10^4	3.6158×10^4
	Change	-7.93%	-7.80%	-13.29%
LCoE (HK$/kWh)	2-D wake model	1.0317	1.1848	1.0312
	3-D wake model	1.1206	1.2866	1.1892
	Change	8.62%	8.59%	15.32%

The 3-D wake model is more accurate than the 2-D wake model. The 2-D wake model tends to overestimate the wind speed and energy outputs. In all three optimized layouts, the maximum and the minimum outputs of wind turbines from the 2-D wake model are larger. The 2-D wake model's energy yields of O1, O2 and O3 arrangements overestimate by 7.93%, 7.80% and 13.29%, respectively. Correspondingly, the LCoE underestimate by 8.62%, 8.59% and 15.32%.

7.4 Summary

This chapter conducted the investigation on offshore wind farm layout optimization.

Repowering strategy has been applied in the optimization process. The significant summaries are drawn as follows:

(1) From the perspective of maximizing the benefit of offshore wind farms, some wind farm repowering measures are adopted to increase the total energy yield and reduce the total cost. The repowering strategies can significantly decrease the LCoE as when the wind turbine foundations reused, huge structure cost and construction cost are saved. In the calculation process, to estimate wind losses caused by wind turbine wakes more precisely, a modified 2-D wake model is applied. The MALTAB software is utilized as the calculation tool, and all calculation models are expressed by matrixes to improve computation performance. As for the optimization aspect, the MPGA is selected as the optimization tool, which shortens the computational time. Finally, a case study in Waglan Island sea area in Hong Kong is demonstrated. From the results, the offshore wind farm layout optimization method is proved to be practical and effective.

(2) Hong Kong is a coastal region with high population density, which apparently needs huge demand of energy input. Hong Kong is also an ideal region to utilize offshore wind energy power as its offshore wind resource is vast. Taking the chosen Waglan Island offshore area (3,740 m×5,828 m) as an example, this offshore wind farm (the number of 4.2 MW wind turbine is 54) can generate 2.15×10^4 GWh electricity in 20 years. If the repowering strategy is applied, by reusing the wind turbine foundations and replacing the original wind turbines with the optimized wind turbine combination, the LCoE is expected to reduce by nearly 16.63% and to only 1.0310 HK$/kWh. So this study also provides a good reference for Hong Kong's government to develop its offshore wind industry.

(3) Furthermore, though the 2-D wake model can predict energy yield more precisely than the Jensen wake model, it still cannot describe wake's characteristics clearly. More research have been conducted on applying the 3-D wake model in the optimized layout of wind farms. The 3-D wake model is more accurate than the 2-D wake model. From the comparisons, the 2-D wake model tends to overestimate wind speeds and energy outputs, which is meaningful to the wind engineering.

(4) There are more research should be conducted in the future. The 3-D wake models can be applied in the wind farm layout optimization process. The repowering strategy provides a good idea to reduce the cost of the offshore wind farm. Actually some more aspects can also be considered in the optimization process. The strategies related to other issues like cable layout, power dispatch and restricted zone etc. will also be considered in the further studies.

Chapter 8

Wind Farm Optimization with the Directional Restriction

In this chapter, a new Directional Restriction method is presented to restrict the spacing between wind turbines. Compared to the existing restrictions, the new method additionally considers the influence of wind directions, and the restriction for each wind turbine is related to its rotor diameter. Therefore, the method is especially effective for the site with obvious prevailing wind directions. With the Directional Restriction, a wind farm optimization process applying the MPGA has been presented. The optimization can exploit the wind resource more effectively and can be used to optimize the layout of nonuniform wind farm. Four representative cases are then studied and discussed. The results demonstrate that the proposed optimization method is practical in designing wind farms. The coastal area in Hong Kong is the ideal region to develop offshore wind power.

8.1 Directional Restriction

Actually, in real projects, some representative wind farms do not adopt the traditional Omnidirectional Restriction, because of the characteristics of the local wind conditions. Tehachapi Pass Wind Farm (Wikipedia), as shown in Figure 8.1, is a large-scale wind farms installed in early year in the U.S.. The local prevailing wind direction is highly-centralized. Corresponding to the wind condition, its layout is also characteristic, with the very small crosswind intervals between wind turbines (some are even smaller than 1.5D) and the much larger downwind intervals (some are larger than 5D). This layout makes the best use of the wind resource, and the parallel installed wind turbines have little influence to each other as well.

Figure 8.1 Aerial view of the Tehachapi Pass Wind Farm (Wikipedia)

Therefore, inspired by the Tehachapi Pass Wind Farm, a new Directional Restriction is presented in this study, as shown in Figure 8.2 (Sun, Yang, & Gao, 2019). The Directional Restriction tends to take good use of wind resources, save the occupied area of wind farm and decrease the cost of energy. When adopting the Directional Restriction, the restrained area varies with the wind direction. For a particular wind direction, the restrained distance in the downwind direction is 5D, and that distance in the crosswind direction is much smaller, 3D is set in this study. It can be seen that the restrained area of the new Directional Restriction is much smaller than that of the Omnidirectional Restriction. The application of the Directional Restriction in layout optimization is also different from of the Omnidirectional Restriction. When adopting the Directional Restriction, see Figure 8.2, if one wind turbine (WT2) is put into the restrained area of another wind turbine (WT1), only WT2 is regarded as out of work, whereas wind turbine1 is still assumed to work normally. This assumption is much closer to reality compared to the Omnidirectional Restriction.

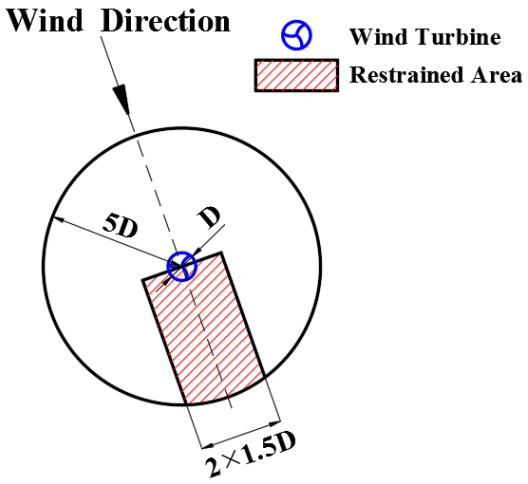

Figure 8.2 Restrained area in the Directional Restriction

So far, no research has been conducted on the Directional Restriction or other wind direction dominant restrictions. This study tries to fill in this research gap. The newly presented Directional Restriction is applied to both aligned and optimized wind farm layouts. The advantages and the feasibilities are studied and discussed from the aspect of energy output. This study is of value to the wind farm development in the region where the wind is highly-concentrated.

8.2 Calculation models

In this chapter, the significant wind turbine model models used in this study are introduced in details. The wind farm model and the wake model are the same as those in Chapter 7, which are therefore not introduced in this chapter.

To investigate the wind farm optimization problem with multiple types of wind turbines, five differing types of wind turbines are adopted in this study. The wind turbines are chosen from ENERCON products (ENERCON GmbH, 2015), and the five types are E-126, E-126 EP4, E-

101, E-82 and E-44. The rated powers range from 900 kW to 7580 kW, and the service time is assumed to be 20 years for each wind turbine. The key parameters of wind turbines are listed in Table 8.1. It is clear that not only the hub heights are diverse, the rotor diameters, cut-in speeds and rated speeds are different as well.

Table 8.1 The parameters of wind turbines (ENERCON GmbH, 2015)

Parameters	E-126	E-126 EP4	E-101	E-82	E-44
Rated power (kW)	7580	4200	3050	2000	900
Rotor diameter (m)	127	127	101	82	44
Cut-in speed (m/s)	3	3	2	2	3
Rated speed (m/s)	17	14	13	13	17
Cut-off speed (m/s)	25	25	25	25	25
Hub height (m)	135	135	99	78	45
Service years	20	20	20	20	20

The power curves of wind turbines are utilized to estimate the wind farm's output. Figure 8.3 and Figure 8.4 demonstrate the power curves and the power coefficient curves of the five chosen wind turbines respectively (ENERCON GmbH, 2015).

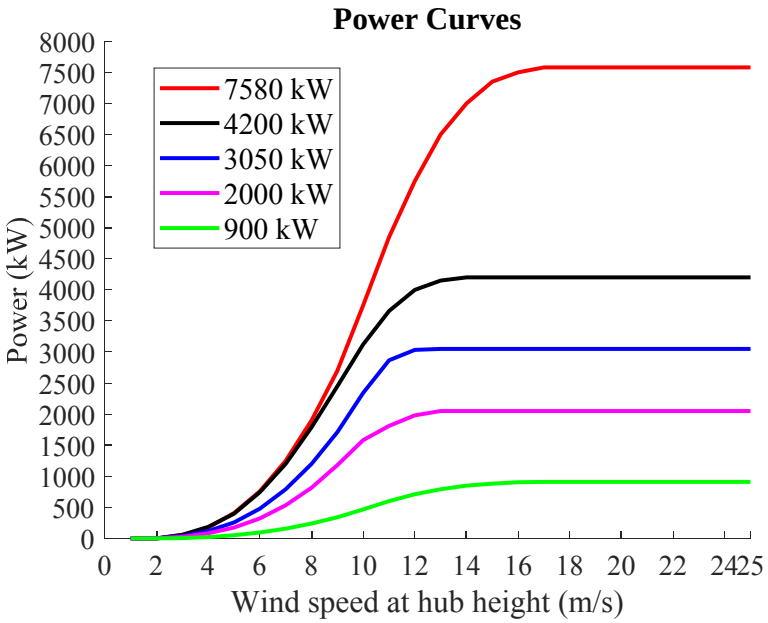

Figure 8.3 Power curves of the chosen wind turbines

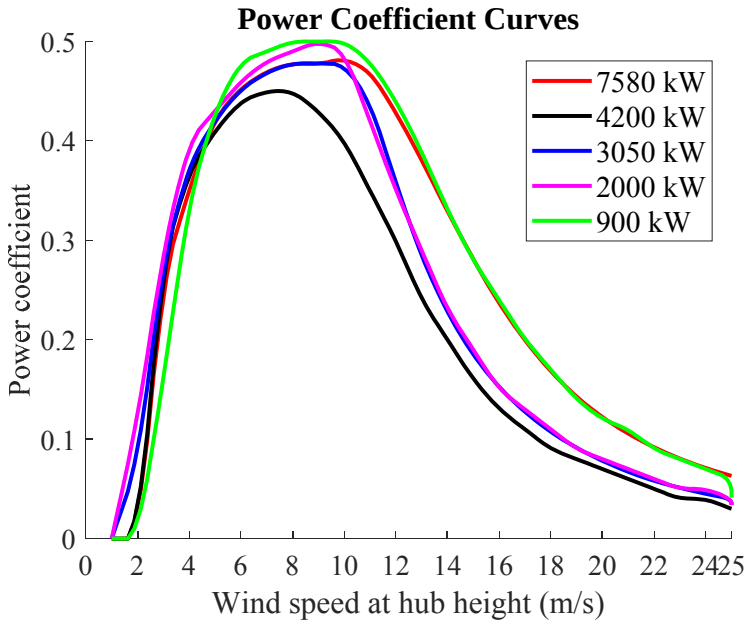

Figure 8.4 Power coefficient curves of the chosen wind turbines

8.3 Case study

In this study, four cases are demonstrated and discussed. To validate the effectiveness of the

Directional Restriction and the optimization method, the wind speeds assumed in the first three cases are smaller than the rated speeds for the wind turbines. If the wind speed is set larger than the rated speeds, 20 m/s for example, all wind turbines will generate energy as the rated power as long as they are installed meeting the qualifications of the restriction. It can be explained that the wind deficit caused by wake effect is limited, so the remaining wind speeds are still higher than the rated wind speeds of the wind turbines. Therefore, the proper setting of the incoming wind speed is really significant. In each case, the wind speed is identified. The potential wind farms in all cases are the square areas of 4 km by 4 km.

8.3.1 Case 1: aligned layout of uniform wind turbines

The first case is about an aligned arrangement of uniform wind turbines. The type of the wind turbine is E-82, and the rated power is 2,000 kW. The number of wind turbines is 48, which means the capacity of the whole wind farm is 98.4 MW. To compare the performances of the two restrictions in the concentrated wind direction, a constant wind condition is adopted. The only direction of the wind is the north, and the wind speed at the hub height is 8.0 m/s, which is smaller than the rated wind speed 13 m/s.

When the Omnidirectional Restriction is adopted, the wind turbines are aligned with 6 rows and 8 columns, as shown in Figure 8.5. The minimum interval between wind turbines is longer than 5D distance (410 m). Whereas, when the Directional Restriction is adopted, the wind turbines are aligned with 3 rows and 16 columns, as shown in Figure 8.6. The crosswind interval is shortened but larger than 3D distance (246 m), and the downwind intervals increase correspondingly.

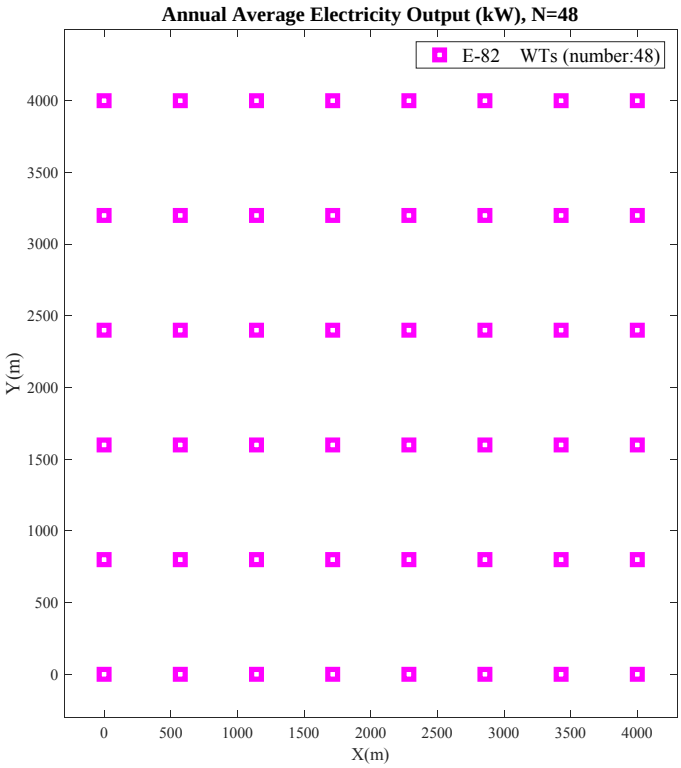

Figure 8.5 Aligned layout with the Omnidirectional Restriction

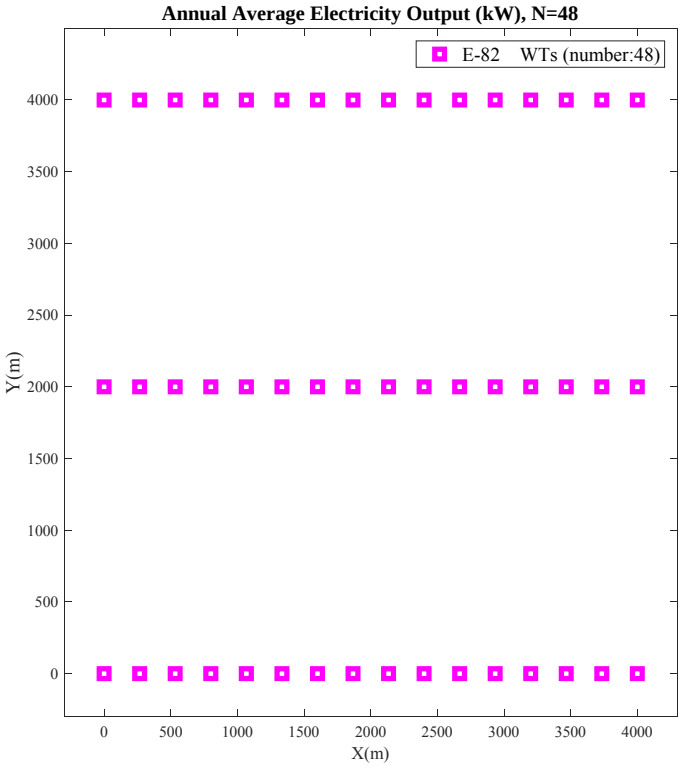

Figure 8.6 Aligned layout with the Directional Restriction

Table 8.2 lists the comparisons of the energy output of two restrictions. Theoretical output at given wind speed is also listed in the table. For E-82 wind turbine, according its power curve in Figure 8.3, the energy output is 837 kW at 8 m/s, which makes the total theoretical output as 40.18 MW.

Table 8.2 Comparisons of two types of restriction

Parameters	Omnidirectional Restriction	Directional Restriction
Number of wind turbine	48	48
Capacity (MW)	96.00	96.00
Theoretical output at given wind speed (MW)	40.18	40.18
Total Output (MW)	32.88	38.68
Utilization rate	81.83%	96.27%
Maximum wind turbine output (kW)	837	837
Minimum wind turbine output (kW)	650	787

To compare the effectiveness of different layouts, the utilization rate of wind farm is adopted, of which the formula is as follows:

$$\text{Utilization rate} = \frac{\text{Total output}}{\text{Theoretical output at given wind speed}} \times 100\% \quad (8.1)$$

From the results, the Directional Restriction has tremendous advantages under the circumstance

of constant wind condition. When the type and the number of wind turbines are same, the layout with the Directional Restriction can avoid much more energy losses caused by the wake effect. The average power of the layout with Directional Restriction is 38.68 MW and the energy utilization ration is 96.27%, which are much more than the 32.88 MW output power and 81.83% utilization rate of the layout with the Omnidirectional Restriction. The increment of the utilization rate is 14.44%. The maximum wind turbine outputs in both layouts are the same at 837 kW. The wind turbines with the maximum output are apparently those stand in the first line, facing the wind directly and are not affected by any wakes. However, the situations of other wind turbines are much differing. The minimum wind turbine output in the layout with the Directional Restriction is 787 kW, larger than that with the Omnidirectional Restriction (650 kW). This also attributes to the difference of the total energy outputs of two layouts. From the first case, it is indicated that the Directional Restriction is of practical use in aligned layout windfarm under the constant wind condition.

8.3.2 Case 2: optimized layout of uniform wind turbines

The Case 2 further investigated the optimization of the scattered arrangement. In this case, the type of wind turbine, the total wind turbine number and the wind condition are all the same as those in Case 1.

The optimization tool adopted in this study is the MPGA, the same as before. The number of wind turbine is 48, which represents the number of individual in optimization process is 48.

Figure 8.7 shows the optimized layout with the Omnidirectional Restriction, and Figure 8.8 shows the optimized layout with the Directional Restriction. Also, the comparisons of the

energy output of two restrictions are listed in Table 8.3.

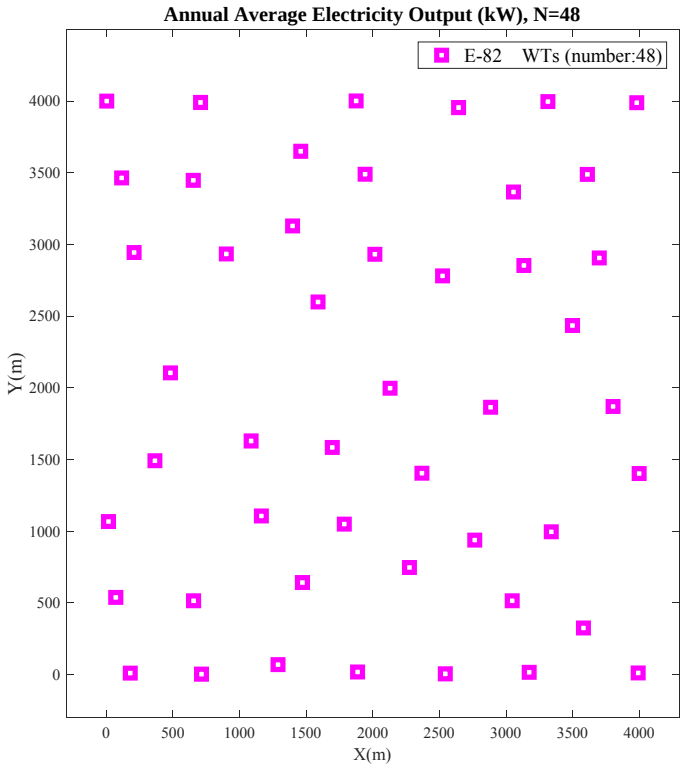

Figure 8.7 Optimized layout with the Omnidirectional Restriction

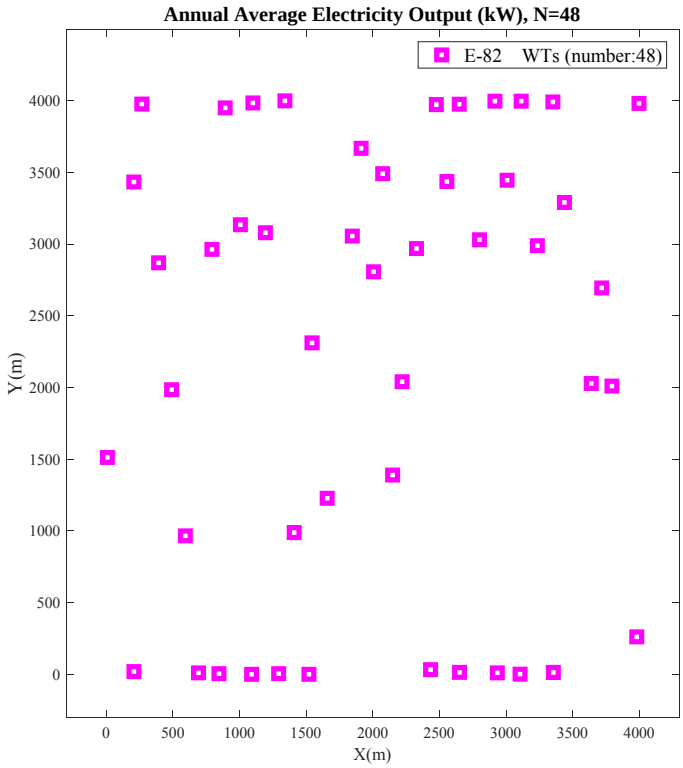

Figure 8.8 Optimized layout with the Directional Restriction

Table 8.3 Comparisons of two restrictions

Parameters	Omnidirectional Restriction	Directional Restriction
Number of wind turbine	48	48
Capacity (MW)	96.00	96.00
Theoretical output at given wind speed (MW)	40.18	40.18
Actual Output (MW)	39.35	39.72
Utilization rate	97.93%	98.86%
Maximum wind turbine output (kW)	837	837
Minimum wind turbine output (kW)	757	800

Case 2 not only demonstrates the comparison of two restrictions, but also verifies the effective of the MPGA once again. Through the optimization process, the layout with the Omnidirectional Restriction improves the energy output compared to that of the aligned layout in Case 1. To be specific, the increment of power output is from 32.88 MW to 39.35 MW, and the utilization rate increases by 16.10%, from 81.83% to 97.93%. As for the optimized layout with the Directional Restriction, it also raises the power output compared to the aligned layout, from 38.68 MW to 39.72 MW, with a utilization rate increases of 2.59% from 96.27% to 98.86%. The power output increment of the Directional Restriction is not prominent, just from 39.35 MW to 39.72 MW, and the utilization rate increases by 0.93%, from 97.93% to 98.86%, which is similarly not remarkable. This is because the efficiency of the original Directional Restriction is as high as 97.93%, so the room for improvement of utilization rate is really limited.

8.3.3 Case 3: optimized layout with multiple wind turbines

In this case, a nonuniform wind farm with multiple wind turbines is studied. The five adopted wind turbines have been introduced in section 8.2. The total number of wind turbine is 45 and the number of each type is 9, hence the capacity of wind farm is 159.57 MW. The wind constantly blows from north and the speed is 10.0 m/s at the hub height of 135 m. The MPGA is applied as the optimization tool. In this case, the Directional Restriction is applied, the restricted area of which is 5D distance in downwind direction and 2.5D distance in crosswind direction. Since diameters of wind turbines are different, the corresponding restricted areas are different as well.

In this case, the wind speed variation with height is also taken into account. The Power law is applied, which has been introduced in section 3.1.3. Figure 8.9 demonstrates the final optimal

layout. From the layout pattern, it is seen clearly that the restricted area is unique for each type of wind turbine, especially in the crosswind direction.

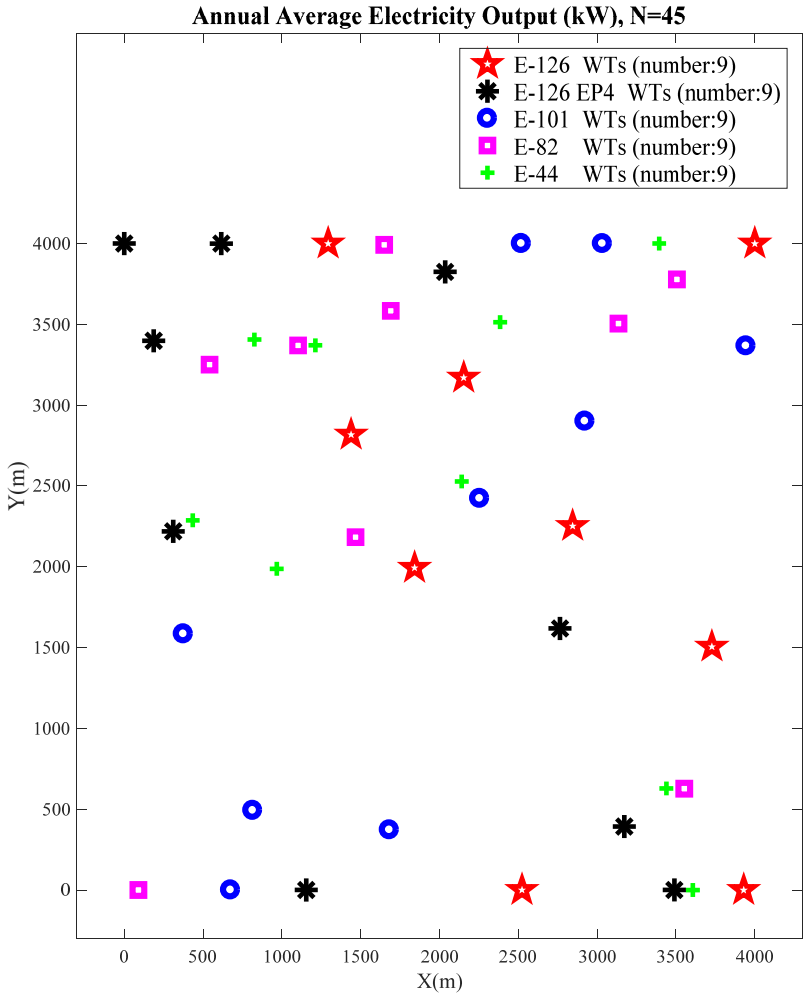

Figure 8.9 optimized layout with nonuniform wind turbines

The detailed analysis results of Case 3 are listed in Table 8.4. Since hub heights of wind turbines are different, the corresponding wind speeds at different hub heights are calculated and listed in the table. The maximum wind speed is 10.0 m/s at the height of 135 m, whereas the minimum one is 6.4 m/s at the height at 88 m. The theoretical outputs of each wind turbines are obtained from the wind power curves. The theoretical wind farm output is the sum of theoretical output

of all wind turbines in the wind farm.

Table 8.4 Analysis of Case 3

Parameters	E-126	E-126 EP4	E-101	E-82	E-44
Wind speed at hub height (m/s)	10.0	10.0	8.8	8.0	6.4
Theoretical wind turbine output (kW)	3750	3097	1631	837	119
Number of wind turbine	9	9	9	9	9
Maximum wind turbine output (kW)	3750	3097	1631	837	119
Utilization rate (maximum output)	100%	100%	100%	100%	100%
Minimum wind turbine output (kW)	3596	3016	1564	789	117
Utilization rate (minimum output)	95.89%	97.38%	95.89%	94.27%	98.32%
Capacity (MW)	159.57				
Theoretical maximum wind farm output (MW)	84.91				
Optimized wind farm output (MW)	84.24				
Utilization rate of wind farm	99.21%				

From the table, the theoretical outputs of wind turbines are 3750 kW, 3097 kW, 1631 kW, 837 kW and 119 kW respectively. In wind farm, because of the wake effect, not every wind turbine generates power as the predicted theoretical output. The maximum outputs and the minimum outputs of every type of wind turbines are also listed. Through the optimization process, the maximum outputs are all the same as the theoretical outputs, whereas the minimum outputs are 3596 kW, 3016 kW, 1564 kW, 789 kW and 117 kW respectively. Of all wind turbines in the wind farm, the minimum utilization rate is 94.27%, and the output of wind farm is 84.24 MW, which makes the utilization rate as high as 99.21%. The effectivenesses of the Directional

Restriction and optimization method are further confirmed.

8.3.4 Case 4: a commercial nonuniform offshore wind farm

In this case, a real commercial wind farm is designed. Five types of wind turbines are used, the wind speeds come from the observation data, and the wind speed variation with height is also considered, which has been introduced in Case 3. The MPGA is still the optimization tool and the Directional Restriction is also applied, with the restriction of 5D distance in downwind direction and 3D distance in crosswind direction.

The potential wind farm site is chosen from Hong Kong sea areas. According to the study of Gao et al. (2014b), four potential sea areas are suitable to build offshore wind farm in Hong Kong. Sha Chau Island sea area, as shown in Figure 8.10, has huge sea area and good potential of offshore wind energy to build offshore wind farms, which is therefore selected here. The size of the chosen offshore area is 4 km × 4 km. The satellite image of Sha Chau Island is shown in Figure 8.11.

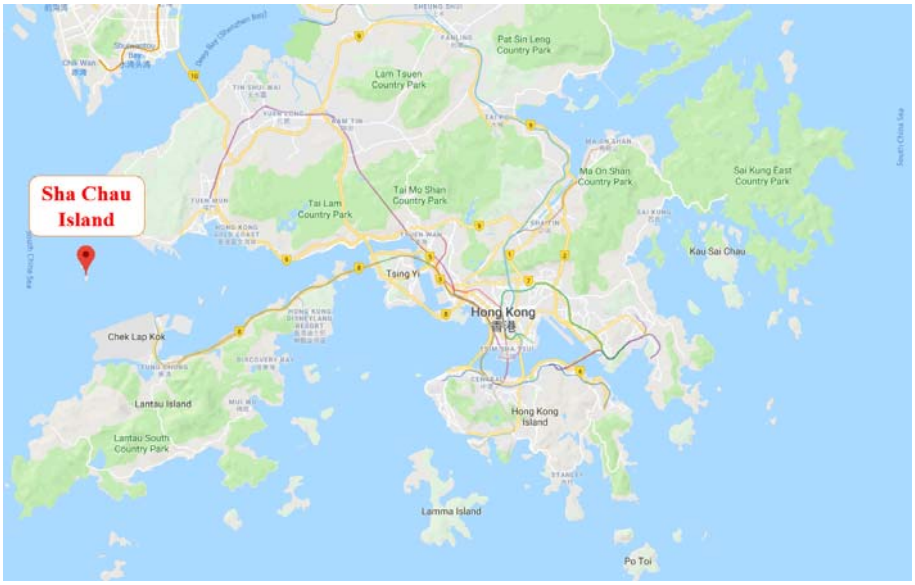

Figure 8.10 The location of Sha Chau Island (Google Map, 2018a)

Figure 8.11 Satellite image of Sha Chau Island (Wikipedia)

With the first-hand wind data of the Sha Chau Island sea area, the wind rose diagram can be obtained, as shown in Figure 8.12.

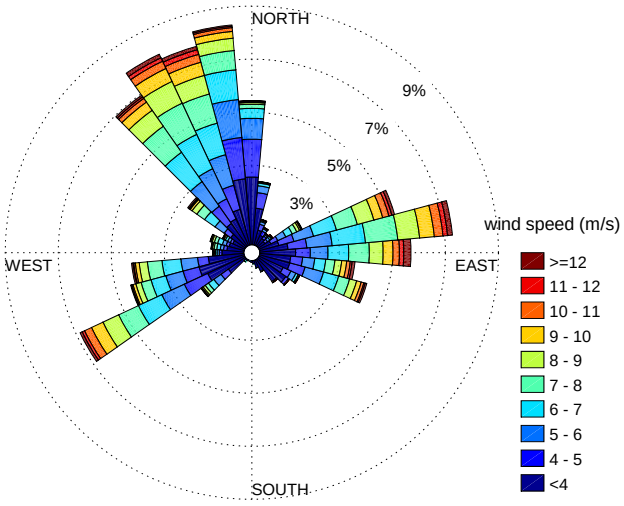

Figure 8.12 Wind rose diagram of Sha Chau

From the wind rose diagram, the wind direction is not centralized but distributed to three major directions. Next, the wind speed frequency distribution is also obtained, as shown in Figure 8.13.

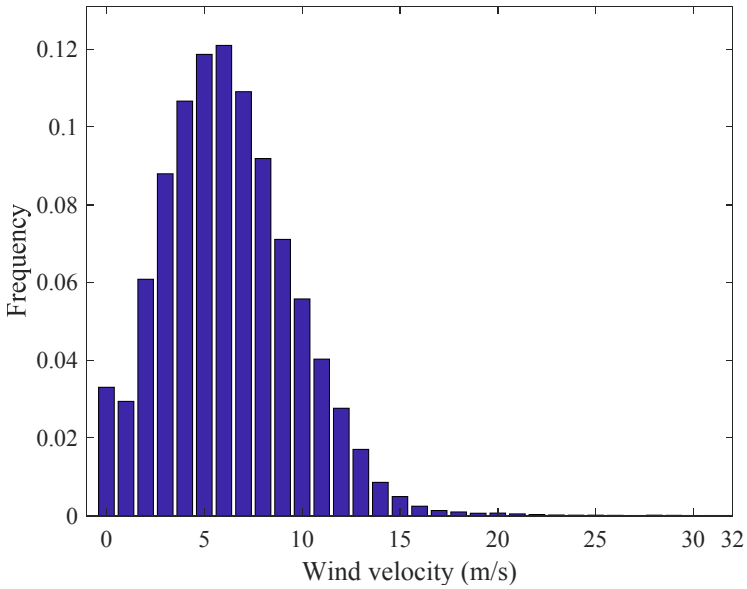

Figure 8.13 Wind speed frequency of Sha Chau

The wind farm is also designed with five types of wind turbines. The number of each type of

the wind turbine is 9, and the capacity of wind farm is also 159.57 MW. Figure 8.14 demonstrates the final layout pattern of the optimized result. The directivity of the layout is not as obvious as the first three cases, this is because that the incoming wind direction is not highly-centralized.

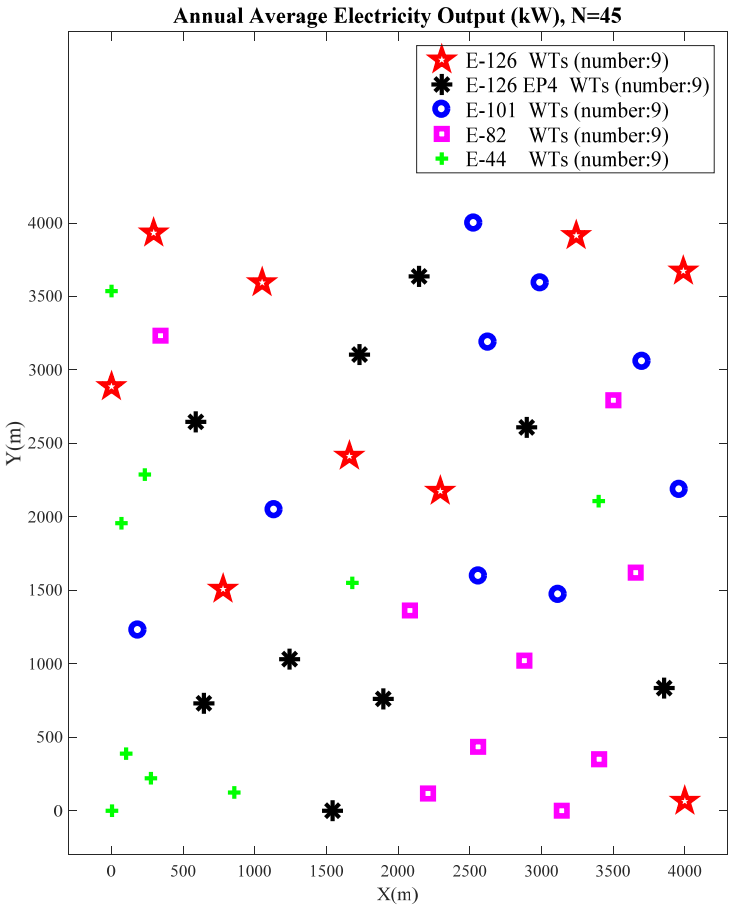

Figure 8.14 optimized layout of a commercial wind farm with nonuniform wind turbines

The analysis of Case 4 is listed in Table 8.5.

Table 8.5 Analysis of Case 4

Parameters	E-126	E-126 EP4	E-101	E-82	E-44
Number of wind turbine	9	9	9	9	9
Maximum wind turbine output (kW)	4420	2822	2029	1304	481
Minimum wind turbine output (kW)	4335	2756	1990	1260	472
Capacity (MW)	159.57				
Optimized wind farm output (MW)	98.57				

With the Directional Restriction, this nonuniform offshore wind farm has the annual average power output of 98.57 MW. For the same type of wind turbine, the differences between the maximum and the minimum power are very small. The maximum difference is only 85 kW from E-126 wind turbines. The average power output of wind turbines also demonstrates that the adopted optimization method is effective.

8.4 Summary

This chapter conducted the research on the spacing restrictions of wind farms and the layout optimization problem of nonuniform wind farms. An original Directional Restriction has been presented, which was applied in the optimization process of the nonuniform wind farm with various types of wind turbines. Four typical cases were studied to validate the presented Directional Restriction and the optimization method. Through this study, the main conclusions can be drawn:

(1) The presented Directional Restriction is effective for the wind farm where the direction of the prevailing wind is distinct. In the aligned layout design, where the wind direction was

fixed and wind speed was constant, the Directional Restriction improved the energy utilization ration in a uniform wind farm by 14.44%. The similar increase in the optimized layout design was 0.93%.

(2) The MPGA is a useful tool to solve the wind farm optimization problem. In the uniform wind farm, with the Omnidirectional Restriction, the optimization made an increase of 16.10% in energy utilization rate. The same increasing trend in the wind farm with the Directional Restriction was 2.59%.

(3) The nonuniform layout is effective in making use of the spatial wind source. In the nonuniform wind farm with five types of wind turbines, the optimization process with the Directional Restriction considered the wind speed variation with height. The utilization rate of the whole wind farm was as high as 99.21%. The five maximum utilization rates of different types of wind turbines were all 100%, and the minimum utilization rate of all wind turbines was 94.27%.

(4) The Directional Restriction and the MPGA were used in the layout optimization of a commercial nonuniform offshore wind farm. The potential site was chosen in Sha Chau Island seawater area in Hong Kong and the real measured wind data were adopted. The designed nonuniform offshore wind farm had an annual average power output of 98.57 MW. It demonstrated that the proposed optimization method is practical in designing wind farm, and Hong Kong offshore area is an ideal region to develop the offshore wind power.

Chapter 9

Conclusions and Recommendations for Future Work

9.1 Conclusions

A detailed research work on the wake effect and the wind farm optimization problems has been investigated and reported. Firstly, the new 3-D wake models for a single and multiple wind turbines have been developed and validated by published wind tunnel experimental data. Secondly, full-scale wind field experiments have been performed to investigate the characteristics of wakes and further study the wake models. Thirdly, some new strategies have been proposed for solving the offshore wind farm layout optimization problems. The conclusions are as follows.

An analytical 3-D wind turbine wake model for a single wind turbine has been proposed. The wake model considers the wind variation in the vertical direction. Then, the wake model for multiple wind turbines has been further developed. The wake models have been validated to have excellent accuracies with the wind tunnel experimental data. A series of wake profiles predicted by the 3-D wake models have been demonstrated. The wake models have the potential to optimize the layout of wind turbines in nonuniform wind farms. The method to calculate the average wind speed of a single wind turbine has also been proposed. The hub height, rotor radius and power exponent all have influence on the average wind speed. The reduction of average wind speed should be considered especially for wind turbines that have large rotor radius, stand at high positions and are built in the terrain with large irregular objects.

The full-scale measurements in the complex-terrain wind fields have been conducted to study

the characteristics of wakes and to validate the proposed wake models. From the experiments, the range of the wake-influenced area expands along the downstream direction, whereas the largest wind speed deficit decreases gradually. The wake centerlines of the upstream and downstream wind turbines can be different. Fluctuations of wind speeds were observed in the far-wake zone. With the experimental data, the presented 3-D wake models have been proved to have good overall accuracies. In the vertical direction, the wake models tended to have better predictions in all higher positions than those in near-ground positions. For horizontal directions, the 3-D wake models showed good accuracies at the far wake positions and also near the inflow measuring site. Deficits of wind speed exist before an operating wind turbine, which could not be estimated from the wake models. Comparing to the 3-D wake models, the traditional 2-D wake model tends to overestimate wind speeds and wind energy outputs.

Strategies for offshore wind farm layout optimization problem have been presented. Repowering strategy has been proposed for the optimization process, which can significantly decrease the LCoE. A case study in Waglan Island sea area in Hong Kong is demonstrated. If the repowering strategy is applied, the LCoE could reduce by nearly 16.63% and to only 1.0310 HK$/kWh. A new Directional Restriction has been presented to restrict the distance between wind turbines. The method separately limits the interval between wind turbines in downwind and crosswind directions, which could make better use of wind resources. For the region with highly-centralized wind directions, the Directional Restriction works more effectively. The application of the Directional Restriction can also improve the capacity of wind farms by installing more wind turbines.

The outcomes of the research work reported in this thesis could make impacts on the wind energy research and engineering. The study have been carried out from the aspects of the

development of 3-D wake models, full-scale wind field measurements and the offshore wind farm layout optimization issues. The mentioned research is expected to be globally applicable, and particularly useful in regions like Hong Kong where full of offshore wind energy resources.

9.2 Future work

Following the successful completion of the research work reported in this thesis, a number of future related possible studies are proposed as follows.

According to the results reported in Chapter 3 and Chapter 4, some errors have be found between the wind simulations and the measured data. This may be because the power law function has been adopted to simulate the incoming wind, which brings errors to the final estimations of the downstream wind speeds. In addition, the power function cannot predict some complicate wind profiles in real wind industry as well. To complete the 3-D wake model, some additional research should be further conducted. The proper function to simulate the incoming wind distribution is significant. The power law function applied in this study may be the one reasons for the error in the incoming wind. It also complicates the calculation to some extent. Therefore, a more accurate and simple function to replace the present power function is required. In addition, some parameters in the 3-D wake model should be adjusted to fit in different operating conditions.

The published wind tunnel experimental data are not quite enough to continue an in-depth investigation of the presented wake model. According to the analysis, some experimental errors affected the validation of the wake model to some extent. The published measurement data are not enough to conduct an in-depth study of the proposed model. Therefore, well-directed wind tunnel tests should be conducted in the near future to determine the parameters and complete

the validation of the 3-D wake models.

The experimental investigation presented in Chapter 5 provides a better understanding of the wind turbine wake characteristics in the complex-terrain wind farm. However, not much of the terrain factors have been involved in this study so far. Therefore, further study would be conducted focusing on how terrains influence the wake effect. Attention needs to be paid to the relationship between inflows and wakes, as some previous experiments only measured wakes downstream of a wind turbine, which cannot explain or predict the development of wakes. In addition, the vast majority of the previous experiments were carried out at onshore wind farms, however, with the increasing development of offshore wind industry, more attentions should be paid on the experimental study on offshore wind energy.

The complex terrain of the tested wind farm makes the inflow and the wind distribution at the near-wake zone more complicated, which may beyond the prediction of the presented 3-D wake models. Therefore, involving more practical factors of complex terrain in the wake models is a very important future research field. The accuracies of the models could be improved with the increase of the downstream distance and the distance from the centerline. Comparing the wind speeds in the two symmetrical side sections, different distributions were demonstrated in the same downwind positions, which contributed to the errors of the wake models. The asymmetrical characteristics of wakes also deserve further studies.

The repowering strategy and the Directional Restriction provide good ideas to reduce the cost of the offshore wind farm and increase the energy output. However, these are theoretical studies looking for ways to increase the utilization of wind energy in a given ocean area, some aspects of building a real wind farm are neglected. Therefore, more aspects can also be considered in

the optimization process. The strategies related to other issues like cable layout, power dispatch and restricted zone etc. could also be considered in the further studies. On the other hand, to fully utilize the resources of wind farms and the benefit of the Directional Restriction, further study should be conducted on how to use the Directional Restriction to improve the capacity of the wind farm in a specific area.

References

Ainslie, J. F. (1988). Calculating the flowfield in the wake of wind turbines. *Journal of Wind Engineering and Industrial Aerodynamics, 27*(1-3), 213-224.

Aitken, M. L., Banta, R. M., Pichugina, Y. L., & Lundquist, J. K. (2014). Quantifying wind turbine wake characteristics from scanning remote sensor data. *Journal of atmospheric and oceanic technology, 31*(4), 765-787.

Aitken, M. L., & Lundquist, J. K. (2014). Utility-scale wind turbine wake characterization using nacelle-based long-range scanning lidar. *Journal of atmospheric and oceanic technology, 31*(7), 1529-1539.

Amaral, L., & Castro, R. (2017). Offshore wind farm layout optimization regarding wake effects and electrical losses. *Engineering Applications of Artificial Intelligence, 60*, 26-34.

Annealing, S., & Machines, B. (1991). A Stochastic Approach to Combinatorial Optimization and Neural Computing. In: Chichester (Wiley).

Aubrun, S., Garcia, E. T., Boquet, M., Coupiac, O., & Girard, N. (2016). *Wind turbine wake tracking and its correlations with wind turbine monitoring sensors. Preliminary results.* Paper presented at the Journal of Physics: Conference Series.

Banta, R. M., Pichugina, Y. L., Brewer, W. A., Lundquist, J. K., Kelley, N. D., Sandberg, S. P., . . . Weickmann, A. M. (2015). 3D volumetric analysis of wind turbine wake properties in the atmosphere using high-resolution Doppler lidar. *Journal of atmospheric and oceanic technology, 32*(5), 904-914.

Barthelmie, R. J., Folkerts, L., Larsen, G. C., Rados, K., Pryor, S. C., Frandsen, S. T., . . . Schepers, G. (2006). Comparison of wake model simulations with offshore wind turbine wake profiles measured by sodar. *Journal of atmospheric and oceanic technology, 23*(7), 888-901.

Barthelmie, R. J., Folkerts, L., Ormel, F. T., Sanderhoff, P., Eecen, P. J., Stobbe, O., & Nielsen,

N. M. (2003). Offshore wind turbine wakes measured by sodar. *Journal of atmospheric and oceanic technology, 20*(4), 466-477.

Barthelmie, R. J., Frandsen, S. T., Nielsen, M. N., Pryor, S. C., Rethore, P. E., & Jorgensen, H. E. (2007). Modelling and measurements of power losses and turbulence intensity in wind turbine wakes at Middelgrunden offshore wind farm. *Wind Energy, 10*(6), 517-528.

Barthelmie, R. J., Hansen, K., Frandsen, S. T., Rathmann, O., Schepers, J. G., Schlez, W., . . . Chaviaropoulos, P. K. (2009). Modelling and Measuring Flow and Wind Turbine Wakes in Large Wind Farms Offshore. *Wind Energy, 12*(5), 431-444.

Barthelmie, R. J., Pryor, S. C., Frandsen, S. T., Hansen, K. S., Schepers, J. G., Rados, K., . . . Neckelmann, S. (2010). Quantifying the Impact of Wind Turbine Wakes on Power Output at Offshore Wind Farms. *Journal of atmospheric and oceanic technology, 27*(8), 1302-1317.

Barthelmie, R. J., Pryor, S. C., Wildmann, N., & Menke, R. (2018). *Wind turbine wake characterization in complex terrain via integrated Doppler lidar data from the Perdigao experiment.* Paper presented at the Journal of Physics: Conference Series.

Bastankhah, M., & Porté-Agel, F. (2014). A new analytical model for wind-turbine wakes. *Renewable Energy, 70*, 116-123.

Bastine, D., Wächter, M., Peinke, J., Trabucchi, D., & Kühn, M. (2015). *Characterizing wake turbulence with staring lidar measurements.* Paper presented at the Journal of Physics: Conference Series.

Bingöl, F., Mann, J., & Larsen, G. C. (2010). Light detection and ranging measurements of wake dynamics part I: one-dimensional scanning. *Wind Energy: An International Journal for Progress and Applications in Wind Power Conversion Technology, 13*(1), 51-61.

Bodini, N., Zardi, D., & Lundquist, J. K. (2017). Three-dimensional structure of wind turbine wakes as measured by scanning lidar. *Atmospheric Measurement Techniques, 10*(8), 2881-2896.

Bonou, A., Laurent, A., & Olsen, S. I. (2016). Life cycle assessment of onshore and offshore wind energy-from theory to application. *Applied Energy, 180*, 327-337.

Cao, J., Wang, T., Long, H., Ke, S., & Xu, B. (2015). Dynamic loads and wake prediction for large wind turbines based on free wake method. *Transactions of Nanjing University of Aeronautics and Astronautics, 32*(2), 240-249.

Carbajo Fuertes, F., Markfort, C. D., & Porté-Agel, F. (2018). Wind Turbine Wake Characterization with Nacelle-Mounted Wind Lidars for Analytical Wake Model Validation. *Remote Sensing, 10*(ARTICLE), 668.

Carper, M. A., & Porté-Agel, F. (2008a). Subfilter-scale fluxes over a surface roughness transition. Part I: Measured fluxes and energy transfer rates. *Boundary-Layer Meteorology, 126*(1), 157-179.

Carper, M. A., & Porté-Agel, F. (2008b). Subfilter-scale fluxes over a surface roughness transition. Part II: A priori study of large-Eddy simulation models. *Boundary-Layer Meteorology, 127*(1), 73-95.

Carrasco, J. M., Bialasiewicz, J. T., Guisado, R. C. P., & León, J. I. (2006). Power-Electronic Systems for the Grid Integration of Renewable Energy Sources A Survey. *IEEE TRANSACTIONS ON INDUSTRIAL ELECTRONICS, VOL. 53, NO. 4*.

Carrillo, C., Montaño, A. O., Cidrás, J., & Díaz-Dorado, E. (2013). Review of power curve modelling for wind turbines. *Renewable and Sustainable Energy Reviews, 21*, 572-581.

Chamorro, L. P., Arndt, R., & Sotiropoulos, F. (2011). Turbulent flow properties around a staggered wind farm. *Boundary-Layer Meteorology, 141*(3), 349-367.

Chamorro, L. P., & Porte-Agel, F. (2011). Turbulent Flow Inside and Above a Wind Farm: A

Wind-Tunnel Study. *Energies, 4*(11), 1916-1936.

Chamorro, L. P., & Porté-Agel, F. (2009). A wind-tunnel investigation of wind-turbine wakes: boundary-layer turbulence effects. *Boundary-Layer Meteorology, 132*(1), 129-149.

Charhouni, N. (2015). Qualification of three analytical wake models. *S12 Fiabilité et robustesse des systèmes mécaniques*.

Chen, K., Song, M. X., & Zhang, X. (2014). The iteration method for tower height matching in wind farm design. *Journal of Wind Engineering and Industrial Aerodynamics, 132*, 37-48.

Chen, K., Song, M. X., Zhang, X., & Wang, S. F. (2016). Wind turbine layout optimization with multiple hub height wind turbines using greedy algorithm. *Renewable Energy, 96*, 676-686.

Chen, Y., Li, H., Jin, K., & Song, Q. (2013). Wind farm layout optimization using genetic algorithm with different hub height wind turbines. *Energy Conversion and Management, 70*, 56-65.

Chowdhury, S., Zhang, J., Messac, A., & Castillo, L. (2012). Unrestricted wind farm layout optimization (UWFLO): Investigating key factors influencing the maximum power generation. *Renewable Energy, 38*(1), 16-30.

Chowdhury, S., Zhang, J., Messac, A., & Castillo, L. (2013). Optimizing the arrangement and the selection of turbines for wind farms subject to varying wind conditions. *Renewable Energy, 52*, 273-282.

Churchfield, M. (2013). *A review of wind turbine wake models and future directions.* Paper presented at the Proceedings of the North American Wind Energy Academy Symposium (NAWEA'13).

Cleijne, J. (1993). Results of sexbierum wind farm: single wake measurements.

Climate Change Capital. (2010). *Offshore Renewable Energy Installation Decommissioning*

Study

Clive, P. J., Dinwoodie, I., & Quail, F. (2011). Direct measurement of wind turbine wakes using remote sensing. *Proc. EWEA 2011*.

Crespo, A., & Herna, J. (1996). Turbulence characteristics in wind-turbine wakes. *Journal of Wind Engineering and Industrial Aerodynamics, 61*(1), 71-85.

Crespo, A., Hernandez, J., Fraga, E., & Andreu, C. (1988). Experimental validation of the UPM computer code to calculate wind turbine wakes and comparison with other models. *Journal of Wind Engineering and Industrial Aerodynamics, 27*(1-3), 77-88.

Debnath, M., Iungo, G. V., Ashton, R., Alan Brewer, W., Choukulkar, A., Delgado, R., . . . Wolfe, D. (2018). Vertical profiles of the 3-D wind velocity retrieved from multiple wind lidars performing triple range-height-indicator scans. *Atmospheric Measurement Techniques, 10*(2).

Djerf, E., & Mattsson, H. (2000). Evaluation of the software program windfarm and comparisons with measured data from alsvik. *The aeronautical research institute of Sweden*.

Dobesch, H., & Kury, G. (2006). *Basic meteorological concepts and recommendations for the exploitation of wind energy in the atmospheric boundary layer*: Zentralanstalt für Meteorologie und Geodynamik.

Dodd, J. (2015). Decommissioning - Should they stay or should they go? Retrieved from http://www.windpowermonthly.com/article/1349270/decommissioning-stay-go

Dolman, S., & Simmonds, M. (2010). Towards best environmental practice for cetacean conservation in developing Scotland's marine renewable energy. *Marine Policy, 34*(5), 1021-1027.

Dufresne, N. P., & Wosnik, M. (2013). Velocity deficit and swirl in the turbulent wake of a wind turbine. *Marine Technology Society Journal, 47*(4), 193-205.

Eecen, P., Barhorst, S., Braam, H., Curvers, A., Korterink, H., Machielse, L., . . . van Der Werff, P. (2006). *Measurements at the ECN wind turbine test location Wieringermeer.* Paper presented at the Proc. EWEC.

Ekins, P., Vanner, R., & Firebrace, J. (2006). Decommissioning of offshore oil and gas facilities: A comparative assessment of different scenarios. *J Environ Manage, 79*(4), 420-438.

Ela, E., Milligan, M., Kirby, B., Eamonn Lannoye, Flynn, D., O'Malley, M., & Zavadil, B. (2010). *Evolution of Operating Reserve Determination in Wind Power Integration Studies*. Paper presented at the IEEE Power & Energy Society General Meeting, Minneapolis, Minnesota.

ENERCON GmbH. (2015). ENERCON product overview. https://www.enercon.de/fileadmin/Redakteur/Medien-Portal/broschueren/pdf/en/ENERCON_Produkt_en_06_2015.pdf

Eroğlu, Y., & Seçkiner, S. U. (2012). Design of wind farm layout using ant colony algorithm. *Renewable Energy, 44*, 53-62.

Feng, J., & Shen, W. Z. (2017). Design optimization of offshore wind farms with multiple types of wind turbines. *Applied Energy, 205*, 1283-1297.

Fleming, P., Annoni, J., Scholbrock, A., Quon, E., Dana, S., Schreck, S., . . . Schlipf, D. (2017). *Full-Scale Field Test of Wake Steering.* Paper presented at the Journal of Physics: Conference Series.

Forsting, A. M., Bechmann, A., & Troldborg, N. (2016). *A numerical study on the flow upstream of a wind turbine in complex terrain.* Paper presented at the Journal of Physics: Conference Series.

Frandsen, S., Barthelmie, R., Pryor, S., Rathmann, O., Larsen, S., Højstrup, J., & Thøgersen, M. (2006). Analytical modelling of wind speed deficit in large offshore wind farms. *Wind Energy, 9*(1-2), 39-53.

Gao, X., Yang, H., & Lu, L. (2014a). Investigation into the optimal wind turbine layout patterns for a Hong Kong offshore wind farm. *Energy, 73*, 430-442.

Gao, X., Yang, H., & Lu, L. (2014b). Study on offshore wind power potential and wind farm optimization in Hong Kong. *Applied Energy, 130*, 519-531.

Gao, X., Yang, H., & Lu, L. (2016). Optimization of wind turbine layout position in a wind farm using a newly-developed two-dimensional wake model. *Applied Energy, 174*, 192-200.

Global Wind Energy Council. (2016). Global wind 2015 report Annual Market Update. *Global Wind Energy Council (GWEC), Brussels, Belgium*.

Global Wind Energy Council. (2019). Global wind 2018 report Annual Market Update. *Global Wind Energy Council (GWEC), Brussels, Belgium*.

Google Map (Cartographer). (2018a). Sha Chau Island

Google Map (Cartographer). (2018b). Waglan Island

Grady, S., Hussaini, M., & Abdullah, M. M. (2005). Placement of wind turbines using genetic algorithms. *Renewable Energy, 30*(2), 259-270.

Hand, D. (1994). Genetic algorithms in search, optimization and machine learning. *Statistics and Computing, 4*(2), 158.

Heba Hashem. (2014). Offshore decommissioning market is emerging, but is wind industry prepared? Retrieved from http://analysis.windenergyupdate.com/operations-maintenance/offshore-decommissioning-market-emerging-wind-industry-prepared

Herbert-Acero, J.-F., Franco-Acevedo, J.-R., Valenzuela-Rendón, M., & Probst-Oleszewski, O. (2009). *Linear wind farm layout optimization through computational intelligence.* Paper presented at the Mexican International Conference on Artificial Intelligence.

Heritage, S. N. (2013). Research and guidance on restoration and decommissioning of onshore wind farms.

Hirth, B. D., & Schroeder, J. L. (2013). Documenting wind speed and power deficits behind a

utility-scale wind turbine. *Journal of Applied Meteorology and Climatology*, *52*(1), 39-46.

Hirth, B. D., Schroeder, J. L., Gunter, W. S., & Guynes, J. G. (2012). Measuring a utility-scale turbine wake using the TTUKa mobile research radars. *Journal of atmospheric and oceanic technology*, *29*(6), 765-771.

Hirth, B. D., Schroeder, J. L., Gunter, W. S., & Guynes, J. G. (2015). Coupling Doppler radar-derived wind maps with operational turbine data to document wind farm complex flows. *Wind Energy*, *18*(3), 529-540.

Hirth, B. D., Schroeder, J. L., Irons, Z., & Walter, K. (2016). Dual-Doppler measurements of a wind ramp event at an Oklahoma wind plant. *Wind Energy*, *19*(5), 953-962.

Hou, P., Enevoldsen, P., Hu, W., Chen, C., & Chen, Z. (2017). Offshore wind farm repowering optimization. *Applied Energy*, *208*, 834-844.

Hou, P., Hu, W., Soltani, M., & Chen, Z. (2015a). *A novel energy yields calculation method for irregular wind farm layout.* Paper presented at the Industrial Electronics Society, IECON 2015-41st Annual Conference of the IEEE.

Hou, P., Hu, W., Soltani, M., & Chen, Z. (2015b). Optimized Placement of Wind Turbines in Large-Scale Offshore Wind Farm Using Particle Swarm Optimization Algorithm. *Ieee Transactions on Sustainable Energy*, *6*(4), 1272-1282.

Hou, P., Hu, W., Soltani, M., Zhang, B., & Chen, Z. (2016). *Optimization of Decommission Strategy for Offshore Wind Farms.* Paper presented at the 2016 IEEE Power & Energy Society General Meeting.

Hu, B. (2016). *Design of a Simple Wake Model for the Wind Farm Layout Optimization Considering the Wake Meandering Effect*

Ilinca, A., McCarthy, E., Chaumel, J.-L., & Rétiveau, J.-L. (2003). Wind potential assessment of Quebec Province. *Renewable Energy*, *28*(12), 1881-1897.

Ishihara, T., Yamaguchi, A., & Fujino, Y. (2004). Development of a new wake model based on a wind tunnel experiment. *Global wind power, 6*.

Iungo, G. V., Wu, Y.-T., & Porté-Agel, F. (2013). Field measurements of wind turbine wakes with lidars. *Journal of atmospheric and oceanic technology, 30*(2), 274-287.

Jensen, L., Mørch, C., Sørensen, P., & Svendsen, K. (2004). *Wake measurements from the Horns Rev wind farm*. Paper presented at the European wind energy conference.

Jensen, N. O. (1983). *A note on wind generator interaction*.

Jimenez, A., Crespo, A., Migoya, E., & García, J. (2007). *Advances in large-eddy simulation of a wind turbine wake*. Paper presented at the Journal of Physics: Conference Series.

Johnson, G. L. (1985). *Wind energy systems*: Prentice-Hall Englewood Cliffs (NJ).

Jowder, F. A. (2009). Wind power analysis and site matching of wind turbine generators in Kingdom of Bahrain. *Applied Energy, 86*(4), 538-545.

Kaldellis, J., Apostolou, D., Kapsali, M., & Kondili, E. (2016). Environmental and social footprint of offshore wind energy. Comparison with onshore counterpart. *Renewable Energy, 92*, 543-556.

Käsler, Y., Rahm, S., Simmet, R., & Kühn, M. (2010). Wake measurements of a multi-MW wind turbine with coherent long-range pulsed Doppler wind lidar. *Journal of atmospheric and oceanic technology, 27*(9), 1529-1532.

Katic, I., Højstrup, J., & Jensen, N. O. (1986). *A simple model for cluster efficiency*. Paper presented at the European wind energy association conference and exhibition.

Korsnes, M. (2016). Ambition and ambiguity: Expectations and imaginaries developing offshore wind in China. *Technological Forecasting and Social Change, 107*, 50-58.

Kumer, V.-M., Reuder, J., Svardal, B., Sætre, C., & Eecen, P. (2015). Characterisation of Single Wind Turbine Wakes with Static and Scanning WINTWEX-W LiDAR Data. *Energy Procedia, 80*, 245-254.

Kuo, J., Rehman, D., Romero, D. A., & Amon, C. H. (2018). A novel wake model for wind farm design on complex terrains. *Journal of Wind Engineering and Industrial Aerodynamics, 174*, 94-102.

Kusiak, A., & Zheng, H. (2010). Optimization of wind turbine energy and power factor with an evolutionary computation algorithm. *Energy, 35*(3), 1324-1332.

Lange, B., Waldl, H. P., Guerrero, A. G., Heinemann, D., & Barthelmie, R. J. (2003). Modelling of offshore wind turbine wakes with the wind farm program FLaP. *Wind Energy, 6*(1), 87-104.

Larsen, G. C. (2009). *A simple stationary semi-analytical wake model*

Larsen, G. C., Carlen, I., & Schepers, G. (1999). *Fatigue life consumption in wake operation.* Paper presented at the 2nd IEA Symposium on Wind Conditions for Wind Turbine Design.

Larsen, G. C., Højstrup, J., & Madsen, H. A. (1996). *Wind fields in wakes.* Paper presented at the 1996 European Union wind energy conference. Proceedings.

Larsen, G. C., Madsen Aagaard, H., Bingöl, F., Mann, J., Ott, S., Sørensen, J. N., . . . Thomsen, K. (2007). *Dynamic wake meandering modeling* (8755036023)

Larsen, G. C., Madsen, H. A., & Sørensen, N. N. (2003). *Mean wake deficit in the near field.* Paper presented at the 2003 European Wind Energy Conference and Exhibition.

Lee, J., Kim, D. R., & Lee, K.-S. (2015). Optimum hub height of a wind turbine for maximizing annual net profit. *Energy Conversion and Management, 100*, 90-96.

Lee, J. C., & Lundquist, J. K. (2017). Observing and Simulating Wind-Turbine Wakes During the Evening Transition. *Boundary-Layer Meteorology, 164*(3), 449-474.

Li, Q. a., Maeda, T., Kamada, Y., & Mori, N. (2017). Investigation of wake characteristics of a Horizontal Axis Wind Turbine in vertical axis direction with field experiments. *Energy, 141*, 262-272.

Li, Q. a., Maeda, T., Kamada, Y., & Mori, N. (2017). Investigation of wake effects on a Horizontal Axis Wind Turbine in field experiments (Part I: Horizontal axis direction). *Energy, 134*, 482-492.

Lissaman, P. B. S., Zambrano, T. G., & Gyatt, G. W. (1983). Wake structure measurements at the Mod-2 cluster test facility at Goodnoe Hills.

Lu, L., Yang, H., & Burnett, J. (2002). Investigation on wind power potential on Hong Kong islands—an analysis of wind power and wind turbine characteristics. *Renewable Energy, 27*(1), 1-12.

Lundberg, S. (2003). *Performance comparison of wind park configurations* (1401-6176)

Lundquist, J., Churchfield, M., Lee, S., & Clifton, A. (2015). Quantifying error of lidar and sodar Doppler beam swinging measurements of wind turbine wakes using computational fluid dynamics. *Atmospheric Measurement Techniques (Online), 8*(NREL/JA-5000-62369).

Lundquist, J. K., Takle, E. S., Boquet, M., Kosović, B., Rhodes, M. E., Rajewski, D., . . . Friedrich, K. (2014). *Lidar observations of interacting wind turbine wakes in an onshore wind farm.* Paper presented at the EWEA meeting proceedings.

MacHielse, L. A. H., Eecen, P. J., Korterink, H., Van Der Pijl, S. P., & Schepers, J. G. (2007). *ECN test farm measurements for validation of wake Models.* Paper presented at the European Wind Energy Conference and Exhibition 2007, EWEC 2007.

Magnusson, M., Rados, K., & Voutsinas, S. (1996). A study of the flow downstream of a wind turbine using measurements and simulations. *Wind Engineering*, 389-403.

Manuel, L., Veers, P. S., & Winterstein, S. R. (2001). Parametric models for estimating wind turbine fatigue loads for design. *Journal of solar energy engineering, 123*(4), 346-355.

McCarthy, J. (2015). Wind Farm Decommissioning: A Detailed Approach to Estimate Future Costs in Sweden. In.

Mirocha, J. D., Rajewski, D. A., Marjanovic, N., Lundquist, J. K., Kosović, B., Draxl, C., & Churchfield, M. J. (2015). Investigating wind turbine impacts on near-wake flow using profiling lidar data and large-eddy simulations with an actuator disk model. *Journal of Renewable and Sustainable Energy, 7*(4), 043143.

Mittal, P., Kulkarni, K., & Mitra, K. (2016). A novel hybrid optimization methodology to optimize the total number and placement of wind turbines. *Renewable Energy, 86*, 133-147.

Mosetti, G., Poloni, C., & Diviacco, B. (1994). Optimization of wind turbine positioning in large windfarms by means of a genetic algorithm. *Journal of Wind Engineering and Industrial Aerodynamics, 51*(1), 105-116.

Niayifar, A., & Porté-Agel, F. (2016). Analytical modeling of wind farms: A new approach for power prediction. *Energies, 9*(9), 741.

Ott, S., Berg, J., & Nielsen, M. (2011). Linearised CFD models for wakes. *Risø National Laboratory, Roskilde, Denmark.*

Parada, L., Herrera, C., Flores, P., & Parada, V. (2017). Wind farm layout optimization using a Gaussian-based wake model. *Renewable Energy, 107*, 531-541.

Park, J., & Law, K. H. (2015). Layout optimization for maximizing wind farm power production using sequential convex programming. *Applied Energy, 151*, 320-334.

Pérez, B., Mínguez, R., & Guanche, R. (2013). Offshore wind farm layout optimization using mathematical programming techniques. *Renewable Energy, 53*, 389-399.

Perveen, R., Kishor, N., & Mohanty, S. R. (2014). Off-shore wind farm development: Present status and challenges. *Renewable and Sustainable Energy Reviews, 29*, 780-792.

Peterson, E. W., & Hennessey Jr, J. P. (1978). On the use of power laws for estimates of wind power potential. *Journal of Applied Meteorology, 17*(3), 390-394.

Politis, E. S., Prospathopoulos, J., Cabezon, D., Hansen, K. S., Chaviaropoulos, P., &

Barthelmie, R. J. (2012). Modeling wake effects in large wind farms in complex terrain: the problem, the methods and the issues. *Wind Energy, 15*(1), 161-182.

Pookpunt, S., & Ongsakul, W. (2013). Optimal placement of wind turbines within wind farm using binary particle swarm optimization with time-varying acceleration coefficients. *Renewable Energy, 55*, 266-276.

Rados, K., Larsen, G., Barthelmie, R., Schlez, W., Lange, B., Schepers, G., . . . Magnisson, M. (2001). Comparison of wake models with data for offshore windfarms. *Wind Engineering, 25*(5), 271-280.

Rajewski, D. A., Takle, E. S., Lundquist, J. K., Oncley, S., Prueger, J. H., Horst, T. W., . . . Spoth, K. K. (2013). Crop wind energy experiment (CWEX): observations of surface-layer, boundary layer, and mesoscale interactions with a wind farm. *Bulletin of the American Meteorological Society, 94*(5), 655-672.

Reichardt, K., Negro, S. O., Rogge, K. S., & Hekkert, M. P. (2016). Analyzing interdependencies between policy mixes and technological innovation systems: The case of offshore wind in Germany. *Technological Forecasting and Social Change, 106*, 11-21.

Renkema, D. J. (2007). *Validation of wind turbine wake models.* (Master of Science), Delft University of Technology,

Rhodes, M. E., & Lundquist, J. K. (2013). The effect of wind-turbine wakes on summertime US midwest atmospheric wind profiles as observed with ground-based doppler lidar. *Boundary-Layer Meteorology, 149*(1), 85-103.

Samorani, M. (2013). The wind farm layout optimization problem. In *Handbook of wind power systems* (pp. 21-38): Springer.

Sanderse, B. (2009). Aerodynamics of wind turbine wakes. *Energy Research Center of the Netherlands (ECN), ECN-E–09-016, Petten, The Netherlands, Tech. Rep*.

Schepers, J. G., Obdam, T. S., & Prospathopoulos, J. (2012). Analysis of wake measurements from the ECN Wind Turbine Test Site Wieringermeer, EWTW. *Wind Energy, 15*(4), 575-591.

Schlez, W., Tindal, A., & Quarton, D. (2003). *GH wind farmer validation report*

Schmidt, J., & Stoevesandt, B. (2015). *The impact of wake models on wind farm layout optimization.* Paper presented at the Journal of Physics: Conference Series.

Sedaghatizadeh, N., Arjomandi, M., Kelso, R., Cazzolato, B., & Ghayesh, M. H. (2018). Modelling of wind turbine wake using large eddy simulation. *Renewable Energy, 115*, 1166-1176.

Shakoor, R., Hassan, M. Y., Raheem, A., & Wu, Y.-K. (2016). Wake effect modeling: A review of wind farm layout optimization using Jensen′s model. *Renewable and Sustainable Energy Reviews, 58*, 1048-1059.

Song, M., Chen, K., & Wang, J. (2018). Three-dimensional wind turbine positioning using Gaussian particle swarm optimization with differential evolution. *Journal of Wind Engineering and Industrial Aerodynamics, 172*, 317-324.

Song, M. X., Wu, B. H., Chen, K., Zhang, X., & Wang, J. (2016). Simulating the wake flow effect of wind turbines on velocity and turbulence using particle random walk method. *Energy, 116*, 583-591.

Song, Z., Zhang, Z., & Chen, X. (2016). The decision model of 3-dimensional wind farm layout design. *Renewable Energy, 85*, 248-258.

Sørensen, T., Thøgersen, M. L., Nielsen, P., & Jernesvej, N. (2008). Adapting and calibration of existing wake models to meet the conditions inside offshore wind farms. *EMD International A/S. Aalborg*.

Sun, H., Gao, X., & Yang, H. (2019). Investigation into offshore wind farm repowering optimization in Hong Kong. *International Journal of Low-Carbon Technologies, 14*(2),

302-311.

Sun, H., & Yang, H. (2018). Study on an innovative three-dimensional wind turbine wake model. *Applied Energy, 226*, 483-493.

Sun, H., & Yang, H. (2020). Numerical investigation of the average wind speed of a single wind turbine and development of a novel three-dimensional multiple wind turbine wake model. *Renewable Energy, 147*, 192-203.

Sun, H., Yang, H., & Gao, X. (2017). Study on offshore wind farm layout optimization based on decommissioning strategy. *Energy Procedia, 143*, 566-571.

Sun, H., Yang, H., & Gao, X. (2019). Investigation into spacing restriction and layout optimization of wind farm with multiple types of wind turbines. *Energy, 168*, 637-650.

Thogersen, M. L., Sorensen, T., Nielsen, P., Grotzner, A., & Chun, S. (2006). Introduction to wind turbine wake modelling and wake generated turbulence. *DNV/Risø, 2nd ed.: Risø National Laboratory, EMD International A/S*.

Tian, L. L., Zhu, W. J., Shen, W. Z., Zhao, N., & Shen, Z. W. (2015). Development and validation of a new two-dimensional wake model for wind turbine wakes. *Journal of Wind Engineering and Industrial Aerodynamics, 137*, 90-99.

Tian, W., Ozbay, A., & Hu, H. (2014). An experimental study on the effects of incoming wind conditions on wind turbine aeromechanics.

Tong, W., Chowdhury, S., Zhang, J., & Messac, A. (2012). *Impact of different wake models on the estimation of wind farm power generation.* Paper presented at the 12th AIAA Aviation Technology, Integration, and Operations (ATIO) Conference and 14th AIAA/ISSMO Multidisciplinary Analysis and Optimization Conference.

Topham, E., & McMillan, D. (2017). Sustainable decommissioning of an offshore wind farm. *Renewable Energy, 102, Part B*, 470-480.

Trujillo, J. J., Bingöl, F., Larsen, G. C., Mann, J., & Kühn, M. (2011). Light detection and

ranging measurements of wake dynamics. Part II: two-dimensional scanning. *Wind Energy, 14*(1), 61-75.

Twidell, J., & Gaudiosi, G. (2009). *Offshore wind power*. Essex, United Kingdom: Multi Science Pub.

van Dooren, M. F., Trabucchi, D., & Kühn, M. (2016). A methodology for the reconstruction of 2d horizontal wind fields of wind turbine wakes based on dual-Doppler lidar measurements. *Remote Sensing, 8*(10), 809.

Vanderwende, B. J., Lundquist, J. K., Rhodes, M. E., Takle, E. S., & Irvin, S. L. (2015). Observing and simulating the summertime low-level jet in central Iowa. *Monthly Weather Review, 143*(6), 2319-2336.

VanLuvanee, D. R. (2006). *Investigation of observed and modeled wake effects at Horns Rev using WindPRO.* (Master), Technical University of Denmark,

Vasel-Be-Hagh, A., & Archer, C. L. (2017). Wind farm hub height optimization. *Applied Energy, 195*, 905-921.

Vasiljević, N., Palma, J. M., Angelou, N., Matos, J. C., Menke, R., Lea, G., . . . Gomes, V. M. (2017). Perdigão 2015: methodology for atmospheric multi-Doppler lidar experiments. *Atmospheric Measurement Techniques, 10*(9), 3463-3483.

Wang, H., & Barthelmie, R. (2015). *Wind turbine wake detection with a single Doppler wind lidar.* Paper presented at the Journal of Physics: Conference Series.

Wang, L., Tan, A. C. C., Cholette, M., & Gu, Y. (2016). Comparison of the effectiveness of analytical wake models for wind farm with constant and variable hub heights. *Energy Conversion and Management, 124*, 189-202.

Wang, P., Goel, L., Ding, Y., & Chang, L. P. (2009). *Reliability-based long term hydro/Thermal reserve allocation of power*. Paper presented at the IEEE Power & Energy Society General Meeting.

Wikipedia. Sha Chau. Retrieved from https://en.wikipedia.org/wiki/Sha_Chau

Wikipedia. Tehachapi Pass Wind Farm. Retrieved from https://en.wikipedia.org/wiki/Tehachapi_Pass_Wind_Farm

Wikipedia. Waglan Island. Retrieved from https://en.wikipedia.org/wiki/Waglan_Island

Wildmann, N., Kigle, S., & Gerz, T. (2018). *Coplanar lidar measurement of a single wind energy converter wake in distinct atmospheric stability regimes at the Perdigao 2017 experiment*. Paper presented at the Journal of Physics: Conference Series.

Wu, Y.-K., Lee, C.-Y., Chen, C.-R., Hsu, K.-W., & Tseng, H.-T. (2014). Optimization of the Wind Turbine Layout and Transmission System Planning for a Large-Scale Offshore WindFarm by AI Technology. *IEEE Transactions on Industry Applications, 50*(3), 2071-2080.

Wu, Y.-T., & Porté-Agel, F. (2011). Large-eddy simulation of wind-turbine wakes: evaluation of turbine parametrisations. *Boundary-Layer Meteorology, 138*(3), 345-366.

Yang, X., & Sotiropoulos, F. (2013). *On the predictive capabilities of LES-actuator disk model in simulating turbulence past wind turbines and farms*. Paper presented at the American Control Conference (ACC), 2013.

Yanguas Miñambres, Ó. (2012). *Assessment of current offshore wind support structures concepts: challenges and technological requirements by 2020*.

Zambrano, T. G., & Gyatt, G. W. (1983). WAKE STRUCTURE MEASUREMENTS AT THE MOD-2 CLUSTER TEST FACILITY AT GOODNOE HILLS, WASHINGTON. *IEE Proceedings A: Physical Science. Measurement and Instrumentation. Management and Education. Reviews, 130*(9), 562-565.

Zhang, C., Hou, G., & Wang, J. (2011). A fast algorithm based on the submodular property for optimization of wind turbine positioning. *Renewable Energy, 36*(11), 2951-2958.

Zhou, H. F., Dou, H. Y., Qin, L. Z., Chen, Y., Ni, Y. Q., & Ko, J. M. (2014). A review of full-

scale structural testing of wind turbine blades. *Renewable and Sustainable Energy Reviews, 33*, 177-187.

Ziegler, L., Gonzalez, E., Rubert, T., Smolka, U., & Melero, J. J. (2018). Lifetime extension of onshore wind turbines: A review covering Germany, Spain, Denmark, and the UK. *Renewable and Sustainable Energy Reviews, 82*(Part 1), 1261-1271.